RAMAN SPECTROSCOPIC STUDIES OF SELECTED ENZYME SYSTEMS

A thesis submitted for the Degree of Doctor of Philosophy at the University of York.

Department of Chemistry

Janina Austin

August 1989

ABSTRACT

Raman, resonance Raman (RR) and surface enhanced Raman (SER) spectroscopies have been applied to the study of the dehydrogenase enzymes and their coenzyme nicotinamide adenine dinucleotide (NAD^+). RR and time-resolved RR (TR^3) spectroscopic techniques have been used to study the heme enzyme catalase and a heme model system, iron(III)tetraphenylporphyrin, $(TPP)Fe^{(III)}$.

Three methods for the analysis of the Raman amide I band have been used to estimate secondary structure in the apo- and holo-forms of the enzyme glyceraldehyde-3-phosphate dehydrogenase (GAPDH). The three methods were critically assessed, and compared with the corresponding X-ray data. Despite the apparent flaws in the methods, there was a generally good agreement with the X-ray data, reflecting a very small (almost negligible) secondary structure change between apo- and holo- GAPDH.

Ultraviolet RR (UVRR) spectra of the enzymes lactate, malate, and alcohol dehydrogenase and GAPDH have been obtained. UVRR spectra obtained using 260 nm excitation showed the spectrum of the enzyme-bound coenzyme. The spectral differences between enzyme-bound and free coenzyme were discussed. UVRR spectra were also obtained for an enzyme-substrate intermediate of GAPDH.

SER spectra have been obtained for the coenzyme NAD^+ and related compounds adsorbed onto colloidal silver. The surface selection rules that have been used to deduce orientational information from SER spectra were discussed in the light of the probable contributions to Raman enhancement from both an electromagnetic and a chemical mechanism. From data obtained at different coenzyme concentrations, and at different pH's, the form of NAD^+ adsorption was deduced. NAD^+ appears to adsorb primarily *via*

its negatively charged phosphate groups, with secondary binding *via* adenine. The nicotinamide moiety approaches closer to the silver surface at lower coenzyme concentrations.

RR and UV-vis. absorption spectra of catalase and various catalase complexes were obtained. In particular, attempts were made to obtain the RR spectrum of catalase compound I. While the UV-vis. spectrum showed complete conversion to compound I, the RR spectrum was more complex, probably reflecting some photodecomposition to compound II. The photoreactions of a heme model system, $(TPP)Fe^{(III)}$ were investigated on the nanosecond timescale. The dimeric species $[(TPP)Fe^{(III)}]_2O$ did not appear to photodissociate in large enough amounts to observe any spectral changes. However, a triplet state species was observed for both the dimer and the monomer species, $(TPP)Fe^{(III)}Cl$.

ACKNOWLEDGEMENTS

I would like to thank my supervisor and mentor Professor Ron Hester for his guidance, patience and strong support throughout my years at York. My thanks also go to Mr. Reuben Girling for his expert help with the Raman equipment at York, and to the past and present members of the York Raman group. Particular thanks are due to Drs. Steve Bell and Siva Umapathy for setting up the excellent CCD Raman system at York, and for their invaluable guidance at the Rutherford Appleton Laboratory. I am indebted to the dedicated staff at the Laser Support Facility, Rutherford Appleton Laboratory, for their expert technical assistance with the UVRR experiments.

On the biochemical side, particular thanks go to Drs. Chris Wharton, Birmingham University, and Tony Clarke, Bristol University, for sharing their knowledge of the dehydrogenase enzymes. My thanks also go to the biochemistry group at York for all their help.

TABLE OF CONTENTS

ABBREVIATIONS

Listed in alphabetical order.

A	Adenine
ADH	Alcohol dehydrogenase
ADP	Adenosine diphosphate
Ala	Alanine
AR	Analytical reagent
Asp	Aspartic acid
Asn	Asparagine
C	Cytosine
CcO	Cytochrome c oxidase
CcP	Cytochrome c peroxidase
CT	Charge transfer
c.w.	Continuous wave
Cys	Cysteine
Cyt	cytochrome
DNA	Deoxyribosenucleic acid
DPG	1,3-diphosphoglycerate
EM	Electromagnetic
EDTA	Ethylenediaminetetraacetic acid
FBP	Fructose 1,6-bisphosphate
G	Guanosine
GAP	Glyceraldehyde-3-phosphate
GAPDH	Glyceraldehyde-3-phosphate dehydrogenase

Gln	Glutamine
Glu	Glutamic acid
Hb	Hemoglobin
HbO_2	Oxyhemoglobin
His	Histidine
HRP	Horseradish peroxidase
Ile	Isoleucine
IR	Infrared
LADH	Liver alcohol dehydrogenase
LDH	Lactate dehydrogenase
Mb	Myoglobin
MDH	Malate dehydrogenase
MEM	Maximum Entropy Method
Met	Methionine
M.W.	Molecular weight
NAD^+	Nicotinamide adenine dinucleotide
NADH	Nicotinamide adenine dinucleotide (reduced)
NR	Normal Raman
OEP	Octaethylporphyrin
PAA	Peroxyacetic acid
Phe	Phenylalanine
PP	Protoporphyrin

PZC	Potential of zero charge
RIP	Reference intensity profile
RR	Resonance Raman
SCE	Saturated calomel electrode
SER	Surface enhanced Raman
Ser	Serine
SERRS	Surface enhanced resonance Raman
SERS	Surface enhanced Raman spectroscopy
T	Thymine
TPP	Tetraphenylporphyrin
Tris	Tris(hydroxymethyl)aminomethane
Trp	Tryptophan
TR^3	Time resolved resonance Raman
Tyr	Tyrosine
U	Uracil
UV	Ultraviolet
UVRR	Ultraviolet resonance Raman
UV-vis.	Ultraviolet-visible
Val	Valine
YADH	Yeast alcohol dehydrogenase

CHAPTER ONE: INTRODUCTION

1.1 GENERAL INTRODUCTION

Raman spectroscopy has been increasingly used over the past two decades for the study of biological systems. Its suitability to certain biological problems has been amply demonstrated by the many recent reviews and texts on the subject [1-7]. Its advantages and limitations have been discussed at length in refs. [2], [5] and [7].

Normal Raman (NR) scattering is an intrinsically weak process; however, resonance Raman (RR) and surface enhanced Raman (SER) scattering can be orders of magnitude stronger. Both RR and SER spectroscopy have been applied (in addition to NR spectroscopy) to the study of the biological systems discussed in the following chapters. A brief general introduction to NR, RR, and SER spectroscopies is given below, in sections 1.2, 1.3 and 1.4, respectively. Particular attention has been given to the type of information that can be gained from the study of biological systems.

The work presented in this thesis is concerned with the application of NR, RR and SER spectroscopies to the dehydrogenase enzymes and to the heme enzyme, catalase. The general biochemistry of these systems is briefly described in sections 1.5 and 1.6 following. A separate section (1.7) is devoted to the description of the molecule nicotinamide adenine dinucleotide (NAD^+), which is the coenzyme for many dehydrogenase enzymes.

1.2 NR SPECTROSCOPY OF PROTEINS

The NR spectrum of a protein will show characteristic bands due to the vibrations of the aromatic amino acid side chains, and due to the vibrations of the polypeptide backbone [8, 9]. If there are disulphide links in the protein, the NR spectrum will also show bands characteristic of vibrations of these. Information can thus be

obtained on the environment and bonding of tyrosine and tryptophan residues in a protein. For example, the relative intensities of the two bands in the 850/830 cm^{-1} 'Fermi' doublet of tyrosine is considered to be an accurate indicator of tyrosine hydrogen bonding [9]. NR bands arising from phenylalanine vibrations are generally considered to be insensitive to such environmental effects [9]. Disulphide links give rise to bands in the region 500-550 cm^{-1}. The band position(s) can be used to determine the precise geometry of the C-C-S-S-C-C linkage [9]. Further details of other bands that are useful in yielding such specific information are given in ref. [9]. Table 1.1 provides a summary of the most commonly used bands in the NR spectra of proteins.

The vibrations of the polypeptide backbone of a protein give rise to the bands in the NR spectrum called the amide I and amide III bands [9]. The amide II band is not Raman active, but is observed in the infrared (IR) spectrum at *ca.* 1550 cm^{-1}. The amide I band arises predominantly from the peptide carbonyl stretching vibration (see Fig. 1.1 (a)) and is found at around 1660 cm^{-1}. The amide III band arises from a vibration consisting of *ca.* 40% C-N stretch and 30% N-H in plane bend, with smaller contributions from $C-C_{\alpha}$ and C=O stretching (see Fig. 1.1 (b)). The amide III band is found between 1230 and 1300 cm^{-1}. The amide I and III bands have both been shown to be sensitive to the secondary structure of the polypeptide backbone (see Fig. 1.1 (c)) [8, 9]. In recent years, these bands have been used to give quantitative estimates of α-helix, β-sheet, and undefined structure in proteins [10-12]. Amide I bands have also been assigned to the various types of β-turn [13, 14], and other types of helix [15]. However, no completely satisfactory method of analysing the quantity of these

Table 1.1 Commonly Used Diagnostic Bands in the NR Spectra of Proteins

Band position	Use
Disulphide links	
500-550 cm^{-1}	Indicator of the geometry of the C-C-S-S-C-C linkage.
Phenylalanine	
1006 cm^{-1}	Intensity standard- considered to be relatively invariant in NR spectra.
Tyrosine	
850/830 cm^{-1} doublet	Indicator of tyrosine hydrogen bonding.
Tryptophan	
1360-1365 cm^{-1}	Indicator of tryptophan solvent exposure.
Peptide Backbone	
Amide III, 1230-1300 cm^{-1}	Indicator of protein secondary structure.
Amide I, 1645-1680 cm^{-1}	Indicator of protein secondary structure.
Sulphydryl (SH)	
2560-2580 cm^{-1}	Identification of 'masked' SH groups in proteins.

Figure 1.1 Representations of (a) the amide I and (b) amide III vibrations of a peptide.

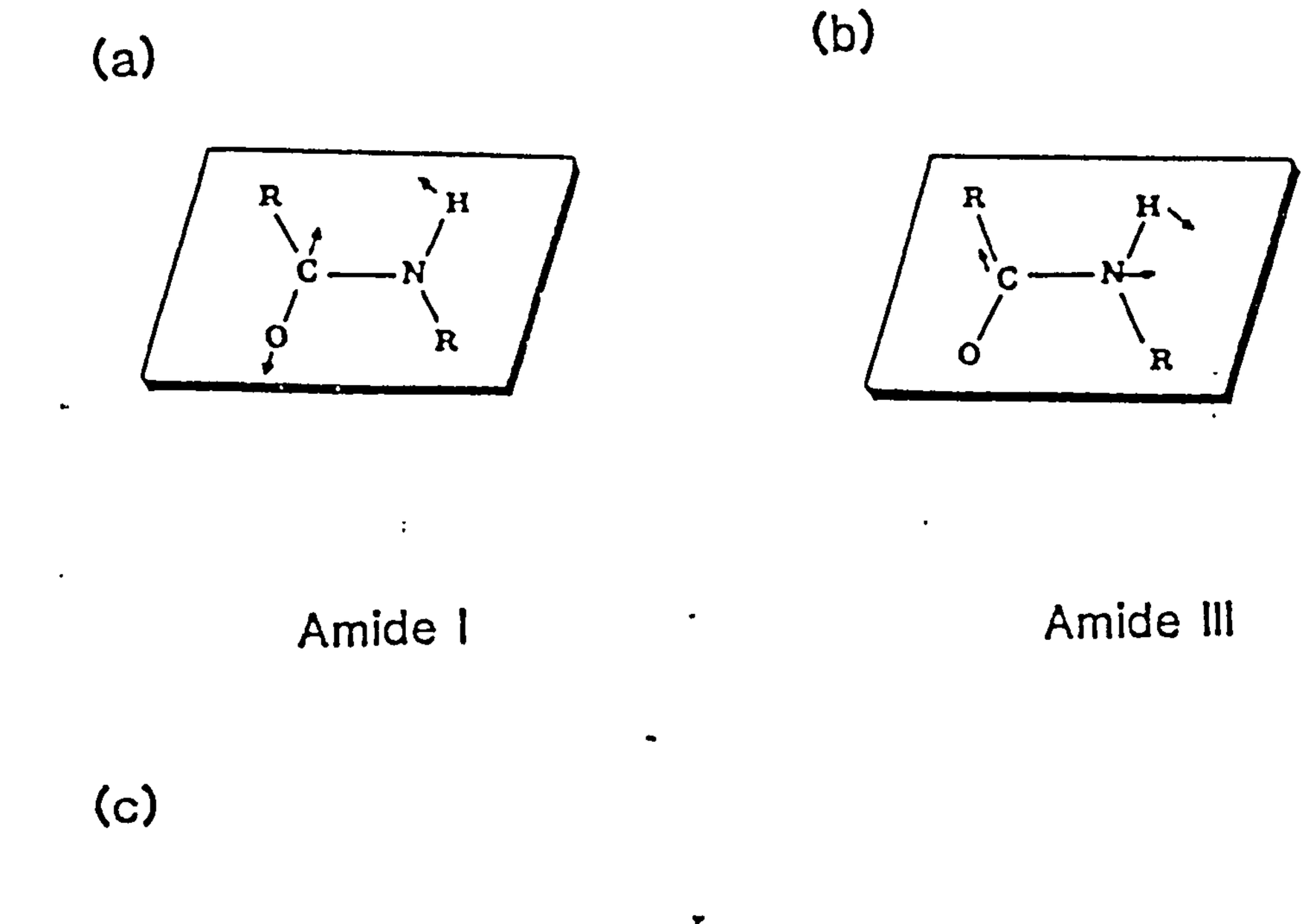

Figure 1.1 (c) Amide I and III band positions for different protein conformations. From ref. [9].

other structures in proteins has yet evolved from the NR studies of proteins. Williams claims accuracy in estimating the amount of β-turn structure in proteins, but does not attempt to subdivide this class into the different types of β-turn that may be present [10].

Chapter 3 of this thesis is concerned with the estimation of secondary structure types in the enzyme glyceraldehyde-3-phosphate dehydrogenase (GAPDH). In this study, several methods of amide I band analysis are used and critically assessed, together with the problem of defining the different types of secondary structure in terms of available X-ray crystallographic data.

1.3 RR SPECTROSCOPY OF BIOLOGICAL SYSTEMS

RR scattering occurs when the incident (exciting) laser wavelength is coincident with (or close to) an electronic absorption band of the molecule under study [2]. Under optimum conditions, the intensity of certain Raman bands may be increased by a factor of 10^6. This allows collection of Raman spectra at low concentrations (typically 10^{-4}-10^{-5} M). The intensity enhancement is selective for Raman bands of the chromophoric part of the molecule. Thus with a heme protein, the RR spectrum obtained with visible excitation will show only bands due to the heme moiety, and no bands from the protein.

There are four different types of RR scattering which may contribute to RR intensity, these being called A-, B-, C-, and D-term scattering [16]. A-term RR scattering is generally the dominant process. It involves just one excited (vibronic) state, and enhances totally symmetric vibrational modes. Overtone and combination bands are also enhanced (activated) by the A-term RR process.

B-term RR scattering involves vibronic coupling of two resonant excited states. The active vibrations are those that have any symmetry contained by the direct product of the representation of the two excited electronic states. Thus, depending on the symmetries of the two excited states, both non-totally symmetric and totally symmetric modes may be active.

C-term RR scattering involves vibronic coupling of the ground state to other excited states and is normally expected to be very small. Similarly, D-term RR scattering is not thought to make a significant contribution to RR intensity in most situations, and need not be considered further here. In addition to the selectivity in RR enhancement that may arise from the contribution of a certain type of RR scattering process, it is generally true that there is a further selectivity which originates from the geometries of the excited (resonant) and ground electronic states. The RR bands that are most enhanced arise from those vibrations along whose normal co-ordinates the molecular geometry would distort on going from the ground electronic state to the resonant excited electronic state [17].

Many biological molecules have convenient visible or near-ultraviolet chromophores which can be relatively easily studied by RR spectroscopy. Hemeproteins, flavoproteins, photosynthetic reaction centres, and rhodopsins have all been studied by RR spectroscopy, producing a wealth of detailed structural and kinetic information on these systems [1, 2, 3, 18]. However, many biological systems, including the dehydrogenase enzymes, do not contain visible chromophores, although in some cases, artificial substrates have been used to provide suitable chromophoric labels [2, 19, 20]. The recent development of ultraviolet lasers has initiated a new growth

in the use of RR spectroscopy of biological systems. Aromatic amino acids absorb in the wavelength regions 250-280 nm and 200-230 nm, and the amide group absorbs at *ca.* 190 nm, so all proteins can be studied by ultraviolet RR (UVRR) spectroscopy. Chapter 4 of this thesis is concerned with the use of UVRR spectroscopy to study the dehydrogenase enzymes and their coenzyme NAD^+, which also absorbs strongly in the ultraviolet (UV) region.

In chapter 6 of this thesis, RR spectra are presented for the heme enzyme catalase, and for a model heme system. RR spectroscopy is particularly suited to the study of heme proteins and metalloporphyrin models. This is in part due to the fact that they are strong Raman scatterers, and their electronic absorption bands are easily accessible to Ar^+ and Kr^+ lasers. It is now also true that their RR spectra are generally well understood; there is a wealth of published information available to aid the interpretation of spectra [1, 3, 21, 22]. Normal co-ordinate analyses of nickel octaethylporphyrin (NiOEP) and nickel tetraphenylporphyrin (NiTPP) have provided accurate mode descriptions of metalloporphyrin vibrations, as well as a systematic mode labelling system [23, 24]. The NiOEP species is considered to be the better model for biological hemes, such as protoporphyrin (PP) IX. The sensitivity of heme RR spectra to various factors have been discussed at length in various reviews [21, 22, 25], a short summary will be given in section 1.3.1 below.

1.3.1 RR Spectroscopy of heme systems

General Principles

Fig. 1.2 shows a generalised porphyrin structure, with

substituents X, Y, and Z on the C_β atoms of the pyrrole rings, and W on the methine bridging C_m atoms. The subsituents vary widely between the various biological heme and model metalloporphyrin systems; a few examples are listed at the bottom of the figure. One or two ligands may co-ordinate the heme iron in the axial positions above and below the plane of the porphyrin nitrogens. In heme proteins one ligand is provided by the protein itself, e.g. histidine in hemoglobin (Hb) and myoglobin (Mb), tyrosine in catalase.

The electronic absorption spectrum of a metalloporphyrin in the near-UV and visible regions shows a strong 'Soret' absorption band ($\epsilon \simeq 10^5$ $M^{-1}cm^{-1}$) in the near-UV, and generally two weaker bands in the visible region called the α and β bands ($\epsilon \simeq 10^4$ $M^{-1}cm^{-1}$). The two fundamental electronic transitions giving rise to the Soret and α bands are due to the $\pi \rightarrow \pi^*$ electronic transitions of E_u symmetry, in which no change of vibrational quantum number occurs (i.e. 0 -> 0 transitions). The β band, found between the Soret and α bands, is due to the envelope of all the active vibronic transitions in which the vibrational quantum number changes from 0 to 1. The electronic absorption spectra of some iron porphyrins are more complex than this [26], due to contributions from porphyrin to metal $\pi \rightarrow d\pi$ charge transfer transitions, the 0 -> 2 vibronic envelope (counterpart of the β band), and very weak contributions from metal d -> d transitions. The absorption spectra have been fully discussed elsewhere [26, 27], and will not be discussed further here.

The RR spectrum of a heme is strongly dependent on the absorption band used for resonance enhancement. Laser excitation in the Soret region gives rise to A-term RR scattering (see section

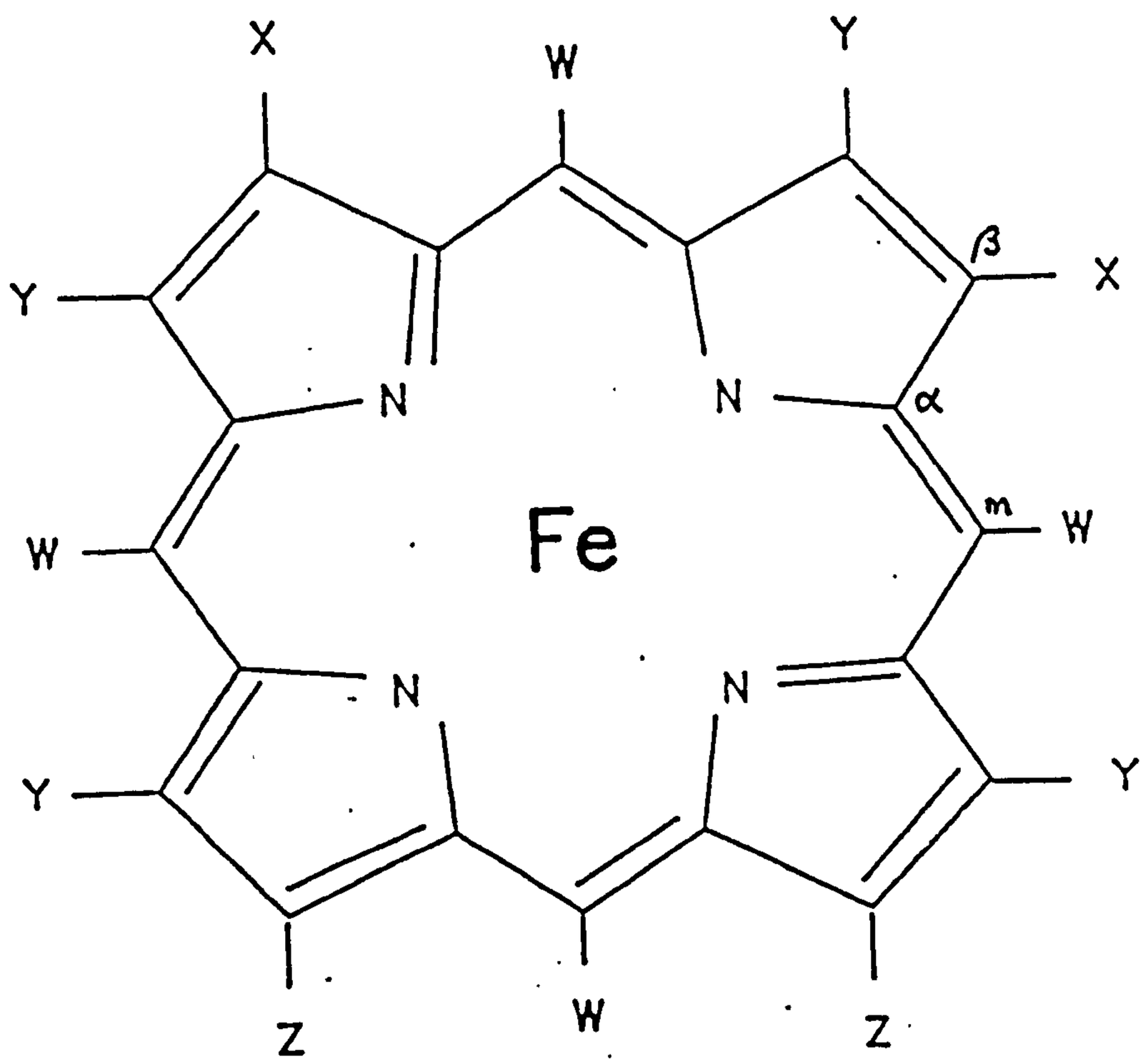

Figure 1.2 Structure of an iron porphyrin. For tetraphenyl-porphyrin (TPP), X=Y=Z=H, W=phenyl. For octaethyl-porphyrin (OEP), X=Y=Z=ethyl, W=H. For protoporphyrin IX (PP), X=vinyl, Y=methyl, Z=propionyl, W=H.

1.3); the RR spectrum is thus dominated by the totally symmetric A_{1g} modes of the heme. Excitation in the visible α, β region gives rise to enhancement by the B-term process; the RR spectrum then becomes dominated by non-totally symmetric B_{1g}, B_{2g} and A_{2g} modes of the heme. Further discussion of this phenomenon is given in refs. [2, 7, 22, 28]. The vibrations of the different symmetries give rise to different depolarizarion ratios of the scattered light. Vibrations of A_{1g} symmetry give rise to 'polarized' RR bands (depolarization ratio, $\rho \leq 0.75$). Vibrations of B_{1g} and B_{2g} symmetry give rise to 'depolarized' RR bands ($\rho = 0.75$), and A_{2g} vibrations give rise to 'anomalously' polarized ($\rho \geq 0.75$) RR bands [28]. Measurement of the depolarization ratio of a band gives a simple indication of the symmetry and thus assignment of any RR band [2]. For right-angle scattering, the ratio ρ is measured as $I_{\perp} / I_{\parallel}$, the intensities of Raman radiation polarized perpendicular and parallel to the plane normal to the incident beam.

Heme structure and RR spectra

The high wavenumber (1000-1700 cm^{-1}) region of a heme RR spectrum shows bands that are mostly due to stretching vibrations of the porphyrin ring [22, 23]. The lower wavenumber region below 1000 cm^{-1} contains bands that arise from iron-ligand stretching vibrations and porphyrin deformation vibrations.

It was noticed in the early days of heme RR spectroscopy that the wavenumbers of bands above 1300 cm^{-1} were particularly sensitive to the oxidation and spin state of the heme iron [28]. Choi *et al.* later correlated these changes with the change in porphyrin core size, measured from crystallographic studies as the distance C_t-N, the average distance from the four pyrrole N atoms to

the centre of the ring [29]. Some of these correlations are shown in Fig. 1.3, which shows the wavenumber dependence of vibrations of various protoporphyrin complexes with C_t-N. In addition to the core size effect, there are also superimposed effects of heme doming and back-donation of d_π electrons from metal to porphyrin [22]. The core size and doming effects have recently been reviewed and updated to include new data [30].

The spin state of the heme iron has a large effect on the porphyrin core size. High spin $Fe^{(III)}$ and $Fe^{(II)}$ have substantially larger radii than the corresponding low spin species; the porphyrin core size reflects this change. When there is only one axial ligand, the iron atom is displaced out of the porphyrin plane, allowing the core size to decrease to some extent despite the effects of spin state.

Heme doming is thought to cause the deviations from core size correlation observed for the 2-methylimidazole adducts of $Fe^{(II)}$ porphyrins (see Fig. 1.3) [22]. Heme doming has been observed in the crystal structures of deoxyHb and deoxyMb, showing the pyrrole rings tilted out of the porphyrin plane, following the out-of-plane Fe.

The oxidation state of the iron has a small effect of the porphyrin core size, as Fe^{3+} has a higher effective nuclear charge, and thus smaller radius, than Fe^{2+}. However, in the region above 1450 cm^{-1}, the effects of spin state are dominant. The ν_4 band (ν_n assignments as in refs. [22] and [23]), which occurs between 1345 and 1380 cm^{-1}, has been found to be the most sensitive oxidation state marker, and is often called the oxidation state marker band. The reasons for its sensitivity are not entirely straightforward, and are given in detail in ref. [22]. However, in heme proteins, it

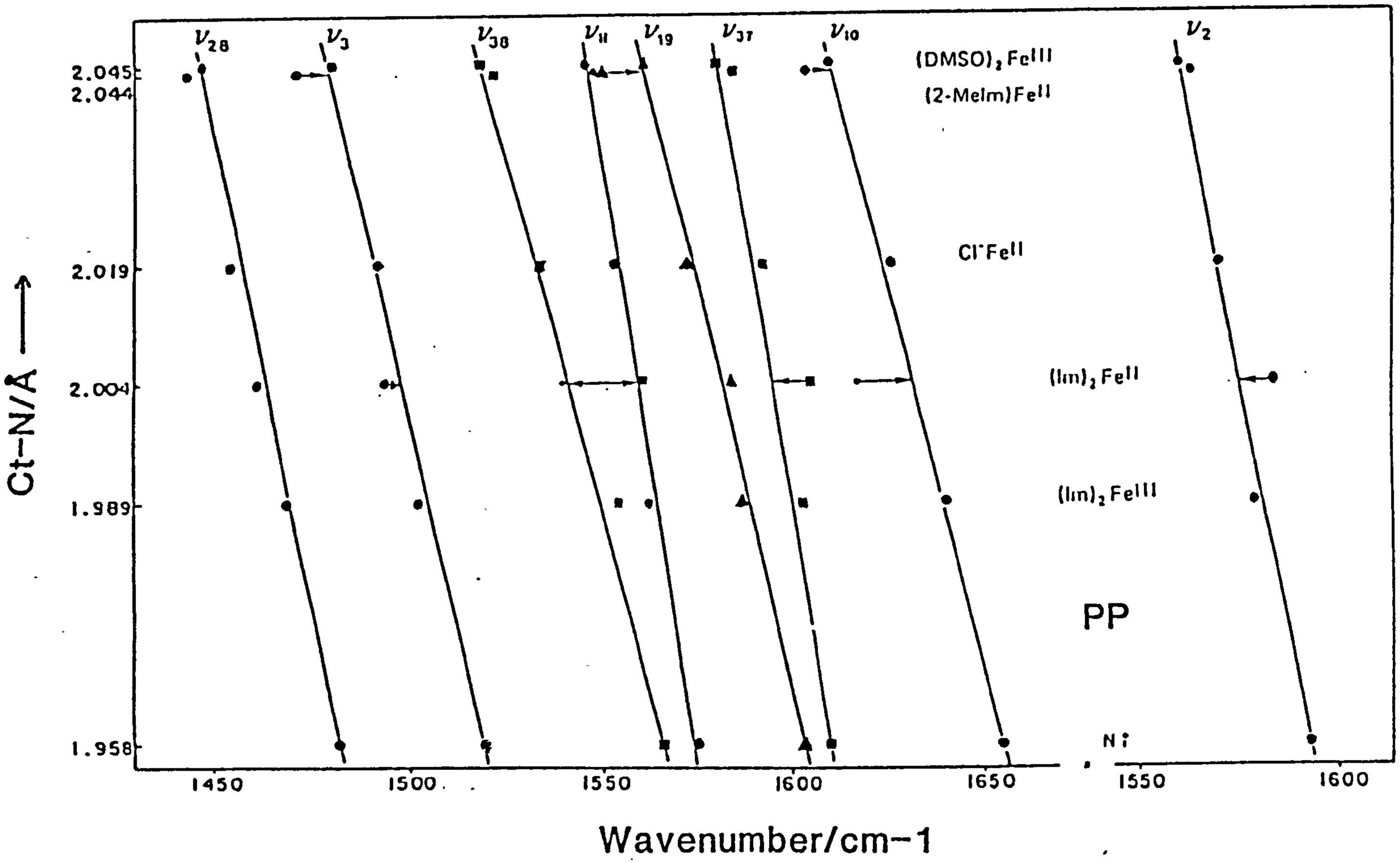

Figure 1.3 Correlation of selected porphyrin vibrational mode wavenumbers with core size (Ct-N) for various protoporhyrin (PP) complexes. From ref. [22].

Table 1.2 RR bands of selected Heme Proteins and Model Compounds: Correlations with iron spin and oxidation state.

		Wavenumber/cm^{-1}		
Low spin $Fe^{(III)}$		ν 4	ν 3	ν 10
core	(6c) Hb(CN)	1374	1508	1642
size	HRP(CN)	1375	1497	1642
↓	Low spin $Fe^{(II)}$			
	(6c) HRP(CN)	1362	1498	1620
	(PP)Fe(Im)$_2$	1359	1493	1617
	High spin $Fe^{(III)}$			
	(5c) (PP)FeCl	1373	1495	1632
	(6c) aquometHb	1373	1481	1623
	(6c) (PP)Fe(DMSO)$_2$	1370	1475	1610
	High spin $Fe^{(II)}$			
	(5c) deoxyHb	1358	1473	1607
	(5c) reduced HRP	1358	1472	1605

Data obtained from refs. [2] and [82].

is generally true that $Fe^{(II)}$ hemes have $\nu 4$ at *ca.* 1360 cm^{-1}, whilst $Fe^{(III)}$ hemes have $\nu 4$ at *ca.* 1375 cm^{-1}. There are some notable exceptions to this rule. For example, HbO_2 has $\nu 4$ at 1377 cm^{-1}, but is considered to be an $Fe^{(II)}$ heme. This has been explained in terms of effective back-donation of the iron $d\pi$ electrons into low lying O_2 π^* orbitals instead of into the porphyrin orbitals [22].

As indicated above, an excellent review of heme RR spectra interpretation can be found in ref. [22]. Table 1.2 presents some typical data for a few exemplary heme systems, indicating 'at a glance' the correlations between the RR spectra and heme iron oxidation and spin state.

1.4 SERS OF BIOLOGICAL MOLECULES

By adsorption onto a metal surface (usually silver), the Raman scattering of the adsorbed molecule may be enhanced by 3 to 6 orders of magnitude [31]. This effect, named surface enhanced Raman scattering, or SERS, and was recognised in 1977 [32] after an earlier experiment by Fleischmann *et al.* [33]. SERS has been the focus of many theoretical discussions over the last decade; many reviews have been published [31, 34-37]. A brief overview of the theories for SERS is given in chapter 5, section 5.1 of this thesis.

Due to the large enhancements that can be observed, many workers have used SERS (often in conjunction with RR) in the study of biological molecules [7, 38, 39]. For example, the SERRS (SERS and RR combined) spectrum of hemoglobin can be obtained at hemoglobin concentrations in the range 10^{-6} to 10^{-8} M, with no apparent loss in its ability to reversibly bind ligands [7]. However, there have been many 'casualties', especially in the early

days of SERS [40-43]. These have been in part due to undesirable chemical effects such as heme loss from Hb [40] (which can be largely avoided [7]), but also due to the lack of understanding of the effect itself.

Chapter 5 of this thesis is concerned with the SERS study of NAD^+, and the possible application of SERS to the study of the dehydrogenase enzymes is discussed.

1.5 THE NAD^+-LINKED DEHYDROGENASE ENZYMES

The NAD^+-linked dehydrogenases belong to a large class of enzymes that catalyse the reversible oxidation of a wide range of substrates using the coenzyme, NAD^+, which is reduced to NADH in the substrate oxidising reaction. The coenzyme is reduced by a stereospecific hydride transfer from the substrate to the coenzyme nicotinamide ring, viz..

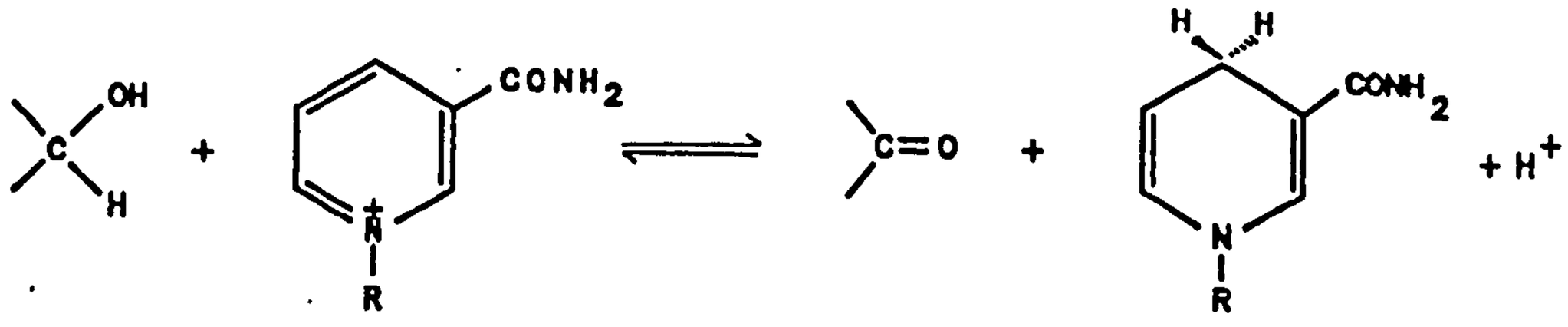

Studies using deuterium labelling have shown that the hydride transfer can occur to different 'faces' of the nicotinamide ring in different enzymes [44]. This is controlled by the orientation of the ring in the coenzyme binding pocket of the enzyme (see section 1.7).

The dehydrogenases are divided into two classes, A and B, depending on the stereochemistry of the hydride transfer.

The X-ray structures of the dehydrogenase enzymes (several have been solved) show a degree of structural homology [45]. All the enzymes appear to consist of two or more identical subunits, within which there are two domains, a catalytic and a nucleotide binding domain. While the catalytic domain varies widely from enzyme to enzyme, the nucleotide binding domain shows a remarkable structural (but not sequence) homology. In all cases, the NAD^+ molecule binds in approximately similar extended conformation (see chapter 4, section 4.4.2, and this chapter, section 1.7, for further details of NAD^+ structure and enzyme binding). Being an important class of enzymes, several thorough reviews have been published on various aspects of dehydrogenase kinetics, mechanism, and structure [45-47]. A brief summary of some characteristics of the enzymes glyceraldehyde-3-phosphate dehydrogenase (GAPDH), alcohol dehydrogenase (ADH), lactate dehydrogenase (LDH) and malate dehydrogenase (MDH) is given in the subsections below.

1.5.1 Glyceraldehyde-3-phosphate dehydrogenase

The glycolytic pathway enzyme GAPDH catalyses the oxidation and phosphorylation of D-glyceraldehyde-3-phosphate (GAP) to 1,3-diphosphoglycerate (DPG), as depicted in Fig. 1.4 [48, 49]. The reaction of the SH group of the active cysteine-149 residue with the substrate forms the hemithioacetal (A). The OH of the thioacetal is deprotonated by the base action of the nearby histidine-176 residue. The simultaneous hydride transfer to the nicotinamide ring from the hemithioacetal causes the formation of a relatively stable intermediate species (B). This acylenzyme intermediate contains the

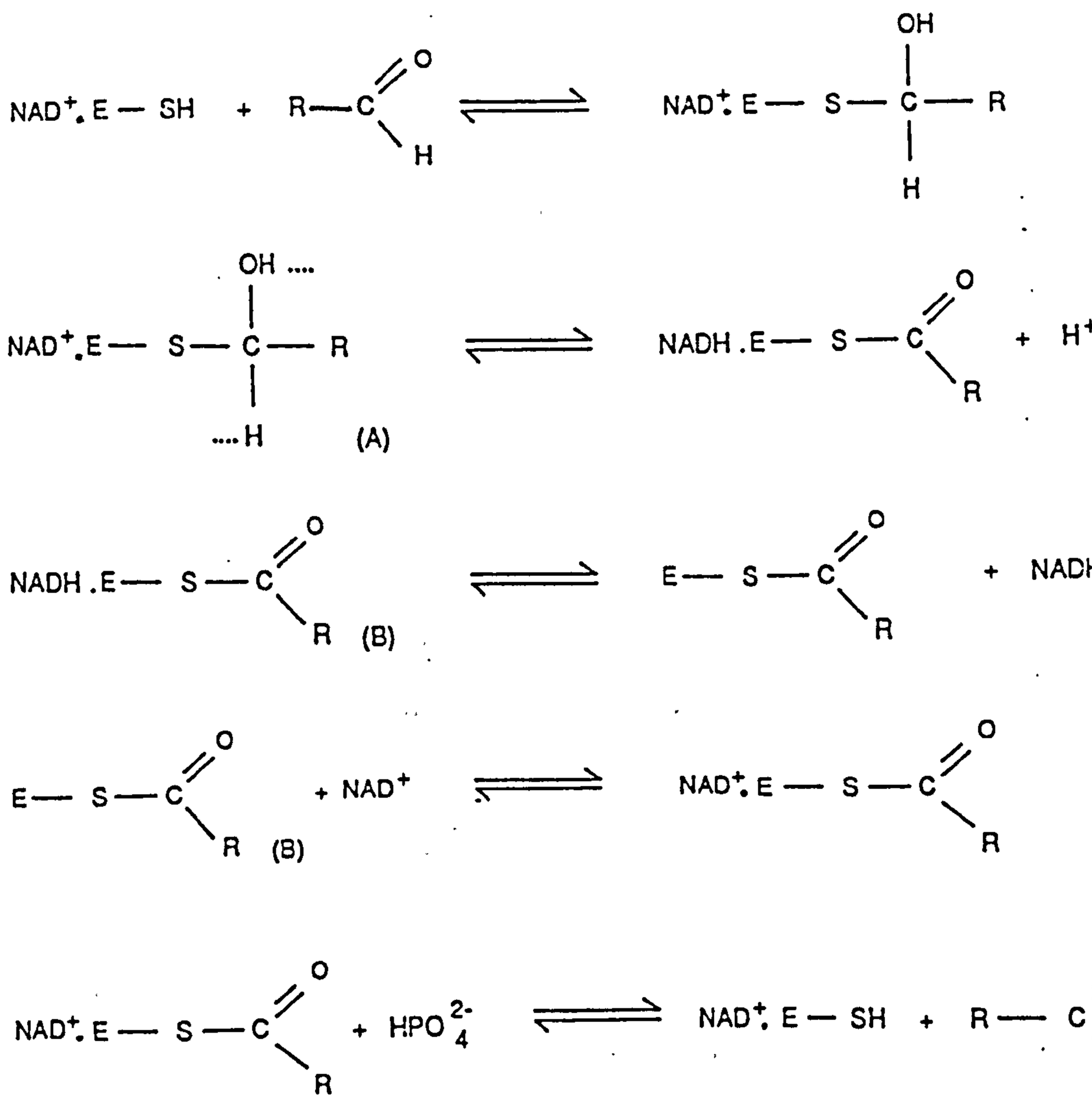

Figure 1.4 Mechanism of GAPDH catalysis.

thioester moiety R(CO)SR. The acylenzyme may be broken down by nucleophilic attack by phosphate (or hydroxide) only after the loss of NADH and subsequent replacement by NAD^+.

Although GAPDH is a tetrameric enzyme consisting of four identical subunits, many workers claim that the enzyme shows only half-of-site reactivity [50 and references therein], i.e. that the enzyme acylates at only two out of its four possible catalytic sites. This phenomenon has not yet been adequately explained, although the medium resolution X-ray structure of the enzyme from lobster muscle indicated a 'dimer of dimers' structure [51], in contrast to the subsequent (higher resolution) bacterial enzyme structure [52]. The coenzyme can bind at all four sites, but coenzyme binding (to all but the yeast enzyme) shows strong negative co-operativity, the fourth coenzyme molecule being very easily dissociated. X-ray structures of the apoenzyme (no bound coenzyme) [53], holoenzyme (fully coenzyme bound) [52], and 1-NAD^+-bound holoenzyme [54], show that there are sequential coenzyme-induced conformational changes which are the root of the observed co-operativity. The structural changes observed on coenzyme binding are fairly small (see chapters 3 and 4); no large change in secondary structure is observed.

1.5.2 Alcohol dehydrogenases

ADH from horse liver (liver ADH, LADH) has been extensively studied by both spectroscopists and crystallographers, providing a detailed picture of the intricate working of this enzyme [55]. As its name suggests, ADH catalyses the oxidation of a wide range of alcohols to aldehydes. In this respect, it is a much less specific enzyme than GAPDH; both aliphatic and aromatic alcohols (with very

different sizes and properties) may be oxidised.

Unlike GAPDH, ADH does not form a covalent intermediate with its substrate. Moreover, a metal ion, Zn^{2+}, is a principal part of the active site and is involved in the catalytic mechanism. It has been proposed that the zinc co-ordinates directly to the alcohol *via* the alcohol's oxygen atom; crystallographic studies of a ternary complex support this view [56]. The X-ray structures [56-59] have also allowed a plausible mechanism to evolve with considerable detail. It has been postulated that the alcohol becomes largely ionised (i.e. $R\text{-}O^{-}\cdots Zn$) when enzyme bound, which may in turn be facilitated by an effective proton-relay chain, involving the histidine-51 and serine-48 residues of the enzyme [60]. Spectroscopic studies using stable ternary complexes have attempted to clarify the nature of the substrate after it has become bound at the active site [20, 61].

LADH is a dimeric enzyme, with two identical subunits; whereas the yeast enzyme (YADH) is a tetramer. The 3D structure of LADH has been obtained in various forms, holo [57], apo [59], and inhibitor complexed forms [62, 62], as well as substrate-bound forms as mentioned above [56, 58]. The enzyme shows large tertiary and quaternary structure changes on binding coenzyme [57], and again on binding an aldehyde substrate with the coenzyme analogue H_2NADH [58]. A thorough review of the basic kinetics and mechanism of ADH's can be found in ref. [55]; a shorter, but more up to date account can be found in ref. [60].

1.5.3 Lactate dehydrogenase

The tetrameric enzyme LDH catalyses the oxidation of L-lactate to pyruvate, viz.

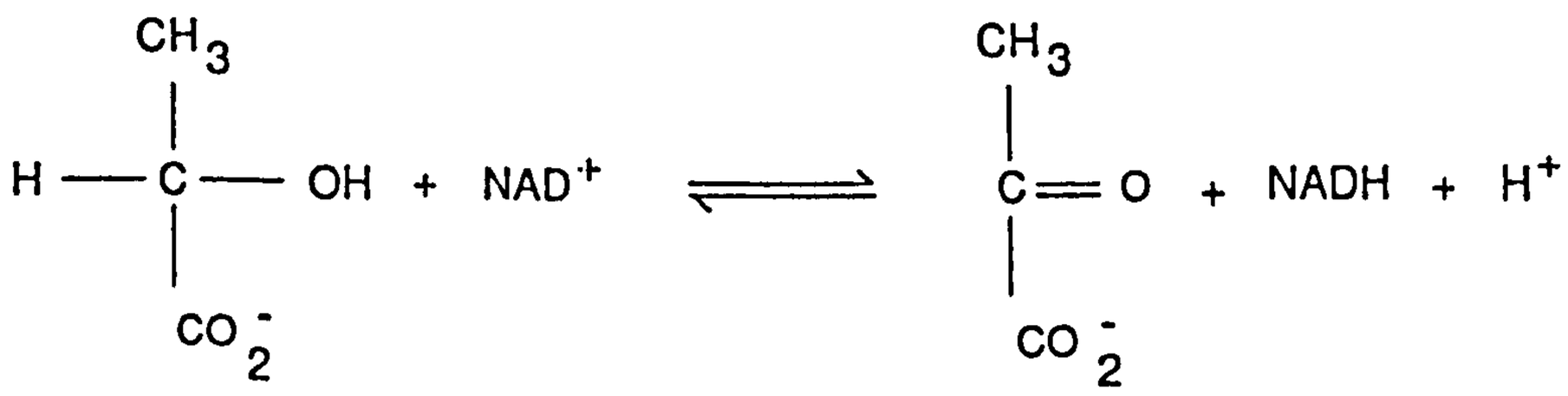

As in ADH, there is no covalent enzyme-substrate intermediate for the reaction. The mammalian enzyme can exist in two slightly different forms, H (predominant in heart muscle) and M (predominant in skeletal muscle). There are small differences in primary sequence between the two forms, but they associate readily to form mixed tetramers. The structures of the dogfish M4 apoenzyme and various ternary complexes have been established [64], and with information from other studies [65], show the possible importance of the amino acid residues histidine-195, arginine-171 and aspartate-168 in the catalytic mechanism. A thorough review of the structure and of kinetic aspects of LDH reactions is given in ref. [66].

1.5.4 Malate dehydrogenase

The dimeric enzyme MDH catalyses the oxidation of malate to oxaloacetate, viz.

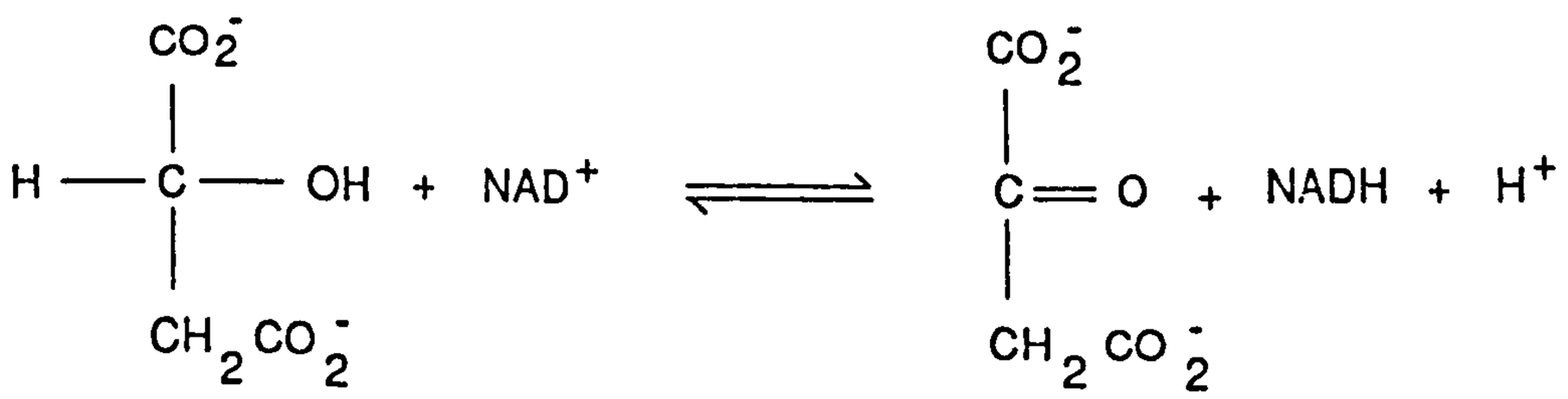

MDH is thought to be very similar in structure and mechanism to LDH; indeed, both MDH and LDH have been shown to contain catalytically important histidine and aspartate residues. An X-ray structure of (porcine) cytoplasmic MDH was obtained without knowledge of the amino acid sequence [67]; a tentative 'X-ray' primary structure was originally deduced largely from refinements of the X-ray data [68]. More recent experiments have resulted in publication of a further refined MDH structure [83]. A review of the properties and structure of MDH can be found in ref. [69].

1.6 CATALASE

Catalase is an extremely common enzyme, occurring in almost all aerobically respiring organisms. It is a large tetrameric enzyme (M.W. $\simeq 2.1\text{-}2.7\times10^5$ $gmol^{-1}$), with each identical subunit containing a heme moiety (protoporphyrin IX, see Fig. 1.2). The X-ray structure of the enzyme from bovine liver has been published [70] and shows (unusually) a tyrosine residue as the fifth ligand to the heme iron. The heme in its protein environment catalyses the decomposition of

peroxides, particularly hydrogen peroxide, through a catalytic intermediate called compound I [71]. This compound I intermediate has distinctive spectral properties (see chapter 6), and was long ago identified as being an intermediate that is common to the peroxidase-catalase family of enzymes [72].

The reaction of the peroxide molecule with the $Fe^{(III)}$ heme in catalase or peroxidase leaves an oxygen atom on the heme centre, and H_2O is released. The compound I intermediate formed by this initial oxidation process is nominally an Fe(V) species. However, spectroscopic measurements have shown that compound I has an Fe(IV)=O (ferryl) centre [73]. The extra oxidising equivalent is generally thought to be stored as a cation radical of the porphyrin in horse radish peroxidase (HRP) and catalase [73]. Cytochrome c peroxidase (CcP) has a compound I spectrum that is quite unlike other compound I species; indeed, e.s.r. studies have shown that although it has the Fe(IV)=O centre, the extra oxidising equivalent is not stored on the porphyrin, but on a nearby amino acid residue [74].

In HRP, compound I reacts with a substrate (usually phenol or amine) to form a radical species. Compound II is one oxidising equivalent below compound I, and is believed to be a non-radical heme species with the ferryl Fe(IV)=O heme centre [73]. Compound II then reacts with another substrate molecule, to regenerate the native enzyme, viz.

$$E + H_2O_2 \longrightarrow \text{Compound I} + H_2O$$

$$\text{Compound I} + AH_2 \longrightarrow \text{Compound II} + {}^{\cdot}AH$$

$$\text{Compound II} + AH_2 \longrightarrow E + {}^{\cdot}AH$$

$$2\,{}^{\cdot}AH \longrightarrow A + AH_2$$

In catalase, the reaction of compound I with a second

molecule of H_2O_2 does not produce an observable compound II intermediate; free catalase is apparently generated without the production of another stable intermediate. Indeed, catalysis of H_2O_2 decomposition by catalase is inhibited by compound II formation [72]. Catalase compound II is formed under conditions of excess ethyl or methyl hydroperoxide [75], or under conditions where H_2O_2 is generated slowly and continuously [76]. It is also formed in the presence of a large excess of peroxyacetic acid (PAA) [72]. Catalase compound II is only slowly regenerated to native catalase.

In chapter 6 of this thesis the RR spectra of catalase and various catalase derivatives are reported. Particular efforts have been made to establish the RR spectrum of catalase compound I.

1.7 STRUCTURAL ASPECTS OF NAD^+

The X-ray structure of $Li^+.NAD^+$ was determined by Reddy *et al.* [77], and is shown in Fig. 1.5 (a). A schematic representation, showing the atom numbering used in this thesis is given in Fig. 1.5 (b). The $Li^+.NAD^+$ structure shows the negatively charged pyrophosphate moieties co-ordinated to lithium ions, preventing intramolecular stacking of the adenine and nicotinamide rings. This extended conformation is generally similar to that found when NAD^+ is bound to the dehydrogenases [45, 78]. The crystal conformation of NAD^+ differs from the solution conformation. Spectroscopic studies (almost exclusively n.m.r.) have shown that the adenine and nicotinamide rings of NAD^+ may stack in solution, to produce a folded conformation [79, 80]. The folded conformation is believed to be in equilibrium with the extended conformation (see chapter 4).

The angle χ_N indicated in Fig. 1.5 (b) can vary by 180° to produce 'syn' and 'anti' conformers of NAD^+. The anti orientation,

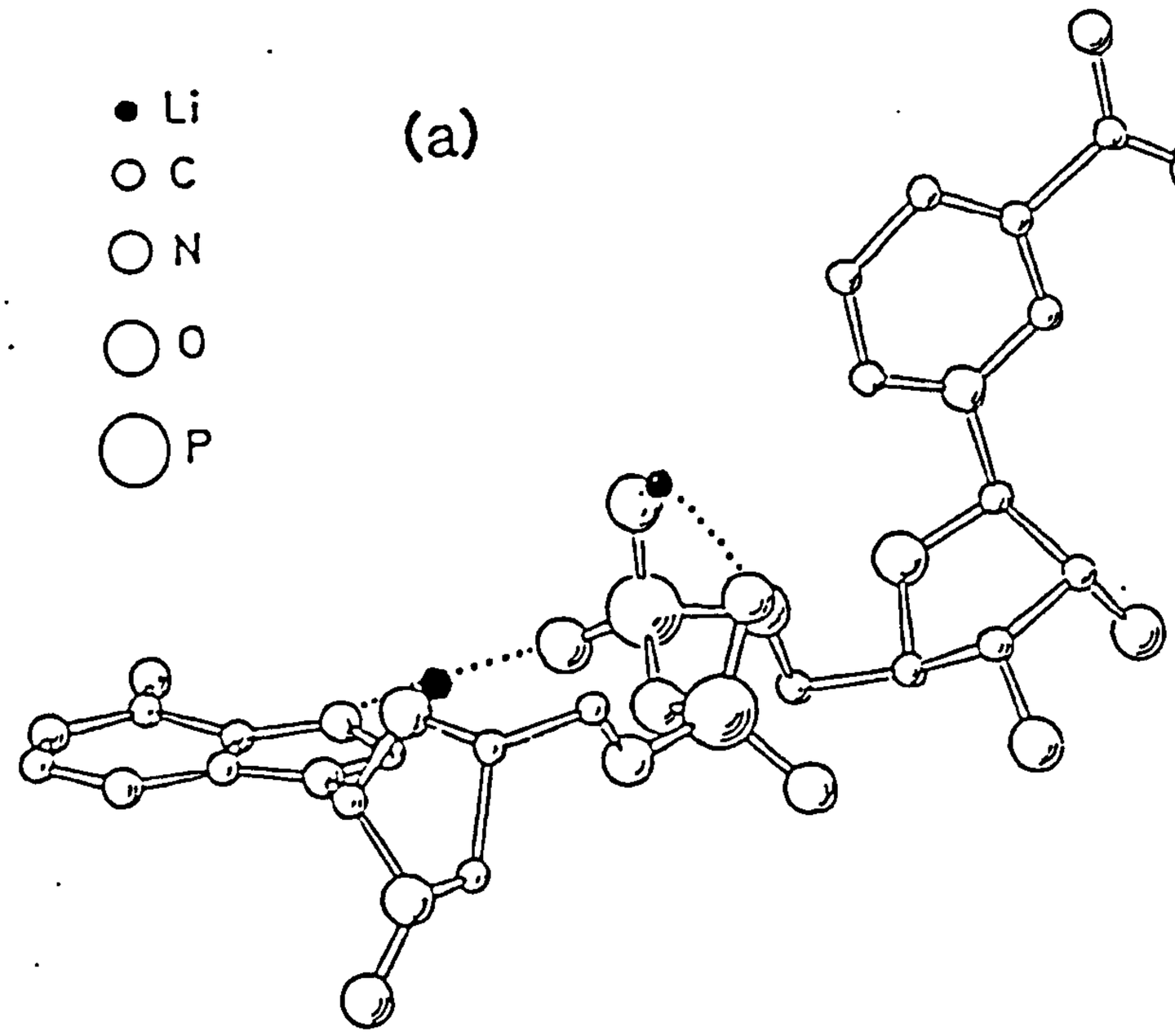

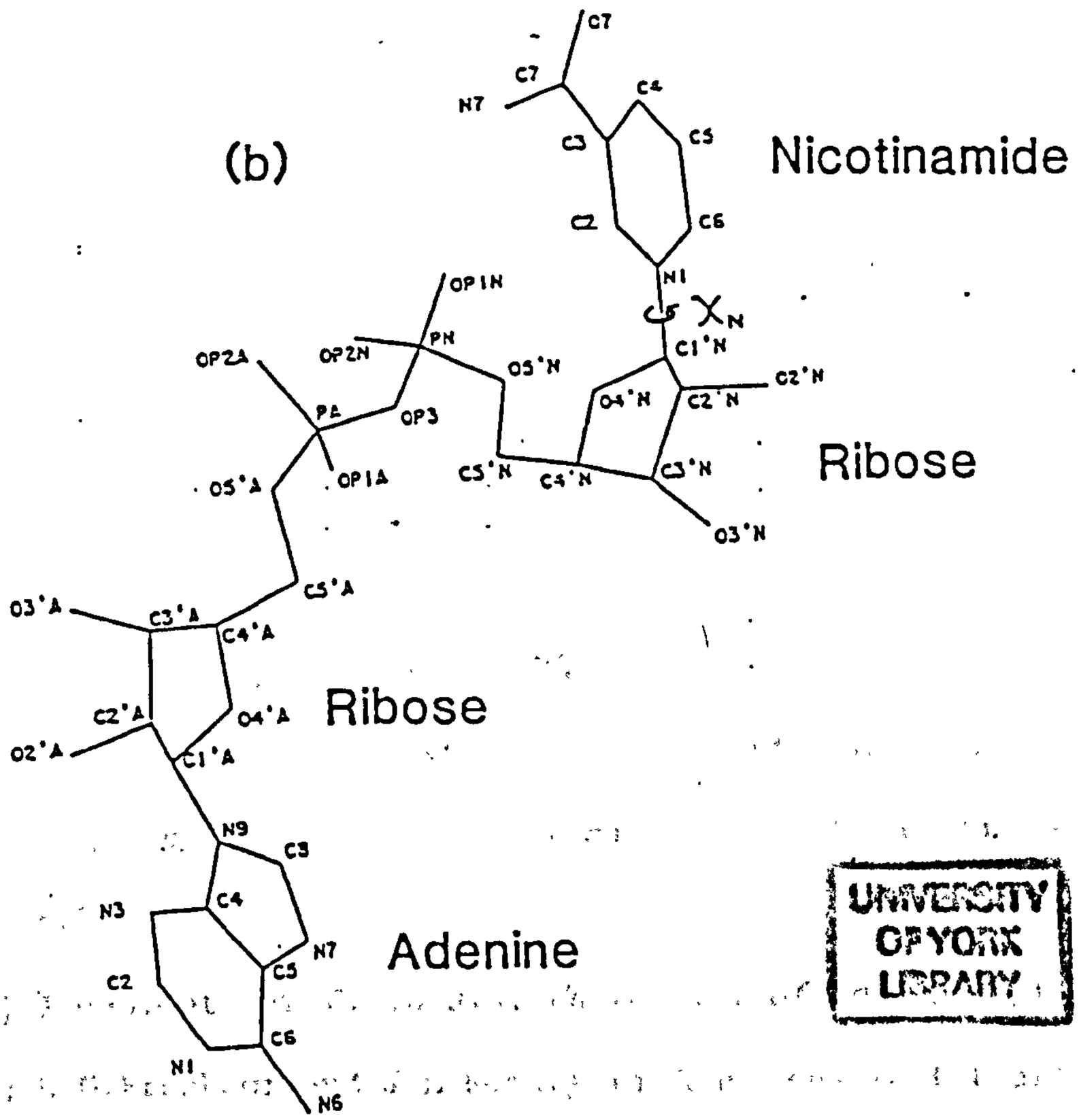

Figure 1.5 (a) Structure of NAD^+ in $Li^+.NAD^+$, from ref. [77].

(b) Representation of NAD^+, showing the atom numbering used in this thesis.

found in $Li^+.NAD^+$ and in the A-type dehydrogenases (LADH, LDH, MDH, see section 1.5), has the amide group of nicotinamide pointing away from the ribose moiety [78]. In the syn orientation, found in the B-type dehydrogenases (GAPDH), the amide group lies above the ribose moiety. Both syn and anti nicotinamide orientations are thought to exist in solution [81]. The terms syn and anti are also used to refer to the orientation of the adenine ring with respect to its adjacent ribose moiety. In the dehydrogenases, the adenine assumes an approximate syn orientation.

1.8 REFERENCES

[1] R.J.H.Clark and R.E.Hester, Eds., *"Advances in Infrared and Raman Spectroscopy, Vol. 13: Spectroscopy of Biological Systems"* (Wiley, Chichester, 1986).

[2] P.R.Carey, *"Biological Applications of Raman and Resonance Raman Spectroscopies"* (Academic Press, London, 1982).

[3] T.G.Spiro, Ed., *"Biological Applications of Raman Spectroscopy"* Vols. 1-3 (Wiley, New York, 1987).

[4] E.D.Schmid, F.W.Schneider, and F.Siebert, Eds., *"Spectroscopy of Biological Molecules- New Advances"* (Wiley, Chichester, 1988).

[5] C.W.Wharton, *Biochem. J.* **233** 25 (1986).

[6] F.S.Parker, *"Applications of Infrared, Raman and Resonance Raman Spectroscopies in Biochemistry"* (Plenum Press, New York, 1983).

[7] J.deGroot, *Ph.D. Thesis, University of York* (1987).

[8] B.G.Frushour and J.L.Koenig in "Advances in Infrared and Raman Spectroscopy, Vol. 1" Ch. 2 (Heyden and Sons, London, 1975).

[9] A.Tu in ref. [1]

[10] R.Williams, *Meth. Enz.* **130**, 311 (1986).

[11] M.Byler and H.Susi, *ibid.* p.290.

[12] M.Berjot, J.Marx, and A.J.P.Alix, *J.Raman Spectrosc.* **18**, 289 (1987).

[13] B.A.Seaton, *Spectrochimica Acta* **42A**, 227 (1986).

[14] J.W.Fox, A.T.Tu, V.J.Hruby, and M.I.Mosberg, *Arch.Biochem.Biophys.* **211**, 628 (1981).

[15] B.J.Frushour and J.L.Koenig, *Biopolymers* **14**, 379 (1975).

[16] R.J.H.Clark and T.J.Dines, *Angew.Chem., Int.Edn.* **25**, 131 (1986).

[17] A.Y.Hirakawa and M.Tsuboi, *Science* **188**, 359 (1975).

[18] B.Robert, E.Nabedryk, and M.Lutz in *"Advances in Spectroscopy, Vol. 18: Time-Resolved Spectroscopy"* Eds. R.J.H.Clark and R.E.Hester, p.301 (Wiley, Chichester, 1989).

[19] A.C.Storer, D.J.Phelps, and P.R.Carey, *Biochemistry* **20**, 3454 (1981).

[20] R.H.Callender, D.Chen, J.Lugtenburg, C.Martin, K.W.Rhee, D.Sloan, R.Vandersteen, and K.T.Yue, *Biochemistry* **27**, 3672 (1988).

[21] N.-T.Yu, *Meth.Enz.* **130** 350 (1986).

[22] T.G.Spiro, *Advances in Protein Chemistry* **37**, 111 (1985).

[23] M.Abe, T.Kitagawa, and Y.Kyogoku, *J.Chem.Phys.* **69**, 4526 (1978).

[24] X.-Y.Li and T.G.Spiro, *J.Phys.Chem.* in press (1989).

[25] T.G.Spiro and X.-Y.Li, in ref. [3], Vol. 3, Chapter 1.

[26] M.Gouterman in *"The Porphyrins, Vol. 3: Physical Chemistry, Part A"* Ed. D.Dolphin, p.69 (Academic Press, New York, 1978).

[27] F.Adar, *ibid.* p.167.

[28] T.G.Spiro and T.C.Strekas, *J.Am.Chem.Soc.* **96**, 338 (1974).

[29] S.Choi, T.G.Spiro, K.C.Langry, K.M.Smith, L.D.Budd, and G.N.LaMar, *J.Am.Chem.Soc.* **104**, 4345 (1982).

[30] N.Parthasarathi, G.Hansen, S.Yamaguchi, and T.G.Spiro, *J.Am.Chem.Soc.* **109**, 3865 (1987).

[31] M.Moskovits, *Rev.Mod.Phys.* **57**, 783 (1985).

[32] (a) A.Albrecht and J.A.Creighton, *J.Am.Chem.Soc.* **99**, 5215 (1977).

(b) D.L.Jeanmaire and R.P.Van Duyne, *J.Electroanal.Chem.* **84**, 1 (1977).

[33] M.Fleischmann, P.Hendra, and A.J.McQuillan, *Chem.Phys.Lett.* **26**, 163 (1974).

[34] R.K.Chang and B.L.Laube, *CRC Crit.Rev. in Solid State and Mater.Sci.* **12**, 1 (1984).

[35] A.Otto, *Ind.J.Pure and Appl.Phys.* **26**, 141 (1988).

[36] R.K.Chang and T.E.Furtak, Eds., *"Surface Enhanced Raman Scattering"* (Plenum Press, New York, 1982).

[37] J.A.Creighton in *"Advances in Spectroscopy, Vol. 16: Spectroscopy of Surfaces"* Eds. R.J.H.Clark and R.E.Hester, p.37 (Wiley, Chichester, 1988).

[38] T.M.Cotton, *ibid.* p.91.

[39] E.Koglin and J.M.Sequaris in *"Topics in Current Chemistry"* **134**, 1 (Springer-Verlag, Berlin, 1986).

[40] G.Smulevich and T.G.Spiro, *J.Phys.Chem.* **89**, 5168 (1985).

[41] R.E.Holt and T.M.Cotton, *J.Am.Chem.Soc.* **109**, 1841 (1987).

[42] E.Gantner, D.Steinert, and J.Reinhardt, *Anal.Chem.* **57**, 1658 (1985). The published spectra arise from a laser dye contaminant.[7].

[43] O.Siiman, R.Rivellini, and R.Patel, *Inorg.Chem.* **27**, 3940 (1988).

[44] G.Popjak, *"The Enzymes, 3rd Edn."* **2**, 134 (1974).

[45] M.G.Rossmann, A.Liljas, C.-I.Branden, and L.J.Banaszak, *"The Enzymes, 3rd Edn."* **11**, 62 (1975).

[46] K.Dalziel, *ibid.* p.2.

[47] H.Sund, Ed., "Pyridine Nucleotide-Dependent Dehydrogenases" (Walter de Gruyter, Berlin, 1977).

[48] J.I.Harris and M. Waters *"The Enzymes, 3rd Edn."* **13**, 1 (1976).

[49] D.R.Trentham, *Biochem.J.* **122**, 59 (1971).

[50] O.P.Malhotra and S.A.Bernhard, *J.Biol.Chem.* **243**, 1243 (1968).

[51] D.Moras, K.W.Olsen, M.N.Sabesan, M Buehner, G.C.Ford, and M.G.Rossmann, *J.Biol.Chem.* **250**, 9137 (1975).

[52] T.Skarzynski, P.C.E.Moody, and A.J.Wonacott, *J.Mol.Biol.* **193**, 171 (1987).

[53] T.Skarzynski and A.J.Wonacott, *J.Mol.Biol.* **203**, 1097 (1988).

[54] A.G.W.Leslie and A.J.Wonacott, *J.Mol.Biol.* **178**, 743 (1984).

[55] C.-I.Branden, H.Jornvall, H.Eklund, and B.Furugren, *"The Enzymes, 3rd Edn."* **11**, 104 (1975).

[56] H.Eklund, B.V.Plapp, J.-P.Samama, and C.-I.Branden, *J.Biol.Chem.* **257**, 14349 (1982).

[57] H.Eklund, J.-P.Samama, and T.A.Jones, *Biochemistry* **23**, 5982 (1984).

[58] E.Cedergren-Zeppezauer, J.-P.Samama, and H.Eklund, *Biochemistry* **21**, 4895 (1982).

[59] H.Eklund, B.Nordstrom, E.Zeppezauer, G.Soderlund, I.Ohlsson, T.Boiwe, B.-O.Soderburg, O.Tapia, C.-I.Branden, and A.Akeson, *J.Mol.Biol.* **102**, 27 (1976).

[60] A.Fersht *"Enzyme Structure and Mechanism, 2nd Edn."* (Freeman, New York, 1985).

[61] P.W.Jagodinski, G.F.Funk, and W.L.Peticolas, *Biochemistry* **21**,

2193 (1982).

[62] H.Eklund, J.-P.Samama, and L.Wallen, *Biochemistry* **21**, 4858 (1982).

[63] J.-P.Samama, E.Zeppezauer, J.F.Biellmann, and C.-I.Branden, *Eur.J.Biochem.* **81** 403 (1977).

[64] J.L.White, M.L.Hackert, M.Buehner, M.J.Adams, G.C.Ford, P.J.Lentz, I.E.Smiley, S.J.Steindel, and M.G.Rossmann, *J.Mol.Biol.* **102**, 759 (1976).

[65] A.R.Clarke, H.M.Wilks, D.A.Barstow, T.Atkinson, W.N.Chia, and J.J.Holbrook, *Biochemistry* **27**, 1617 (1988).

[66] J.J.Holbrook, A.Liljas, S.J.Steindel, and M.G.Rossmann, *"The Enzymes, 3rd Edn."* **11**, 191 (1975).

[67] J.J.Birktoft and L.J.Banaszak, *J.Biol.Chem.* **258**, 472 (1983).

[68] J.J.Birktoft, R.A.Bradshaw, and L.J.Banaszak, *Biochemistry* **26**, 2722 (1987).

[69] L.J.Banaszak and R.A.Bradshaw, *"The Enzymes, 3rd Edn."* **11**, 369 (1975).

[70] I.Fita and M.G.Rossmann, *J.Mol.Biol.* **185**, 21 (1985).

[71] G.R.Schonbaum and B.Chance, *"The Enzymes, 3rd Edn."* **13**, 363 (1976).

[72] D.N.Middlemiss, *Ph.D.Thesis, University of Newcastle-upon-Tyne* (1973).

[73] J.E.Frew and P.Jones in *"Advances in Inorganic and Bioinorganic Mechanisms, Vol. 3"* Ed. A.G.Sykes, p.175 (Academic Press, London, 1984).

[74] B.Hofman, J.E.Roberts, C.H.Kang, and E.Margiolash, *J.Biol.Chem.* **256**, 6556 (1981).

[75] B.Chance, *J.Biol.Chem.* **179**, 1341 (1949).

[76] B.Chance, *Biochem.J.* **46**, 387 (1950).

[77] B.S.Reddy, W.Saenger, K.Muhlegger, and G.Weimann, **J.Am.Chem.Soc. 103**, 907 (1981).

[78] W.Saenger, B.S.Reddy, K.Muhlegger, and G.Weimann, in ref. [47], p.222.

[79] B.A.Gruber and N.J.Leonard, *Proc.Natl.Acad.Sci. U.S.A* **72**, 3966 (1986).

[80] N.J.Oppenheimer, L.J.Arnold, and N.O.Kaplan, *Biochemistry* **17**, 2163 (1978).

[81] B.Birdsall, N.J.M.Birdsall, J.Feeny, and J.M.Thornton, *J.Am.Chem.Soc.* **97**, 2845 (1975).

[82] T.G.Spiro, J.D.Stong, and P.Stein, *J.Am.Chem.Soc.* **101**, 2648 (1979).

[83] J.J.Birktoft, G.Rhodes and L.J.Banaszak, *Biochemistry* **28**, 6064 (1989).

CHAPTER TWO: INSTRUMENTATION

2.1 INSTRUMENTATION AT YORK UNIVERSITY

2.1.1 Jobin-Yvon (JY) Ramanor HG2 Spectrometer System

This spectrometer and its detection system has been fully described in a previous thesis [1], where details of spectral response and sampling optics are also given. The spectrometer was controlled by a Nicolet 1074 computer, which was interfaced to the University of York mainframe computer (VAX) via a PDP-11 (DEC) minicomputer. For both this system and the Spex (see 2.1.2 following) all specific details of the instrumental settings and sample handling relevant to the work described are given in the experimental sections of each chapter.

2.1.2 Spex Model 1403 Spectrometer System

This spectrometer system has been described in detail in a previous thesis [1], and will not be discussed further here.

2.1.3 Lasers at the University of York

An Argon ion laser (Spectra Physics model 2025) was used for obtaining laser light of selected wavelengths between 351.1 and 514.5 nm. A Krypton ion laser (Spectra Physics model 170) was used for obtaining laser light of selected wavelengths between 350.6 and 647.1 nm.

2.1.4 The CCD Raman system

The potential of a charge coupled device (CCD) as a sensitive detector for Raman spectroscopy was noted by Murray [2]. The CCD Raman system recently developed at York has been designed to combine the extremely sensitive detection with good light collection

efficiency. It is thus ideal for use with weak Raman scatterers, low laser powers, or for studies where spectra need to be collected quickly (1-200 seconds). Its limitations are (1) it does not have very good spectral resolution at near-uv or uv wavelengths, and (2) the system does not have very efficient stray light rejection (it only has a single grating), thus hampering analysis of low wavenumber spectral regions.

The system uses a single grating spectrograph (JY HR640) equipped with a high efficiency holographic grating (1200 groove/mm). The detector is a CCD camera (Wright Instruments), which is interfaced to a microcomputer (Tandon TM7002), where control of data collection and manipulation of data can be carried out (using Wright Instruments Software). The detailed characteristics and performance of this system are given elsewhere [3].

The sampling optics used were simple; the laser beam was focussed onto the sample at 90° to the collected scattered light. The scattered light was collected and focussed by two lenses onto the entrance slit of the spectrometer. A polarization scrambler was placed in front of the entrance slit of the spectrograph.

2.2 INSTRUMENTATION AT THE LASER SUPPORT FACILITY, RUTHERFORD APPLETON LABORATORY

2.2.1 Laser Radiation

Visble laser light was obtained from a XeCl excimer (Lumonics HX460) - pumped dye laser (Lambda Physik FL3002), or a KrF excimer laser (Lumonics HX460) - pumped dye laser (Lambda Physik FL3002). UV radiation in the range 220 to 260 nm was produced by frequency doubling the dye laser output using a β-barium borate

crystal (Laser Line, Banbury, UK). The excimer lasers were generally run at 30 Hz, and the laser pulse width was *ca.* 10 ns (FWHH).

2.2.2 The Spex Triplemate Spectrometer and Multichannel Detection System

The Spex Triplemate spectrometer has been described in a previous thesis [1]. For UVRR experiments, 1200 groove/mm holographic gratings were used in the filter stage of the spectrometer, and 2400 or 3600 groove/mm holographic gratings in the spectrograph stage. For visible-RR experiments, 600 groove/mm gratings were used in the filter stage, and 1200 groove/mm gratings in the spectrograph stage. The internal mirrors were all coated with MgF_2 for optimum UV reflectivity.

The OSMA (Spectroscopic Instruments) intensified diode array was used to detect scattered light. The intensifier could be gated synchronously so as to allow collection of scattered light only at the time of the probe laser pulse (see section 2.2.3 below). The data collection and limited data handling were controlled by a dedicated minicomputer and software. For more extensive data handling, the data was transferred to a BBC minicomputer, for which Raman software has been written [4].

2.2.3 Gating/Timing System for UVRR and TR^3 Experiments

A gating and timing set-up for two-colour TR^3 experiments is shown in Fig. 2.1. It allows independent control of both laser pulses with respect to the gate pulse, and can thus be used for single laser experiments equally well.

A pulse generator sends a T_o pulse (C) to charge up the pump laser (1). This pulse generator also sends a fire pulse (F) delayed

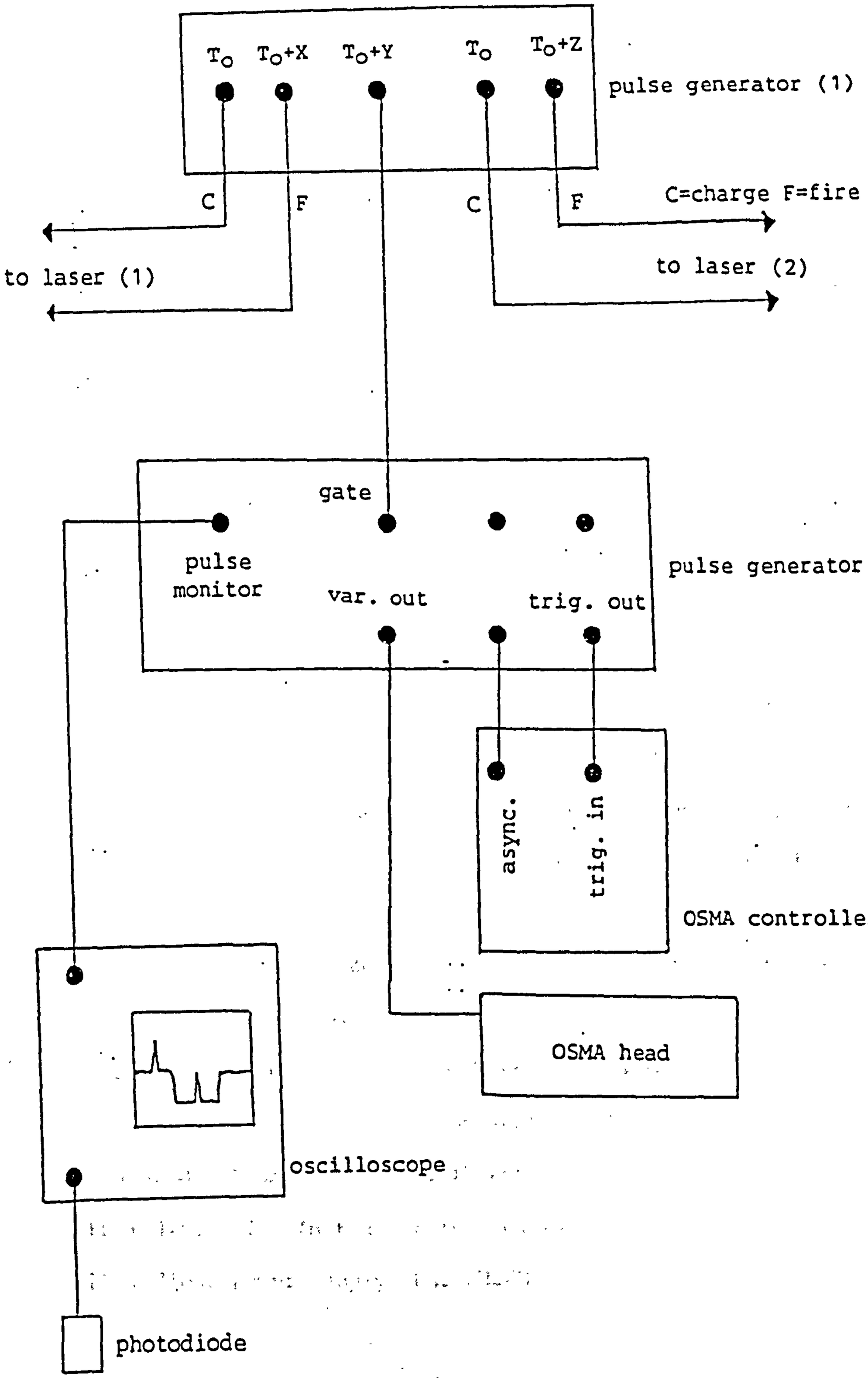

2.1 Diagram of timing system for TR^3 experiments

by set time, X, after T_o (to the same laser) and a gate pulse (to a second pulse generator) at a different delay time, Y. The second laser (if used) is also controlled from this pulse generator: a charge pulse is sent at T_o, and a fire pulse at some specified time, Z, after T_o. This last fire pulse may then be used to control the delay between the two laser pulses. The second pulse generator, on receiving the gate pulse from the first pulse generator, sends a gate pulse (labelled 'trig. out' in Fig. 2.1) of controllable width and delay to the OSMA controller ('trig. in'). This allows the OSMA detector to be intensified for only the duration of the gate pulse. The other connection from the second pulse generator (2) to the OSMA controller ('async.') avoids spectral artefacts that can be introduced by the gating process. The gate pulse is monitored by an oscilloscope. The two laser pulses are monitored by a photodiode (connected to the oscilloscope) at a point where the beams are co-linear. A beam splitter can be used to send a small proportion of the laser pulses to the photodiode, so that the timing of the two pulses with respect to the gate can be monitored throughout the experiment.

The model numbers and suppliers of the various items shown in Fig. 2.1 are listed below.

Pulse generator (1): Stanford Research Systems DG535

Pulse generator (2): Princeton Instruments PG100

350 Mz Oscilloscope: Tektronix 2467

Photodiode: ITL Instrument Technology

Photodiode power supply: EMI PM28B

2.3 REFERENCES

[1] J. deGroot, *Ph.D. Thesis, University of York* (1987)

[2] S.B.Dierker and C.A.Murray, *J.Opt.Soc.Am. A* 3, 2151 (1986).

[3] S.Umapathy, S.E.J.Bell, J.C.Austin and R.E.Hester, *RAL Annual report* (1989)

[4] R.S.Chittock, OSMA data handling software for the BBC minicomputer (available from SERC Rutherford Lab., Laser Div.).

CHAPTER THREE: SECONDARY STRUCTURE OF GAPDH FROM THE RAMAN AMIDE I BAND

3.1 INTRODUCTION

The analysis of Raman and IR amide I bands to yield quantitative estimates of protein secondary structure is now commonplace. The technique is being usefully applied to give preliminary information on proteins that have not had their 3D structures determined by X-ray crystallography. It also has allowed the observation of secondary structure changes caused by pH, the presence of metal ions, or coenzyme or substrate binding. A number of examples may serve to illustrate the range of applications and differing procedures.

The pH and temperature-induced changes in β-lactoglobulin B have been studied by analysis of the IR amide I band [1]. Deconvolution of this band revealed five components, due to antiparallel β-sheet structure, β-turns, α-helix and random structure. Changes were observed in bands due to β-sheet structure that reflected dimerization of the protein at low pH. Thomas and Agard [2] have used Fourier deconvolution of the Raman amide I bands of viruses, where bands from DNA can overlap the amide I band. The same method was subsequently applied to the protein phosvitin [3], to determine its structure in the solid state, and in solution at several different pHs. Phosvitin appeared to be a rather unusual protein, with large, unidentified changes in structure on raising the pH. The solid state structure was most similar to the structure found at low pH, and not similar to the structure found at physiological pHs. A study of two different forms of lysozyme (human airway and hen-egg white lysozymes) found subtle differences in secondary structure [4]. These, and other differences in the Raman spectra were disscussed in the light of the quite different activities of the two lysozymes. Some groups have concentrated their

efforts on the application of amide I analysis to membrane proteins. The proteins gramicidin A [5], melittin [6], and Na^+ and K^+ ATPases [7] have all been investigated by various methods, with convincing results.

Perhaps a bewildering factor in this rapidly expanding field is the diversity of methods used for the analysis of the amide I band. Most of the above examples have used different approaches; these will be outlined below.

3.1.1 The Reference Intensity Profiles (RIP) Method [8].

The reference intensity profiles (RIP's) are model Raman amide I bands corresponding to bands of pure classes of secondary structure. The RIP's are fitted to any amide I band, and the quantitative estimate of secondary structure made from the relative amounts of the RIP's. The RIP's were generated using the amide I bands of a number of proteins with well defined structures (as determined by X-ray crystallography). The authors found that better results were obtained when four RIPs were used (as opposed to three). The four RIPs correspond to the structure types $\alpha 1$ and $\alpha 2$ (α -helix structure), β -sheet and undefined. The differences between the two α -helical structures is not entirely clear. The band positions are quite different ($\alpha 1$ at 1640 cm^{-1}, $\alpha 2$ at 1652 cm^{-1}), but the division is not related to clear structural differences, it is more of an experimentally determined improvement. The authors found that for proteins of mainly α -helical structure, the amide I band could still vary enormously. The Fd-phage protein (100% α -helix) had an amide I band at 1649 cm^{-1}, whereas poly-L-lysine (100% α -helical form at pH 12) had a much lower amide I band, near 1640 cm^{-1}. Clearly, these amide I bands would have been

difficult to 'fit' using just one α -helix RIP, so two were employed. However, there were apparently no correlations between the two α -helix RIPs and the ordered and disordered helix structures defined by Williams [9]. A recent review by Krimm has included a discussion of the vibrational frequencies of α -helix structures [10]. Vibrational spectra and normal co-ordinate analyses of two model α -helical polypeptides, $\alpha(Ala)_n$ and $\alpha(GluH)_n$ showed significant differences in the amide band positions. This was interpreted as a demonstration of the sensitivity of such vibrational modes of α-helices to side chain structure. Clearly, other factors (environment, length of helix) may also affect backbone vibrational modes. Hopefully, further work will accurately establish the source of the experimentally observed variation in amide I band positions.

3.1.2 The Williams Method [9]

This earlier method is similar to the RIP method, in as much as it uses reference amide I spectra for proteins with well defined structures. However, it avoids the calculation and use of reference intensity profiles, by directly fitting a linear combination of amide I bands of the reference proteins to the amide I band of the 'unknown' protein. The solution of this fit is then used to calculate the fraction of each structure type. Essentially, the fraction of any one structure type is determined by summing the products $C_p.F_{sp}$, where C_p is the contribution of the spectrum of reference protein p to the fit, and F_{sp} is the fraction of structure s in protein p. Six structure types are defined in the Williams analysis: disordered and ordered α -helix, parallel and antiparallel β -sheet, turns and undefined structure.

3.1.3 Deconvolution Methods

Many groups have used Fourier self deconvolution to resolve the components of the amide I band. The strategies for obtaining secondary structure estimates after this point fall into three categories: (1) direct measurement of areas of deconvolved bands [2], (2) curve fitting to the deconvolved spectrum and subsequent measurement of the areas of fitted bands [11], and (3) identification of bands from deconvolution, followed by curve fitting to the original spectrum. Method (2) and the method used in this chapter (3) also use second derivative spectra to increase the confidence of band assignments. No group has yet used the maximum entropy method (MEM) to resolve the amide I band, although other applications of the MEM look promising [12].

3.2 EXPERIMENTAL

3.2.1 Enzyme Preparation

GAPDH from rabbit and porcine muscle were obtained from Sigma, as suspensions in solutions containing 4M ammonium sulphate, 1mM EDTA and 4mM mercaptoethanol. Purity of the enzyme from rabbit muscle was estimated by SDS-PAGE to be above 98% (with respect to protein contamination). The GAPDH suspension was centrifuged and the supernatant removed. The wet solid was then dissolved in either en (0.01 M 1,2-diaminoethane hydrochloride) or phosphate buffer, pH 6.0 - 7.0, with $NaNO_3$ or KNO_3 added to 0.1 M as an internal intensity standard in some preparations. The amount of buffer added was less than or equal to the volume required to equal the original volume of suspension taken. The final concentration of enzyme was estimated from the absorption at 280 nm using $\epsilon = 1.38 \times 10^5\ M^{-1}{}_{cm}{}^{-1}$

[13]. Enzyme concentrations were typically 1-2 x 10^{-4} M. Dilute (0.2 M) dithiothreitol (Sigma) was added to enzyme solutions (50 μl to 1 ml) to restore maximum enzyme activity (see Chapter 4).

The NAD^+ content of untreated enzyme preparations was estimated spectroscopically by the absorption ratio A_{280}/A_{260} (see Fig. 3.1). Holo-enzyme preparations were found to contain 2-3 NAD^+ per tetramer. Apo-GAPDH was prepared by incubation of the holo-GAPDH solutions with activated charcoal (5% $^w/_v$) for *ca.* 20 minutes. The charcoal was removed by centrifugation.

Deuterated GAPDH was prepared by dissolving the 'solid' enzyme in an excess (at least 10x excess compared with the normal volume of buffer added) volume of D_2O. The solution was allowed to exchange for 2 hours, then was reconcentrated to an appropriate concentration (i.e. final volume less than or equal to the original suspension volume) for Raman spectroscopy using an Amicon concentrator. All enzyme preparations were used immediately and discarded after one day. The holoenzyme is reasonably stable in solution for 1-2 days at 0-4°C. The apoenzyme is less stable; solutions start to turn cloudy within a day (at 0-4°C).

3.2.2 Raman Spectroscopy

The instrumentation at York has been described in detail elsewhere [14] and outlined in chapter 2 of this thesis. For amide I band analysis, laser excitation of wavelength 488 or 514.5 nm was used, at laser powers of not more than 100 mW at the sample. Right-angle illumination was employed in all cases, using the Spex instrument with a 6 cm^{-1} spectral slit width. Spectra were collected for long times (8 hours or more) to obtain good signal-to-noise ratios. To prevent enzyme denaturation over the collection period,

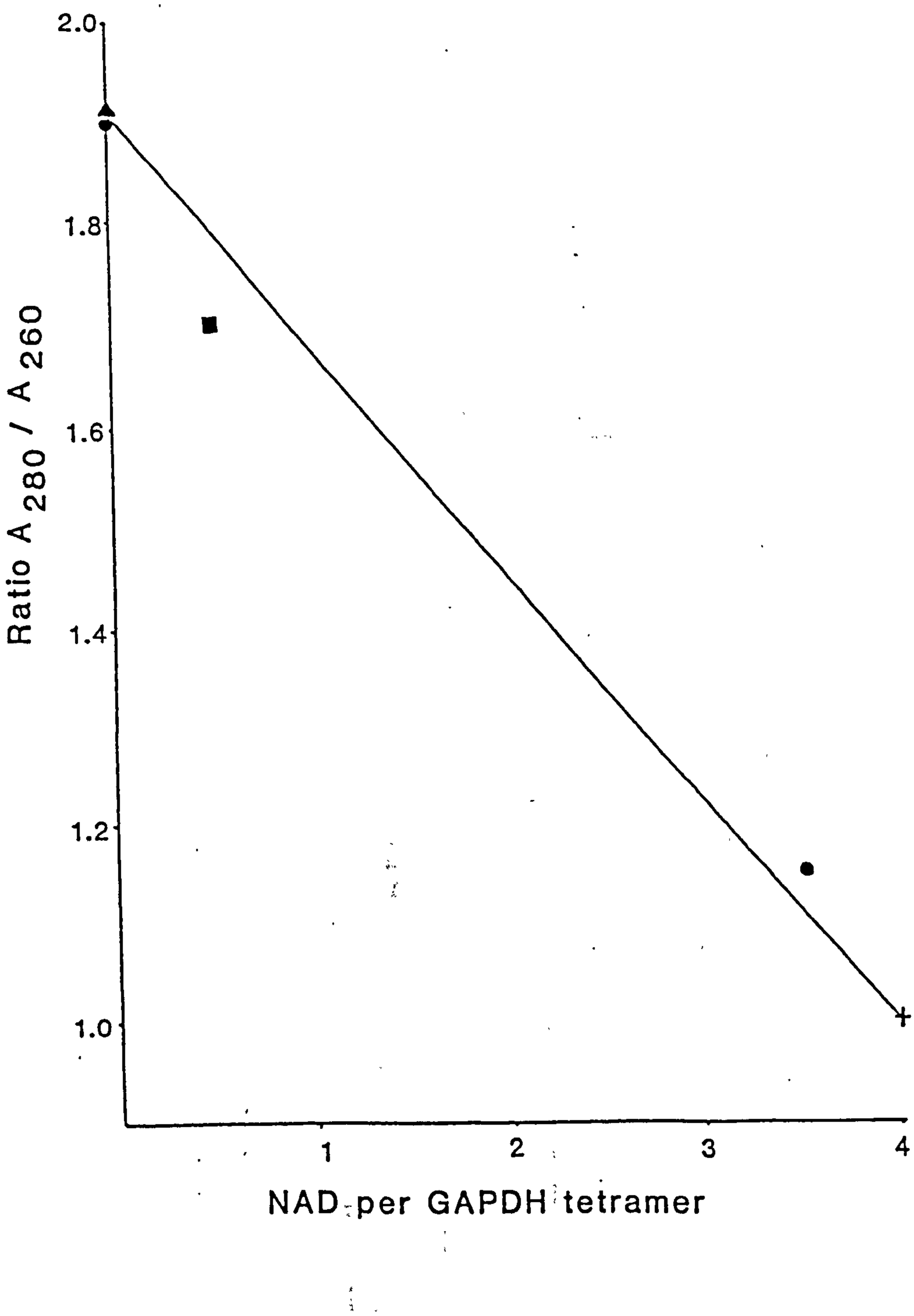

Figure 3.1 Dependence of absorbance ratio A_{280}/A_{260} on the number of NAD^+ molecules bound per GAPDH tetramer. ▲ = data from [36], ● = data from [37], ■ = data from [38], ϕ = data point calculated using ϵ for GAPDH from [13] and ϵ_{280} for NAD^+ as 4500 $M^{-1}cm^{-1}$, ϵ_{260} for NAD^+ as 17800 $M^{-1}cm^{-1}$.

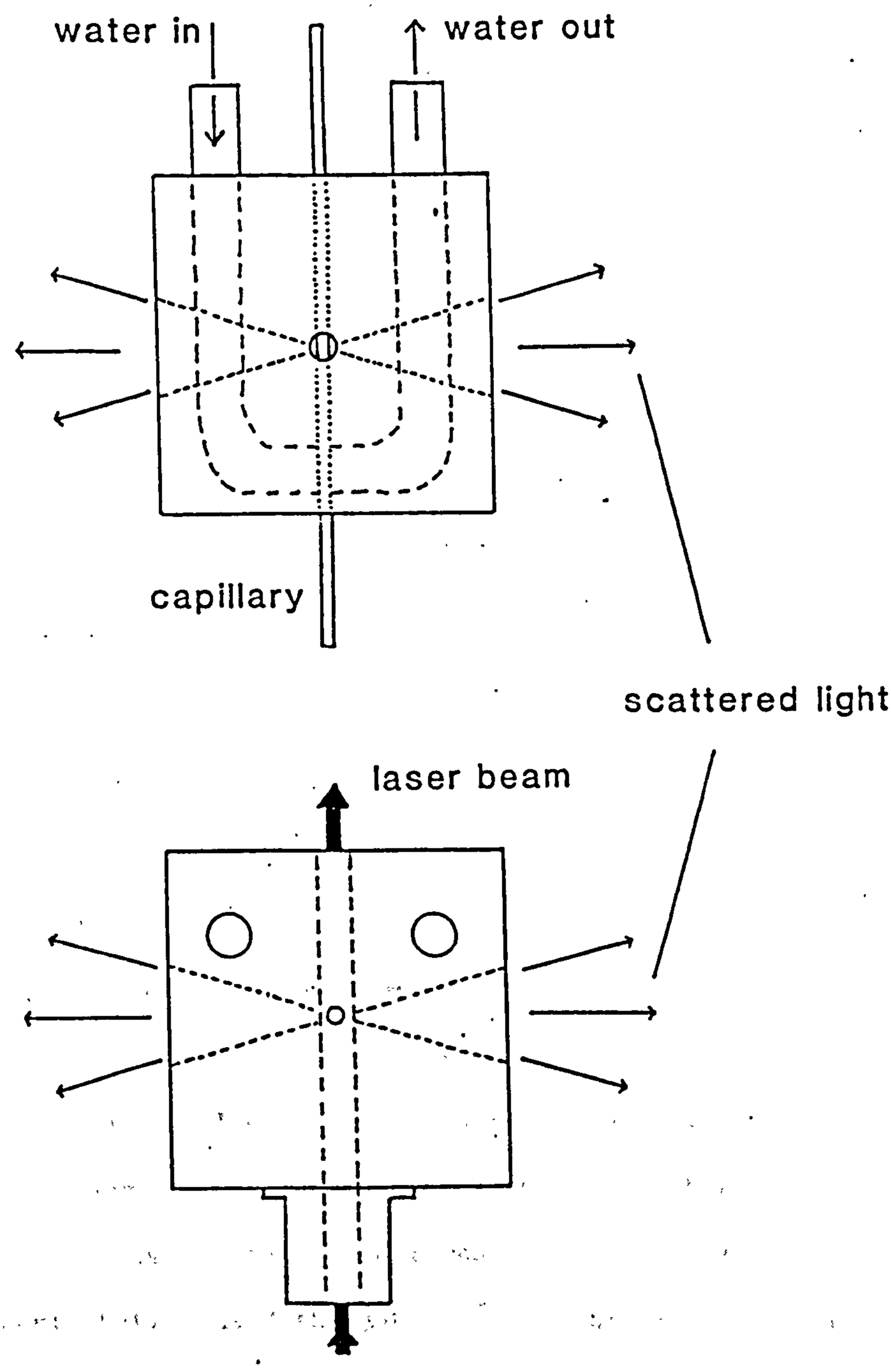

Figure 3.2 Diagram of water-cooled block capillary holder.

small (10μl) volumes of enzyme were put into thin (*ca.* 1mm internal diameter) capillary tubes, and the bulk of the enzyme preparation kept in the 'fridge (0-4°C). Fresh samples could then be used as required. Moreover, the capillaries were cooled during laser illumination by placing them in an ice-water-cooled block (see Fig. 3.2). Denaturation was easily identified by an increase in fluorescence and a shift in the amide I band to higher wavenumber. In addition, gross denaturation caused the accumulation of coagulated enzyme (white solid) on the walls of the tube.

3.2.3 Processing of Spectra

Initially, spectra were calibrated for accurate wavenumber positions using the CCl_4 peak at 459 cm^{-1}, and assuming a linear spectrometer response. This was later found to be inadequate, and an indene spectrum was run to more accurately establish wavenumber values in the amide I region (see Fig. 3.3). The implications of this are discussed later in this chapter.

Before analysis by any method, the contribution to the amide I spectrum from the water deformation mode at *ca.* 1640 cm^{-1} must be removed. This was achieved in most cases by subtraction of a buffer spectrum (also 0.1 M in nitrate) until the nitrate peak at *ca.* 1047 cm^{-1} was completely removed. The accuracy of this method is discussed later in this chapter. An alternative method for removal of the water contribution used the 3400 cm^{-1} O-H stretching band as an estimate of water content in the enzyme preparation; subtraction of the buffer spectrum was accomplished by normalising to the 3400 cm^{-1} band of the enzyme spectrum.

In the deuterated sample, the transformation of residual H_2O to HOD was essentially complete. The HOD content was estimated to be

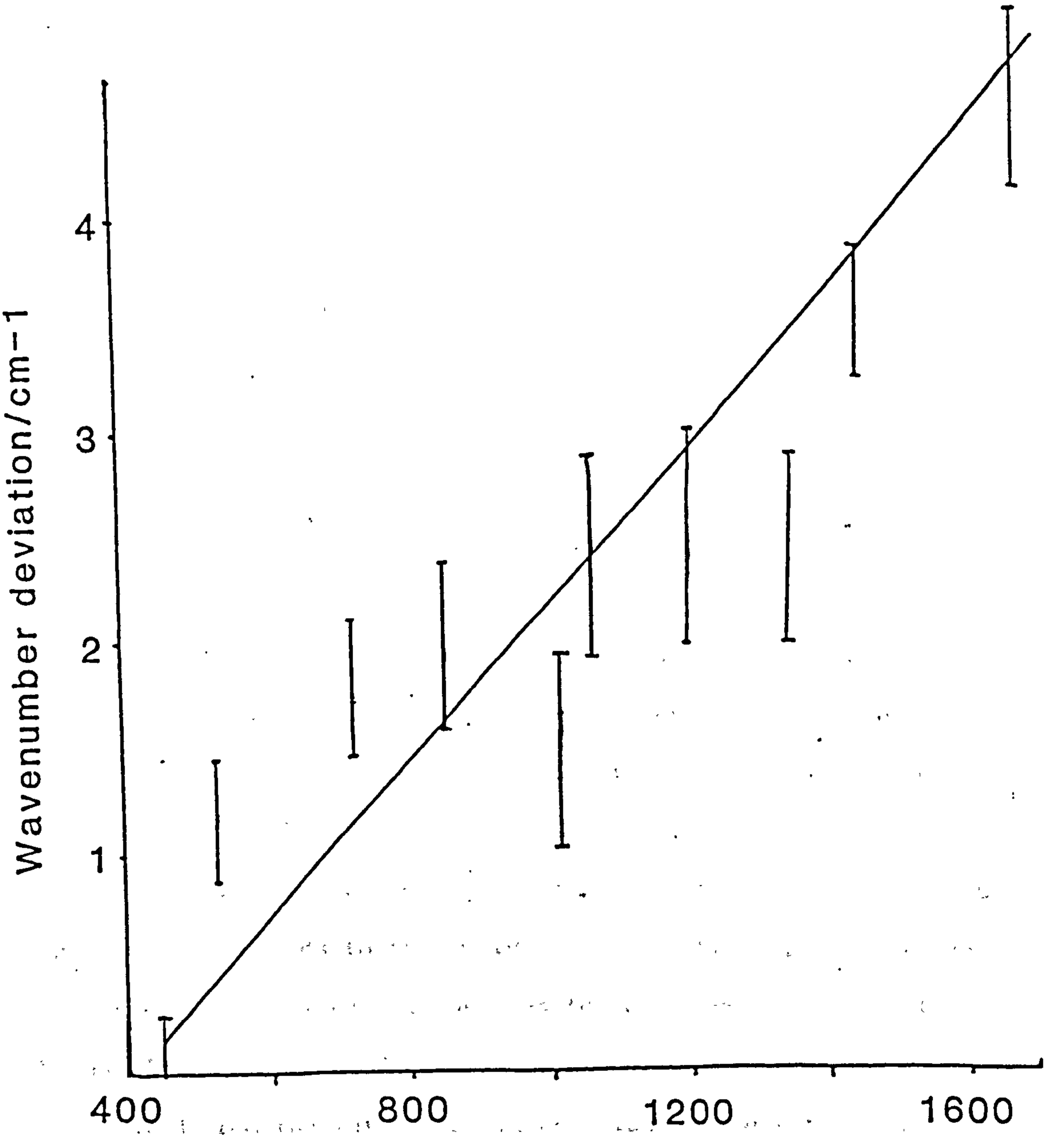

Figure 3.3 Indene calibration of Spex spectrometer for 488 nm excitation. Wavenumber deviation = expected wavenumber minus observed wavenumber.

ca. 5% by measurement of the D_2O and HOD peak heights at *ca.* 2400 and 3300 cm^{-1}. Since the HOD deformation mode occurs at 1455 cm^{-1}, it does not interfere with the amide I band, so a subtraction is not necessary.

For analysis by the RIP [8] and Williams [9] methods, contributions to the 1500-1800 cm^{-1} region of the enzyme spectrum from amino acid side chain vibrations need to be removed. This was accomplished using the NEWRES least squares curve fitting program [15], which fits peaks with varying widths, heights and fractions of Gaussian and Lorentzian character. Best fits were obtained when peaks were assumed to be *ca.* 90% Lorentzian, 10% Gaussian. The widths of the bands due to aromatic amino acid side chains were assumed to be *ca.* 20 cm^{-1}, but were allowed to vary by 5 cm^{-1} in the iterative procedure. The smaller bands above 1685 cm^{-1} (for discussion of assignment, see results section) were assumed to have half widths of *ca.* 17 cm^{-1}, and again were allowed to vary by 5 cm^{-1}. The general procedure for amide I analysis by these two methods and a detailed description of the running of the programs has been written by Hari Virdee [16].

The alternative method of analysis used the curve fitting program to fit bands to the individual structure types (α-helix, β-sheet and undefined), as well as to the amino acid side chain bands. The percentage of each secondary structure type was calculated from the integrated intensities of the fitted bands (assuming that the total % of α, β and u structures = 100%). Judgement of band positions to be used for curve fitting was made after careful examination of the second derivative and Fourier self-deconvolved spectra. The latter spectra were obtained using the FORTRAN programs developed at York [17, 18]. The Fourier

deconvolution program is based on an original procedure by Kauppinen *et. al.* [19]. The derivative spectrum program was written by Stewart [18]. Such spectra are prone to the formation of spurious 'bands'; also wavenumber values from such spectra may be distorted. Thus comparison of both second derivative and Fourier self-deconvolved spectra is necessary for accurate assignments. Comparison with the corresponding deuterated spectra also aided the assignment of the structural components.

The choice of a band width for each secondary structure type is difficult. From comparison with the RIP's used by Berjot *et. al.* [8], a suitable band width appeared to be 30-35 cm^{-1}. In fact, 'best fits' were generally obtained with somewhat higher (up to 40 cm^{-1}) widths for α, β and u bands. However, there appeared to be a general problem with curve fitting so many closely overlapping bands. Depending on the amount of variation allowed on initial estimated values for positions, heights and widths, quite different results could be obtained. Thus, quite different relative areas of α, β and u bands could arise from two apparently equally good curve-fits. Generally, the positions of α, β and u bands were allowed to vary within only 1 cm^{-1} of the values obtained from analysis of deconvolved and derivative spectra, and the 1687 cm^{-1} band was restrained to a small height. If more variation was allowed, then there was a tendency for the α band to dominate the curve fit, with bands due to u and β structures upshifted and reduced in size, and thus (probably) underestimated. This problem is discussed further below.

3.3 RESULTS

In cases where the nitrate peak was used to estimate water

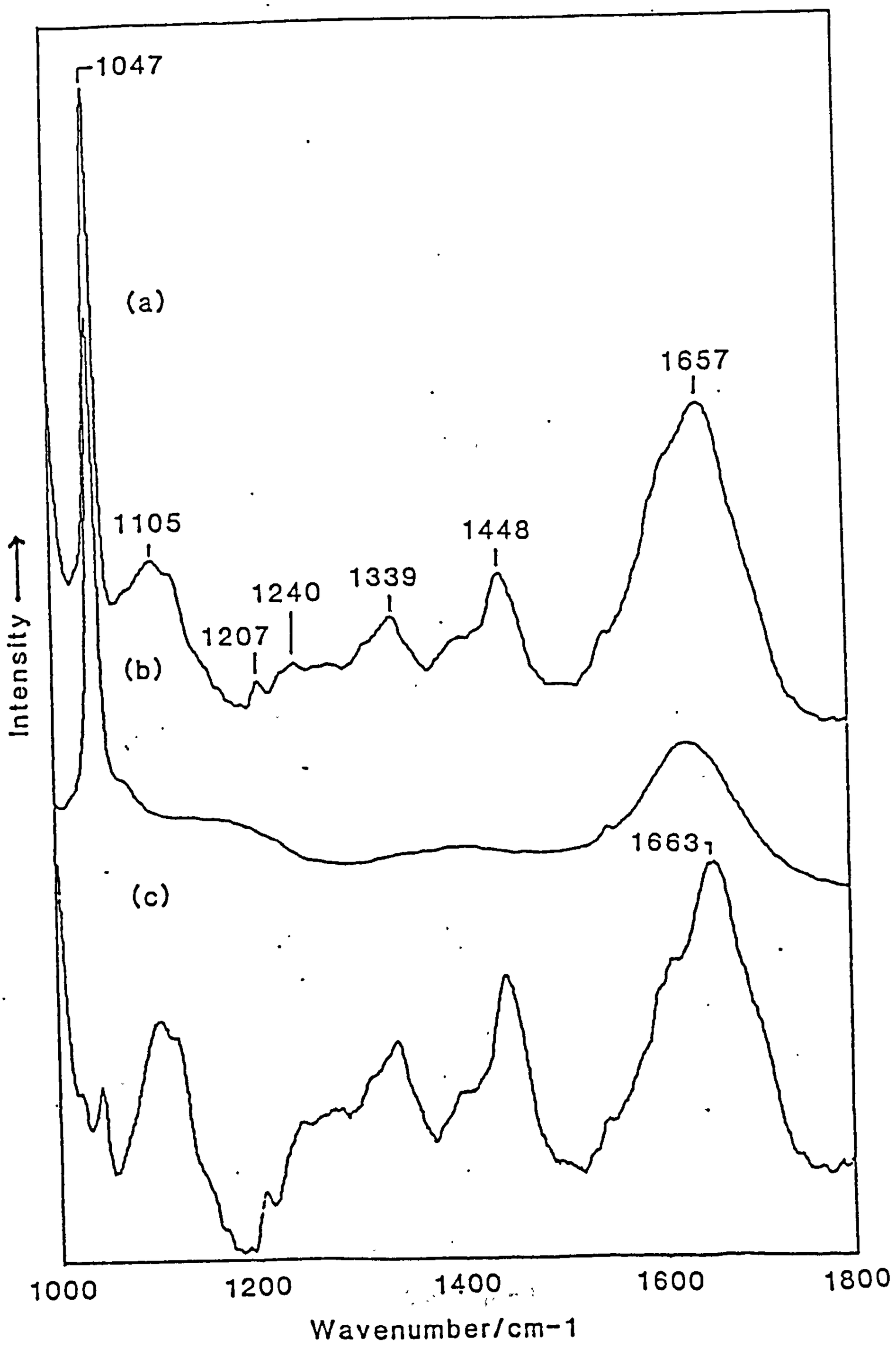

Figure 3.4 (a) Raman spectrum of apo-GAPDH in phosphate buffer, 0.1 M in $NaNO_3$.

(b) Raman spectrum of phosphate buffer spectrum (also 0.1 M in $NaNO_3$).

(c) (a)-(b) difference spectrum.

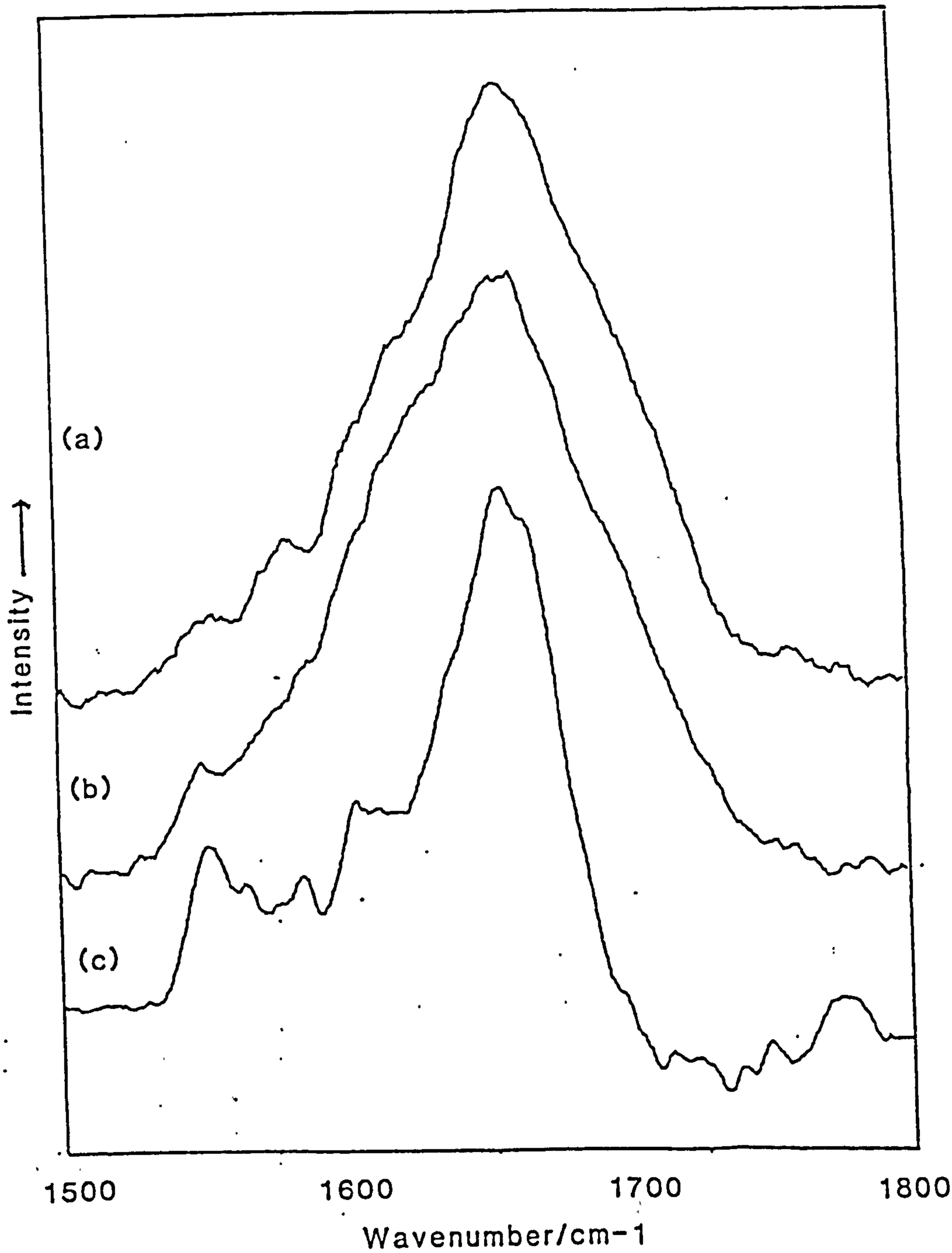

Figure 3.5 (a) Raman spectrum of rabbit muscle holo-GAPDH.

(b) Raman spectrum of porcine holo-GAPDH.

(c) Raman spectrum of rabbit muscle holo-GAPDH in D_2O.

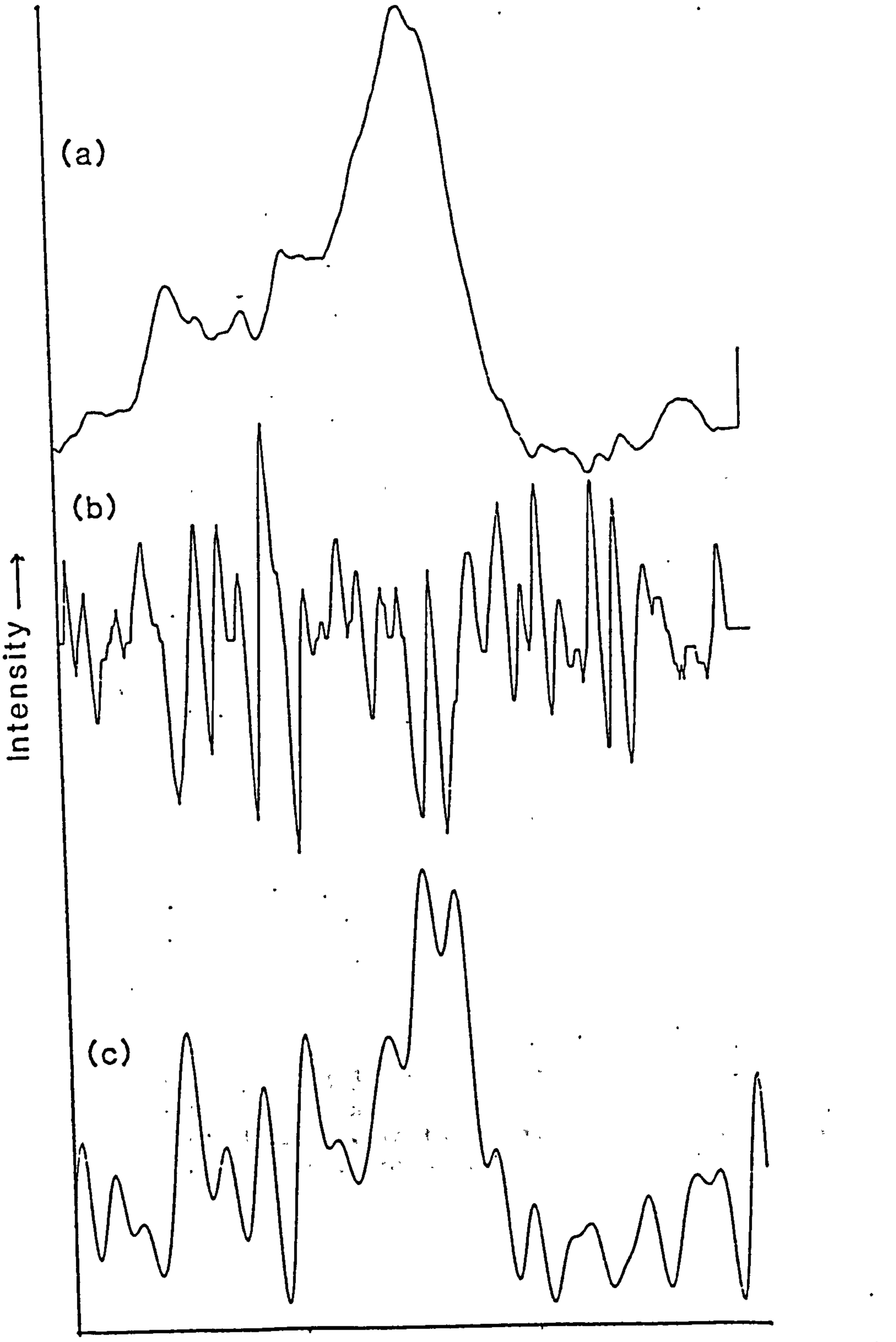

Figure 3.6 Comparison of (a) original, (b) second derivative, and (c) Fourier self-deconvolved spectra of GAPDH in D_2O.

Table 3.1: Assignments of bands in the GAPDH Raman spectrum

(a) Assignments for apo-GAPDH, 1000-1500 cm^{-1} region.

Wavenumber/cm^{-1}	Assignment [2, 20, 21]
1047	Nitrate
1105	)
1124	) ν (C-N)
1207	Phe, Tyr
1240-1300	Amide III
1339	δ (C-H), Trp
1405	ν_s (COO^-)
1448	δ (CH_2)

(b) Assignments for apo-GAPDH and holo-GAPDH in both H_2O and D_2O, 1500-1800 cm^{-1} region*

apo	holo	holo(D_2O)	Assignment
Wavenumber/cm^{-1}			
1554	1554	1554	Trp
		1570	
1587	1584	1587	Phe, Tyr
1604	1605	1605	Phe, Tyr
1619	1621	-	Trp, Tyr
1647	1650	1639	α -helix
1660	1661	1657	undefined
1674	1674	1669	β -sheet
1691	1695	1687	Gln, Asn
1709	a	a	Glu, Asp

* Values corrected using Fig. 3.3, identification from deconvolved and derivative spectra (see text).

[a] Bands were not observed clearly in the derivative or deconvolved spectra, but were assumed to be present.

contribution to enzyme spectra, the spectral region from 1000 to 1800 cm^{-1} was collected. Fig. 3.4(a) shows the spectrum of apo-GAPDH, and compares the buffer spectrum (b) with the (a)-(b) subtraction spectrum, (c). Band assignments are given in Table 3.1(a) for the peaks in the 1000-1500 cm^{-1} region. Fig. 3.5 shows the amide I region (1500-1800 cm^{-1}) of (a)rabbit holo-GAPDH, (b) porcine holo-GAPDH and (c) GAPDH in D_2O. The band assignments for this region are given in Table 3.1(b). The assignments have been made by comparison with data from the literature [2, 20, 21]. The most debatable assignments are those of the bands above 1685 cm^{-1}. Bands due to vibrations of COOH moieties are expected to contribute some intensity between 1700 and 1750 cm^{-1}. Thus, it is possible that the side chains of glutamic and aspartic acid residues contribute to the observed intensity in the region 1700-1710 cm^{-1}. Bands around 1690 cm^{-1} have in the past been assigned to β-turn structures [22, 23]. However, it is likely that significant intensity in this region arises from the amide vibrations of glutamine and asparagine side chains [2]. It should be noted that such bands would be expected to be weak, as these residues constitute only a small proportion of the total number of amide groups. As previously discussed, the overlapping bands in this region are best identified by the careful comparison of second derivative and Fourier deconvolved spectra. Such a comparison is shown in Fig. 3.6 for holo-GAPDH in D_2O. The curve fitting procedure for processing spectra before RIP and Williams analyses was found to be most successful when bands due to both aromatic amino acid vibrations (below 1625 cm^{-1}) and to other vibrations (above 1685 cm^{-1}) were taken into account. A typical NEWRES fit is shown in Fig. 3.7(a) for holo-GAPDH. A similar curve fit result is shown in Fig. 3.7(b), but with bands due to α, β, and

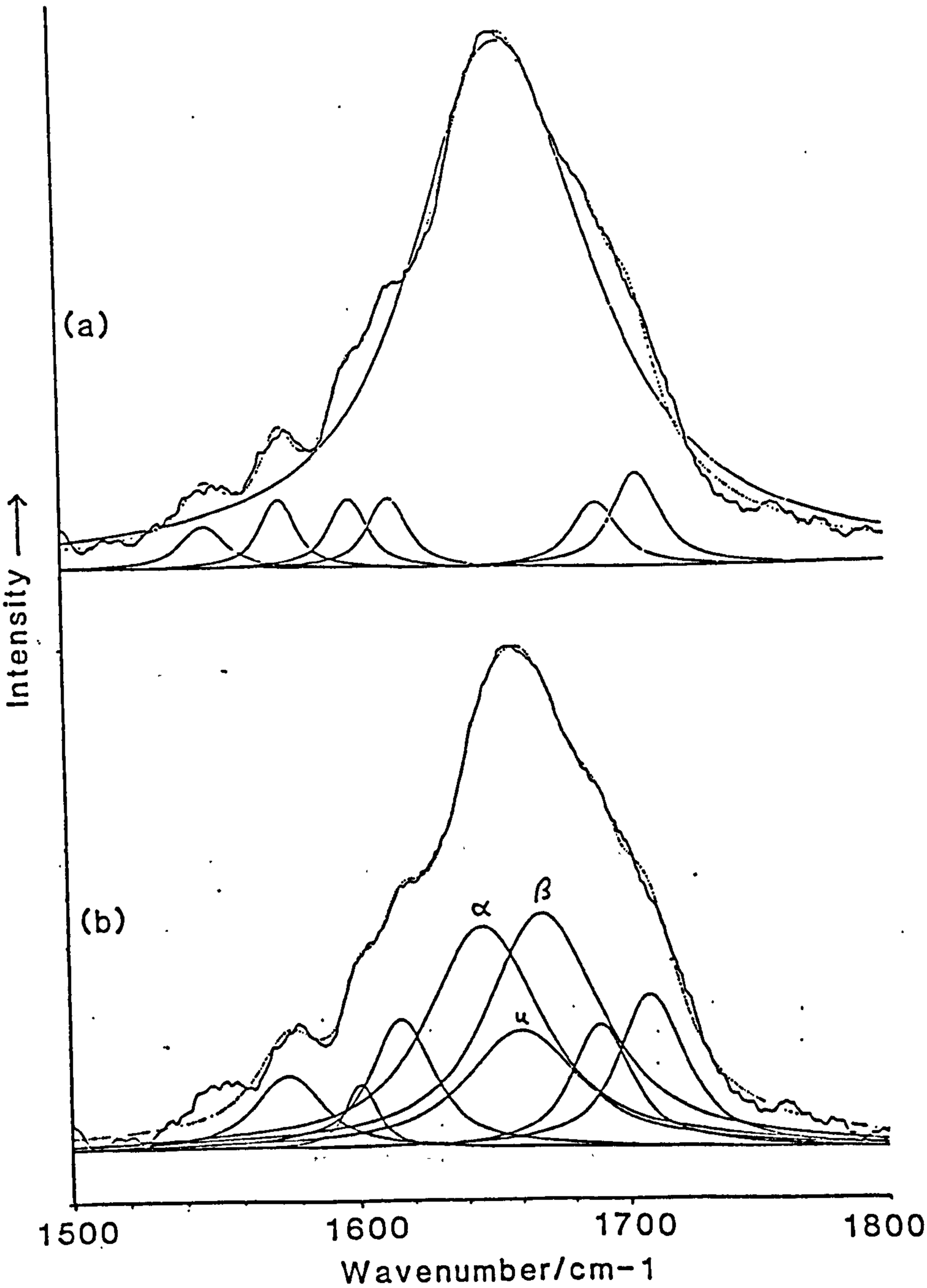

Figure 3.7 Typical NEWRES curve-fits to holo-GAPDH spectrum,

(a) without individual secondary structure components,

(b) including fitting of individual secondary structure components.

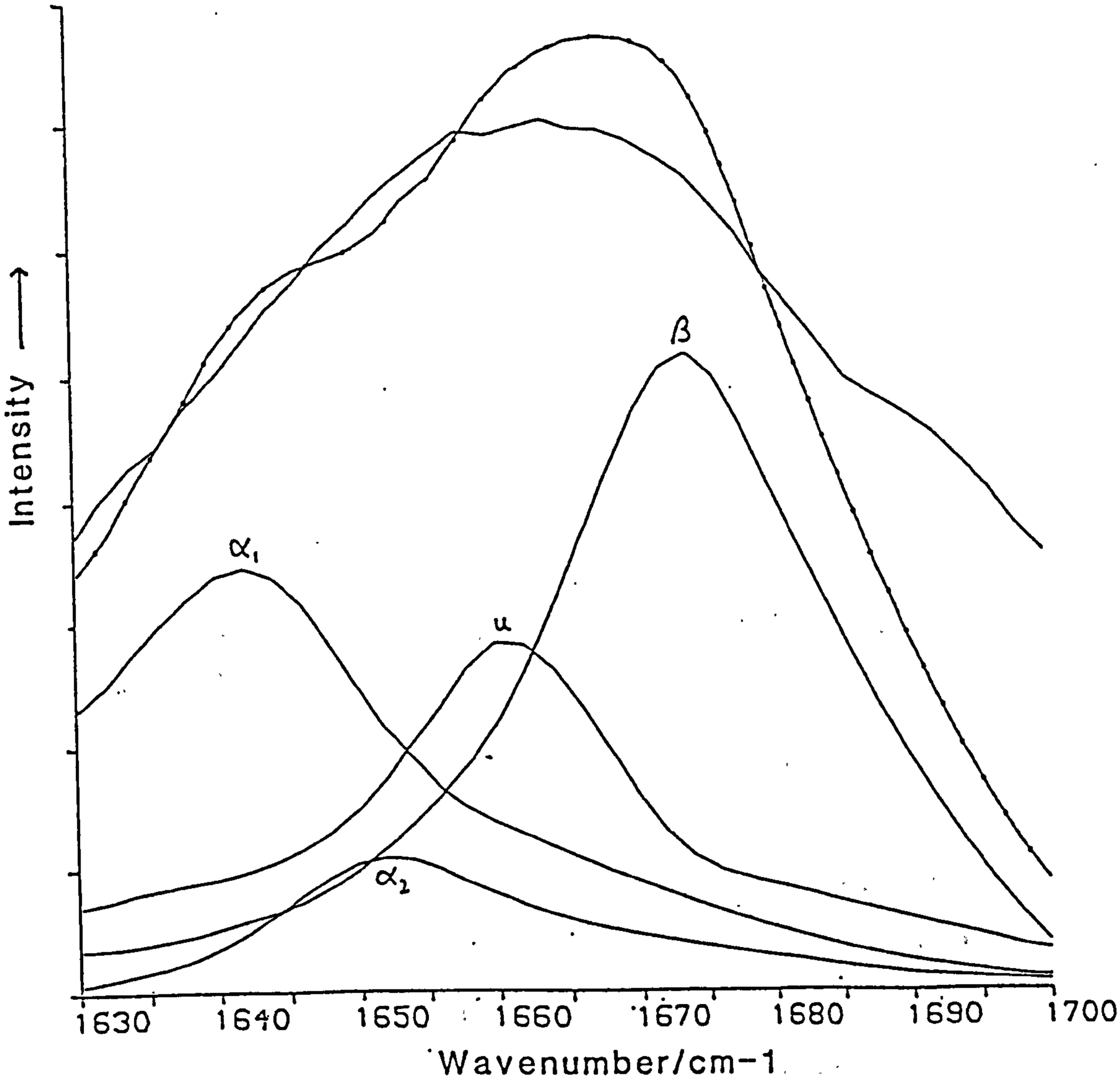

Figure 3.8 Typical fit of RIP's to apo-GAPDH spectrum.

undefined structures also included. The curve fitting of the RIP's for α 1, α 2, β and undefined structures to the processed apo-GAPDH data is shown in Fig. 3.8. The quantitative results, and the corresponding X-ray and CD data are summarized in Table 3.2.

3.4 DISCUSSION

The results summarised in Table 3.2 show that there is at most only a small change in overall secondary structure in GAPDH on binding NAD^+. There appears to be an approximate 2% shift towards less α -helix, and more β -sheet structure on coenzyme binding. This is in agreement with the X-ray crystallographic data for holo- and apo- GAPDH [24, 25, 26]; which show that, although there are significant conformational changes, the underlying secondary structure is not affected. The main changes appear to be in the detailed structure of the catalytic domain, and in the relative positions of structural elements in the coenzyme binding domain. There are some differences in the positions of the NAD^+ binding site residues: the coenzyme binding seems to induce a 'tightening' or contraction of the immediate area around the coenzyme. It is perhaps this contraction that precipitates the other structural changes. The absolute quantitative values for holo- and apo- GAPDH agree well with the secondary structure values given by the original authors of the lobster holo-GAPDH structure [27] (see Table 3.2). However, the definition of a certain type of secondary structure is not absolutely fixed, and the values given by the original authors are subjective values, made by simple inspection of the structure. Other groups have tried to make the quantitative values for secondary structure in proteins more objective by the use of recognition algorithms.

Table 3.2: Comparison of secondary structure estimates.

(a) **Apo-GAPDH**[a]

	Structure type/ %					
	∝ 1	∝ 2	∝t	βt	u[b]	t
RIP	26.0	7.8	33.8	37.6	22.2	-
Williams'	30.2	4.4	34.7	34.1	25.6	13.4
Curve fit[c]	-	-	41.0	37.0	22.0	-

(b) **Holo-GAPDH**[a]

	∝ 1	∝ 2	∝t	βt	u[b]	t
RIP	22.9	9.5	32.4	38.3	23.1	-
Williams'	27.5	4.6	32.1	35.1	25.7	13.8
Curve fit	-	-	39.0	41.0	20.0	-
X-ray (1)	-	-	35.0	39.0	-	-
(2)	-	-	30.5	36.9	-	-
(3)	-	-	22.0	21.0	-	-
ORD[d]	-	-	40.0	-	-	-

[a] Unless otherwise specified, values given are for rabbit muscle GAPDH.
[b] For the Williams' analysis this figure is the sum of the turn and undefined structure types. The separate turn contribution is also given (t).
[c] The curve fit that generated these results was restrained to avoid over-estimation of the band at 1687 cm^{-1}; wavenumber positions were also restrained.
[d] From [39]; the authors admit that their value may be in error due to interfering effects from coenzyme.
(1) Values given by the original authors [27].
(2) Values from structure in [40], using secondary structure definition defined by Levitt and Greer [28].
(3) Values from structure in [27], using secondary structure definition defined by Kabsch and Sanders [29].

Levitt and Greer first developed an algorithm for recognising α, β, and reverse turn structures [28]. Various algorithms were tested on a set of proteins with structures known to high, medium and low resolution. The algorithms were based on recognition of either (1)inter C_α-C_α distances, (2) H-bond patterns or (3) inter C_α torsion angles. By comparing the amounts of structure recognised by the various methods with the original authors estimates, they concluded that the best objective method combined both C_α-C_α distance and H-bonding pattern recognition. It has been suggested that this method is not realistic and overestimates the amounts of α and β structure types. Subsequently, Kabsch and Sanders developed a different secondary structure recognition algorithm based solely on the recognition of hydrogen bonding patterns [29]. It is generally accepted that this method, in contrast to that of Levitt and Greer, tends to underestimate the amount of secondary structure (see Table 3.2).

The two established methods for estimating secondary structure content from Raman amide I bands are both largely based on the use of secondary structure values determined by Levitt and Greer. The Williams method further modifies the structure values to incorporate further division of structure types into two types of helix (disordered and ordered), and two types of sheet (parallel and antiparallel). Consequently, the Raman data from these two methods correlates well with the secondary structure values from Levitt and Greer. The method using simple curve fitting would not necessarily be expected to show such a good correlation with Levitt and Greer values. In the case of amide I analysis, since the amide I mode consists mainly of C=O stretching vibration, it might be expected that the (amide I band and thus) secondary structure estimates would

be most sensitive to hydrogen bonding, and thus best reflect the Kabsch-Sanders values. However, it is clear from Table 3.2 that this is not the case. The 'undefined' structure estimates are much lower in the curve fitting analysis, leading to a correspondingly larger estimate for α and β structures, since total structure=100%.

3.4.1 Accuracy/Reliability of Data

As outlined in the experimental section, the amide I band analysis is subject to two major sources of error: the wavenumber accuracy and the subtraction of the water band. The 'error' induced by the subjectivity of the curve fitting procedures used is difficult to quantify (see following section). The wavenumber accuracy of the data is extremely important when using either of the two literature methods that use reference spectra. It was found (from the standard indene spectrum) that the Spex spectrometer gave wavenumber values that were *ca.* 4 cm^{-1} 'low' at 1600 cm^{-1}; thus the original data had to be corrected to allow for this. At best, the spectra are likely to be accurate to 1 cm^{-1}, which would induce an error in the structure estimate of 1-1.5%.

The subtraction of the water spectrum by normalisation to the nitrate peak (see experimental section) should be accurate to better than 5%. However, the sample was wet before the buffer was added; this may have affected the water content considerably (and unquantifiably). The best approach to the subtraction of the water band is by normalisation to the water band at 3400 cm^{-1} (see experimental section). An incomplete subtraction of the water band would be expected to lead to falsely high α-helix structure estimates. A 5% 'over-subtraction' of the estimated water content was made in one set of data: this was found to decrease the α-helix

content by less than 1%.

3.4.2 Assessment of Methods

RIP and Williams Analyses

Once problems of accuracy (wavenumber position and water subtraction) have been overcome, these methods both appear to produce plausible and reproducible estimates for protein secondary structure. Because the methods both rely on Levitt and Greer data, the secondary structure estimates are really only comparable with other Levitt and Greer data; i.e they reflect the secondary structure as defined by Levitt and Greer. The methods have the advantage of being reasonably objective. Some subjectivity is introduced in the subtraction of bands due to amino acid side chains.

The major drawback of the two methods is their inability to cope with 'abnormal' data. For example, the methods would not have produced meaningful estimates for the protein phosvitin, which has an amide I band reported at 1685 cm^{-1} [3]. As yet, no satisfactory explanation has been proposed to explain this unusual amide I band.

A less extreme example is that of insulin. This protein has an amide I band with two distinct components at 1662 and 1680 cm^{-1} (Bovine Zn insulin) [30, 31]. The two components have been assigned to α -helix and undefined structures, respectively. Both band positions are unusually high, (the RIP band positions are 1640(α), 1652(α), and 1660(u)) and would therefore lead to inaccurate secondary structure values. The α -helix estimate would be too low and the β -sheet estimate too high. There does indeed seem to be a large difference between the X-ray and Raman estimates for α and β

structure in the Porcine Zn-free enzyme, as reported by Stewart *et. al.* [32]. The Williams analysis does in fact use insulin in the reference data set (amide I bands at 1656 and 1677 cm^{-1}, lower than the other literature values, but the insulin used may not have been the Bovine Zn form). The correlation between X-ray and Raman data for insulin reported by Williams is quite satisfactory [9]. This is in part due to the fact that modified Levitt and Greer criteria were used for insulin, so as to reduce the amount of α-helix and increase the amount of β-sheet. This may be perfectly valid. The RIP method also uses insulin in the generation of the RIP's. After RIP generation, the authors tested their method by applying it to their reference proteins. For insulin, again the structure correlation was good, but the statistical parameters (judging the error from the curve-fit) were by far the worst of the data set of 17 proteins.

Deconvolution and Curve-fitting methods

Such methods are potentially more satisfactory than either RIP or Williams' methods. They allow greater flexibility (would be applicable to 'extreme' cases), and do not rely on the use of arbitrary secondary structure criteria, which may not be suitable for Raman spectroscopy, nor realistic in the absolute sense. They are also less prone to error from wavenumber inaccuracy. Several different approaches have employed deconvolution and/or curve fitting procedures. Thomas and Agard used a constrained, iterative deconvolution procedure to directly yield quantitative estimates for α and β structures [2]. They claim that their deconvolution procedure maintains the correct areas for resolved peaks, and thus simply calculate quantities of α and β structures from the areas of

the Fourier deconvolved bands. Byler and Susi [11], in their analysis of IR data, used 'unrestrained' deconvolution and second derivative spectra to identify the number and positions of bands in the Amide I region, similar to the approach outlined in this chapter. However, curve-fitting was applied to the deconvolved spectra and not to the original spectra. Although the authors note the possibility of area changes during their deconvolution procedure, they claim that if the deconvolution is kept to a minimum, then areas are negligibly affected [19, 33].

The method described in this thesis does not suffer from adverse effects of deconvolution, but appears to suffer from the possibility of erroneous results (see experimental section). In the worst cases, there was a difference in the estimated amount of α-helix structure of 7%, and 10% in the amount of β-sheet structure. This can be avoided by the use of 'sensible' restraints, but the procedure then becomes rather subjective.

All three methods described are based on the assumption that the integrated areas of bands of 'pure' structure type are equivalent; i.e. that the overall amide I band intensity does not change with conformation. The Williams' analysis also makes this assumption, based on the experimental results of Yu *et al.* [34]. Berjot *et al.* [8] have criticised this assumption, and have tried using normalisation coefficients in their RIP analysis. This did not appear to have a significant effect on the end results of the analysis.

3.5 CONCLUSIONS

This chapter has pinpointed two major problems with most of the presently used methods for Raman amide I band analysis: the use

of reference proteins, and the difficulties of curve-fitting. The RIP and Williams methods that use reference spectra and corresponding secondary structure values are limited by the structure definitions that are used. As more comprehensive secondary structure data sets become available, with better secondary structure recognition algorithms, the latter two analysis methods could be revised. Such a data system is currently being constructed [35].

The curve-fitting method presented in this chapter clearly suffers greatly from being too subjective. The restraints imposed to make the curve-fit apparently more realistic were useful, and had some reasonable foundation. However, it would be better to test the method on a larger set of proteins to test the reliability of the procedure. The related work of Byler and Susi [11], analysing IR amide I bands has established good results for 21 proteins.

Perhaps the most straightforward method for amide I band analysis is the iterative Fourier deconvolution method of Thomas and Agard [2]. It bypasses any need for time consuming and problematic curve-fitting, and does not require the subtraction of amino acid side chain bands. It is a pity that the method has not apparently been tested on a set of proteins with well defined structures, nor has been used for protein structure studies outside the Thomas group. The method has been tested by Palmo *et al.* [12], and compared with other deconvolution methods. The authors pointed out the slowness of the iterative procedure and the need for very high signal to noise ratios (or external smoothing). A last point about the method is its apparent lack of success in identifying more than two component bands in any amide I profile. However, this may merely reflect the character of the proteins studied by this method.

3.6 REFERENCES

[1] H.L.Casal, U.Kohler, and H.H.Mantsch, *Biochim.Biophys.Acta* **957**, 11 (1988).

[2] G.J.Thomas, Jr. and D.A.Agard, *Biophys.J.* **46**, 763 (1984).

[3] B.Prescott, V.Renugopalakrishnan, M.J.Glimcher, A.Bhushan, and G.J.Thomas, Jr., *Biochemistry* **25**, 2792 (1986).

[4] J.Marx, J.Jacquot, M.Berjot, E.Puchelle, and A.J.P.Alix, *Biochim.Biophys.Acta* **870**, 488 (1986).

[5] V.M.Naik and S.Krimm, *Biophys. J.* **49**, 1147 (1986).

[6] F.Jahnig and H.Vogel in *"Modern Methods in Protein Chemistry"* Vol. 2, Ed. H.Tschesche, (de Gruyter, 1985).

[7] Yu.A.Ovchinnikov, E.A.Arystarkova, N.M.Arzamazova, K.N.Dzhandzhugazyan, R.G.Efremov, I.R.Nabiev, and N.N.Modyanov, *F.E.B.S Lett.* **227**, 235 (1988).

[8] M.Berjot, J.Marx, and A.J.P.Alix, *J.Raman Spectrosc.* **18**, 289 (1987).

[9] R.W.Williams, *J.Mol.Biol.* **166**, 581 (1983).

[10] S.Krimm in *"Vibrational Spectra and Structure"* Vol. 16, Ed. J.Durig, 59-69, (Elsevier, 1987).

[11] D.M.Byler and H.Susi, *Biopolymers* **25**, 469 (1986).

[12] a S.F.Gull and J.Skilling, *IEE Proc.* **131**, 646 (1984).
b K.Palmo, B.Mannfors, and L.-O.Pietila, personal communication.

[13] T.E.Smith, *Biochemistry* **5**, 2919 (1966).

[14] J.deGroot, *PhD. Thesis, University of York* (1987).

[15] R.E.Hester, University of York (adapted from original program by R.N.Jones; *NRCC Bulletin*, **12**, 1968).

[16] H.R.Virdee, University of York, unpublished results.

[17] R.E.Hester, University of York (after ref. [19]).

[18] R.E.Hester, University of York (original program by B.Stewart).

[19] J.K.Kauppinen, D.J.Moffat, H.H.Mantsch, and D.G.Cameron, *Appl. Spectrosc.*, **35**, 271 (1981).

[20] B.G.Frushour and J.L.Koenig in *"Advances in Spectroscopy"* Vol. 1, Eds. R.J.H.Clark and R.E.Hester, (Wiley, Chichester, 1975).

[21] A.T.Tu in "*Advances in Spectroscopy, Vol. 13: Spectroscopy of Biological Systems*" Eds. R.J.H.Clark and R.E.Hester, (Wiley, Chichester, 1986).

[22] B.A.Seaton, *Biochim.Biophys.Acta* **42A**, 227 (1986).

[23] S.Krimm, *Biopolymers* **22**, 217 (1983).

[24] A.G.W.Leslie and A.J.Wonacott, *J.Mol.Biol.* **178**, 743 (1984).

[25] T.Skarzynski, P.C.E.Moody, and A.J.Wonacott, *J.Mol.Biol.* **193**, 171 (1987).

[26] T.Skarzynski and A.J.Wonacott, *J.Mol.Biol.* **203**, 1097, (1988).

[27] M.Buehner, G.C.Ford, D.Moras, K.W.Olsen, and M.G.Rossmann, *J. Mol. Biol.* **90**, 25 (1974).

[28] M.Levitt and J.Greer, *J.Mol.Biol.* **114**, 181 (1977).

[29] W.Kabsch and C.Sanders, *Biopolymers* **22**, 2577 (1983).

[30] N.T.Yu, B.H.Jo, and C.S.Liu, *J.Am.Chem.Soc.* **94**, 7572 (1972).

[31] N.T.Yu, C.S.Liu, J.Culver, and D.C.O'Shea, *Biochim.Biophys. Acta* **263**, 1 (1972).

[32] B.Stewart, J.deGroot, J.Brameld, and R.E.Hester in *"Studies in Physical and Theoretical Chemistry"* Vol. 45, Eds. J.Stepanek, P.Anzenbacher, and B.Sedlacek (Elsevier, 1987).

[33] W.J.Yang, P.R.Griffiths, D.M.Byler, and H.Susi, *Appl. Spectrosc.* **39**, 282 (1985).

[34] T.J.Yu, J.L.Lippert, and W.L.Peticolas, *Biopolymers* **12**, 2161 (1973).

[35] ISIS data base, Daresbury Laboratory, U.K.

[36] J.B.Fox and W.B.Dandliker, *J.Biol.Chem.* **221**, 1005 (1956).

[37] R.S.Chittock, personal communication.

[38] O.P.Malhotra and S.A.Bernhard, *J.Biol.Chem.* **243**, 1243 (1968).

[39] M.E.Magar, *J.Biol.Chem.* **242**, 2517 (1967).

[40] D.Moras and K.W.Olsen, *J.Biol.Chem.* **250**, 9137 (1975).

CHAPTER FOUR: ULTRAVIOLET RESONANCE RAMAN STUDIES OF THE DEHYDROGENASE ENZYMES

4.1 INTRODUCTION

UVRR spectroscopy is a rapidly developing new field in vibrational spectroscopy. Problems of sensitivity, fluorescence and of interference from visible chromophores may be overcome by judicious choice of the excitation wavelength. A small number of groups are now presenting novel and promising results from biological systems, but there is still much fundamental work to be covered [1]. The UVRR spectra of the individual aromatic amino acids and of nucleic acids have now been determined [1-7]. Initial misassignments of certain bands arising from transient photodecomposition products to new bands of the aromatic amino acids have been corrected [5, 8]; now these bands are clear markers of the loss of spectral integrity.

The study of proteins by UVRR spectroscopy is still at a preliminary stage, with new structure-spectra relationships continually being established. Although many of the bands that are present in normal Raman (NR) spectra can also be observed in UVRR spectra, they do not always retain the same sensitivity to environment and bonding. Secondary structure estimates have been made from the UVRR amide II band, using 192-nm excitation [9]. The amide I band, which is used in NR spectroscopy (see chapter 3), is comparatively weak in UVRR spectra, and no longer an accurate guide to secondary structure [9].

Difficulties in correlating changes in UVRR spectra with known structural changes were pinpointed by Rava and Spiro in an early study of insulin and α-lactalbumin, using 200 and 218 nm excitation [10]. The two systems were chosen for their known changes of conformation with pH, which result in changes in exposure of various aromatic amino acids of the protein to solvent. The authors

experienced problems in correlating relative intensities in the Fermi resonance doublet of tyrosine (850 and 830 cm^{-1}) to tyrosine hydrogen bonding, due to the different enhancements of the two bands. Hildebrandt *et al.* subsequently established the new dependence of the ratio of the two bands (when excited with 229 nm radiation) on tyrosine environment and bonding [11]. Other relationships between tyrosine environment and RR bands were also established in this study. By exciting at 229 nm, where the spectrum of tyrosine in the 1580 to 1620 cm^{-1} region dominates contributions from phenylalanine and tryptophan, tyrosine band intensities and wavenumbers could more clearly be followed. The position of the ν 8b (*ca.* 1601 cm^{-1}) tyrosine band was found to depend sensitively on tyrosine hydrogen bond strength, varying from 1600 cm^{-1} for aqueous tyrosine to 1587 cm^{-1} for tyrosine in the protein OMACHA3(-) (ovomucoid third domain protein from chachalaca), at neutral pH. Two further conclusions were drawn from this study: (1) the intensity of the band due to the tyrosine ν 9_a ring mode depends on the hydrogen bonding, and (2) the phenylalanine ν 12 band changes in intensity as its environment changes. In general, it appears from this study that environmental effects play a large role in determining the UVRR band intensities associated with aromatic ring modes, and such effects may obscure the effects of hydrogen bonding on certain marker bands.

In this chapter, UVRR spectra of the enzyme GAPDH obtained using 220 and 240 nm excitation are described. These show strong enhancement of bands due to aromatic amino acid vibrations. Unfortunately, without the insights provided by the recent papers cited above, the excitation wavelengths chosen did not give complete selectivity of enhancement. However, the spectra enable some conclusions to be drawn about the effects of substrate and

coenzyme binding to GAPDH.

The coenzyme NADH has UV chromophores at *ca.* 220, 260 and 340 nm. It was realised in the early days of UVRR spectroscopy that different parts of this coenzyme could be selectively studied by UVRR, by choice of the excitation wavelength. The UVRR spectra of NADH excited at 273 and at 330 nm have been presented by Rodgers and Peticolas [12]. The 273 nm-excited spectrum showed bands due to the adenine ring, whereas the 330 nm-excited spectrum showed bands due to the nicotinamide moiety [12, 13]. This selectivity and intensity enhancement has not previously been exploited to study the interactions between this coenzyme and enzymes. The results of preliminary investigations of such coenzyme-enzyme interactions by UVRR spectroscopy are presented in this chapter.

The adenine ring is, of course, a fundamental structural component of the coenzyme NADH. UVRR studies of nucleic acids, DNA and RNA are thus closely related to the present study. The UVRR spectra of the nucleosides [14] and nucleotides [15] have been obtained with excitation wavelengths from 200 to 266 nm, allowing the resonance enhancement patterns to be analysed. This has yielded information about the character of the modes active in the RR spectra [16]. Following on from this point, efforts have been directed at establishing correlations between nucleotide UVRR spectra and factors such as base stacking, hydrogen bonding, and conformation. Fodor and Spiro obtained UVRR spectra of the nucleic acid duplexes poly(dA-dT) and poly(dG-dC) that showed clear differences from the spectra of the free nucleotides [17,18]. Base stacking was found to cause Raman hypochromism (associated with a corresponding shift in the UV absorption maximum), which affected the overall intensities of the ring modes of the nucleotides.

Attempts were also made to identify marker bands for the different conformations A, B and Z, found in DNA [17]. Subsequent studies by Grygon and Spiro [19], and by Grygon *et al.* [20] have examined in more detail the effects of base stacking and hydrogen bonding on the UVRR spectra of adenine (A), uracil (U), and thymine (T) - based systems. The observed Raman hypochromism on base stacking was quantified for various modes of different duplexes. It was found that stacking between identical bases gave rise to stronger hypochromism than stacking between non-identical bases [19]. Significant wavenumber shifts were observed for bands due to exocyclic modes of the bases when hydrogen bonded in the duplex structures. However, only small wavenumber shifts on duplex formation were observed for bands due to ring modes [17, 19].

4.2 EXPERIMENTAL

4.2.1 Enzyme preparations

All enzymes and coenzymes (NAD^+ and NADH) for the UVRR (220-260 nm) studies were purchased from the Sigma Chemical Co. and used without further purification. Holo-GAPDH was obtained from rabbit muscle (see chapter 3, section 3.2.1). LADH (horse liver) and YADH were obtained in crystalline form, with specific activities of 2.1 and 310 units, respectively, where 1 unit is equal to 1 μmol of NADH released per minute per milligram of protein, at pH 8.8. LDH (porcine heart, type XVIII) was obtained as a crystalline suspension in a solution containing 1.9 M ammonium sulphate. The specific activity of this preparation was 400-600 units per mg of protein, where one unit converts 1 μmol of pyruvate to L-lactate per minute

at pH 7.5, 37°C. MDH (porcine heart cytoplasmic) was obtained as a crystalline suspension in a solution containing 3.2 M ammonium sulphate and 0.1 M potassium dihydrogen phosphate. MDH activity was 400 units per mg protein, where one unit converts 1 μmol of oxalacetate and NADH to L-malate and NAD per minute at pH 7.5, 25°C. The use of these proteins (excepting GAPDH) without checking purity was far from ideal. However, only contamination with other dehydrogenase enzymes would affect the studies of coenzyme binding; this is unlikely. Low molecular weight contaminants should largely be removed by the charcoal treatment.

For the UVRR experiments undertaken using 350.6 nm excitation, LDH (Bacillus Sterothermophilus) of high purity was a generous gift from Dr. Tony Clarke (Bristol University). Oxamate inhibitor and D-fructose-1,6-diphosphate (FBP) were also provided by Dr. Clarke as their mono- and tri- sodium salts, respectively, and were both at least 98% pure.

For the GAPDH acylenzyme experiments, the substrate GAP was prepared by hydrolysis of the ethyl acetal (Sigma, mono-barium salt), as described by Sigma. Exhaustive washing of the Dowex resin was necessary to avoid artefacts in the UVRR spectra. GAP solutions were stored at 0°C, pH 3. Immediately prior to use, GAP solutions were adjusted to pH 6.0-6.5 with dilute HCl.

GAPDH activity was determined by a single turnover experiment, which directly measures the number of active sites that are acylated per GAPDH tetramer. This was achieved by measuring the amount of NADH released when an excess of GAP was added to GAPDH at pH 6.0 in the absence of phosphate. Under such conditions the amount of NADH released can be assumed to be equivalent to the amount of acylation. The amount of NADH released was measured

spectrophotometrically at 340 nm, using $\epsilon = 6.2 \times 10^3\ M^{-1}cm^{-1}$ [21]. The extent of acylation is sensitive to the amount of NAD^+ present in solution, and to the redox state of the cysteine thiol groups of the active sites. Both EDTA (0.001M) and dithiothreitol were found to maintain the cysteine groups in the reduced state, and thus ensure maximum enzyme activity. However, EDTA was found to be unsatisfactory for use in UVRR experiments, as it absorbs in the UV region. Dithiothreitol was used in all UVRR experiments, at a final concentration of 0.01 M. The dependence of the extent of acylation on the amount of NAD^+ present in solution is shown in Figure 4.1. Clearly, a minimum amount of NAD^+ in solution is preferable for UVRR experiments, to avoid large spectral contributions from free NAD^+, but maximum acylation is also desirable. A six-fold excess of free NAD^+ was used in preparations for the acylenzyme experiments. Under these conditions, the number of acylated sites per GAPDH tetramer was found to be between 1.7 and 2.0. Although there is still some controversy, many other groups have found a maximum of two-site acylation of GAPDH under these conditions [22]. Thus GAPDH activity appears to be close to its maximum.

The ammonium sulphate suspensions of GAPDH, LDH (Sigma) and MDH were centrifuged, and the supernatant solutions removed. The centrifuged enzymes (and LADH and YADH powders) were dissolved in 0.05 M tris(hydroxymethyl)amine (tris) buffer to final concentrations in the range 5×10^{-5} to 6×10^{-6} M. GAPDH solutions were pH 6.0-6.5, ADH solutions pH 7.0-7.5. MDH and LDH solutions were made with pH 6.5 buffer, but mixed with alkaline NADH solutions so as to produce holoenzyme solutions of pH 7.0-7.2. LADH, GAPDH, YADH and bacterial-LDH concentrations were determined from their UV absorptions, using the absorption coefficients in Table 4.1. MDH and

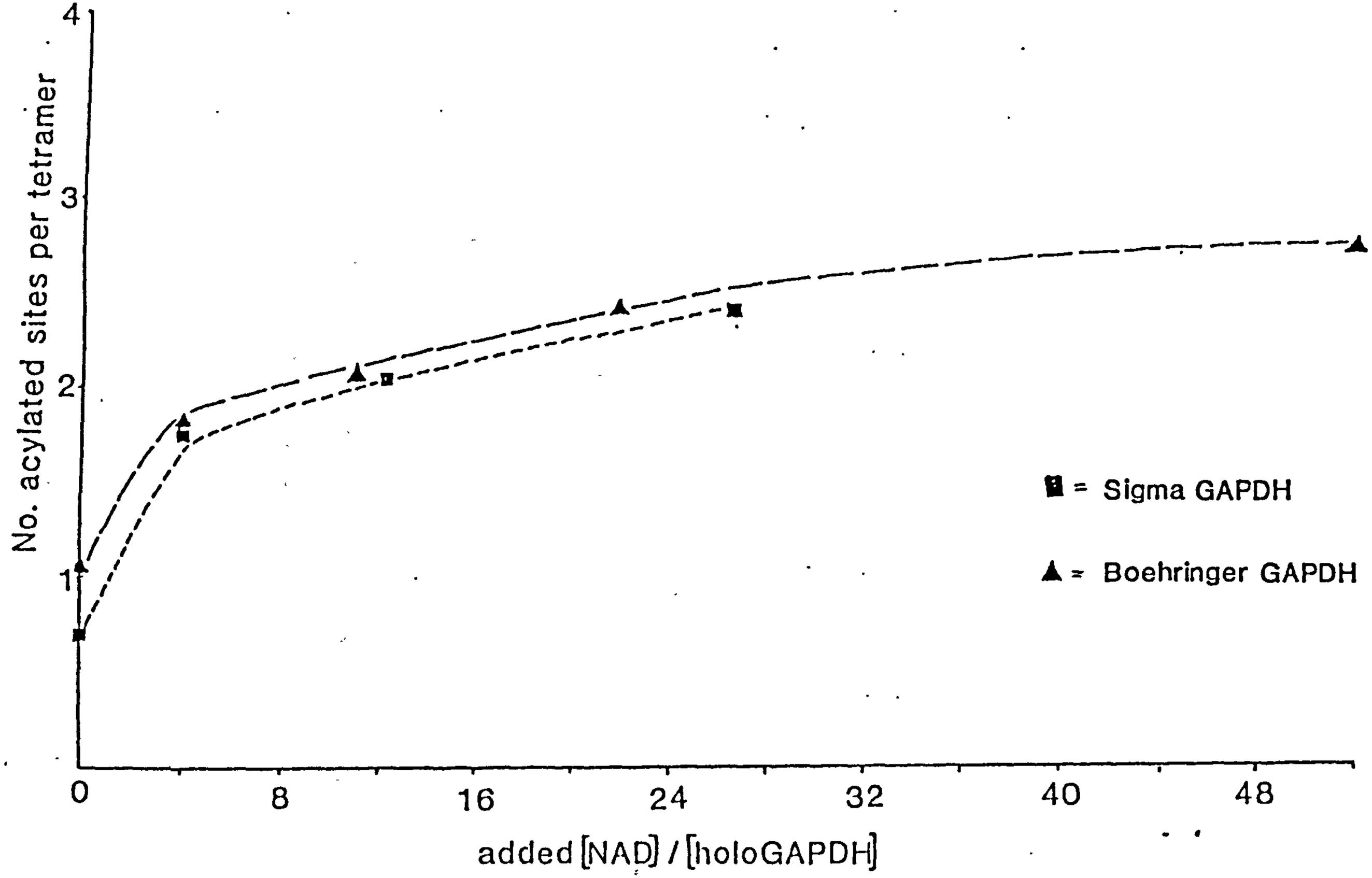

Figure 4.1 Dependence of the extent of GAPDH acylation on the amount of NAD^+ present.

Table 4.1: Absorption coefficients for enzymes and coenzymes in the far ultraviolet.

	$10^{-3}\epsilon/M^{-1}cm^{-1}$		
	220 nm[a]	240 nm[a]	260 nm
NAD^+	11	10	17.8
NADH	12.7	7.8	14.9
GAPDH	2000	240	100[b]
LADH	800	50	20.4[c]
YADH	-	187	104[c]

LDH (bacterial) $\epsilon_{280} = 6 \times 10^4\ M^{-1}cm^{-1}$.

[a] Values estimated from absorption spectra, using 260 nm absorption coefficients.

[b] Values for holoenzyme with *ca.* 2 NAD^+ per tetramer, using $\epsilon_{280} = 1.38 \times 10^5\ M^{-1}cm^{-1}$ (3.25 NAD^+ per tetramer [49]).

[c] Values for apoenzyme using 280 nm absorption coefficients from Sund and Theorell [50].

porcine-LDH concentrations were estimated from the volume of suspension used (with known concentration in mg/ml) and their known molecular weights. The bacterial LDH was also stored as a suspension in ammonium sulphate (430 mg to 1 ml of solution), but for use, sulphate was removed, as it is thought to interfere with coenzyme and oxamate binding. The LDH suspension was dialysed against 10 mM tris buffer containing *ca.* 1% $^{w}/v$ charcoal outside the dialysis sac. The dialysed enzyme was reconcentrated using a Centricon concentrator (M.W. cut-off 30000 $gmol^{-1}$).

Apoenzymes were prepared by incubation of the enzyme with activated charcoal at room temperature for 15-20 minutes (see also chapter 3 section 3.2.1). Holoenzymes of YADH, LADH, MDH, and LDH were prepared by stoichiometric addition of NADH to the enzymes, so as to occupy half the coenzyme binding sites (i.e 2 NADH per YADH, one NADH per LADH), and thus ensure complete binding of the coenzyme if estimates of concentration (from inaccurate ϵ values or mass of enzyme used) are inaccurate. In the case of LADH and YADH, NADH was added to the enzymes a few minutes before laser irradiation. MDH and LDH were mixed with NADH a few seconds before laser irradiation, using the flow-mixing device described below (see also Fig. 4.2). The UV absorption spectrum of the MDH holoenzyme was recorded after collection of the Raman spectrum. The peak of the nicotinamide absorption was found at 335 nm.

The extent of coenzyme binding at any concentration can be estimated, if necessary, by using the dissociation constant $K_{e.nadh}$ or $K_{e.nad}$. However, the literature values for these constants vary quite widely [23], and may only give an approximate estimate of the extent of coenzyme binding.

The estimation of the extent of coenzyme binding to YADH is

made as follows:

$$K_d = \frac{[N].[E]}{[NE]}$$

[N]=concentration of coenzyme

[E]=concentration of enzyme

[NE]=concentration of complex

$[N]=[N]_{initial}-y = (2.4\times10^{-5}M)-y$

$[E]=[E]_{initial}-y = (4.8\times10^{-5}M)-y$

$[NE]=y$

Thus, $K_d.y = 11.5\times10^{-10} - y^2 - 7.2\times10^{-5}y$

and $0 = 11.5\times10^{-10} - y^2 - (7.2\times10^{-5} - K_d)y$

The quadratic equation is solved using K_d=11 μM [23], then [NE] can be found. In the above case of YADH, the % of coenzyme binding is approximately 40%. For LADH K_d is much lower (see Table 4.2), so that, at the concentration employed, the coenzyme is entirely bound. This was confirmed spectroscopically by observing the shift of the nicotinamide absorption from 340 to 325 nm. The binding of NAD^+ to GAPDH is negatively co-operative [24]. The K_d value for the first coenzyme molecule binding is thus very low, and gradually increases (see Table 4.2). It is again likely that all the NAD^+ is bound to GAPDH in the holoenzyme preparations. Table 4.2 lists the K_d values for other holoenzymes that can usefully be compared with the enzymes used in this study.

The LDH ternary complex, LDH.NADH.oxamate was produced by the addition of excess oxamate and FBP to the holoenzyme. FBP enhances the affinity of the enzyme for oxamate. A 10-20 fold excess of oxamate, and a 2-3 fold excess of FBP were used in the LDH ternary complex preparations.

The relative activities of holo- and apo- GAPDH were

Table 4.2 Dissociation constants for enzyme.NAD^+ (or NADH) complexes.

Enzyme	pH	$K_{e.nad}/\mu M$	$K_{e.nadh}/\mu M$
LADH	6.0	266	0.23
	7.0	160	0.3
	9.0	12	0.66
YADH	7.0	350	11.0
MDH[a]	6.0-8.0	280	1.0
LDH[b]	7.2	300	0.9
GAPDH, K_1[c]	7.4	0.023	-
GAPDH, K_2[d]	7.4	0.2	-
GAPDH, K_3[e]	7.4	0.55	-

All values obtained from ref. [23].

[a] Value for mitochondrial porcine heart enzyme.

[b] Value for porcine heart enzyme.

[c], [d], [e] Values for first, second and third bound NAD^+ molecule (to rabbit muscle enzyme), respectively.

monitored before and after esposure to pulsed 260 nm irradiation. The initial rates of NADH production during the reaction of enzyme with GAP and phosphate in the presence of excess NAD^+ at pH 7.5 were compared. Holo-GAPDH lost only 4% activity after laser irradiation for the duration of the Raman experiments, whereas apo-GAPDH lost 16-20% activity. These results were assumed to also reflect the stability of the other enzymes to pulsed laser irradiation. Holoenzymes were sometimes passed through the laser beam more than once. Apoenzymes were never re-used, as effects on spectra from denatured enzyme could become significant.

UVRR experiments using 220-260 nm-excitation were undertaken at the Rutherford Appleton Laboratory. The general experimental set-up and instrumentation is described in chapter 2 of this thesis. Samples were flowed through a quartz capillary tube at a rate sufficient to present a fresh sample to each pulse of the laser (generally *ca.* 1 ml per minute). In addition, the capillary tube was slowly translated through the beam to avoid any build up of decomposed enzyme on the walls of the tube. The acylenzyme was flowed in the same manner, but a simple mixing device was employed so as to freshly form acylenzyme shortly before laser irradiation (see Fig.4.2).

Experiments using the 340 nm absorption band of NADH for resonance enhancement were undertaken at York. The 350.6 nm line of a c.w. Kr ion laser was always used, with the experimental set-up and instrumentation described in chapter 2, section 2.1.4 of this thesis. Samples were placed in a spinning cell and irradiated using conventional right angle scattering geometry.

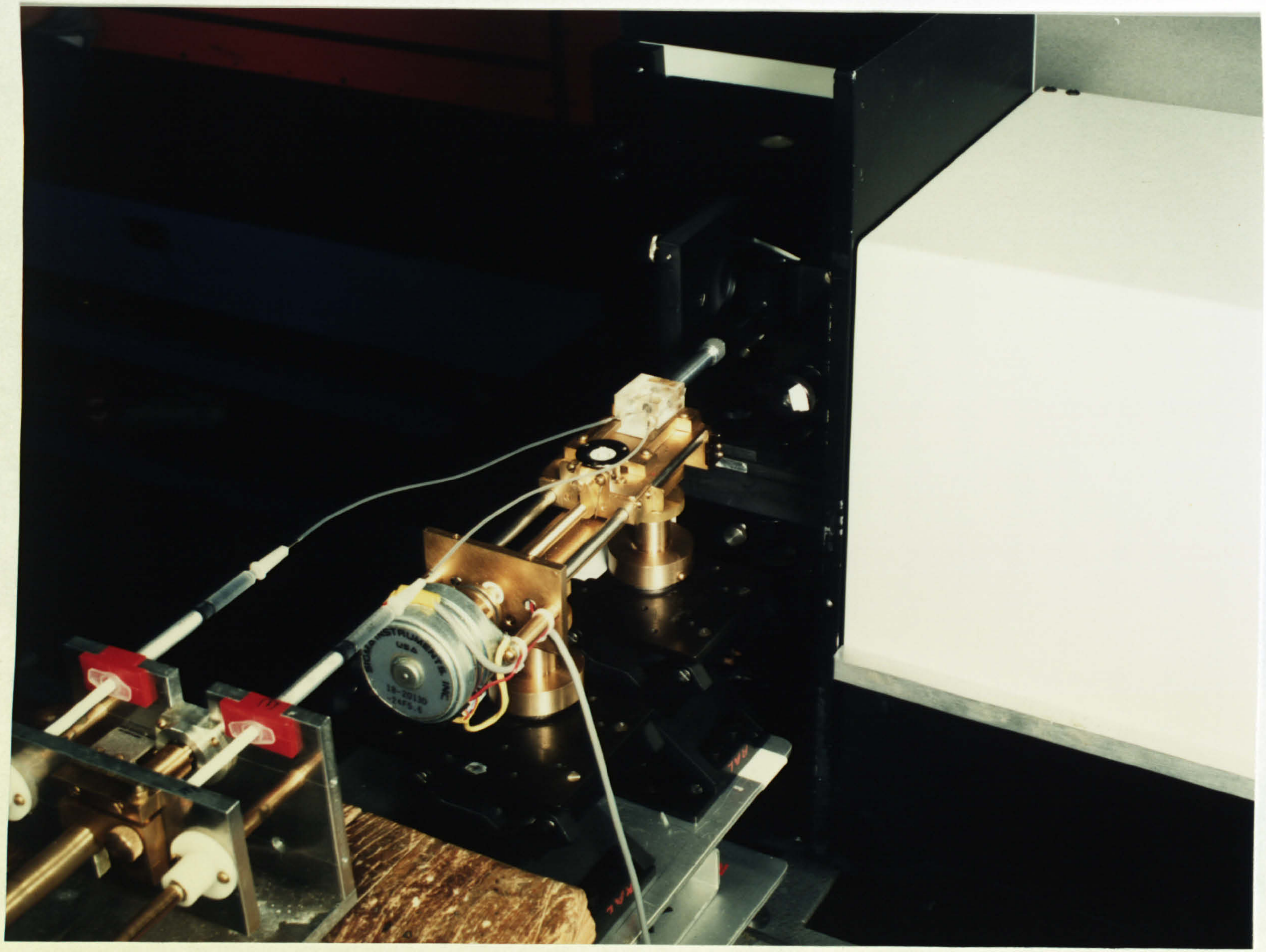

Figure 4.2 Flow-mixing device used for UVRR experiments.

4.3 RESULTS

4.3.1 Coenzyme binding study using 260 nm excitation

Both NAD^+ and NADH gave strong, fluorescence free RR spectra with 260 nm excitation (see Figs. 4.3(a) and 4.4(a)). Consistent with the fact that the 260 nm absorption bands of NAD^+ and NADH are mainly due to the absorption by the adenine moiety, the 260 nm RR spectra of NAD^+ and NADH are virtually identical. The bands in the RR spectra are, with the exception of a small nicotinamide band at *ca.* 1030 cm^{-1} (Fig. 4.3(a)), assigned to adenine vibrations [16,25]. The spectrum of NAD^+ in Fig. 4.3(a) is also closely similar to that of NADH excited at 273.0 nm [12]. The wavenumber values for NAD^+ are listed in Table 4.3.

The 260 nm excited RR spectra of holo- and apo- GAPDH are shown in Fig. 4.3. Both spectra had large fluorescence backgrounds which have been subtracted as simply as possible. However, a broad 'hump', centred at 1300 cm^{-1}, is an indication of an imperfect subtraction. This appeared as a major problem in all the dehydrogenase spectra obtained using 260 nm-excitation. The fluorescence was short-lived (could not be reduced by gating), and was not removed by the charcoal treatment. Fortunately, the apo- and holo- enzyme spectra had very similar fluorescence backgrounds, so that a holo- minus apo- subtraction not only removed enzyme bands, but also conveniently removed the large backgrounds. As can be seen from Fig. 4.3(b) and (c), interference from aromatic amino acid bands is not a major problem, but a (b)-(c) subtraction was used to obtain accurate wavenumber values for bound NAD^+. The latter values are given in Table 4.3.

The spectra of NADH bound to the alcohol dehydrogenases are

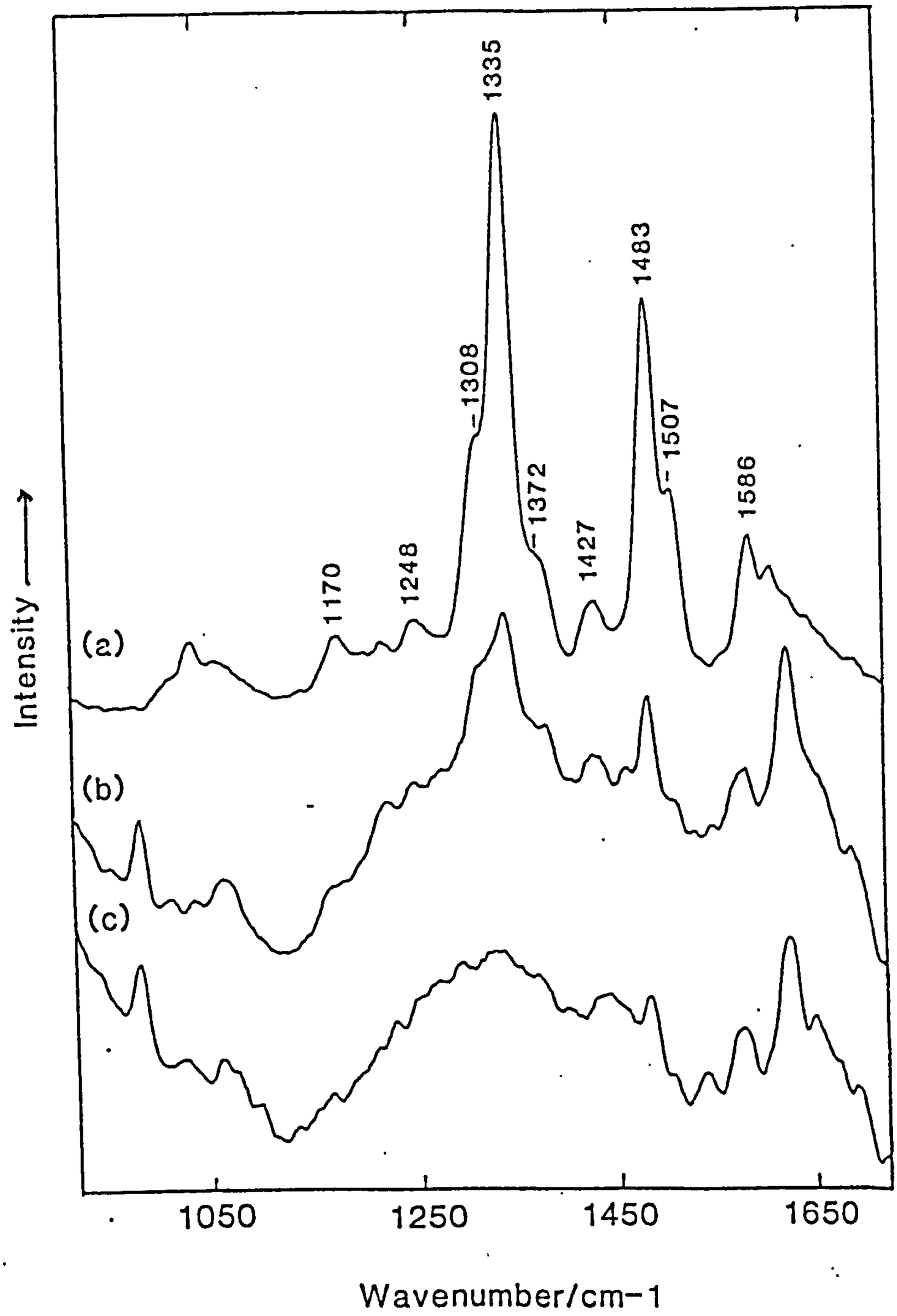

Figure 4.3 260 nm-excited RR spectra of

(a) NAD^+ ($3x10^{-4}$ M, pH 6.8)

(b) holo-GAPDH ($2x10^{-5}$ M, pH 6)

(c) apo-GAPDH ($2x10^{-5}$ M, pH 6)

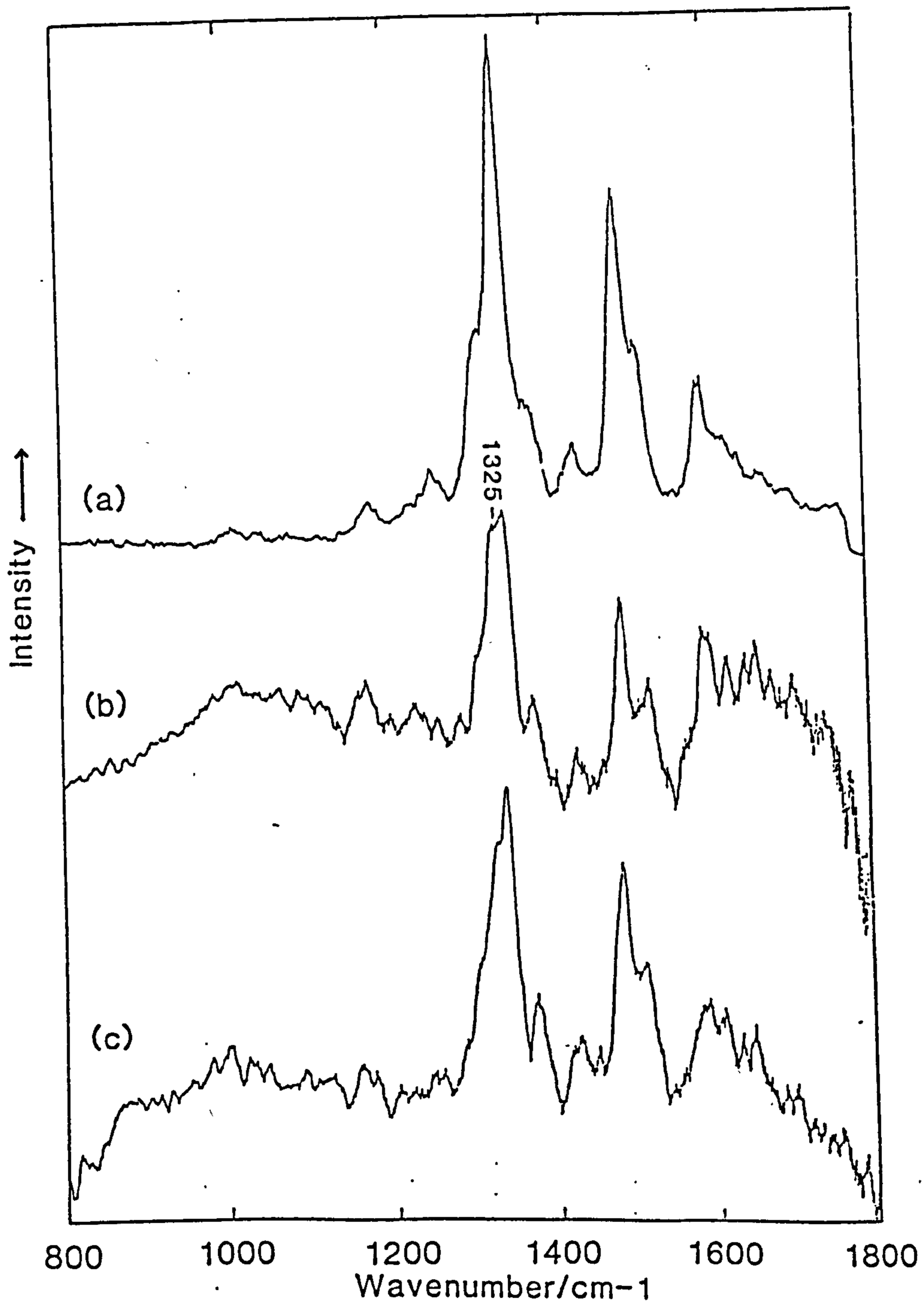

Figure 4.4 260 nm-excited RR spectrum of NADH ($8x10^{-4}$ M, pH 7.5), (a), and 260 nm-excited RR difference spectra of

(b) NADH bound to LADH ($4.3x10^{-5}$ M, pH 7.5)

(c) NADH bound to YADH ($4.8x10^{-5}$ M, pH 7.5); *ca.* 40% of NADH is not enzyme bound. In (b) and (c) the holoenzyme minus apoenzyme difference spectra are shown.

Table 4.3: Wavenumber values (cm^{-1}) for NAD^+ and NADH in solution and enzyme bound.

free NAD^+ (NR)[a]	free NAD^+ (RR)	NAD^+.GAPDH	NADH.YADH	NADH.LADH
730 s	730 w		–	–
1032 vs	1030 w		–	–
–	1170 mw	*ca.*1172 w	1160/ 1173 w	1166 mw
1254 mw	1248 mw	–	–	–
1308 m	1308 m	1314 m	*ca.*1304 sh. m	*ca.*1301 sh. w
			1325 s	1325 s
1338 s	1335 s	1336 s	1335 s	1335 s
1378 m	1372 m	1378 m	1371 m	1369 m
1422 m	1427 mw	1422 m	*ca.*1420 mw	1420 w
1484 mw	1483 s	1483 s	1480–1 s	1480 s
1510 mw	1507	1509 m	1505 m	1510 m
1580 m	1586 m	1590 m	1582 mw	1584 m
–	1609 mw	–	*ca.*1607 mw	1609 mw

w=weak, m=medium, s=strong, v=very, sh=shoulder

[a] Taken from Yue *et al.* [25]

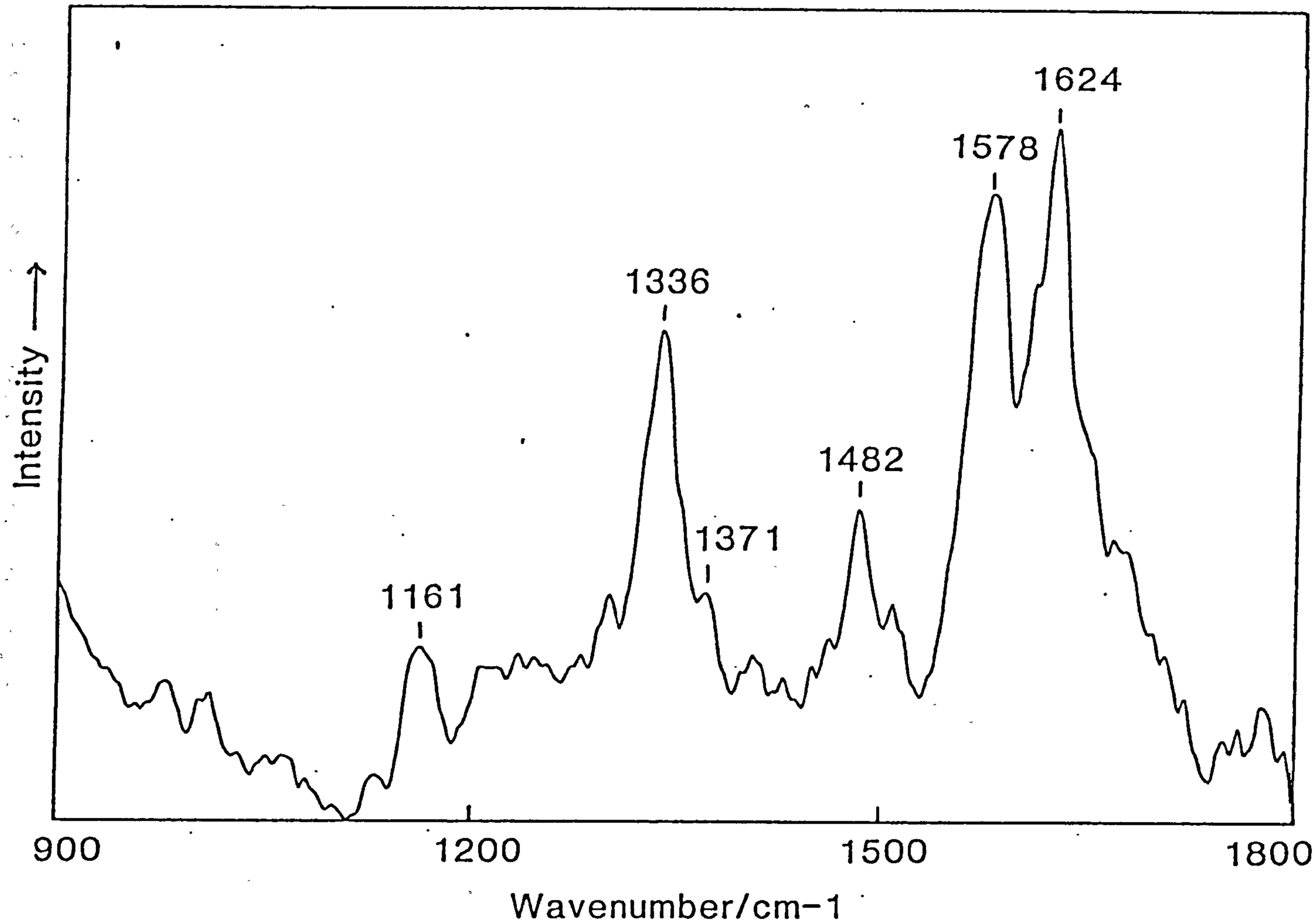

Figure 4.5 260 nm-excited RR spectrum of NADH (4.8×10^{-5} M, pH 7.5) in the presence of YADH (2.4×10^{-5} M, pH 7.5). A fluorescence background has been subtracted.

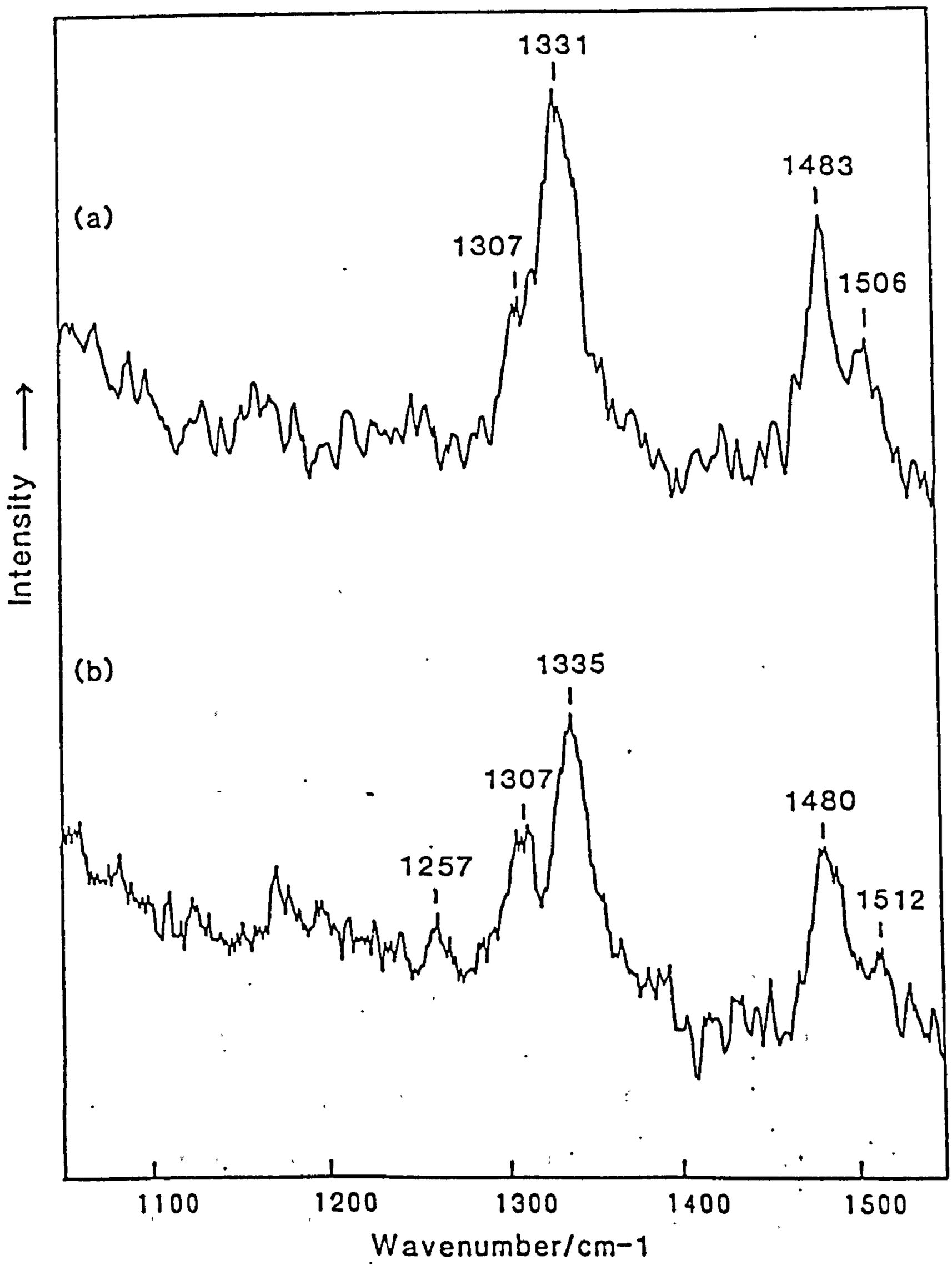

Figure 4.6 260 nm-excited RR difference spectra of (a) NADH ($5x10^{-5}$ M) bound to LDH ($2x10^{-5}$ M), pH 7. (b) NADH ($5x10^{-5}$ M) bound to MDH ($5x10^{-5}$ M), pH 7. The holoenzyme minus apoenzyme difference spectra are shown in both cases.

shown in Figs. 4.4(b) (LADH) and (c) (YADH). The spectrum in Fig. 4.4(c) shows a superposition of spectra of bound and free coenzyme; only *ca.* 40% of the coenzyme is bound (see experimental section). The band wavenumbers are listed in Table 4.3. The aromatic amino acid bands in the 1580-1630 cm^{-1} region of the ADH spectra were quite strong (see Fig.4.5), and imperfect subtractions may have left spurious bands and slight negative peaks in this region.

The corresponding spectra of NADH bound to MDH and LDH were of poorer quality than the ADH- bound NADH spectra. This was mainly due to poor alignment of the Triplemate spectrometer and the degradation of the mirror coatings in its spectrograph stage. Consequently, the difference spectra only clearly showed the major bands at *ca.* 1330 and 1480 cm^{-1}. The two difference spectra are shown in Fig. 4.6.

4.3.2 Acylenzyme study using 240 and 248 nm excitation

The 240 nm excited RR spectra of holo-GAPDH, with and without substrate, GAP, are shown in Fig. 4.7. The spectra show bands due to tryptophan (trp) and tyrosine (tyr) vibrations of GAPDH, and also due to the free NAD in solution. The corresponding 248 nm excited spectra were dominated by the contribution from free NAD^+, but still showed a band at *ca.* 1620 cm^{-1} due to tyr and trp.

Previous experiments using the 248 nm pulsed output of a line-narrowed KrF excimer laser had apparently revealed a new band in the acylenzyme spectrum at 1590 cm^{-1} [26]. This band was only present in the acylenzyme spectrum, and disappeared as expected on the addition of arsenate (arsenate converts acylenzyme back to enzyme and substrate). This result was not reproduced by the subsequent (more reliable) experiments presented in this section. It

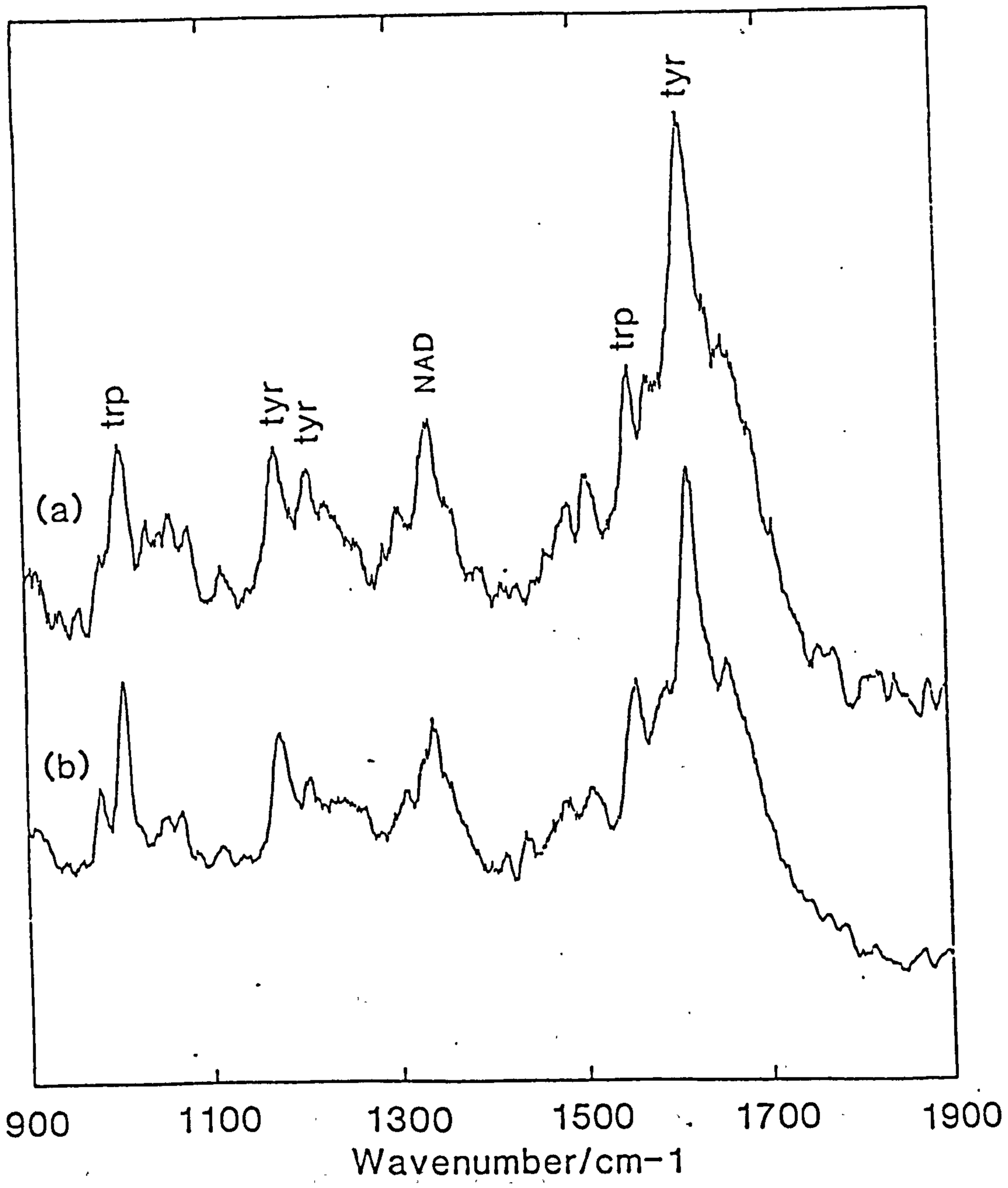

Figure 4.7 240 nm-excited RR spectra of

(a) GAPDH (2×10^{-5} M) with NAD^+ (1.2×10^{-4} M) at pH 6.0

(b) GAPDH (2×10^{-5} M) with NAD^+ (1.2×10^{-4} M) and substrate, GAP (*ca.* 10^{-4} M) at pH 6.0.

In both (a) and (b) a small amount of dithiothreitol (DTT) was added to the GAPDH to restore full enzyme activity.

is difficult to explain the result which showed a 1590 cm^{-1} band in the acylenzyme spectrum, but a peak was observed in this region when samples of GAP were contaminated with a substance of unknown composition that originated from the Dowex resin used in GAP preparation.

4.3.3 Coenzyme binding to GAPDH: 220 nm RR study

The 220 nm excited RR spectra of holo- and apo- GAPDH are shown in Fig. 4.8. The spectra show only bands due to vibrations of the aromatic amino acid residues of GAPDH. The wavenumbers and assignments of the bands in Fig. 4.8 are given in Table 4.4. The spectra are essentially identical, with only a slight distortion of the intensity of the broad band at 1613 cm^{-1}, due to slightly differing contributions from the water band at 1640 cm^{-1}.

4.3.4 Coenzyme and inhibitor binding to LDH: 350.6 nm study

The 350.6 nm excited RR spectra of free NADH could easily be obtained on the Spex monochannel system (see chapter 2, section 2.1.2), as decomposition was slow at c.w. laser powers of 100 mW (focused) at the sample. No significant NADH decomposition was observed after 1.5 hours in the laser beam. However, the photodecomposition of NADH when bound to enzyme (either GAPDH or LDH) was much faster (from 5 to 30 minutes), and fluorescence from enzyme obscured NADH bands. In the case of LDH, the NADH absorption at 350.6 nm (and thus resonance enhancement) decreased significantly on binding to enzyme. Thus, an entire spectrum with an adequate signal-to-noise ratio could not be obtained using monochannel detection. Problems with fluorescence (and decomposition) completely prevented any 350.6 nm UVRR study of NADH bound to GAPDH. The LDH

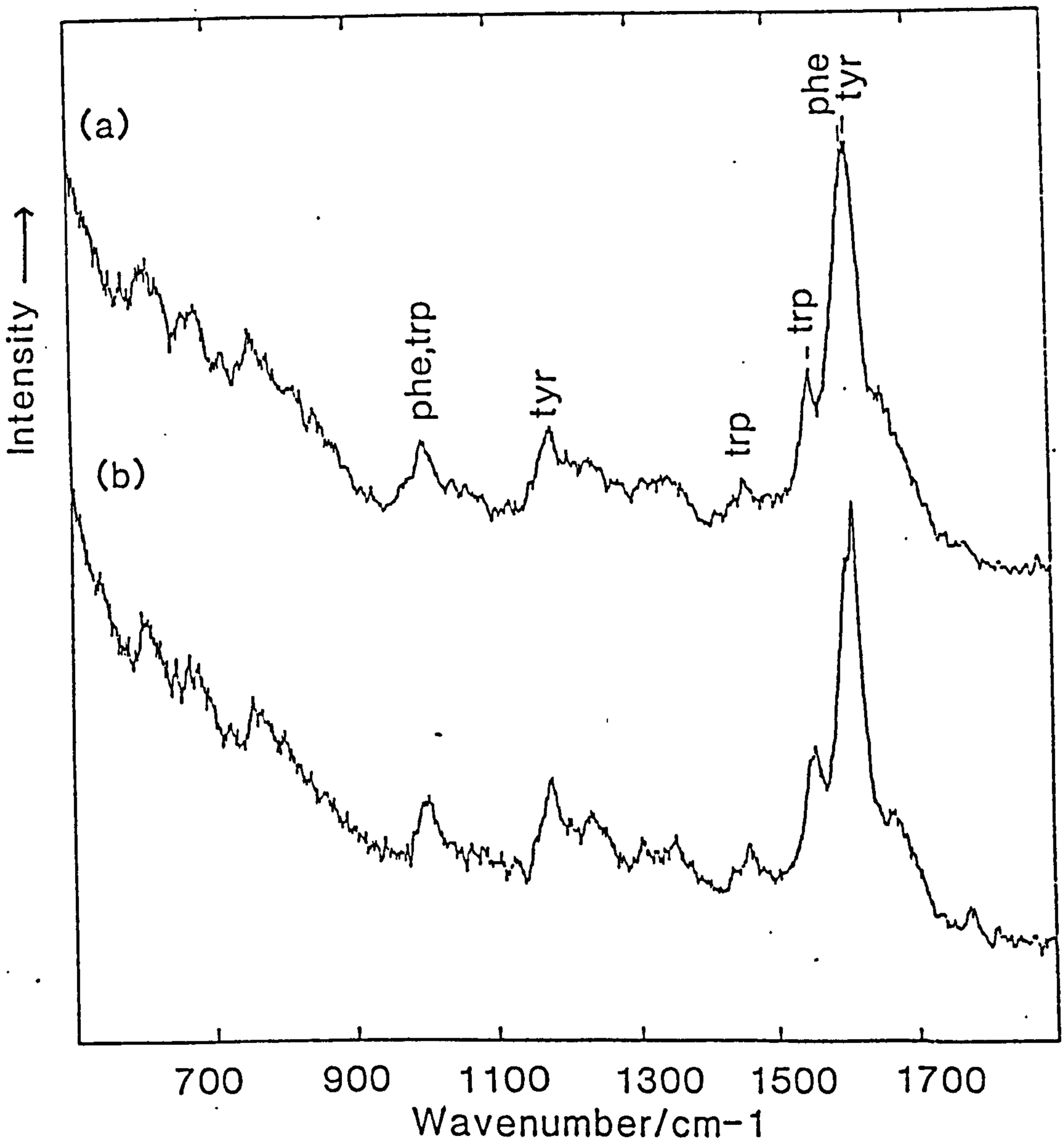

Figure 4.8 220 nm-excited RR spectra of

(a) holo-GAPDH ($6x10^{-6}$ M, pH 6)

(b) apo-GAPDH ($6x10^{-6}$ M, pH 6).

Table 4.4 Assignments and positions of bands in the 220 nm-excited spectrum of GAPDH.

Wavenumber/cm^{-1}	Assignment
760	trp
1001	phe
1010 (shoulder)	trp
1178	tyr[a], phe
1231	trp
1355	trp
1461	trp
1554	trp
1613 (broad)	tyr, phe

[a] Tyr is probably the dominant component [5].

system was less fluorescent, and seemed to be less susceptible to photodecomposition. Thus attempts were made to record RR spectra of NADH bound to LDH using the multichannel CCD system (see chapter 2, section 2.1.4). The complex of LDH.NADH with inhibitor, oxamate, is reported to be very (thermally) stable, with a low quantum yield for fluorescence [27], making it the preferred candidate for such a study.

The 350.6 nm-excited RR spectrum of NADH is shown in Fig. 4.9. The resolution and wavenumber accuracy of the spectrum is not as good as could be obtained using the monochannel system, but the acquisition time was only 60 seconds, as compared with 30 minutes for monochannel collection. The spectrum is similar to that reported by Bowman and Spiro [13], and shows bands due to vibrations of the nicotinamide moiety.

The LDH.NADH complex was very fluorescent, and saturated the detector within 30-60 seconds (depending on the power used, and perhaps on the cleanliness of the preparation; see section 4.4.5). A spectrum of NADH bound to LDH is shown in Fig. 4.9, and is the sum of sixteen 60-second accumulations. The ternary complex with oxamate was slightly less fluorescent. The rate of photodecomposition seemed to be variable, sometimes taking about 30 minutes to completely decompose (see discussion). The short acquisition time and large fluorescence background resulted in a very poor signal-to-noise ratio, and differences in either relative intensities or band wavenumbers were not thought to be reliable. When just a small region of the spectrum (1650 to 1700 cm^{-1}) was scanned using the monchannel system, an apparent downshift from 1687 to 1683 cm^{-1} was observed when NADH bound to LDH with oxamate. However, the spectra obtained on the multichannel system did not confirm this result.

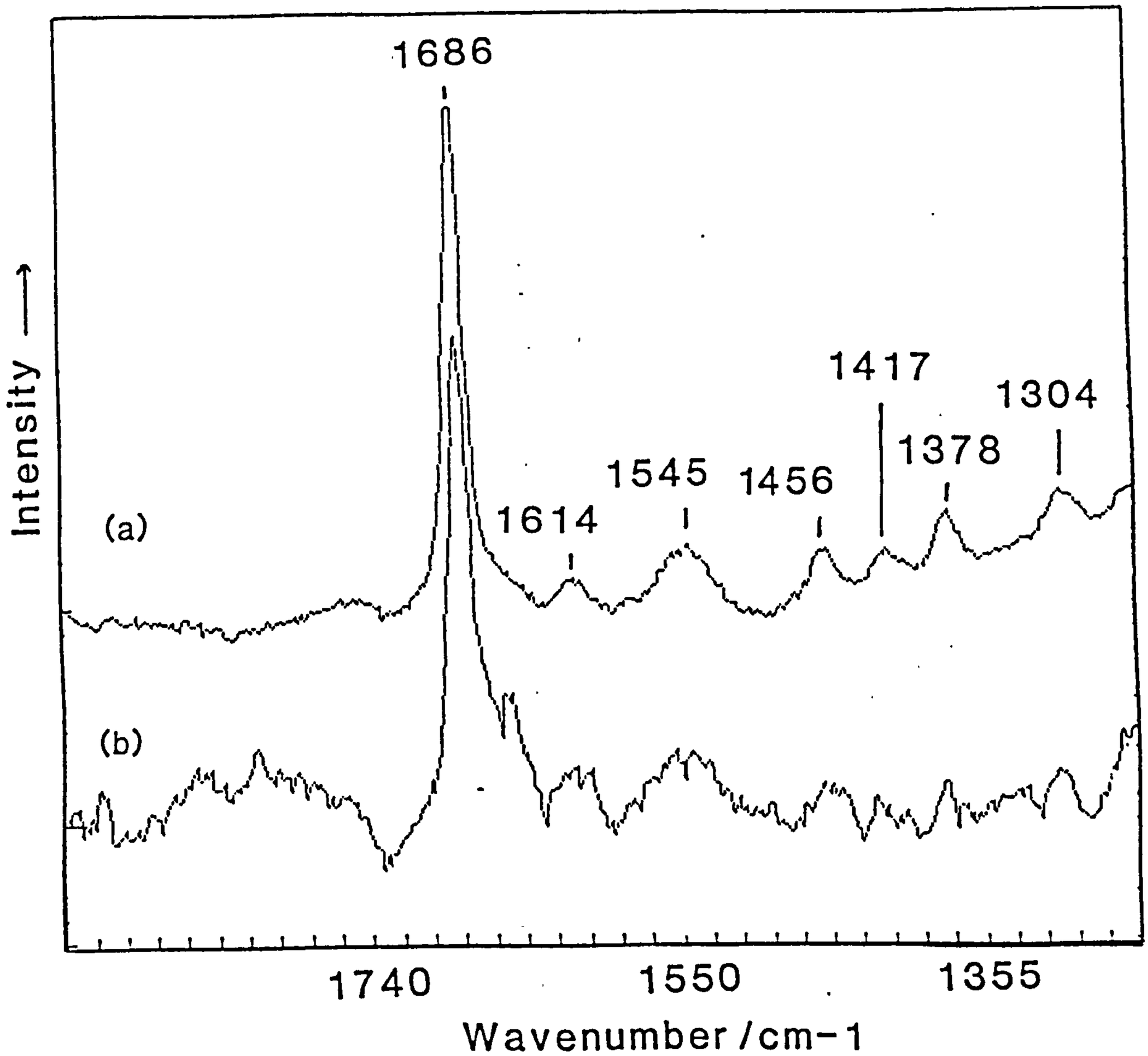

Figure 4.9 350.6 nm-excited RR spectra of

(a) NADH, *ca.* 1 mM

(b) NADH (0.2 mM) bound to LDH (0.2 mM). Fluorescence backgrounds have been subtracted from both spectra. A contribution from the water band at 1640 cm^{-1} can be observed in (b).

4.4 DISCUSSION

4.4.1 Saturation phenomena

Johnson *et al.* have pointed out that it is common for saturation phenomena to occur in UVRR experiments using pulsed lasers [8]. Both non-linear effects (such as stimulated Raman scattering [28]) and saturation of absorption come under the rather general term of saturation phenomena, although they have quite different effects on the Raman spectrum. In the case of non-linear effects, some Raman bands show an increased dependence (e.g. square dependence) on the laser power density. In the case of absorption saturation, all the Raman bands show a decrease in their dependence on the laser power density as the ground state of the molecule is depleted. No power dependence studies were made in the UVRR experiments presented in this thesis. It is thus difficult to judge whether such phenomena could be affecting our results. However, it is clear from the results of Johnson *et al.* that it is absorption saturation (not the onset of non-linear effects) that is most likely in UVRR experiments. This would affect all the Raman bands to the same extent. Thus, while this phenomenon would affect a Raman excitation profile measurement, the comparison of relative intensities of NADH bands is not affected.

In the case of tyrosine and tyrosinate, saturation is preceded by reversible photodecomposition, which is characterised by the appearance of new peaks in the RR spectrum [8]. The transient species produced, thought to be the tyrosinyl radical, has a lifetime of *ca.* 10 ns, and absorbs strongly at 240 nm. A 240 nm-excited RR spectrum should show the extent of photodecomposition, and thus whether saturation may be occurring. RR spectra of aqueous

tyrosine obtained using 240 nm-excitation, under similar conditions to the enzyme experiments, show quite a significant photodecomposition peak at 1516 cm^{-1}; see Fig. 4.10. However, the spectra presented in Fig. 4.7 show only a small peak at 1510 cm^{-1}, which is partly due to free NAD^+. It is possible that the tyrosine residues in the enzyme are less susceptible to radical anion formation. Because of this, it is difficult to say with certainty whether the spectra are free from saturation effects or not. It is even more difficult to estimate possible effects at other laser wavelengths, where the transient photoproduct peaks are not resonantly enhanced. It seems likely that, in these experiments in which samples were partly shielded by the capillary tube and the laser beam only loosely focused, saturation was not taking place.

Tyrosinate is clearly very susceptible to reversible photodecomposition in UVRR experiments. It is not known whether NAD^+ and NADH undergo any similar reversible photo-decomposition. The experiments on bound coenzyme were conducted at lower concentration, and thus higher photon-per-molecule levels, than the experiments on free coenzyme (there is an estimated 6-fold difference in photon-per-molecule level). It is possible that some of the changes in the bound coenzyme spectra are due to the formation of new photo-induced transient species. However, the spectra of NADH bound to LADH and YADH show different amounts of the bands at 1335 cm^{-1} and 1325 cm^{-1}, despite being obtained under very similar experimental conditions. This difference is more likely to be due to diffences in the amount of coenzyme bound to enzyme (see section 4.2.1) than to variation in laser intensity.

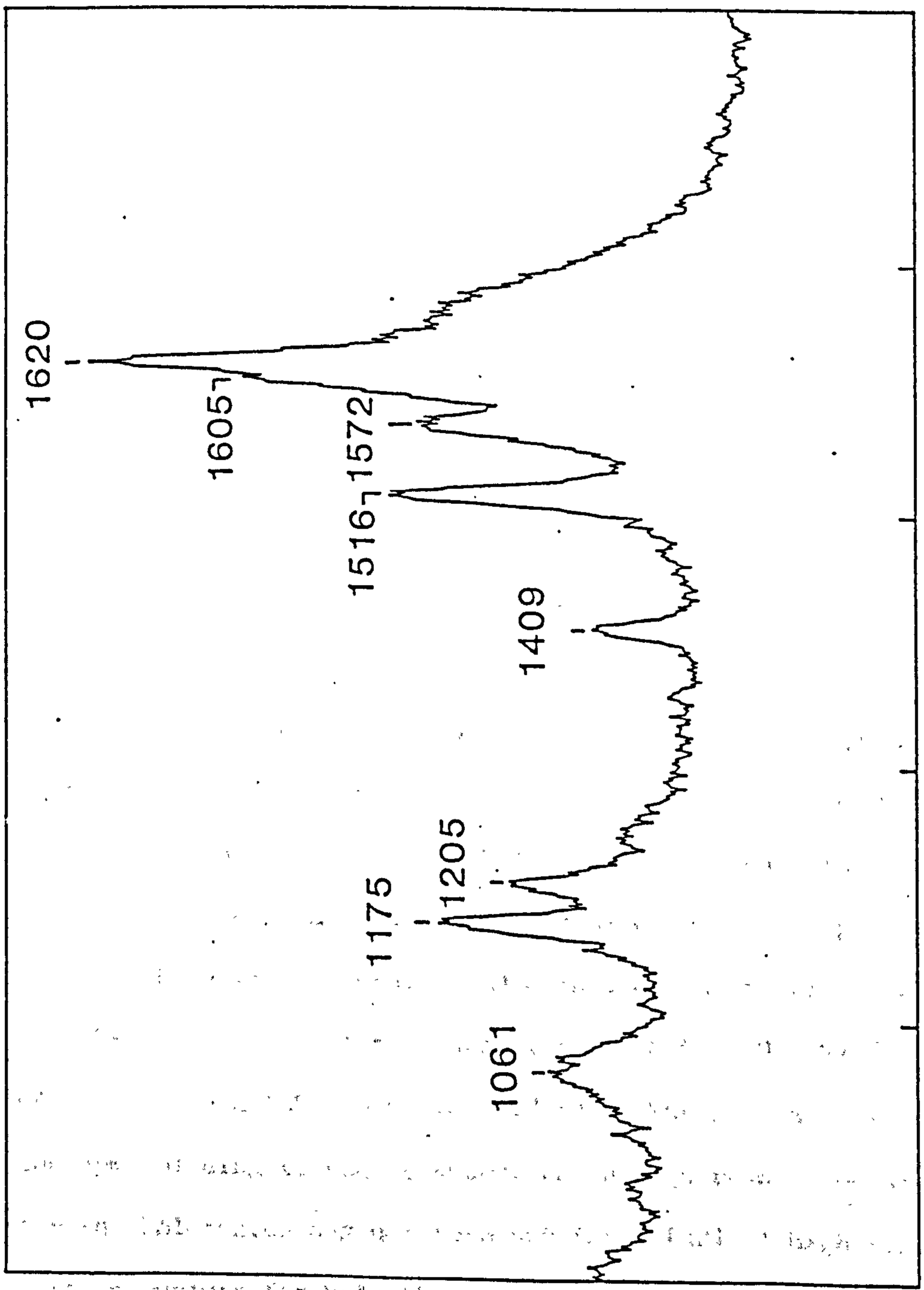

Figure 4.10 244 nm-excited RR spectrum of tyrosine (1 mM, pH 6), obtained using *ca.* 1 mJ laser pulse energy.

4.4.2 Coenzyme binding: 260 nm study

The RR spectrum of NAD^+ bound to GAPDH is somewhat different from that of free NAD^+ (Fig. 4.3(a) and (b)). The 1308 cm^{-1} band is upshifted to 1314 cm^{-1}, and the 1372 cm^{-1} band upshifted to 1378 cm^{-1} on binding enzyme. The 1335 cm^{-1} band remains unshifted but lowered in intensity relative to its neighbouring bands (but see previous section). The 1483 cm^{-1} and 1509 cm^{-1} bands appear little changed, although the 1483 cm^{-1} band is lowered in intensity in the bound NAD^+ spectrum. The overall spectrum of GAPDH-bound coenzyme is seen to be significantly though only subtly changed from that of the free coenzyme.

On binding LADH or YADH, the coenzyme bands are more dramatically changed. A strong new band is observed at 1325 cm^{-1}, alongside the 1335 cm^{-1} band. The 1308 cm^{-1} band becomes a weak shoulder at 1301 cm^{-1}. The 1372 cm^{-1} band is indistinct, but appears to downshift slightly (1-3 cm^{-1}). The main band in the LDH-bound NADH spectrum also appears to take this general form; the 1308 cm^{-1} band is unresolved, and the main band is centred at 1331 cm^{-1}. The MDH-bound NADH spectrum is arguably most like the spectrum of NAD^+ bound to GAPDH, shown in Fig. 4.3(b). The main band is unshifted, and the 1307 cm^{-1} band is clearly resolved (but not upshifted).

The X-ray structures and detailed conformational parameters have been determined for crystalline $Li^+.NAD^+$ [29], NAD^+ bound to GAPDH [30], and NADH bound to LADH [31]. The general form of coenzyme binding to LDH is known, but a high resolution structure for the holoenzyme has not been published [32]. A high resolution X-ray structure for holo-LDH has been determined (but not published [33]). Molecular graphics representations of the adenine binding site of LDH have been made using the new co-ordinates. The

similarity of the LDH and MDH structures allows a reasonably meaningful representation of the adenine binding site of MDH to be made by superposition of the MDH primary structure onto the LDH co-ordinates [34]. The modelling of the MDH 'structure' was performed to provide a guide to the MDH coenzyme pocket, as the most recent X-ray data for MDH [51] are not yet available. A comparison of the LDH and (postulated) MDH adenine-binding sites is made in Figs. 4.11, 4.12, 4.13 and Table 4.5.

NAD^+ (and NADH) binds to all the above dehydrogenases in an 'open', extended conformation [32]. This is in contrast to the generally accepted solution conformation, where the open form is in equilibrium with a folded (ring-stacked) conformer [35,36]. Some of the changes in coenzyme spectra on binding to enzyme could be due to this shift in conformation from predominantly folded (in solution) to entirely open (in enzyme). In particular, changes in overall intensity might be expected, as the loss of ring stacking could give rise to hyperchromism. The solution equilibrium is thought to be shifted in favour of the open form at high temperatures (above 70°C [36]). RR spectra of NADH at both 20 and 75°C were found to be virtually identical, in both relative and absolute intensities, and in band positions. This is in general agreement with the results of Grygon and Spiro [19], who studied the effects of adenine (A) and thymine (T) base stacking on the UVRR spectrum of adenine. Little change was observed in the positions of bands, or in relative intensities when adenine was stacked with thymine. However, strong Raman hypochromism was observed, suggesting that the A-T stacking interaction is still much greater than between the adenine and nicotinamide rings of NADH. Alternatively, the evidence for a significant change in the amount of stacking in NADH accompanying

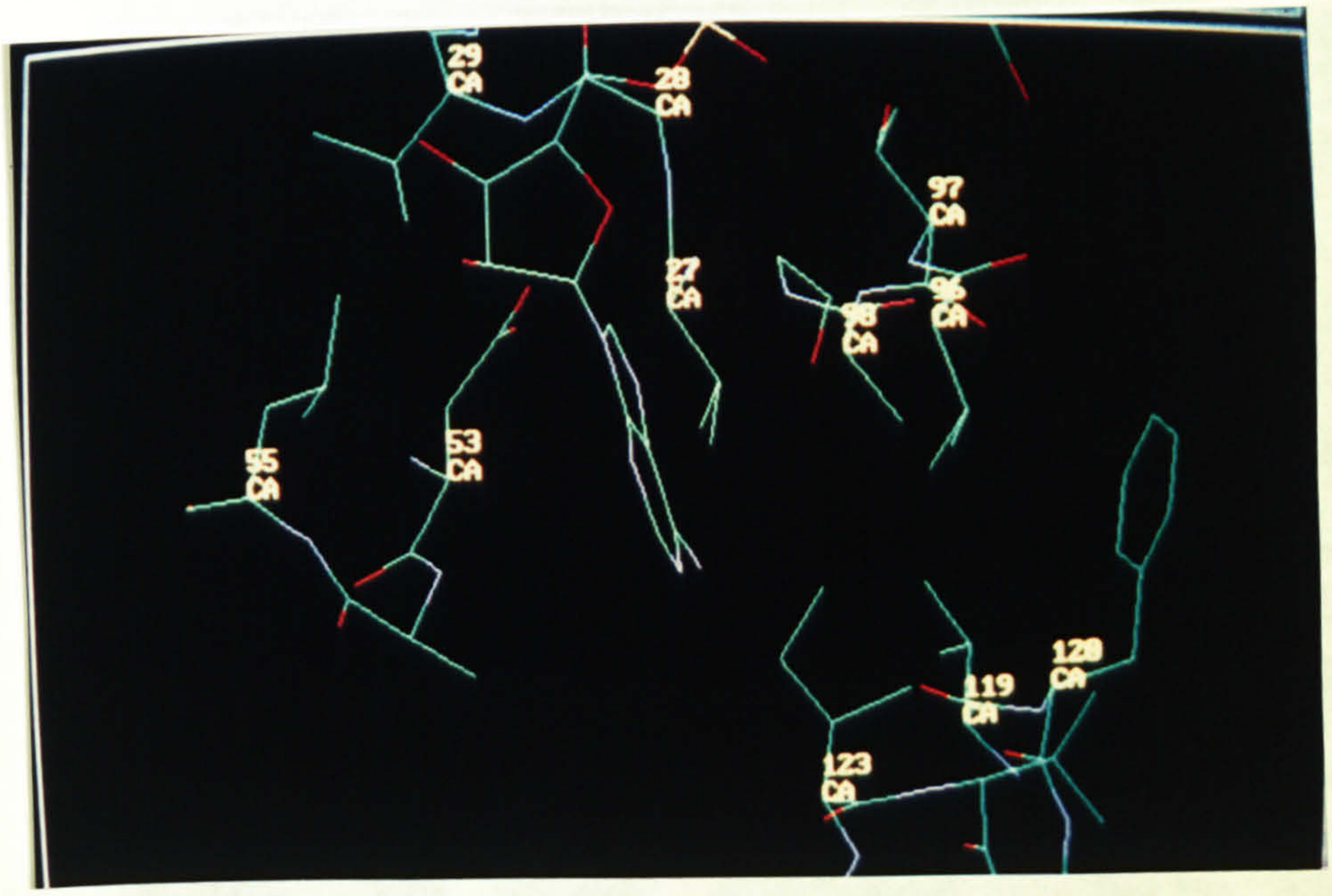

Figure 4.11 Molecular graphics representation of LDH (upper) and MDH (lower) adenine binding sites. View (1).

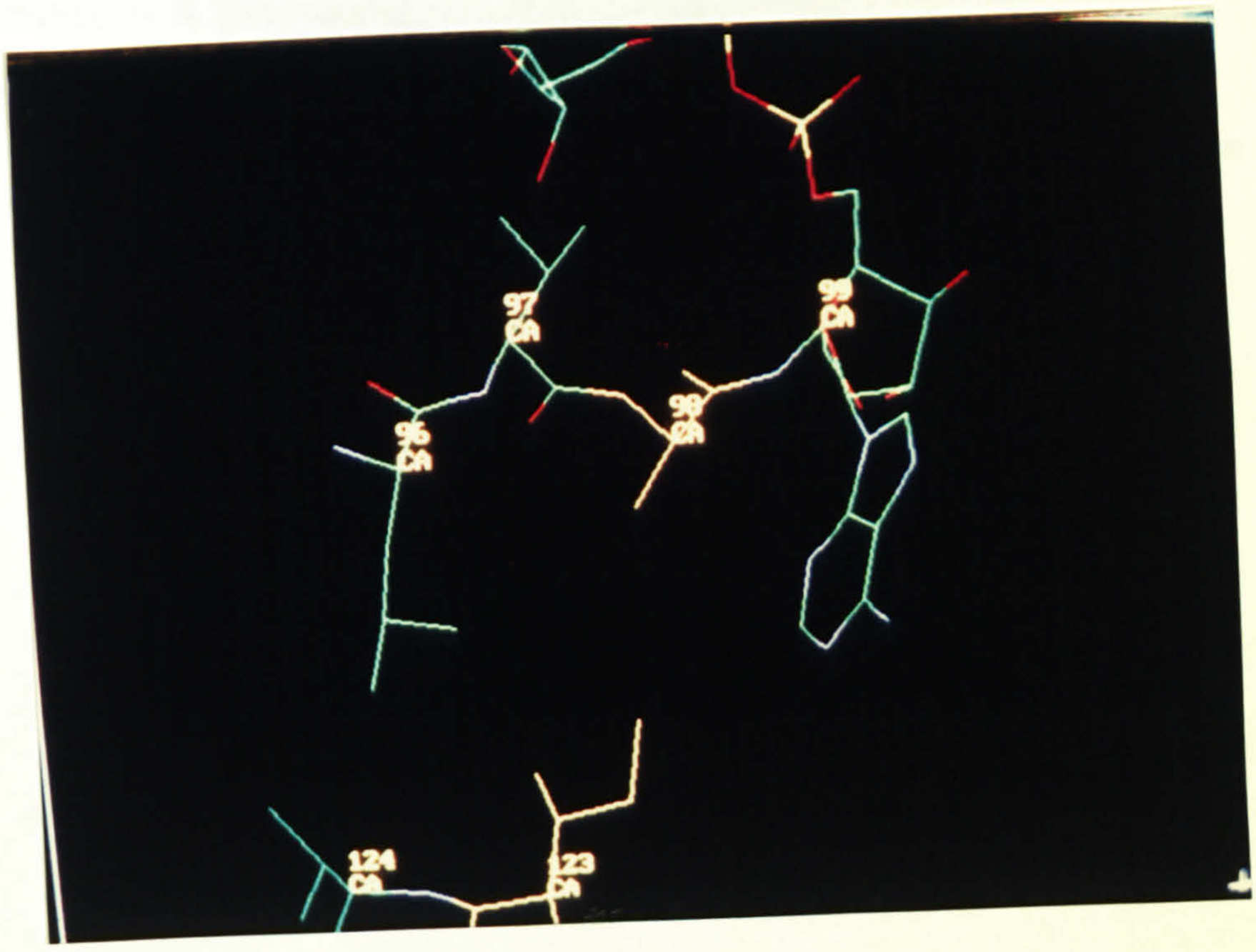

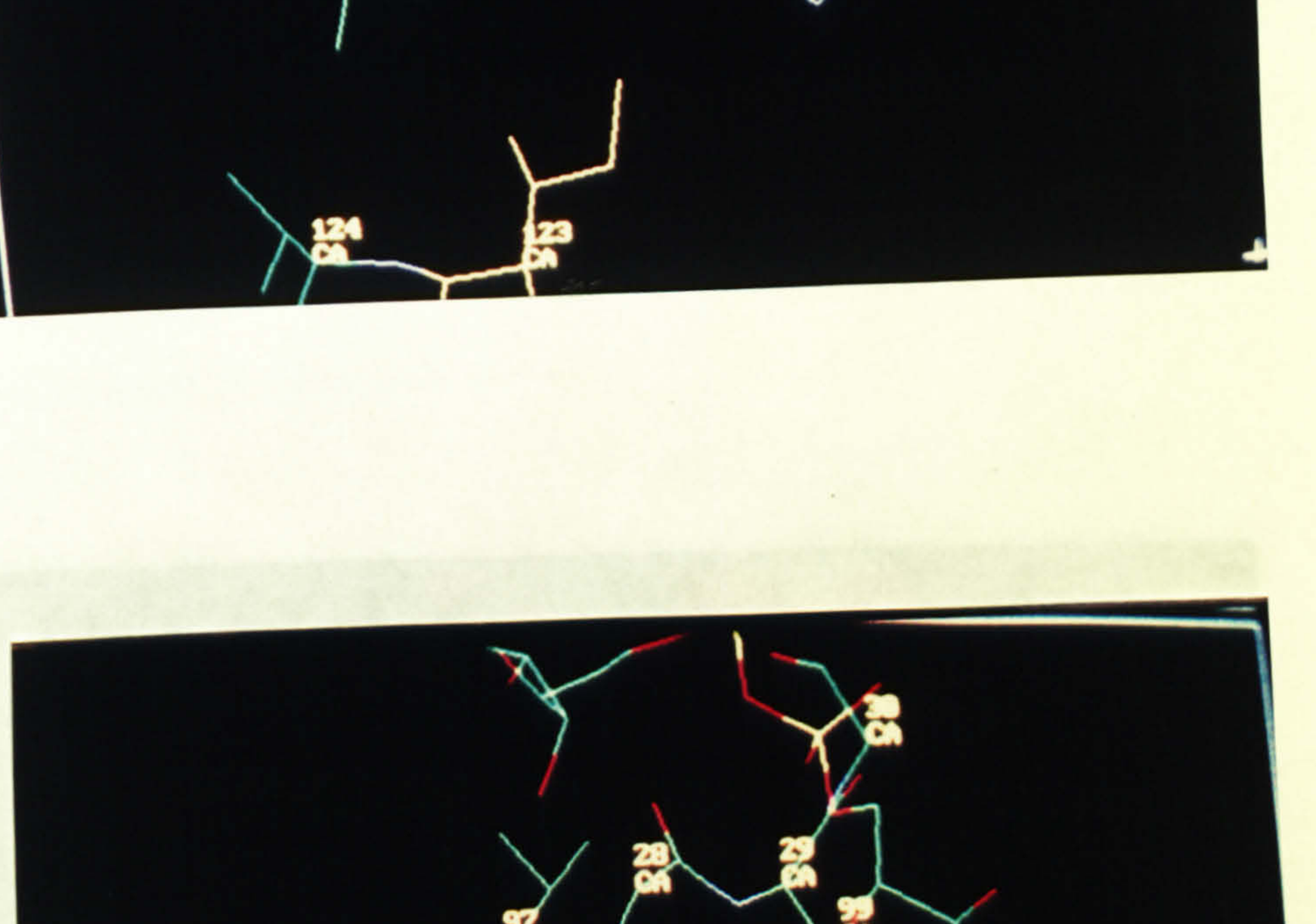

Figure 4.12 Molecular graphics representation of LDH (upper) and MDH (lower) adenine binding sites. View (2). In LDH, two residues (Ile and Ala) are shown in gold.

Table 4.5 Estimates of selected protein - coenzyme distances (in Å) in MDH[a]

Adenine	Ser (O)	Gln (O or N) amide
N_1	3.5	2.7
N_3	4.3	3.4
N_{10}	4.2	4.8
N_7	5.1	6.0
N_9	5.4	5.6

[a] The distances shown are estimated from the molecular graphics representation, and are not taken from an X-ray structure.

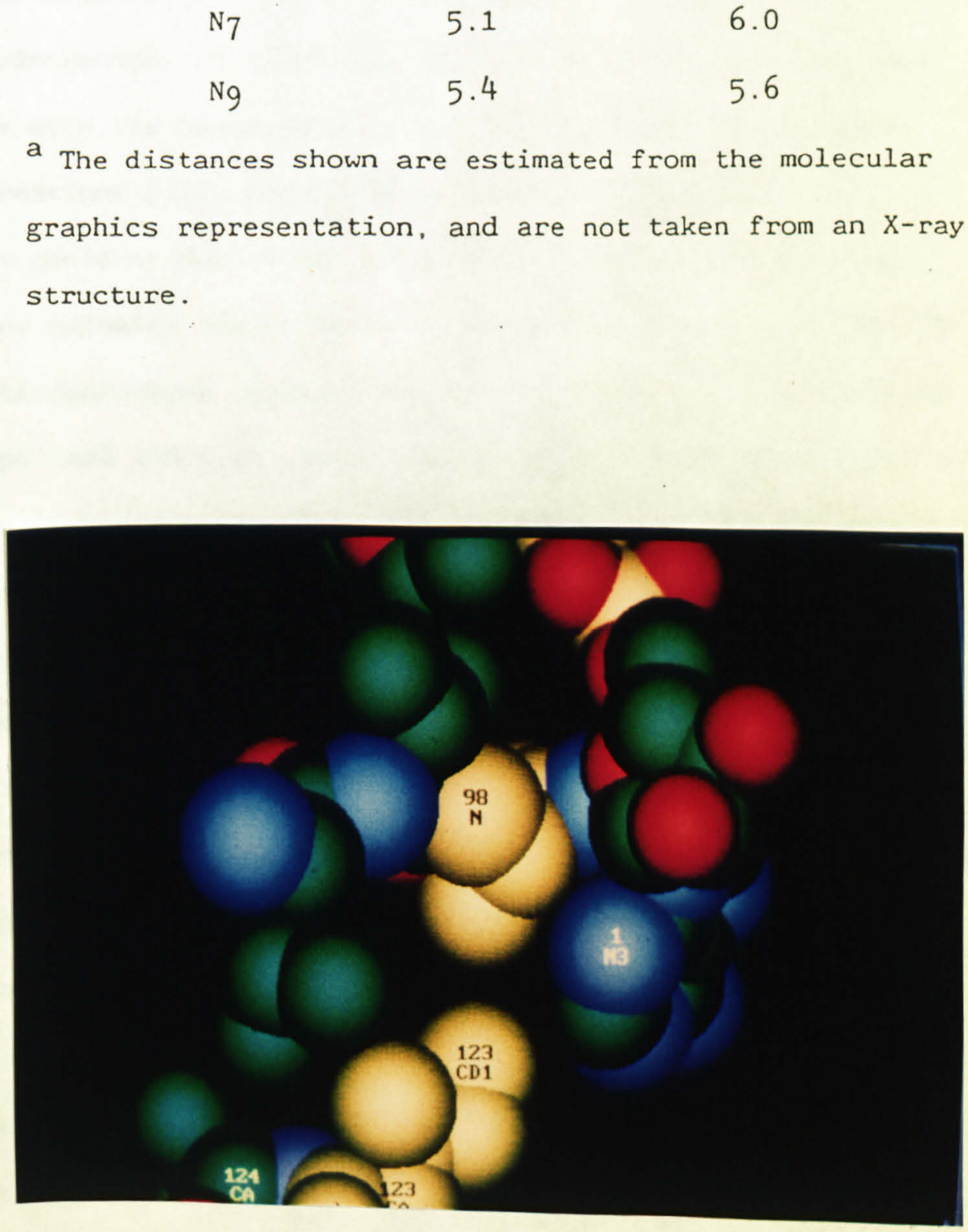

Figure 4.13 Space filling representation of LDH adenine binding site, view (2).

the temperature change from 20 to 75°C [36] could be incorrect.

In $Li^+.NAD^+$ crystals, both the adenine and nicotinamide heterocycles are in anti orientation (χ = 30° for anti conformation, χ = -150° for a syn conformation, see Fig. 1.5) [29]. This conformation is also approximately assumed by the coenzyme in LADH, LDH and MDH, which are A-type dehydrogenases. In GAPDH, the nicotinamide ring is in a syn orientation and the enzyme is called a B-type dehydrogenase. In solution, there is evidence from nmr that NAD^+ exists with its nicotinamide ring in a 2:1 ratio of syn and anti conformations [37]. Accordingly, some of the RR spectral differences could be due to the differences in nicotinamide ring orientation. Assuming the solution spectrum is that of a 2:1 mix of syn and anti conformers, then in the simplest view, a superposition of 1 'A-type' and 2'B-type' bound coenzyme spectra should produce a free coenzyme spectrum. This is clearly not the case, as one might expect considering the remoteness of the conformational change from the 260 nm RR active centre.

Recent normal Raman (NR) studies of NADH bound to LDH and LADH have been interpreted as showing protonation of the adenine N_3 nitrogen atom on binding to enzyme [38]. The NR spectra, produced by careful subtraction of the apoenzyme spectrum from the holoenzyme spectrum, are quite different from the corresponding RR spectra presented in this chapter. There are some general similarities; for example, a weak feature at 1325 cm^{-1} appears in the NR spectrum on binding to enzyme. However, the 1335 cm^{-1} band, which persists as a strong band in all the RR spectra (except in that of LDH, where it shifts) completely disappears in the NR spectra. It is difficult to reconcile these two widely differing results, and perhaps it is reasonable to be sceptical about the accuracy of the NR data in

reporting the complete disappearance of this band. Being the strongest band in the RR spectrum allows clear distinction from protein bands, in contrast to the NR spectra, where the band is weak.

The NR data have been interpreted as indicating protonation of adenine on binding to enzyme [38]. The evidence cited for protonation is the observed change in the 1300-1400 cm^{-1} region of the spectrum; the loss of the 1335 cm^{-1} band and the appearance of weak features at 1325 and 1340 cm^{-1}. When the adenine ring of NAD^+ is protonated at N_1 (at pH 3.9 or less), substantial changes occur in this region of the spectrum (see Fig. 4.14 and ref. [25]). Since the changes observed in the NR spectra on N_1 protonation were not exactly the same as the changes observed on enzyme binding, the authors proposed that N_3, and not N_1, was protonated. They indicated the possibility of forming a stabilising salt bridge between Asp (COO^-) and the protonated N_3. However, there are no Raman data for NAD^+ (or NADH) where N_3 is protonated, as N_3 is not protonated until below pH 1 [39](see Fig. 4.15 for pK_a values for the closely related molecule, ADP). Although changes in pKa's of groups buried in enzymes are well documented, a change of pKa of 8 or more units (the LADH NR experiments were conducted at pH 9.6) is extremely unlikely. The proposed protonation of adenine at N_3, is therefore a poor explanation of the observed spectral changes.

In agreement with the NR data, the RR data do not support N_1 protonation. The similarities with the protonated spectra (compare the band in Fig. 4.14 at 1329 cm^{-1} with the band in Fig. 4.4(b) at 1325 cm^{-1}) could perhaps indicate specific hydrogen bonding between adenine and protein. Deng *et al.* [38] have suggested that N_3 hydrogen bonding to a protonated Asp (COOH) residue is an

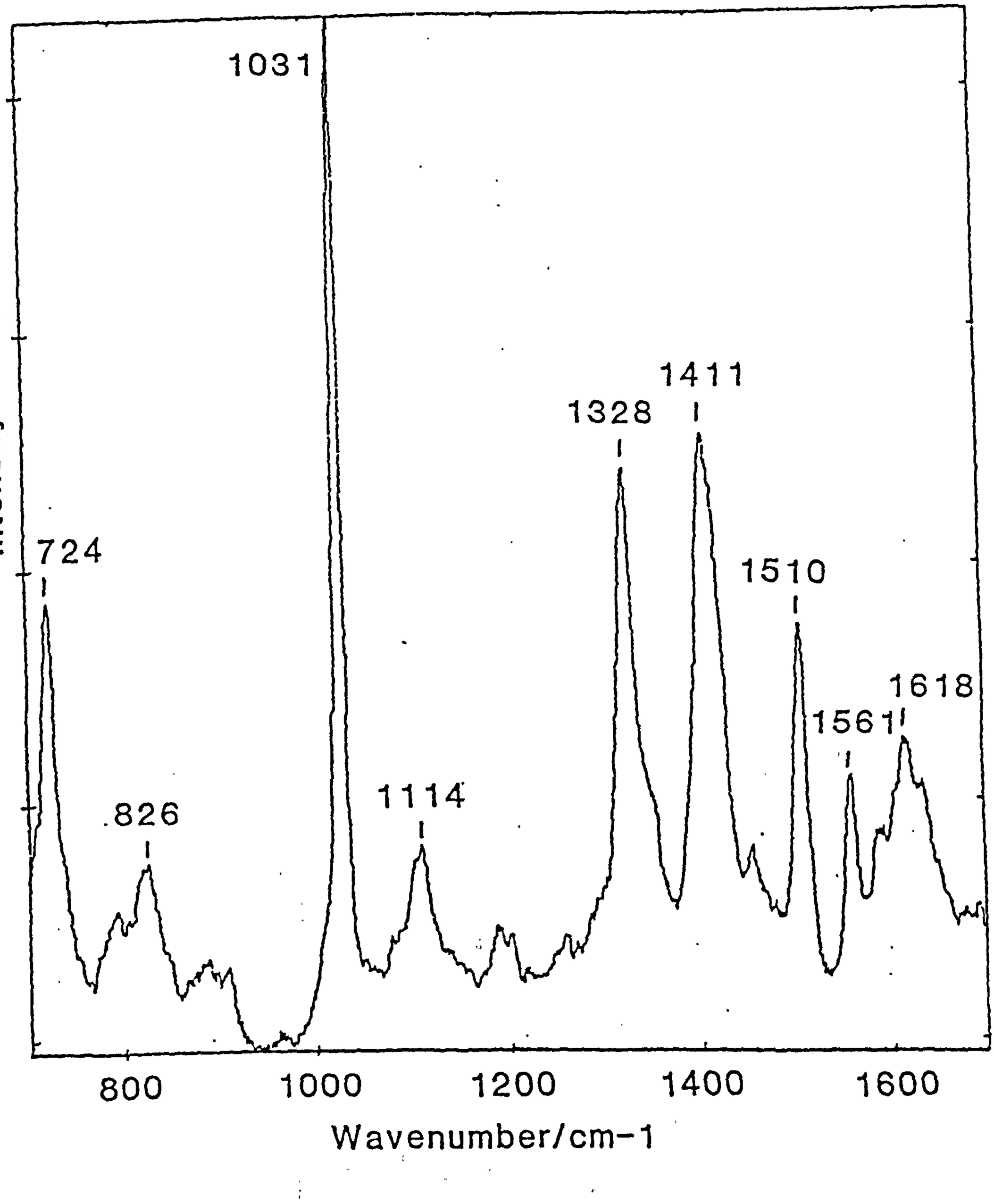

Figure 4.14 NR spectrum of NAD^+, 50 mM, pH 2-3. The spectrum was recorded using the Spex instrument, 488 nm-excitation and a spectral slit width of *ca.* 5 cm^{-1}. The wavenumber values have been corrected (see Figure 3.3).

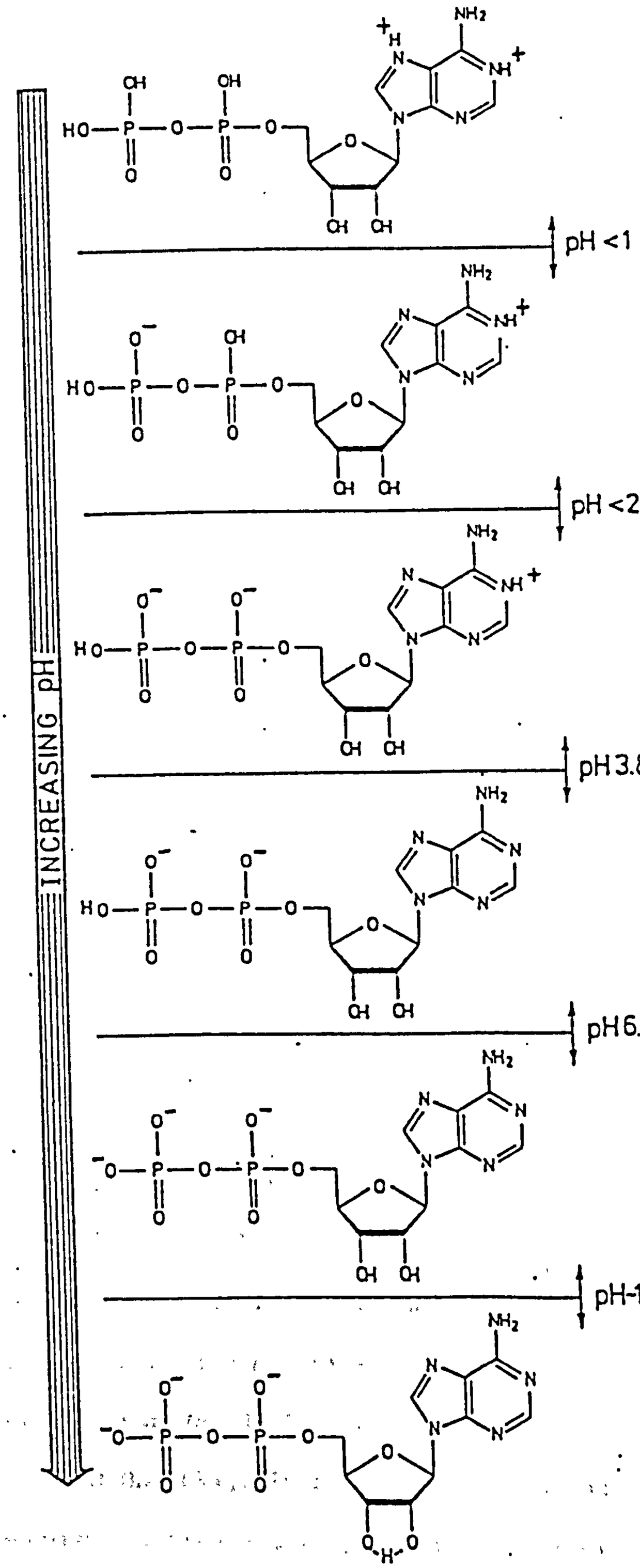

Figure 4.15 pK_a values and sites of protonation for ADP. From ref. [39].

alternative to protonation. The pKa of the Asp residue would need to shift to pKa >9.6 (for LADH), which again is well outside the normally observed range in proteins of pKa 3.0 to 4.7 [40]. Hydrogen bonding to N_1 is an alternative possibility. However, UVRR studies of N_1 hydrogen bonded adenine in nucleic acid duplexes do not show similar spectral changes to those observed in NAD^+ and NADH on binding to enzyme [17,19]. In the nucleic acid experiments, the adenine band at 1338 cm^{-1} is unchanged, the band at 1310 cm^{-1} shifts to 1305 cm^{-1}, and the band at 1374 cm^{-1} shifts up to 1380 cm^{-1}. No new band is observed at 1325 cm^{-1} that could be characteristic of N_1 hydrogen bonding. The changes that are observed are not strikingly similar to the changes observed on coenzyme binding to the enzymes studied here, and may be largely due to stacking interactions, not hydrogen bonding.

The X-ray structure of GAPDH has indicated hydrogen bonding to N_1 and N_{10} (NH_2) of adenine [30]. In LADH, N_{10} may be hydrogen bonded to Asp 273 and/or Arg 271 [31]. Asp 223, which is conserved in other dehydrogenases, may hydrogen bond to both O2 of adenine ribose, and to an adenine ring nitrogen. The latter contact is not specified by Eklund *et al.* [31], but could be to N_7 or possibly (as Deng *et al.* suggest [38]) to N_3. In LDH, the conserved Asp residue (Asp 53) is also close to the adenine ring, and may hydrogen bond, see Fig. 4.11 [34]. The molecular graphics representation of MDH highlighted a possible important difference between the adenine binding sites of LDH and MDH [34]. In LDH, residues 98 and 123 are hydrophobic (isoleucine and alanine, respectively), whilst in MDH they are relatively hydrophilic (glutamine and serine). This difference can be seen in Figs. 4.11 and 4.12. In MDH, the serine oxygen is close to adenine N_1 (3.5Å), and the glutamine O or N (of

the amide) is close to N_1 and N_3 (2.7Å to N_1, 3.4 to N_3); all the pertinent distances are given in Table 4.5. Whilst these unconfirmed 'structures' must be viewed critically, there is a strong possibility for hydrogen bonding in MDH which is not present in LDH.

Clearly, a degree of hydrogen bonding to adenine is likely to be present in all the enzymes studied. However, it is not easy (or indeed even possible) to correlate the observed RR spectral changes with differences in hydrogen bonding. In addition, other UVRR data appear to show that hydrogen bonding has only a small effect on the RR spectrum of adenine. Of course, adenine (in NAD^+) would be hydrogen bonded to solvent when not bound to enzyme, and it is possible that the hydrogen bonds which it makes to enzyme are of similar strength to the bonds to solvent.

The positive charge of Arg 271 in LADH, which is close to the adenine ring, could be the cause of the particular spectral changes observed when NADH binds to LADH. This can be discounted on inspection of the YADH primary structure [41]. YADH does not have a positively charged residue in the position of Arg-271. However, the spectrum of NADH bound to YADH is closely similar (apart from the contribution from free NADH) to the corresponding NADH spectrum when bound to LADH. Thus, the presence of the 1325 cm^{-1} shoulder (in both Fig. 4.4(c) and (b)) cannot be due to this charge effect.

The polarity of the adenine binding pocket varies quite widely between the enzymes studied, and may be a major factor in determining the coenzyme RR spectrum. LADH and LDH provide a generally more hydrophobic adenine binding environment for coenzyme than do GAPDH and MDH. Consistent with this, the spectra of the coenzyme when bound to MDH, and particularly GAPDH, resemble the solution spectra more closely than do the corresponding LADH and LDH

spectra. Deng *et al.* have recorded the NR spectra of 9-ethyladenine (a suitable model) in various solvents, including water, propanol, chloroform and p-dioxane [38]. The spectra were said to be very similar, the spectrum recorded in chloroform being the most changed. In chloroform, the 1338 cm^{-1} band shifted to 1330 cm^{-1}, the 1368 cm^{-1} band to 1360 cm^{-1}, and the 1311 cm^{-1} to 1303 cm^{-1}. The authors interpreted their results as an indication of the lack of importance of polarity in determining the NR spectrum. However, these shifts show some similarities to those observed in the RR spectra when NADH binds to ADH and LDH. It is conceivable that polarity changes have a more marked effect on the RR spectra than on the NR spectra, and that the RR spectra obtained reflect largely the polarity differences experienced when the coenzyme binds to different enzymes.

4.4.3 Acylenzyme formation: effects on 240 nm RR spectra.

The spectra in Fig. 4.7 show no differences that could be attributable to a thioester vibration of the acylenzyme intermediate. Despite the proximity of the excitation wavelength to the estimated absorption maximum of the thioester group, the intensity of the thioester absorption is still extremely low ($\epsilon = 3x10^3\ M^{-1}cm^{-1}$ [42]) compared with combined absorption of NAD^+ and GAPDH ($\epsilon = 3x10^5\ M^{-1}cm^{-1}$). Thus, it would be surprising if the thioester band could be resolved above the noise level in these spectra. This is in contrast to the successful study of the thioester acylenzyme intermediate in papain, which showed a new band in the acylenzyme spectrum at 1678 cm^{-1}, attributed to the thioester carbonyl vibration [43]. In papain, the problems of absorbtion by the protein are much reduced, as papain is a much smaller protein

than GAPDH, and does not need NAD^+ to drive the formation of acylenzyme.

Some changes in relative intensities of trp and tyr bands are observed on forming the acylenzyme. The 1206 cm^{-1} band of tyrosine decreases in intensity relative to other tyr bands at 1174 and 1620 cm^{-1}. The 1007 cm^{-1} band of trp appears to increase slightly in relative intensity on forming the acylenzyme. The changes observed are not consistent with the photodecomposition effects noted by Johnson *et al.* [8]. The 1007 cm^{-1} trp band intensity increases in the spectrum of the trp photodecomposition product as the 1549 cm^{-1} (1557) band decreases. In the acylenzyme the 1007 cm^{-1} band increases as the 1557 cm^{-1} band remains unchanged (or increases slightly), and the 1510 cm^{-1} band, another decomposition indicator, decreases. Similarly, none of the 1206, 1620, and 1174 cm^{-1} bands of tyr are associated with photoproduct peaks, so relative intensities of these bands would not be expected to vary, except under conditions of change in environment and bonding.

In GAPDH, tyr-311, which is conserved in all dehydrogenases, is present in the active site pocket. No tryptophan residues appear to be important. The structure of lobster GAPDH at 2.9 Å resolution indicated hydrogen bonding between tyr-311 and the essential His-176 residue [44], while the structure of bacterial GAPDH at 1.8 Å resolution indicated no such bonding [30]. The RR data can be tentatively interpreted as showing that one or more tyr residues are undergoing some change on forming the acylenzyme. However, it is impossible to determine whether it is the active site tyr that is perturbed, or whether it is a more general structural change affecting one or more of the remaining eight tyr residues.

4.4.4 Coenzyme binding: effects on GAPDH

Structures of apo- and holo- GAPDH from thermophilic bacteria give strong evidence for NAD^+-induced sequential conformational changes in the overall tertiary and quaternary structure [30, 45, 46]. The similarity of the two spectra in Fig. 4.8 may be interpreted as showing that the aromatic amino acid residues (14 phe, 9 tyr and 2 trp per subunit) are not significantly perturbed by the conformational changes accompanying binding, or by direct interactions with coenzyme. Raman bands of phenylalanine have not previously been found to be sensitive to environmental changes in studies of other proteins, so the lack of spectral changes here may not be significant. The ν 12 (1000 cm^{-1}) band of phenylalanine has recently been shown to be sensitive to environmental effects in the RR spectra of proteins [11]. However, this band is not strongly enhanced in the RR spectra shown in Fig. 4.8, and is partly overlapped by the tryptophan band at *ca.* 1010 cm^{-1}. Two phe residues (phe 34 and 99) clearly do contribute to the hydrophobic character of the adenine binding pocket. Tyrosine bands in UVRR spectra are sensitive to hydrogen bonding and environment changes; however, only the average tyrosine state is shown in the UVRR spectra. Since there are nine tyr residues per subunit, changes accompanying coenzyme binding would have to be substantial before changes could be accurately pinpointed in the UVRR spectra. In fact, tyr and trp residues are not found in the coenzyme binding site of GAPDH, nor are they implicated as being an integral part of the conformational change observed in the X-ray studies.

4.4.5 NADH binding to LDH: 350.6 nm RR study

The NR data published for NADH and NAD^+ bound to LDH show

marked differences in the nicotinamide bands of the coenzyme spectra on binding enzyme [38]. This would again appear to be in direct contrast to the results obtained from the 350.6 nm excited RR spectra, where the bound and free NADH spectra appear to be generally very similar. The NR data are claimed to show the complete loss of a strong nicotinamide band at 1546 cm^{-1}, and of a weaker band at 1458 cm^{-1}. This is not the case in the RR spectra. It might be expected that the nicotinamide bands, especially in the oxamate-inhibited complex, would show more dramatic differences than have been observed in these RR spectra.

The limiting factors in the collection of the RR data are the high fluorescence, low absorption strength, and photodecomposition. Tuning to the shifted absorption maximum (325 nm) or reducing fluorescence would probably allow spectra of adequate quality to be collected before photodecomposition. The enzyme-accelerated photodecomposition mechanism is unknown, and hitherto not reported. The photodecomposition of NADH in solution has been studied by Raman scattering [47] and by transient absorption methods [48]. While there is some controversy over the exact mechanism (mono- or bi- photonic), and quantum yield, the general process is:-

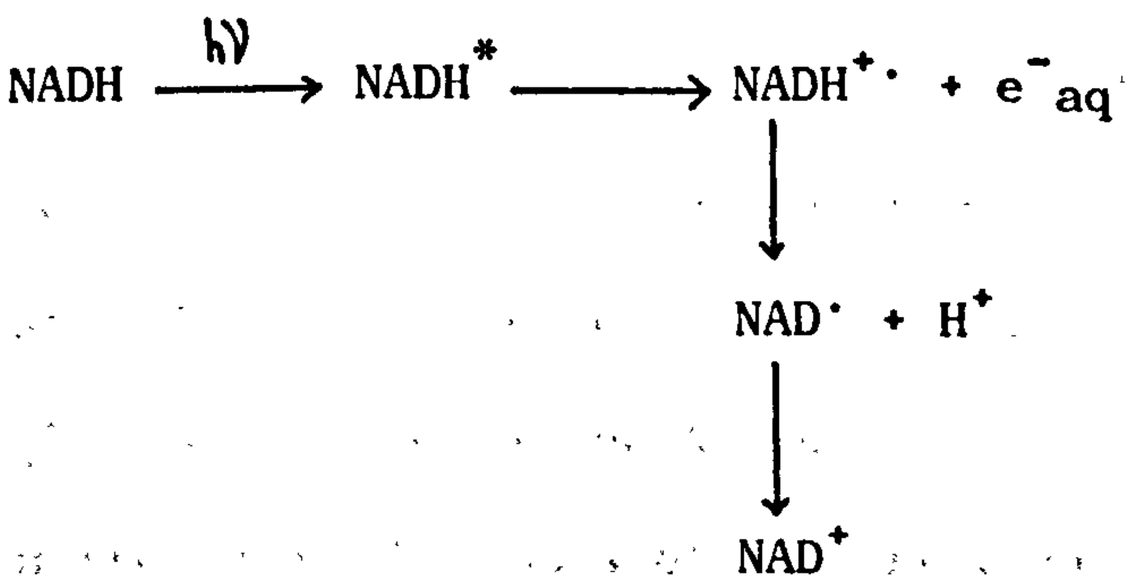

The accelerated rate of photodecomposition of NADH bound to

LDH (and GAPDH) could indicate either (a) some sort of effect of the binding pocket (e.g. changed polarity or conformation) on NADH or (b) a completely different mechanism. In view of the observed variation in rates of decomposition it appears quite likely that there is a new mechanism, involving some other species. The species could be a residue in the enzyme or a contaminant of the solution.

4.5 CONCLUSIONS

4.5.1 Coenzyme binding to dehydrogenase enzymes: adenine environment and bonding.

The following conclusions can be drawn from the 260 nm-UVRR study of NAD^+ and NADH binding to dehydrogenases.

(1) Although there are problems with fluorescence, the spectra of bound coenzyme are largely free from interference from the enzyme spectra, in contrast to the NR spectra.

(2) The factors which may influence the coenzyme spectrum when bound to the dehydrogenase enzymes are numerous, and further studies would be desirable to establish further the relationships between coenzyme spectra, and structure, environment and bonding.

(3) The conformation of the coenzyme when bound to the different enzymes LADH, LDH, GAPDH and MDH does not seem to have a large effect on the 260-nm RR spectrum. Neither the loss of ring stacking, nor the A/B conformational difference (see section 4.4.2) shows a significant influence on the RR spectrum of the adenine moiety.

(4) Protonation of the N_3 (or N_7) nitrogen of adenine is extremely unlikely on the basis of the unusually large pK_a shifts that would be required. Similarly, protonation of Asp-53 in LDH (and corresponding Asp residues found in other dehydrogenases), and

subsequent hydrogen bonding to N_3 or N_7 is unlikely due to the large pK_a shift required. It is possible that a water molecule could fit between adenine and the Asp residue, and hydrogen bond to both.

(5) Hydrogen bonding to adenine N_1 and N_{10} is possible in GAPDH, MDH, and LADH (N_{10} only). However, there is little evidence to suggest that the RR spectral changes reflect differences in hydrogen bonding. In UVRR studies of adenine hydrogen bonding through N_1 and N_{10} to thymine or uracil, effects on adenine ring modes were small, and not similar to the effects observed in the coenzyme UVRR spectra discussed in section 4.4.2.

(6) Coenzyme environment polarity differences do seem to correlate quite well with differences in the UVRR spectra. LADH and LDH have considerably more hydrophobic adenine binding environments than GAPDH and MDH. Consistent with this, the reported NR spectrum of 9-ethyladenine in chloroform is similar to the spectrum of NADH bound to LADH and LDH.

4.5.2 Effects of coenzyme and substrate binding on the UVRR spectra of GAPDH.

While it has been shown that many UVRR bands of aromatic amino acids are sensitive to changes in their environment and bonding [10, 11] it is clear, from the 220 and 240 nm-RR spectra presented in this chapter, that there are problems with overall sensitivity and selectivity. The recent work of Fodor *et al.* [5] established the Raman excitation profiles of many bands of the aromatic amino acids between 192 and 240 nm. This will be useful in future studies for choosing a suitable excitation wavelength to yield information on a particular type of amino acid. In the study of GAPDH, the abundance of phe and tyr residues (14 and 9 per

subunit, respectively) makes the task of looking for changes in their spectra difficult. The assignment of UVRR spectral changes to the environment or bonding differences of a particular residue is almost impossible, unless there is some other evidence for change (e.g. from crystallographic studies). The combination of UVRR with site-directed mutagenesis techniques would be a very powerful tool in determining the precise environment and bonding of particular amino acid residues in proteins.

4.5.3 Coenzyme binding to LDH: nicotinamide environment and bonding.

From the preliminary results presented in this chapter (section 4.3.5), the study (by UVRR) of the nicotinamide moiety when bound to enzymes looks promising, if difficult. The UVRR spectrum of the nicotinamide moiety bound to LDH has no spectral contribution from LDH. Problems of fluorescence would be reduced by using an excitation wavelength closer to the absorption maximum of the enzyme-bound nicotinamide moiety. The nicotinamide moiety of NADH is the 'active' part of the coenzyme, and must undergo significant changes on binding to certain enzymes, especially when a substrate (or analogue) is also bound. This is already partly proved by the large shifts that can be induced in the nicotinamide absorption - for example on binding to LADH or to LDH and oxamate.

4.6 REFERENCES

[1] I.Harada and H.Takeuchi in *"Advances in Spectroscopy, Vol. 13: Spectroscopy of Biological Systems"* Eds. R.J.H.Clark and R.E.Hester (Wiley, Chichester, 1986).

[2] (a) R.P.Rava and T.G.Spiro, *J. Am. Chem. Soc.* **106**, 4062 (1984).

(b) R.P.Rava and T.G.Spiro, *J. Phys. Chem.* **89**, 1856 (1985)

[3] C.R.Johnson, M.Ludwig, S.O'Donnell, and S.A.Asher, *J. Am. Chem. Soc.* **106**, 5008 (1984).

[4] R.A.Copeland and T.G.Spiro, *Biochemistry* **24**, 4960 (1985).

[5] S.P.A.Fodor R.A.Copeland, C.A.Grygon and T.G.Spiro, personal communication.

[6] S.A.Asher, M.Ludwig, and C.R.Johnson, *J. Am. Chem. Soc.* **108**, 3186 (1986).

[7] D.S.Caswell and T.G.Spiro, *J. Am. Chem. Soc.* **108**, 6470 (1986).

[8] C.R.Johnson, M.Ludwig, and S.A.Asher, *J. Am. Chem. Soc.* **108**, 905 (1986).

[9] R.A.Copeland and T.G.Spiro, *Biochemistry*, **26**, 2134 (1986).

[10] R.P.Rava and T.G.Spiro, *Biochemistry*, **24**, 1861 (1985).

[11] P.G.Hildebrandt, R.A.Copeland, T.G.Spiro, J.Otlewski, M.Lasowski, and F.G.Prendergast, *Biochemistry* **27**, 5426 (1988).

[12] E.G.Rodgers and W.L.Peticolas, *J. Raman Spectrosc.* **9**, 372 (1980).

[13] W.D.Bowman and T.G.Spiro, *J. Raman Spectrosc.* **9**, 369 (1980).

[14] W.L.Kubasek, B.Hudson and W.L.Peticolas, *Proc. Natl. Acad. Sci. (USA)* **82**, 2369 (1985).

[15] S.P.A.Fodor, R.P.Rava, T.R.Hays and T.G.Spiro, *J. Am. Chem. Soc.* **107**, 1520 (1985).

[16] M.Tsuboi, Y.Nishimura, A.Y.Hirakawa and W.L.Peticolas in *"Biological Applications of Raman Spectroscopy, Volume 2: Resonance Raman Spectra of Polyenes and Aromatics"*, Ed. T.G.Spiro (Wiley, New York, 1988).

[17] S.P.A.Fodor and T.G.Spiro, *J. Am. Chem. Soc.* **108**, 3198 (1986).

[18] B.Jolles, L.Chinsky, and P.Y.Turpin, *Nuc. Acids Res.* **13**, 2075 (1985).

[19] C.A.Grygon and T.G.Spiro, personal communication.

[20] C.A.Grygon, D.F.Davis, T.G.Spiro and J.R.Fresco, personal communication.

[21] B.L.Horecker and A.Kornberg, *J. Biol. Chem.* **175**, 385 (1948).

[22] O.P.Malhotra and S.A.Bernhard, *J. Biol. Chem.* **243**, 1243 (1968).

[23] K.Dalziel, *The Enzymes (3rd Ed.)* **11**, 40 (1975).

[24] J.I.Harris and M.Waters, *The Enzymes (3rd Ed.)* **13**, 30 (1975).

[25] K.T.Yue, C.L.Martin, D.Chen, P.Nelson, D.L.Sloan and R.H.Callender, *Biochemistry* **25**, 4941 (1986).

[26] R.S.Chittock, C.W.Wharton, J.C.Austin and R.E.Hester, *Biochem. Soc. Trans.* **16**, 49 (1987).

[27] A.R.Clarke, D.B.Wrigley, W.N.Chia, D.Barstow, T.Atkinson and J.J.Holbrook, *Nature* **324**, 699 (1986).

[28] M.D.Levenson, *"Introduction to Nonlinear Laser Spectroscopy"* (Academic Press, 1982).

[29] B.S.Reddy, W.Saenger, K.Muhlegger and G.Weimann, *J. Am. Chem. Soc.* **103**, 907 (1981).

[30] T.Skarzynski, P.C.E.Moody and A.J.Wonacott, *J. Mol. Biol.* **193**, 171 (1987).

[31] H.Eklund, J.-P.Samama and T.Alwyn-Jones, *Biochemistry* **23**

[32] M.G.Rossmann, A.Liljas, C.-I.Branden and L.J.Banaszak, *The Enzymes (3rd Ed.)* **11**, 61 (1975).

[33] J.J.Birktoft and L.J.Banaszak, personal communication to A.R.Clarke.

[34] A.R.Clarke (Bristol University), personal communication.

[35] W.A.Catterall, D.P.Hollis, and C.F.Walter, *Biochemistry* **8**, 4032 (1969).

[36] N.J.Oppenheimer, L.J.Arnold, and N.O.Kaplan, *Biochemistry* **17**, 2613 (1878).

[37] B.Birdsall, N.J.M.Birdsall, J.Feeny, and J.M.Thornton, *J. Am.*

Chem. Soc. **97**, 2845 (1975).

[38] H.Deng, J.Zheng, D.Sloan, J.Burgner, and R.H.Callender, *Biochemistry* **28** 1525 (1989).

[39] W.Saenger, *"Principles of Nucleic Acid Structure"* p.108 (Springer-Verlag 1984).

[40] A.White, P.Handler, and E.L.Smith, *"Principles of Biochemistry"*, 5^{th} *Ed.* p.120 (McGraw-Hill 1973).

[41] H.E.Jornvall, H.Eklund, and C.-I.Branden, *J. Biol. Chem.* **253**, 8414 (1978).

[42] B.Wladislaw, H.Viertler, and E.B.Demant, *J. Chem. Soc.* **B(1)**, 565 (1971).

[43] K.Bajdor, W.L.Peticolas, C.W.Wharton, and R.E.Hester, *J. Raman Spectrosc.* **18**, 211 (1987).

[44] D.Moras, K.W.Olsen, M.N.Sabesan, M.Buehner, G.C.Ford, and M.G.Rossman, *J. Biol. Chem.* **250**, 9137 (1975).

[45] A.J.W.Leslie and A.J.Wonacott, *J. Mol. Biol.* **178**, 743 (1984).

[46] T.Skarzynski and A.J.Wonacott, *J. Mol. Biol.* **203**, 1097 (1988).

[47] K.Bajdor, Y.Nishimura, and W.L.Peticolas, *J. Am. Chem. Soc.* **109**, 3514 (1987).

[48] L.Lindqvist, B.Czochralska, and I.Grigorov, *Chem. Phys. Lett.* **119**, 494 (1985).

[49] T.E.Smith, *Biochemistry* **5**, 2919 (1966).

[50] H.Sund and H.Theorell, *The Enzymes* (2^{nd} *Ed.*) **7**, 25 (1963).

[51] J.J.Birktoft, G.Rhodes, and L.J.Banaszak, *Biochemistry* **28**, 6064 (1989).

CHAPTER FIVE: SURFACE ENHANCED RAMAN SPECTROSCOPY OF NAD^+

5.1 INTRODUCTION

Surface-enhanced Raman spectroscopy (SERS) has proved to be an excellent tool for obtaining the vibrational spectra of molecular species at very low concentration (see chapter 1 for a resume of recent studies). Many controversies about SERS still persist, from fundamental arguments about the enhancement mechanism to more 'applied' arguments about the changes induced in species on adsorption onto metal surfaces, including the possibility of denaturation of proteins [1]. In the SERS study of NAD^+, NADH and GAPDH described in this chapter, many of these questions about SERS have been addressed, including the interpretation of SERS spectra in terms of molecular orientation and the possible denaturing effects of colloidal silver.

Other SERS studies of nucleic acids and NAD^+ have been reported [2-6], and orientations of these species at the metal surface have been suggested. The information on molecular orientation has been deduced on the basis of surface enhancement selection rules; these determine which vibrational modes of a molecule will be surface active in a particular molecular orientation. The theoretical and experimental bases for these rules have recently been reviewed [7], and it has been shown that these are, in general, considerably more complex than the corresponding rules for infrared reflectance spectra. In this chapter it is shown that the commonly used simplification of these rules may give incorrect information on surface orientation. It is also pointed out that it is impossible to determine surface orientation from SERS data where the relative intensity contributions from the charge transfer (CT) mechanism and the electromagnetic (EM) enhancement mechanism are unknown.

Since the discussion in this chapter revolves largely around the relative contributions of the SERS enhancement mechanism, a brief outline of the two major enhancement theories will be given.

Classical Raman theory treats polarisability as the proportionality constant linking the incident electric field, E, with the electric dipole, μ , induced in the molecule, viz.

$$\mu = \alpha \, . \, E \qquad \ldots.(1)$$

Raman band intensities are proportional to the square of the mean molecular polarisability derivatives associated with each of the normal modes of vibration, viz.

$$I \propto (d\alpha/dQ)^2 \qquad \ldots.(2)$$

Taken together with the direct dependence of scattering intensity on the incident light intensity (proportional to E_i^2), this provides the basis for two distinct mechanisms of surface enhancement. The SERS enhancement mechanisms are divided into those that increase E, 'electromagnetic' mechanisms, and those that increase α, 'chemical' mechanisms.

5.1.1 Electromagnetic (EM) enhancement

Many workers have developed the basic EM theory in attempts to explain the very high enhancements observed in SERS. Quantitative field enhancement factors have been calculated for spheres [8], spheroids [9], rough surfaces [10] and clusters [11]. These treatments have been reviewed in detail in [12], and most recently in [7, 13]. Strictly speaking, there are other EM theories apart from those considered here, including the image field theory, and reflectivity modulation theory. However, the most successful EM theory presented to date (that which is specific to rough surfaces) is the localised surface plasmon theory.

For small spheres (smaller than the wavelength of the incident light), the enhancement factor, G, is given by [8, 14], viz.

$$G = \left| \left(1 + \frac{2(\epsilon_i - 1)}{(\epsilon_i + 2)} \right) \left(1 + \frac{2(\epsilon_s - 1)}{(\epsilon_s + 2)} \right) \right|^2 \qquad \ldots.(3)$$

where ϵ_i and ϵ_s are the complex dielectric function of the metal with respect to the surrounding medium at incident and scattered wavelengths, respectively. Thus, enhancement is at a maximum when $\epsilon_i \simeq \epsilon_s = -2$. This condition is satisfied for silver, gold and copper with wavelengths in the visible region. The frequency for $\epsilon = -2$ is called the surface plasmon resonance frequency. This resonance frequency has been shown to depend sensitively on the shape of the spheroid (or surface feature) [8], although the simple equation (2) above does not give a dependence. Similarly, the absolute enhancement factor has been shown to depend critically on the shape of the spheroid, due to what is generally referred to as the 'lightning-rod' effect, where the E field is dramatically increased at sharp features (e.g. tips of spheroids)[9].

Using this theory, various experimental features have been predicted, including a non-specific enhancement of all adsorbed molecules, and a distance dependence of $(c/r)^{12}$, where c is the local radius of curvature and r = c + molecule to surface distance. While the distance dependence has been confirmed by spacer experiments [15], it is clear that SERS is not molecule specific. This latter inconsistency has been taken up by Pettinger in a recent paper and used as a starting point for his 'modified EM' model [16].

The modified EM model attempts to introduce a chemical nature into EM theory. An energy-transfer (ET) mechanism is proposed

(overlaying the classical EM mechanism), that enhances SERS for only those molecules that have available electronic transitions (either already existing or induced on adsorption) that can couple with the transitions of the metal. For such molecules, Pettinger derives an enhancement factor of

$$G = 0.00143.R^{-18}.\epsilon_{eff}^{-6}.\alpha_m^{6} \qquad ....(4)$$

where α_m is a function of the dielectric, ϵ, of the metal, and R is the molecule-metal distance. For 'non-excitable' molecules such as water, a different enhancement factor is derived,

$$G = 0.0127.R^{-12}.\epsilon_{eff}^{-4}.\alpha_m^{4}.\eta_{dd} \qquad ....(5)$$

where η_{dd} is a 'yield for radiative transitions' and is estimated to be *ca.* 0.01, so as to yield an enhancement factor for water of 300-1500.

Pettinger has provided some experimental evidence for his theories [17], but as yet they remain unevaluated by the SERS community. While the theory is appealing, in as much as it introduces large enhancement factors for coloured species, or species like pyridine that can create new charge-transfer transitions on chemisorption, enhancement does not depend explicitly on any properties of the molecule. It does not try to diminish the contribution from the 'true' chemical enhancement that is outlined below.

5.1.2 Chemical enhancement

It is generally believed that a distinct charge-transfer (CT) process contributes to SERS enhancement for certain molecule-metal systems. While many workers describe chemical enhancement rather loosely as a RR enhancement arising from new electronic transitions either from molecule to metal or *vice versa*

[18-20], Otto has described a process that is more specific [21]. In his model, a photon generates an electron in the sp band of the metal, above the Fermi level, and leaves a hole below the Fermi level (step 1). The electron jumps or tunnels to the molecule to form a temporary negative molecular complex (step 2). The electron jumps or tunnels back to the metal (step 3), and combines radiatively (producing Raman shifted radiation) with the electron. Chang [13] has noted that the formation of the negative ion complex by step 2 above is not a prerequisite for this mechanism of enhancement. A photoexcited electron could tunnel or jump into the first excited electronic level of the molecule (more like a molecular RR process). Since the photoexcitation of metal electrons (step 1) is much more favourable at sites of atomic scale roughness [21], then the roughness requirement for SERS is also explained.

Recent experimental work has been undertaken to estimate the relative contributions of the charge-transfer (CT) and EM effects [18, 22-24]. There must be no absolute answer for all molecule-metal systems, as there is clearly a 'spectrum' of cases, from the extreme case of water, where there appears to be little possibility for CT enhancement, to the strongly enhanced pyridine on silver (for which a distinct CT band has been observed [18]). The methods of estimation have varied in emphasis, using complex SERS substrates [22], and using chemical quenching of 'active sites' [23]. The estimates of the CT enhancement factor vary from 10 to 10^3 for the case of pyridine on silver, where there is an overall enhancement factor of 10^5-10^6.

Consideration has been given to the type of RR scattering that may occur in CT SERS [7, 20]. There are four types of RR scattering that may contribute to band intensities [25], commonly

referred to as A-, B-, C-, and D- term RR scattering. These are described in chapter 1, section 1.3 of this thesis. The terms all introduce different selectivity of enhancement into CT SERS, and may account for some of the observed enhancement selectivity in SERS.

5.2 EXPERIMENTAL

5.2.1 Preparation of silver colloids

A detailed description of different methods of preparation of silver colloids is given in ref. [26]. Two methods were employed for the SERS study of NAD^+; using borohydride or citrate reduction of silver. Silver nitrate (May and Baker, AR grade), trisodium citrate (Fisons, AR grade), and sodium borohydride (Fisons, SLR grade) were used without further purification. Water was doubly or triply distilled, using carefully cleaned Pyrex glassware.

"Citrate sols" were prepared by reduction of a boiling solution of silver nitrate (90 mg in 500 cm^3 water) by trisodium citrate (10 cm^3 of a 1% $^w/_v$ solution), as in the method described by Lee and Meisel [27]. These citrate sols were murky grey in appearance, with strong absorption maxima at 405-410 nm, and were stable for many months. "Borohydride sols" were prepared by the addition of 5 cm^3 aqueous silver nitrate solution ($1x10^{-3}$ M) to 10 cm^3 ice-cold aqueous sodium borohydride solution ($8x10^{-3}$ M). The sols produced by this method were bright yellow, again with a strong absorption maximum at 405-410 nm. The borohydride sols were stable only for a few days (at room temperature) and were only used for purposes of comparison. Rapid aggregation was often observed on addition of adsorbates to borohydride sols, making control of experimental conditions difficult.

5.2.2 Samples for Raman Spectroscopy.

NADH, NAD^+, and ADP (adenosine diphosphate) were purchased from the Sigma Chemical Co. and used without further purification. GAPDH (Sigma) was obtained as a lyophilised powder and added directly to the silver sols (at least 2 mg to 5 cm^3). Alternatively, the ammonium sulphate suspension of GAPDH (Sigma) was centrifuged, and the solid resuspended in silver sol. This procedure led to rapid aggregation of the sol, due to the high concentration of sulphate present in the mixture. Desalting was performed by passing 0.1 cm^3 highly concentrated GAPDH down a prepacked Sephadex G25 column (PD-10 column, Pharmacia, UK). The desalted GAPDH solution was added to silver sol; these mixtures were more stable. The NAD^+ content of GAPDH was determined spectroscopically (see chapter 4, section 4.2.1). The above procedures for producing solutions of holo-GAPDH in silver sols resulted in final GAPDH concentrations of > $3x10^{-6}$ M. With *ca.* 3 NAD^+ per tetramer, the resulting NAD^+ concentrations in the GAPDH-sol mixtures were *ca.* 10^{-5} M.

Addition of the SERS adsorbate and/or salts to silver sols caused the sols to darken in colour. These sols gave broad absorption maxima at 550-650 nm in addition to that at 405-410 nm, this former band being attributable to aggregation [28]. Strong SERS was not obtained without aggregation, so potassium nitrate was added (in varying amounts) as necessary to optimise the SERS signal. Other salts (Cl^-, $SO4^{2-}$, I^-) also enhanced the SERS signal by causing aggregation. However, use of halide ions (chloride in particular) gave rise to problems of contamination. Despite extreme care in solution preparation, the use of fresh chemicals, and thorough washing of the Raman cell, use of Cl^- always gave rise

to a SERS spectrum of trisbipyridylruthenium(II).

Sol pH was measured after addition of SERS adsorbates, and adjusted as necessary by addition of dilute potassium hydroxide solution or dilute nitric acid. At extremes of pH (above pH 10, or below pH 3) the sols quickly precipitated. Estimates of surface potential were made according to the method of Wetzel *et al.* [29], which involves measurement of the relative intensities of the ν_1 and ν_{12} bands of pyridine. For these measurements samples were made up in the normal manner in the presence of a low concentration (*ca.* 10^{-4} M) of pyridine. This procedure is given in detail in ref. [26].

For measurement of spectra at different NAD^+ concentrations, and at different excitation wavelengths, acetone was added to 20% $^v/_v$ as an internal intensity standard. All NAD^+ Raman band intensities were normalised to the acetone peak at *ca.* 800 cm^{-1}. Further corrections were made for differential spectrometer response at wavenumber values far from 800 cm^{-1}.

Raman spectra were obtained using laser excitation from either an Ar^+ (Spectra Physics model 2025) or a Kr^+ (Spectra Physics model 170) laser. Raman scattered light was dispersed and detected using either the Jobin-Yvon or Spex instruments as described in chapter 2 of this thesis. In all cases, 90° illumination was used, with the sample in a rotating cell. The cell was spun as fast as was possible, whilst still avoiding sedimentation of sol onto the walls of the cell. Laser powers of up to 100 mW at the sample were used, with a spectrometer band pass of *ca.* 6 cm^{-1}.

5.3 RESULTS

The NR spectrum of NAD^+ (50 mM) is compared with the spectra of NAD^+ and ADP (both at 1 mM) on colloidal silver in Fig.5.1. No Raman signal could be obtained for NAD^+ alone at 1 mM under comparable conditions; thus the spectra in Figs.5.1(b) and (c) are assumed to be entirely the SERS spectra. Table 5.1 lists all the wavenumber values for the spectra in Fig. 5.1. The NAD^+ SERS spectrum shows particular enhancement of bands at 730, 1030 and 1320-1340 cm^{-1}, with weaker bands at 620, 790, 820, 925, 955, 1115, 1244, 1399, 1463, 1509, 1570 and 2940 cm^{-1}. Broad features at 620 and 925 cm^{-1} were not observed in all spectra; these bands were attributed to the sol itself. The 1320-1340 cm^{-1} band in the SERS spectrum is broad, and consists of two unresolved components, one at *ca.* 1325 cm^{-1} and one at 1335 cm^{-1}, see Fig. 5.2(b). The 1378 cm^{-1} band in the NR spectrum of NAD^+ is not prominent in the SERS spectrum. The pH's of NAD^+- and ADP-containing sols were in the range 4.5-6. The spectra did not appear to change with pH above pH 4.5, although some changes were observed below pH4. The SERS spectrum of NAD^+ at pH 3 showed enhancement of a band at *ca.* 1410 cm^{-1}, consistent with the changes observed in the NR spectrum on protonation of adenine N_1 nitrogen [30]. At pH 4.5 the surface potential of the silver was estimated (see experimental section) to be in the range -0.1 to -0.3 V vs SCE. At pH 9.5 the surface potential dropped to -0.55 V vs SCE. Since the PZC for polycrystalline silver is *ca.* -0.9 V vs SCE, the silver surface potentials reflect an absolute positive charge at the silver surface.

The SERS spectra obtained using borohydride sols were

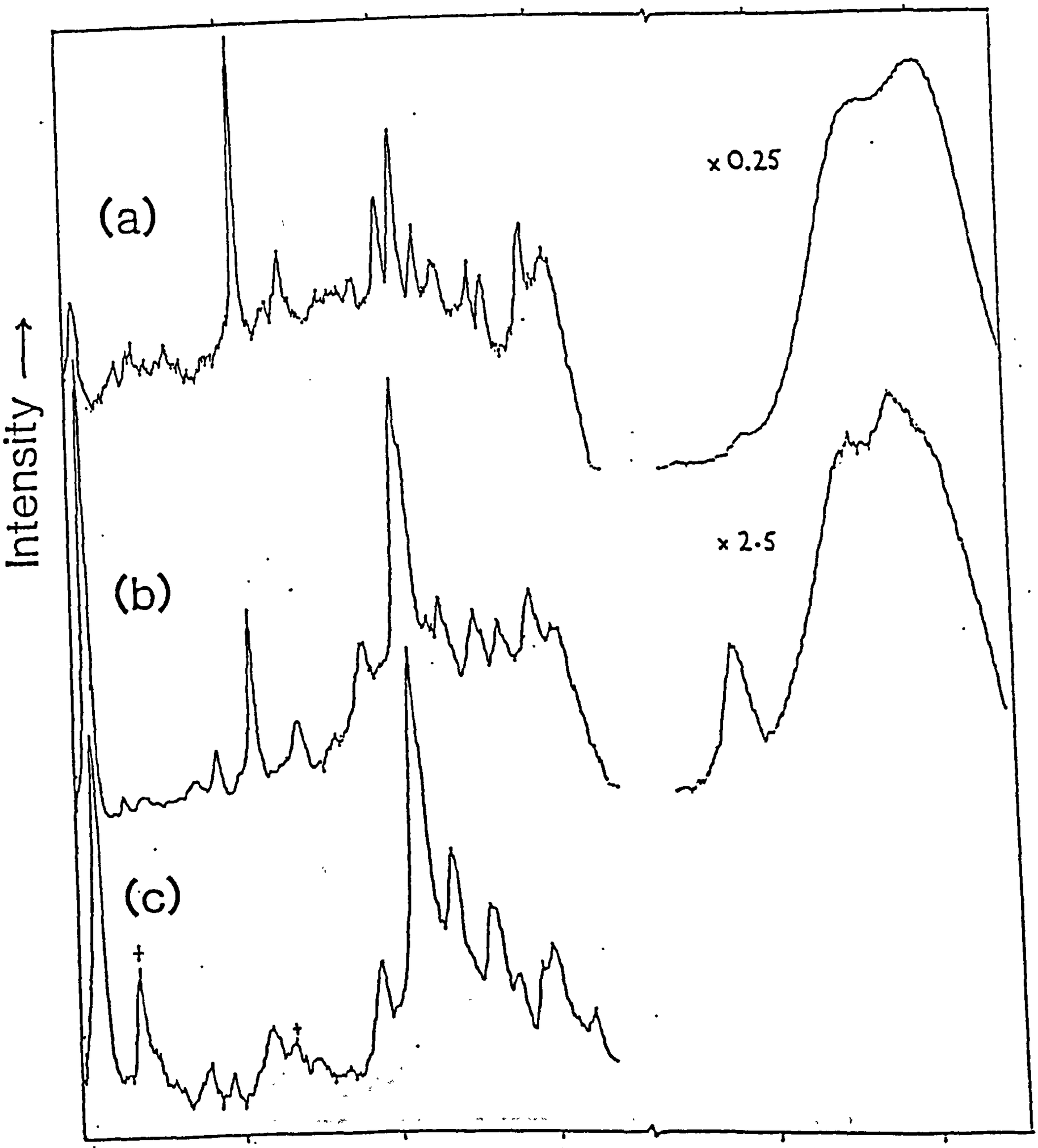

Figure 5.1 (a) NR spectrum of NAD^+ (50 mM, pH 6.0)

(b) SER spectrum of NAD^+ (1 mM)

(c) SER spectrum of ADP (1 mM). Acetone (20% v/v)

peaks are marked (+).

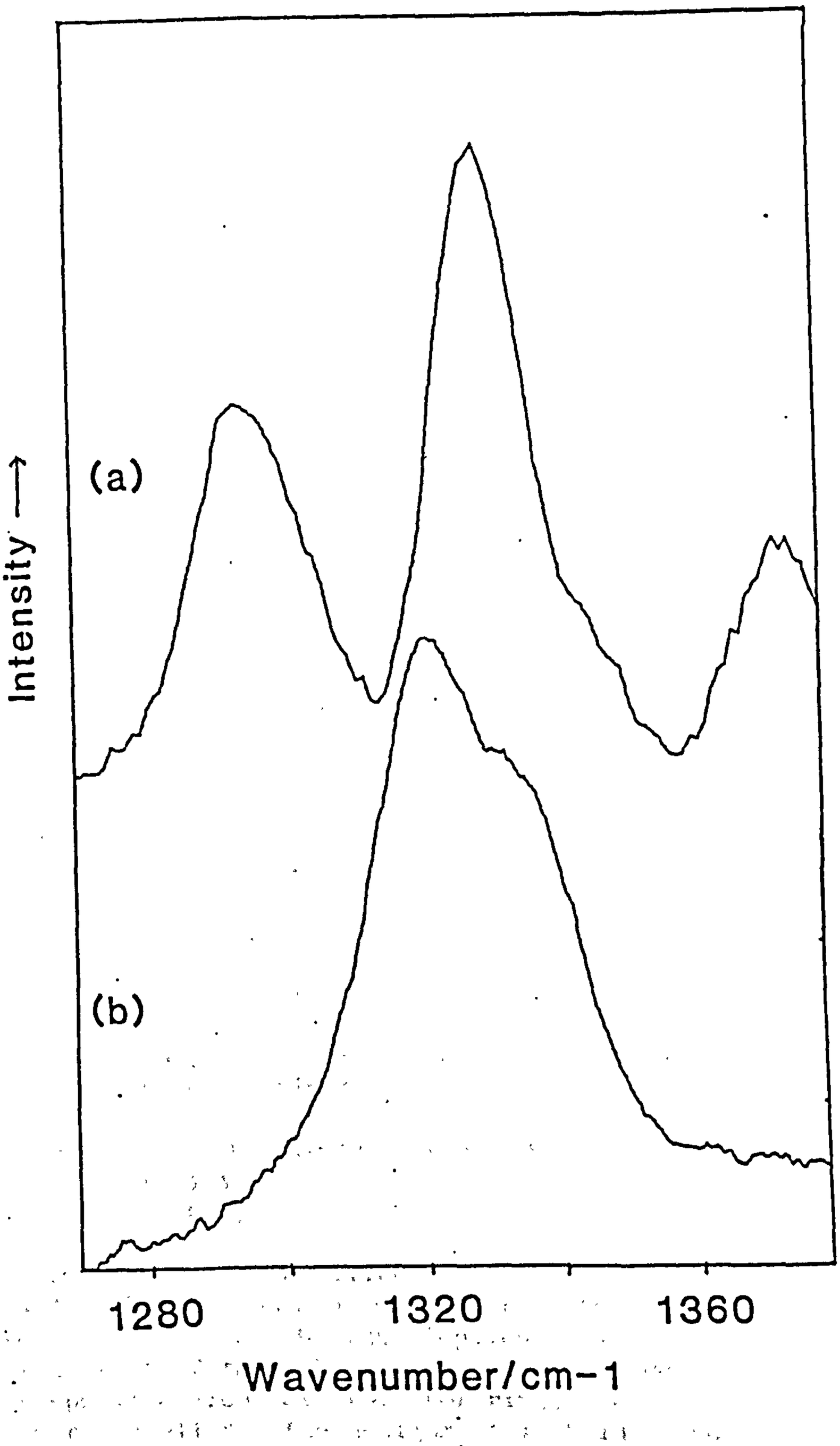

Figure 5.2 (a) NR spectrum of NAD^+, 1300 cm^{-1} region only

(b) SERS spectrum of NAD^+ 1300 cm^{-1} region only

Table 5.1 Wavenumber values[a] and assignments of bands in NR and SERS spectra of NAD^+ and ADP.

NR	SERS		Assignment[d]
NAD^+	NAD^+	ADP	
538w[b]	537w	542w	A 6-ring
564w[b]	561w	562w	P/R
-	619w	625w	Sol contaminant, A 5-ring deformation
642w[b]	-	-	A out-of-plane
730ms	730s	732s	A 6 and 5-ring breathing
802w	790w	-	R_2/N, out-of-plane A
834w	820w	-	P
888w	-	-	P, out-of-plane A
914w[b]	-	922m	P, sol contaminant
-	955m	-	citrate, A **5-ring**
-	-	961mw	
1029s	1030s	-	N ring mode (in-plane)
-	-	1037m	R/P
1087w	-	-	P
1114m	1115m	-	R_2/P
1254w	1244m	1247m	A **6-ring**
1304ms	-	-	A **6-ring**
-	1325s	1326s	A
1336s	1335sh	1335sh	A **6-ring**
1377ms	-	-	A exocyclic (C_2-H, N_9-R)
-	1399m	1395m	
1410m	-	-	
1462w[b]	1463m	1465m	A 6-ring, N_9-R
1480m	-	-	A
1507m	1509m	1512w	A 5-ring
-	-	1554sh	
1582ms	1570m	1575m	A
-	2930m	c	R

w=weak, m=medium, s=strong, sh=shoulder, A=adenine, P=phospate, R=ribose (R_2=ribose near N), N=nicotinamide.

[a] Values not corrected for instrument inaccuracy (see chapter 3, section 3.2.3 and Fig. 3.3).
[b] Reported by Yue *et al.* [30].
[c] Not measured.
[d] Tentative assignments made with additional information from refs. [30, 33-36]. The predominant character of the vibration is denoted where possible, e.g. '6-ring' implies a vibration of the 6-membered ring. Most of the vibrations appear to involve more than just one specific group of atoms (or ring). Where the vibration is more localised, the assignment is bold-typed.

similar to those obtained using citrate sols, but of inferior quality, only showing the same main features at 730 and 1330 cm^{-1}. Due to the greater stability and greater enhancements achieved with the citrate sols, these were used for all experiments in which concentration and excitation wavelength were varied. The spectra presented in Figs. 5.1, 5.2 and 5.5 result from the use of citrate sols.

Fig.5.3 shows the dependence of the corrected SERS band intensities on excitation wavelength for the 730, 1030 and 1330 cm^{-1} bands of NAD^+ (Raman excitation profiles). No significant changes in the relative intensities of any other NAD^+ bands were observed over this wavelength range; i.e. all bands showed a similar wavelength dependence to that of the three bands shown in Fig.5.3. Fig.5.4 shows the dependence of the SERS band intensity on NAD^+ concentration for the 1030 (b) and 1330 cm^{-1} (a) SERS bands of NAD^+. The 1330 cm^{-1} band shows a general decrease in intensity with decreasing concentration, but the intercept is non-zero. A similar decrease in intensity with concentration was observed for the 730 cm^{-1} band, the corresponding plot (not shown) having the same intercept value. Fig.5.5 shows a SERS spectrum of NAD^+ at very low ($2x10^{-5}$ M) concentration.

NADH did not give comparable SERS signals at millimolar concentrations on silver. At neutral pH, weak SERS bands were observed at *ca.* 730 and 1330 cm^{-1}. At higher pH's (> 7.5) little or no SERS signals were observed.

NAD^+ gave no SERS spectrum when bound to GAPDH at NAD^+ concentrations of 10^{-4} to 10^{-5} M, although good spectra could be obtained at these NAD^+ concentrations in the absence of the enzyme (see Fig. 5.5). At higher enzyme concentrations, the sols

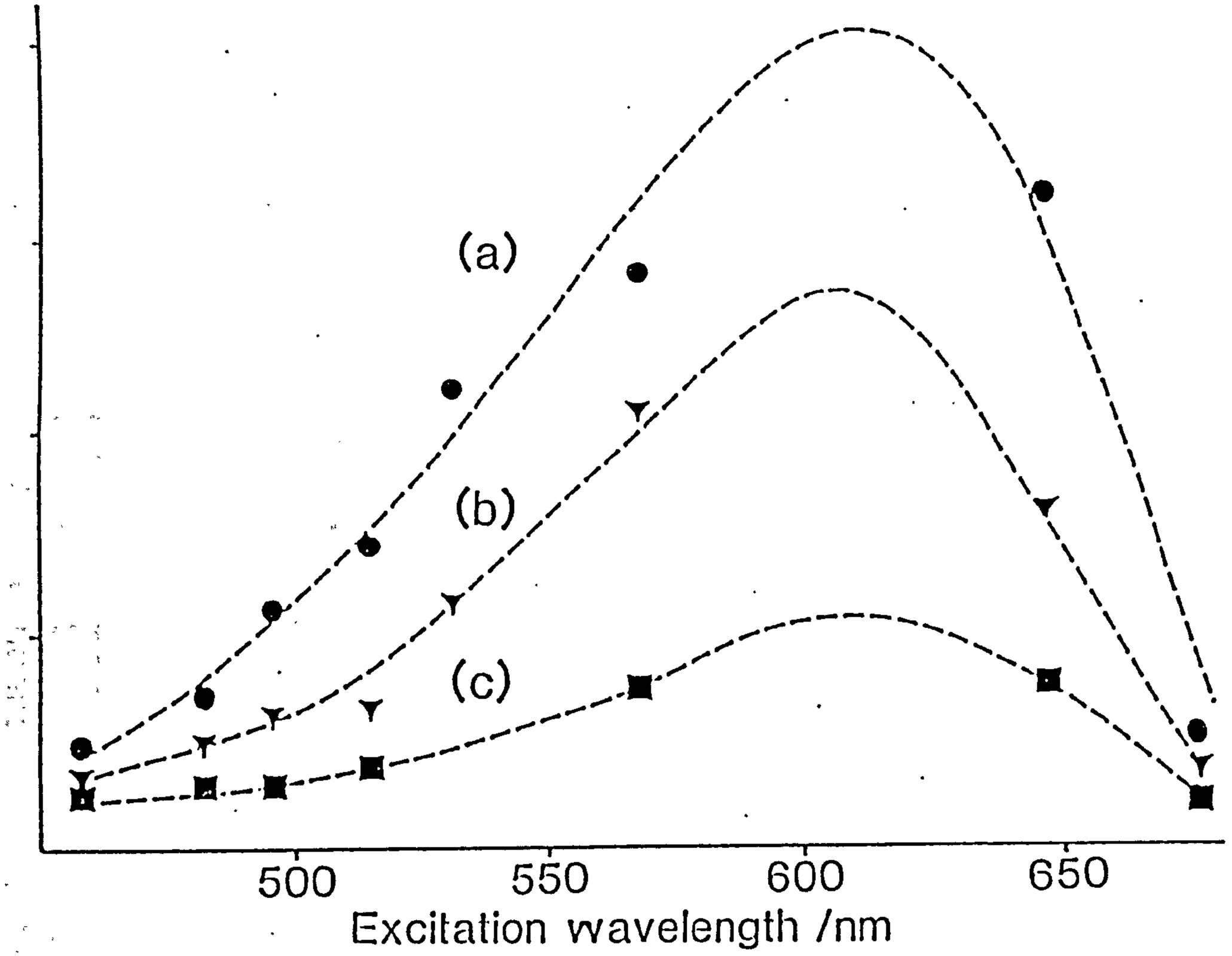

Figure 5.3 Raman Excitation Profiles of SERS bands of NAD^+:

(a) 730 cm^{-1} band

(b) 1330 cm^{-1} band

(c) 1030 cm^{-1} band

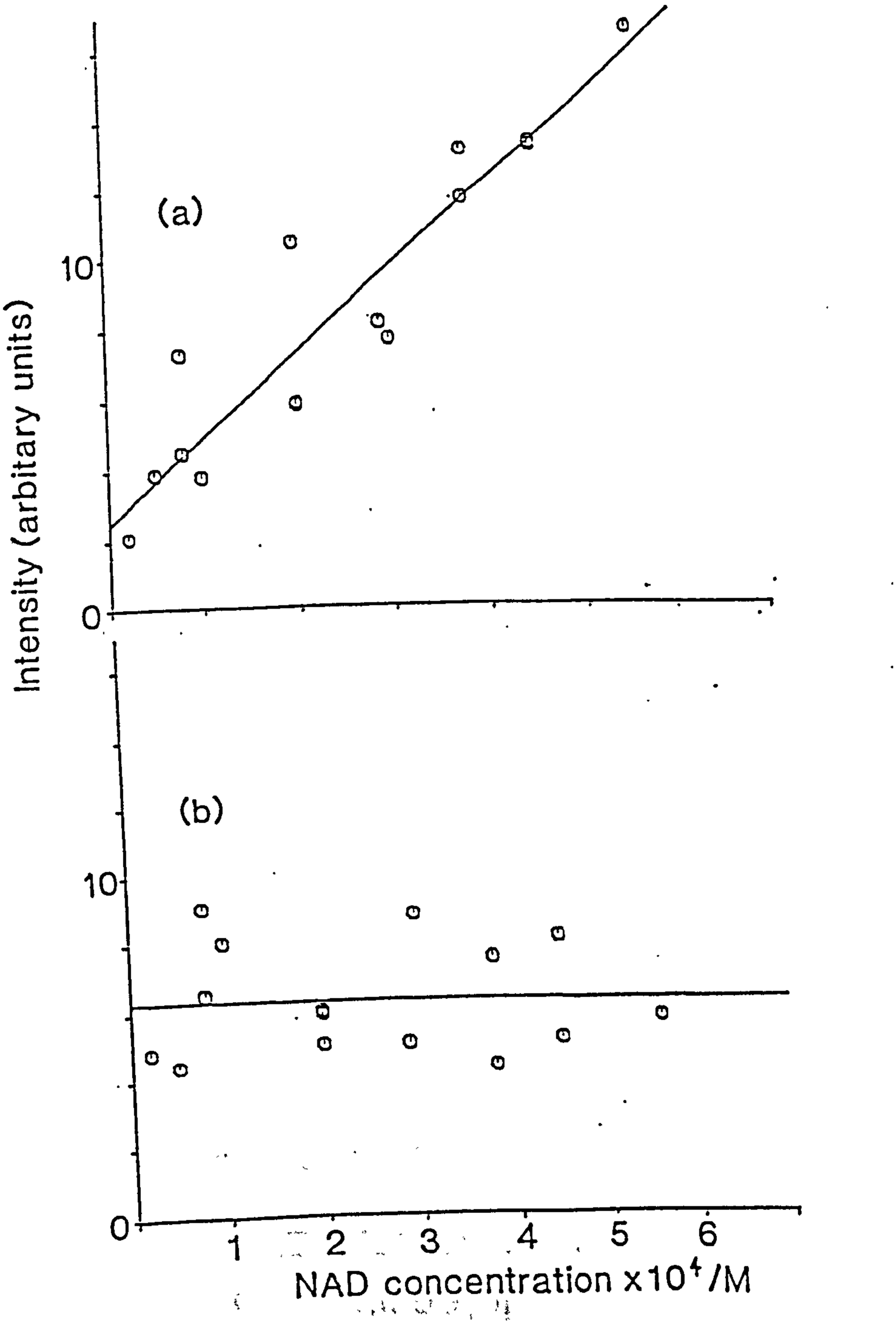

Figure 5.4 Concentration dependance of (a)1330 and (b)1030 cm^{-1} SERS bands of NAD^+.

Figure 5.5 SER spectrum of NAD^+ ($2x10^{-5}$ M). Acetone (20% $^v/_v$) peaks are marked (+).

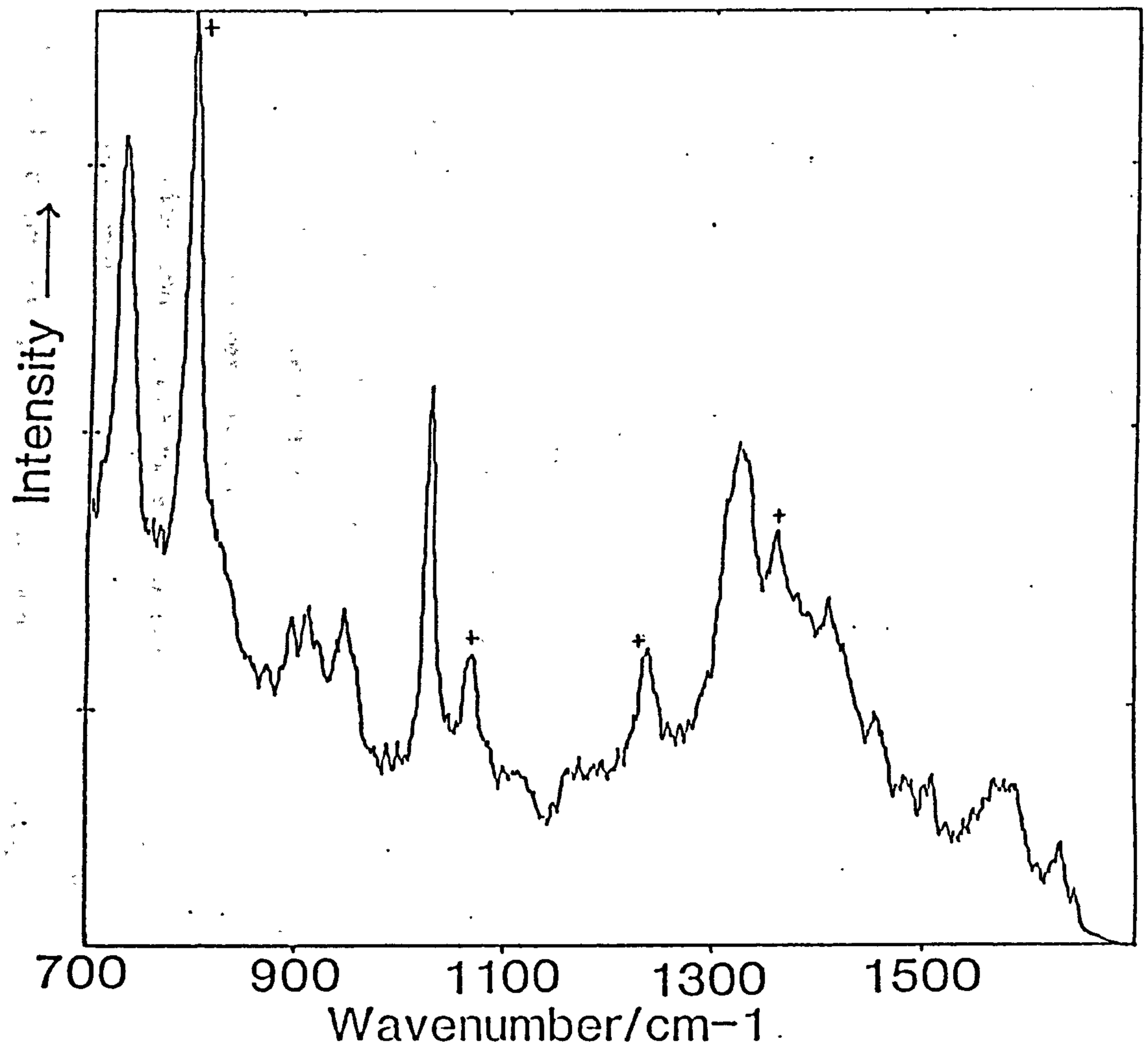

precipitated.

5.4 DISCUSSION

5.4.1 SERS spectra: assignment of bands.

The SERS spectrum of NAD^+ shows strongest enhancement of the adenine in-plane ring vibration at 730 cm^{-1}. The aliphatic C-H stretching vibrations (2940 cm^{-1}) of the ribose moiety are strongly enhanced, whereas the aromatic C-H stretching vibrations (expected at *ca.* 3080 cm^{-1}) are not. The high wavenumber regions of the spectra shown in Fig. 5.1 (a) and (b) are not shown to their correct relative intensities (with respect to the low wavenumber region). The 3400 cm^{-1} band of the NR spectrum in Fig. 5.1 (a) is *ca.* 4 times more intense than the band at 1030 cm^{-1}. The *ca.* 3300 cm^{-1} band in the SERS spectrum in Fig. 5.1 (b) is 2.6 times **less** intense than the 730 cm^{-1} band. Thus the 2940 cm^{-1} band in the SERS spectrum of NAD^+ is in fact only of moderate to weak intensity. This still reflects strong enhancement of the ribose C-H modes with respect to the NR spectrum, where they are too weak to be observed. It should be noted that citrate in solution could give rise to a band at *ca.* 2930 cm^{-1} [31]. However, in the SERS spectrum of citrate, this band is not enhanced [31], and in the NR spectrum it is weaker than other citrate bands at 956 and 1415 cm^{-1}. In addition, no 2930 cm^{-1} band was observed for the spectrum of aggregated citrate sol without NAD^+. The 1030 cm^{-1} band in the SERS spectrum of NAD^+ (Fig. 5.1(b)) is far weaker than the corresponding band in the NR spectrum, in which it has been assigned to an in-plane vibration of the oxidised nicotinamide ring [30]. Since the SERS spectrum of ADP shows no similar band at 1030 cm^{-1}, we may assume that the band at 1030 cm^{-1}

in the NAD^+ SERS spectrum is due to nicotinamide and is not a coincidentally close adenine or ribose band.

The change observed in the 1335 cm^{-1} band of the NAD^+ spectrum on adsorption onto the silver surface (compare Figs. 5.2(a) and (b)) is qualitatively similar to those observed in the NR spectrum of NAD^+ when the pH is lowered to below pH 4. The NR spectrum at low pH shows one band at *ca.* 1328 cm^{-1} (see Fig. 4.14 and [30]), whereas the SERS spectrum shows two bands, at 1335 and 1325 cm^{-1}. The N_1 of adenine becomes protonated below pH 4 (pK_a 3.8 [32]); this is assumed to be the cause of the spectral changes. However, as previously stated, the pH of the NAD^+-containing sol is above 4.5; thus the changes are unlikely to be due to adenine N_1 protonation. It is possible that the pK_a for N_1 protonation could change when NAD^+ is adsorbed on a silver surface. However, protonation is dismissed, as the SERS spectrum does not change in the pH range 4.5-6, but does change below pH 4. The different SERS spectrum obtained below pH 4 is consistent with protonation only in this lower pH range. The fact that the spectrum in Fig. 5.1(b) is similar to the protonated NAD^+ spectrum may indicate strong interaction between the silver surface and the adenine ring, with a particular involvement of adenine N_1. At first glance, it might appear that there are two types of adenine binding at silver that cause the two bands at 1335 and 1325 cm^{-1}. Although other SERS bands are broad, it is difficult to see evidence for other 'doublets', and thus evidence for two binding modes. A more thorough understanding of the vibrational modes of NAD^+, both in N_1-protonated and unprotonated forms, would clearly help to assign the band observed at 1325 cm^{-1}. For the purposes of the discussion below (section 5.4.2), the 1325 cm^{-1} band has been assumed to be an adenine

in-plane ring vibration, due to its high SERS intensity (similar to the 730 cm^{-1} band).

Apart from the change observed in the main 1335 cm^{-1} band of the NAD^+ spectrum on adsorption of the molecule onto colloidal silver, there are other significant differences between the NR and SERS spectra of NAD^+. A band at 1399 cm^{-1} (at 1395 cm^{-1}, and more intense in the SERS of ADP) could be the strongest band in the citrate SERS spectrum [31]. However, citrate bands at 805 and 953 cm^{-1} would also be expected at medium intensity; these bands do not always appear together in the SERS spectra. Moreover, when the concentration of NAD^+ is lowered, it might be expected that citrate bands should become relatively more intense. However, in Fig. 5.5, where NAD^+ is $2x10^{-5}$ M, the band at 1400 cm^{-1} is weak. Thus, while it not certain whether the band at 1399 cm^{-1} is due to adenine or ribose, it does not appear to be a citrate band.

Bands at 1244 (1247 in ADP), 1463 and 1570 cm^{-1} in the NAD^+ SERS spectrum also do not have clear counterparts in the NR spectrum. The bands at 1244 and 1570 cm^{-1} are probably simply downshifted from the bands in the NR spectrum at 1254 and 1582 cm^{-1}. However, these are considerable shifts compared with the nicotinamide and adenine ring modes at 1030 and 730 cm^{-1}, respectively, which are unshifted in the SERS spectrum. At low pH, where N_1 is protonated, the 1580 cm^{-1} band in the NR spectrum of NAD^+ decreases in intensity and a new band grows in at 1560 cm^{-1} [30]. The apparent shift from 1580 to 1570 cm^{-1} on adsorption onto colloidal silver perhaps again reflects some sort of electrostatic interaction of the adenine ring with the silver surface, possibly specifically with N_1 as previously suggested. The band at 1463 cm^{-1} in the SERS spectrum of NAD^+ (at 1465 cm^{-1}, and more intense in the

corresponding ADP spectrum) could be due to a large enhancement of the very weak band at *ca.* 1462 cm^{-1} found in the spectra of NAD^+, AMP, and ADPR [30, 33, 34]. A similar band at 1454 cm^{-1} in the SERS spectrum of adenine has been reported as being both a weak [3, 6] and a strong [2, 6] band in the SERS spectrum, and assigned to an adenine ring vibration [2]. The assignments are summarised in Table 5.1, with the additional information from the data in ref. [30], and from normal co-ordinate analyses [33-36].

5.4.2 NAD^+ on silver: orientational information

The SERS spectrum of NAD^+ on colloidal silver is substantially different from that reported for NAD^+ adsorbed on a silver electrode at potentials between 0 and -1.0 V vs SCE [5]; the electrode spectrum showed strong bands only at 735 and 1335 cm^{-1}. No enhancement of the nicotinamide band at 1030 cm^{-1} was reported and other features were weak. Since our value for the silver surface potential (-0.1 to -0.3 V vs SCE) is well within the range used in the electrode study, a simple potential-induced re-orientation cannot be used to explain the differences between colloid and electrode spectra. Indeed, in the same electrode study, a 1030 cm^{-1} nicotinamide band was observed when gold electrodes were used. Evidently, the nicotinamide ring approaches more closely, and possibly with a different orientation, to the colloidal silver surface than to the silver electrode surface. The results from the electrode study were interpreted as showing a close contact between adenine and the silver surface, with the adenine ring in a perpendicular orientation, binding to the surface via its NH_2 and N_7 nitrogens. This contradicts a surface reflectivity study, the results from which were interpreted in terms of a flat orientation

of the adenine ring [37]. The basis for the assignment of a perpendicular orientation of adenine on the silver electrode was a simplified view of the surface electromagnetic enhancement selection rules; namely, that only vibrations in a plane containing the surface normal, z, are enhanced. Since both strong bands observed in the electrode study were in-plane ring vibrations [33, 34], it was assumed that the plane of the ring must be normal to the surface. However, we shall show that the surface selection rules cannot generally be interpreted in such a simple manner.

The surface selection rules arising from the classical electromagnetic enhancement theory [7, 38-40] state that with excitation at, or to the red of the dipole resonance maximum of the silver particle, vibrations with polarisability derivative components α_{xz} and α_{yz} will be enhanced by a factor of up to $|\epsilon|^2$. Bands from the polarisability derivative component α_{zz} will be enhanced by a factor of up to $|\epsilon|^4$ compared with those vibrations with only α_{xy}, α_{xx}, or α_{yy} components, where ϵ is the effective dielectric constant of the metal relative to the surrounding medium (the difference in values of ϵ at incident and scattered wavelengths being neglected). In the case of adenine (C_s symmetry, molecule in xy plane), the totally symmetric (in-plane) modes may contain a varying degree of α_{zz} character. Considering a vibration involving the whole π-electron system, i.e. a vibration of the C-N skeleton, there might be expected to be a small degree of α_{zz} character out of the ring plane as the π-electron distribution expands and contracts over the ring. An exocyclic vibration, e.g. C-H or $C-NH_2$, involving only σ-type electrons, would contain far less α_{zz} character. Accordingly, adsorption of adenine flat onto a surface would result in the C-H in-plane modes in particular not being

enhanced, whereas C-N skeleton modes may be enhanced to varying extents. Such a treatment has been developed for benzene and extended to adenine SERS by Suh and Moskovits [2]. Out-of-plane adenine modes would, of course, be more enhanced, but still might be weak in the SERS spectrum as they are very weak in the NR spectrum (due to low polarisability derivative values). Conversely, adsorption perpendicular (or partially so) to the surface would result in the in-plane modes, especially C-H modes, becoming much more enhanced (as the bulk of their polarisability derivative would become $\propto \alpha_{zz}$). Out-of-plane modes would show no enhancement.

The data presented in the electrode study unfortunately do not show the high wavenumber region where, if the adenine moiety of NAD^+ is indeed perpendicular to the surface, C-H stretching modes at *ca.* 3080 cm^{-1} would be expected to be strongly enhanced. The observation of enhancement of only in-plane ring modes does fit with the electromagnetic surface-enhancement selection rules, assuming a perpendicular orientation, but it is not the only possible explanation. Indeed a totally different explanation of a similar spectrum, that of adenine itself on a silver colloid, has been proposed [2]. Using the same selection rules, adenine was deduced to be adsorbed parallel to the surface. The main evidence cited for this flat orientation was the observation that the C-H mode at *ca.* 3080 cm^{-1} was not enhanced. However, out-of-plane modes also were not enhanced in this SERS spectrum, contrary to expectations. The 739 and 1339 cm^{-1} bands were strongly enhanced and, although they both arise from similar vibrations involving the C-N skeleton in the NR spectrum (see Table 5.1), the authors reassigned the 739 cm^{-1} band to a coincidentally close strongly enhanced band. The new assignment of this band to a coupled NH_2 deformation and ring

vibration seems rather contrived, since the amount of α_{zz} character in these ring vibrations is unquantified. It might be expected that, similar to the example of benzene [41], these modes might contain sufficient α_{zz} character to be considerably enhanced when the molecule is adsorbed flat on to the surface.

The SERS spectrum of NAD^+ presented in Fig.5.1(b) presents an equally confusing picture. The exocyclic C-H stretching vibrations of adenine, expected at 3080 cm^{-1}, and the predominantly exocyclic C_2-H deformation vibration at 1377 cm^{-1} (see Table 5.1) are not enhanced, whereas most of the other adenine ring vibrations **are** enhanced. The out-of-plane modes do not appear to be strongly enhanced; in fact, on the contrary, the *ca.* 790 cm^{-1} band is the only band in the SERS spectrum that can be assigned to an out-of-plane adenine vibration [34, 36]. These observations appear to be in conflict if the electromagnetic enhancement selection rules are rigidly interpreted.

Complicating the picture is the wavelength dependence of the electromagnetic enhancement selection rules. At wavelengths to the blue of the dipole resonance maximum, modes containing α_{xx}, α_{yy}, and α_{xy} polarisability derivative components may become more enhanced, and indeed the situation can be reached where the rules are completely reversed. The lack of major changes in relative intensities of the SERS bands of NAD^+ with excitation wavelength implies that this 'reversal' situation is not reached for silver sols using excitation wavelengths greater than 457.9 nm, or that SERS intensity from other enhancement mechanisms is dominating the excitation profile.

Neither of the two mentioned studies [2, 5] have made use of a 'chemical' enhancement theory (see Introduction) to explain their

results. As previously discussed, there is much evidence to suggest that chemical enhancement contributes significantly to the overall SERS enhancement; it cannot be dismissed from the studies in refs. [2] and [5]. Since this enhancement mechanism arises from an RR process involving charge transfer (from metal to molecule or *vice versa*), the chemical enhancement mechanism is often called the CT mechanism. This distinguishes it from other molecule-specific or chemisorption-specific EM models [16].

The selection rules for the CT mechanism are not as clear-cut as those that arise from the EM mechanism. Creighton argues that, being an RR process, the CT mechanism will principally enhance totally symmetric vibrations via an A-term RR process [7]. It would also select those vibrations in the 'chromophoric' part of the molecule; in particular those vibrations along whose normal co-ordinates the molecule would relax if the (virtual) electronic transition involved in the RR process were real. Otto has pointed out that since the transient states produced in the CT process are negative ion states (see section 5.1.2), there should be a similarity between the SERS spectrum of benzene and the EELS spectrum of benzene [21]. Although there appears to be some correlation between the spectra, there are many strongly enhanced modes in the SERS spectrum of benzene that are not present in the EELS spectrum. Lombardi *et al.* have discussed the contribution of B and C term RR scattering to SERS [20]. They suggest that for molecule-> metal CT, both A and B terms are important, and that for metal-> molecule CT A and C terms are important, thus allowing for enhancement of non-totally symmetric modes. The arguments for introducing these terms are largely based on the authors observations of (1) lack of enhancement of overtones and (2) enhancement of non-totally

symmetric vibrations in SERS spectra. However, after Lombardi's publication, a SERS spectrum of pyridine clearly showing overtone enhancement was published [42]. Moreover, in all experiments cited by Lombardi, EM enhancement (which must always be present) would enhance some of the non-totally symmetric modes. None of the more recent studies have suggested any orientation selectivity. Yamada and Yamamoto [43] have deviated somewhat from the RR-selectivity. They argued that the CT from the metal to the π^* orbital of pyridine necessarily involves a component of the electric field vector perpendicular to the surface, and might thus be expected to result in the selective enhancement of vibrational modes which also have oscillating polarizablility derivative components in this direction. Yamada has claimed that support for this surface-orientation selection rule is found in her results from pyridine on silver.

For NAD^+ or adenine, with the CT mechanism (and assuming metal->molecule CT), vibrations of the ring skeleton can be enhanced, whereas exocyclic vibrations (e.g. C-H) cannot. It is likely that the CT contributions to the SERS spectra of NAD^+ presented here, and to the SERS spectra of NAD^+ and adenine previously reported [2, 5], are large. Recent estimates of the size of CT enhancement in SERS have varied. A SERS study of pyridine adsorbed on a silver-rhodium substrate attributed an absolute enhancement factor of 15-65 to the CT mechanism [22]. Another silver island film study estimated a CT enhancement factor of 10^3, compared with a factor of $10\text{-}10^2$ from an EM mechanism [18a]. The observation of good SERS spectra at very low NAD^+ concentrations (Fig. 5.5) is in itself evidence for a significant contribution from a CT enhancement mechanism. Such strong enhancement is unlikely to arise from the EM mechanism alone. In addition, the observation of

enhancement of only ring modes (not exocyclic C-H modes) of the adenine moiety is in harmony with a CT mechanism. A large CT enhancement contribution would also adequately explain both previous studies of the adenine moiety at silver, similar enhancements of adenine bands being observed. Particular evidence for the presence of a CT mechanism arises from studies of SERS band intensity variations with electrode potential [19]. At strongly negative potentials the metal donor level is raised closer to the ligand acceptor level. Thus SERS CT bands are able to gain intensity with lower energy red excitation as the electrode potential is made more negative. The electrode study of NAD^+, which used red excitation, does in fact appear to show an increase in band intensities as the electrode potential is lowered from 0 to -0.6 V vs SCE. After this point, the spectra start to lose intensity - probably due to counteracting desorption effects. It is clear that unless the CT mechanism can somehow be dismissed as not contributing to the SERS intensity, the orientation of adenine on silver cannot be determined with certainty. Our low concentration (10^{-5} M) data point to a substantial contribution from a CT mechanism, as does the strong selective enhancement of just two adenine totally symmetric modes. Thus the surface selection rules provided by the EM mechanism cannot be used in isolation to deduce the orientation of the adenine ring with respect to the silver surface.

The evidence cited previously for a strong interaction between the adenine ring and the silver surface does not imply a particular orientation, unless the results are interpreted as showing particular involvement of N_1. The evidence presented does not rule out interaction with N_3 or N_7, since NR spectra do not provide any information about the effects on the spectrum of

complexation/protonation at N_7 or N_3. Most of the adenine vibrational modes are thought to be very delocalized [33-36]; it is thus difficult to correlate specific shifts with perturbation around one atom. A completely flat geometry would be expected to affect the vibrational modes involving not only N_1, N_7 and N_3, but also N_9 and the exocyclic amino group. According to Tsuboi *et al.*, modes involving a significant contribution from the amino group are found at 1606 and 1484 cm^{-1} for AMP [33]. These modes are not strongly enhanced in the SERS spectrum. If the adenine ring were tilted to interact with the surface *via* N_1, the amino group would also come close to the surface. It is difficult to envisage what sort of interaction may be occurring.

The data shown in Fig.5.4 shed some light on the nature of the relative proximity to the surface of the adenine and nicotinamide rings. The adenine band intensities show a clear concentration dependence (Fig.5.4(a)), but the nicotinamide band (Fig.5.4(b)) does not. The only adequate explanation for this observation is that the NAD^+ molecule undergoes reorientation as the concentration is lowered. At high concentrations the nicotinamide ring is further away from the surface than the adenine, and so its Raman spectrum is relatively weakly enhanced. As the concentration is lowered, the nicotinamide moiety is able to get closer to the surface and its SERS band becomes more enhanced. This counteracts the loss of signal due to the lowering of concentration, resulting in the apparent independence of the 1030 cm^{-1} band intensity on concentration (Fig.5.4(b)). Also of interest from Fig.5.4 is the non-zero intercept value (see Results section). This indicates that only molecules giving relatively weakly enhanced Raman bands are being lost over the concentration range 10^{-3} - 10^{-5} M and that these

are the less strongly bound NAD^+ molecules. This is consistent with previous observations of just a few very strongly enhancing sites on the silver surface amongst many moderately enhancing sites [23, 44]. If the sols were being overloaded at high concentration, and there were a significant spectral contribution from free NAD^+, the nicotinamide band would be larger with respect to the adenine bands at high concentration, which is opposite to the observed trend. Any explanation based on multilayer adsorption would have to involve a faster loss of adenine signal than nicotinamide signal, which would only arise if different layers of NAD^+ took different orientations.

The observation of no SERS enhancement for NADH at alkaline pH's is difficult to explain at first sight in terms of adsorption *via* adenine and nicotinamide. Above pH 4 the adenine moiety carries no charge in either NAD^+ or NADH. The nicotinamide moiety is positively charged in NAD^+, but uncharged in NADH. The surface of the colloidal particles has a distinctly positive character at pH 4-5 (PZC for silver is *ca.* -0.9 V vs SCE) but loses its surface charge at alkaline pH (see Results section), presumably due to the formation of co-ordinated hydroxide. Superficially, NADH might be expected to adsorb as readily to the silver surface as NAD^+, giving a similar SERS spectrum, excepting the 1030 cm^{-1} nicotinamide band. In order to account for the observed behaviour, we propose that the primary binding of NAD^+ and NADH to silver is *via* the negatively charged phosphate groups, with only weaker binding *via* adenine. At alkaline pH, the reduction of the positive charge on silver inhibits adsorption of NADH; adenine binding alone being too weak for effective adsorption to take place. Co-ordination *via* the phosphate groups also can explain the strong enhancement of the ribose C-H vibrations. With adsorption *via* phosphate, the adenine ribose of

NAD^+ is necessarily located very close to the surface. SERS spectra of NADH have been reported by Siiman *et al.* [6]. At pH 8-9, and high NADH concentrations, the spectra showed no bands at 730 or 1330 cm^{-1}, but did show bands at 1137, 1180, 1268 and 1363 cm^{-1}, and bands due to citrate. No nicotinamide bands were observed at 1540 or 1688 cm^{-1}. The authors concluded a co-ordination *via* adenine through N_7 and NH_2, and 'end-on' to nicotinamide. At pH 6.5-7 and with lower concentration, only bands due to citrate and a band at 739 cm^{-1} were observed. Although Siiman *et al.* made careful assignments using SERS spectra of nicotinamide, adenine, histidine and imidazole, their data seem to be plagued by citrate SERS. In addition, the sols (with NADH) were left for 1-4 days before running SERS spectra, thus increasing the likelihood of decomposition. Finally, the authors appear to be inconsistent in their interpretations of the EM theory selection rules.

5.4.3 SERS of GAPDH

In the tetrameric enzyme GAPDH, NAD^+ is deeply buried (see Fig. 5.6). Although the X-ray structure [45] shows it to be located at the edge of a subunit, each subunit shields the others from solvent (and the silver surface) and thus entrains the coenzyme within the protein envelope. Accordingly, any SERS signal would have to arise from either a large electromagnetic enhancement or from protein denaturation (either gross structure change or mere dissociation into monomer units). The lack of SERS signals thus provides further proof that silver colloids prepared by citrate reduction do not denature proteins. It is possible that the lack of SERS enhancement is due to a lack of adsorption onto silver. In view of the numerous charged groups at the exterior of the enzyme,

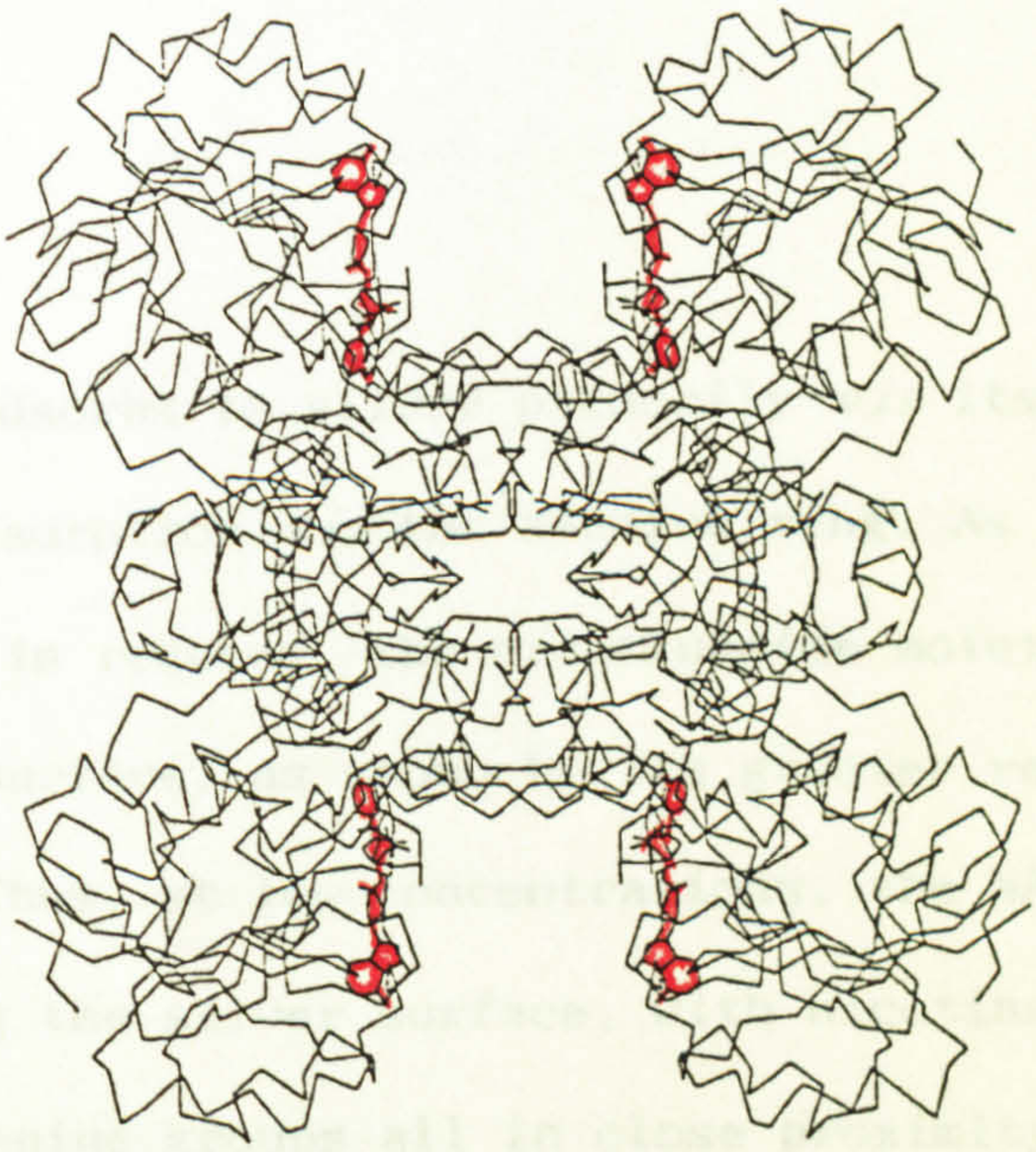

Figure 5.6 Representation of GAPDH tetramer (α carbon backbone only). NAD^+ is highlighted.

however, adsorption seems probable. The lack of enhancement demonstrates rather that the separation of the NAD^+ from the silver surface is too great for even electromagnetic enhancement to be effective.

5.5 CONCLUSION

NAD^+ adsorbs to silver primarily *via* its phosphate groups, with weaker adsorption *via* the adenine ring. As the solution concentration is reduced, the nicotinamide moiety approaches closer to the siver surface, as shown by its greater relative SERS enhancement. Thus, at low concentrations, the NAD^+ molecule is quite extended along the silver surface, with nicotinamide, phosphate, ribose and adenine groups all in close proximity to the surface. In contrast to the strong enhancement seen for NAD^+ on silver, little enhancement is seen for NADH. This is due to adsorption being prevented by co-ordination of hydroxide ions to the silver at the alkaline pH needed for stability of NADH in solution, resulting in a more negative surface potential at the higher pH values.

NAD^+ did not give a SER spectrum when bound to GAPDH. The separation between silver and NAD^+ caused by the protein completely prevents enhancement by any CT mechanism. The separation is sufficiently large for enhancement by the electromagnetic enhancement mechanism to be negligible. The future for study of NAD^+ by SERS when bound to similar large dehydrogenase enzymes appears bleak.

5.6 REFERENCES

[1] G. Smulevich and T.G.Spiro, *J.Phys.Chem.* **86**, 5168 (1985).

[2] J.S.Suh and M.Moskovits, *J.Am.Chem.Soc.* **108**, 4711 (1986).

[3] E.Koglin, J.M.Sequaris, and P.Valenta, *J.Mol.Struct.* **60**, 421 (1980).

[4] C.Otto, F.F.deMul, A.Huizinga, and J.Greve, *J.Phys.Chem.* **92**, 1239 (1988).

[5] I.Taniguchi, K.Umekita and K.Yasukouchi, *J.Electroanal.Chem.* **202**, 315 (1985).

[6] O.Siiman, R.Rivellini, and R.Patel, *Inorg.Chem.* **27**, 3940 (1988).

[7] J.A.Creighton in *"Advances in Spectroscopy, Vol. 16: Spectroscopy of Surfaces"* Eds. R.J.H.Clark and R.E.Hester ch. 2 (J.Wiley & Sons, Chichester, 1988).

[8] M.Kerker, D.-S.Wang, H.Chew, O.Siiman, and L.A.Bumm, in ref. 12, p.109.

[9] J.I.Gersten and A.Nitzan, in ref. 12, p.89.

[10] J.I.Gersten and A.Nitzan, *J.Chem.Phys.* **73**, 3023 (1980).

[11] N.Liver, A.Nitzan, and J.I.Gersten, *Chem.Phys.Lett.* **111**, 449 (1984).

[12] R.K.Chang and T.E.Furtak, Eds. *"Surface Enhanced Raman Scattering"* (Plenum, New York, 1982).

[13] R.K.Chang and B.L.Laube, *CRC Crit.Rev. Solid State and Mater. Sci.* **12**, 1 (1984).

[14] J.A.Creighton in ref. 12, p.331.

[15] C.A.Murray in ref. 12, p.203.

[16] B.Pettinger, *J.Chem.Phys.* **85**, 7442 (1986).

[17] B.Pettinger, K.Krischer, and G.Ertl, *Chem.Phys.Lett.* **151**, 151 (1988).

[18]a H.Yamada, H.Nagata, K.Toba and Y.Nakao, *Surf.Sci.* **182**, 269 (1987).

b H.Yamada, K.Toba, and Y.Nakao, *J.Electron Spectrosc.Relat.Phenom.* **45**, 113 (1987).

[19] T.E.Furtak and S.H.Macomber, *Chem.Phys.Lett.* **95**, 328 (1983).

[20] J.R.Lombardi, R.L.Birke, T.Lu, and J.Xu, *J.Chem.Phys.* **84**, 4174 (1986).

[21] A.Otto, *J.Electron Spectrosc.Relat.Phenom.* **29**, 329 (1983).

[22] X.Jiang and A.Campion, *Chem.Phys.Lett.* **140**, 95 (1987).

[23] T.Watanabe, O.Kawanami, K.Honda, and B.Pettinger, *Chem.Phys.Lett.* **102**, 565 (1983).

[24] H.Yamada, H.Nagata, and H.Teranishi, *J.Phys.Chem.* **90**, 2384 (1986).

[25] R.J.H.Clark and T.J.Dines, *Angew.Chem., Int.Ed.* **25**, 131 (1986).

[26] J.deGroot, *Ph.D Thesis, University of York* (1987).

[27] P.C.Lee and D.Meisel, *J.Phys.Chem.* **86**, 3391 (1982).

[28] J.A.Creighton, C.G.Blatchford and M.G.Albrecht, *J.Chem.Soc. Faraday Trans. II* **75**, 790 (1977).

[29] H.Wetzel, H.Gerischer and B.Pettinger, *Chem.Phys.Lett.* **85**, 187 (1982).

[30] K.T.Yue, C.Martin, D.Chen, P.Nelson, D.Sloan and R.H.Callendar, *Biochemistry* **25**, 4941 (1986).

[31] O.Siiman, L.A.Bumm, R.Callaghan, C.G.Blatchford, and M.Kerker, *J.Phys.Chem.* **87**, 1014 (1983).

[32] W.Saenger, *"Principles of Nucleic Acid Structure"* p.109 (Springer-Verlag, Berlin, 1984).

[33] M.Tsuboi, Y.Nishimura, A.Y.Hirakawa and W.L.Peticolas in *"Biological Applications of Raman Spectroscopy"* Ed. T.G.Spiro, Vol.2, p.109 (J.Wiley & Sons, 1987).

[34] M.Majoube, *J.Raman Spectrosc.* **16**, 98 (1985).

[35] R.Letellier, M.Ghomi, and E.Taillandier, *Eur.Biophys.J.* **14**, 423 (1987).

[36] R.Letellier, M.Ghomi, and E.Taillandier, *Eur.Biophys.J.* **14**, 243

(1987).

[37]a K.Takamura, A.Mori and F.Kusu, *Bioelectrochem.Bioenerg.* **8**, 229 (1981).

b K.Takamura, A.Mori and F.Kusu, *Bioelectrochem.Bioenerg.* **9**, 499 (1982).

[38] J.A.Creighton, *Surf.Sci.* **158**, 211 (1985).

[39] M.Moskovits, *J.Chem.Phys.* **77**, 4408 (1982).

[40] M.Moskovits and J.S.Suh, *J.Phys.Chem.* **88**, 5526 (1984).

[41] M.Moskovits and D.P.DiLella, *J.Chem.Phys.* **73**, 6068 (1980).

[42] J.A.Creighton, *Surf.Sci.* **173**, 665 (1986).

[43] H.Yamada and Y.Yamamoto, *Surf.Sci.* **134**, 71 (1983).

[44] P.Hildebrandt and M.Stockburger, *J.Phys.Chem.* **88**, 5941 (1984).

[45] T.Skarzynski, P.C.E.Moody and A.J.Wonacott, *J.Mol.Biol.* **193**, 171 (1987).

CHAPTER SIX: A RESONANCE RAMAN STUDY OF CATALASE AND A HEME MODEL SYSTEM

6.1 INTRODUCTION

Resonance Raman spectroscopy of heme systems has become an extremely incisive method of determining the environment and bonding of the heme prosthetic group in heme enzymes and other heme proteins. The assignment of the porphyrin vibrational modes, and their sensitivity to factors such as co-ordination, oxidation, and spin state of the metal atom have been discussed in chapter 1. The heme enzymes and their catalytic intermediates have been studied by a number of spectroscopic methods, including RR spectroscopy. The general catalytic mechanism of catalase and of other heme enzymes has been presented in chapter 1, section 1.6, where the compound I and II intermediates were introduced. Two recent reviews [1, 2] have focused on the RR studies of the intermediates of heme enzymes and, in particular, on the intermediates of horseradish peroxidase (HRP), cytochrome c peroxidase (CcP) and cytochrome c oxidase (CcO). Surprisingly few RR (or indeed other spectroscopic) studies have been undertaken on catalase, despite its importance and ubiquity (see chapter 1). In fact, only two RR studies have been presented to date [3, 4], only one of which presents data on a catalase intermediate [3]. A brief review of some of the most recent heme enzyme studies, including the catalase studies, is given in section 6.1.1 below. The conclusions that have been drawn from the work in this chapter will not be mentioned in section 6.1.1.

There is a need for an accurate guide to the effects of environment and bonding on the heme enzyme intermediates, but it is difficult to obtain data on a large range of enzymes. The use of porphyrin models for heme enzyme intermediates is thus important, as they (and their ligands) can be systematically varied, and studied in different solvents. Many spectroscopic studies have been

undertaken on such model porphyrins; reviews can be found in ref. [5]. A short overview of some of the recent RR studies on these model systems (but not including the studies presented in this chapter) is given in section 6.1.2 below. The results from the time-resolved RR (TR^3) study of a model heme system are presented in section 6.3.3 below.

6.1.1 The intermediate compounds I and II of catalase and other heme enzymes.

The relatively stable compound II intermediate of HRP and other peroxidases has been well characterised by spectroscopic methods, including RR spectroscopy [1, 6-8]. The intermediate is e.s.r silent, and has UV-vis. and RR spectra that are consistent with the formulation $Fe^{(IV)}$=O, low spin [9]. While the corresponding compound II of catalase is not an intermediate of the normal catalytic cycle, it is easily formed by the reaction of compound I with donors such as phenols and alcohols [10]. Compound II of catalase has not been extensively characterised by RR spectroscopy. Only one study has produced any data for this species, and these are incomplete [3].

The RR spectrum of HRP compound II shows the oxidation and spin state marker bands characteristically shifted from their postions in native HRP (see also chapter 1) [1, 3, 11, 12]. The oxidation state marker, ν 4, shifts from 1374 to 1381 cm^{-1}. The core size (or oxidation and spin state) markers ν 3, ν 2, ν 10 and ν 11 shift from 1499, 1574, 1630 and 1550 cm^{-1} to 1509, 1584-9, 1644 and 1560 cm^{-1}. As discussed in chapter 1, these positions are characteristic of a low spin heme. The 7 cm^{-1} shift of the oxidation state marker ν 4 is not as large as the (*ca.* 15 cm^{-1}) shift observed

in $\nu 4$ when $Fe^{(II)}$ is oxidised to $Fe^{(III)}$. This has been rationalised by Kitagawa in his recent review in terms of effective backdonation from the porphyrin to the metal [1]. The even smaller shifts (2 cm^{-1}) in $\nu 4$ on forming compounds II of catalase and CcP are discussed by Spiro [13]. The Raman band due to $Fe^{(IV)}$=O (ferryl) stretching in HRP has been identified [14, 15], and has been shown to be affected by changes in pH, which cause a change in hydrogen bonding to the ferryl oxygen [16, 17].

The study of compound I intermediates of peroxidases and catalases is more difficult than the study of compound II, due to the greater reactivity (instability) of compound I. Catalase and chloroperoxidase have, however, been shown to react with peroxyacetic acid (PAA) to form relatively stable (lifetime of minutes) compound I preparations [10, 18, 19]; HRP compound I can be formed with reasonable yield and stability under appropriate conditions (of substrate stoichiometry). The e.s.r spectra of both chloroperoxidase [20] and HRP compound I [21] confirm proposals that compound I is a cation radical of the porphyrin, which is weakly coupled to the $Fe^{(IV)}$=O centre. Catalase compound I has not been studied by e.s.r (excepting preliminary studies at York), but the similarity of its UV-vis spectrum to other compound I species suggests that it is also a porphyrin cation radical species with an $Fe^{(IV)}$=O centre.

Several groups have attempted to obtain and characterise the RR spectra of HRP compound I [22-24]. All of them have experienced difficulty in obtaining the RR spectrum of the intact porphyrin cation radical species; HRP compound I appears to be photolabile. Paeng and Kincaid [24] have recently published convincing spectra of HRP compound I, which agree reasonably well with model compound

studies, if the porphyrin radical cation is assumed to be in an A_{2u} ground state (see below). The RR spectrum of HRP compound I has been shown to be quite different from the spectra of native HRP and HRP compound II. Previous reports of HRP compound I RR spectra were very similar to the spectra of HRP compound II [22, 23]. These spectra of HRP compound I under higher irradiance conditions are thought to arise from a photoproduct of compound I that has lost the radical from the porphyrin, i.e. that is more like compound II [23b].

6.1.2 The use of heme models for compounds I and II.

The use of porphyrin models for the enzyme intermediates compounds I and II allows relatively easy determination of the effects of ligation, solvation and porphyrin ring substituents. A number of studies have been undertaken on model compound II ferryl intermediates [25-28]. Gold *et al.* [29] have presented spectra (UV-vis, nmr, RR) of the ferryl complex of (tetrakis(2,6-dichlorophenyl)porphinato) iron, and have compared their results with spectral data from other ferryl porphyrins. These water-insoluble model systems are very unstable, and all spectra have been recorded in non-aqueous solvents at low temperatures. Water soluble ferryl porphyrins have been shown to be more stable [30, 31] and room temperature RR [30] and UV-vis. spectra [31] have been reported.

All the above studies have employed either chemical oxidising agents or electrochemical methods to generate the ferryl species. Peterson *et al.* instead photochemically generated the ferryl tetraphenylporphine (TPP) complex, $(TPP)Fe^{(IV)}=O$ by photodisproportionation of the μ-oxo-dimer, $[(TPP)Fe^{(III)}]_2O$ [32]. The $Fe^{(IV)}=O$ and $Fe^{(II)}$ species produced were characterised by their

transient absorption spectra, and by trapping the ferryl fragment with triphenylphosphine. The ferryl species could still be observed 5 μs after the photolysis flash, but was only formed with a quantum yield of 10^{-4}. Another transient absorption study [33] of this process has contradicted the observations and interpretation of Peterson *et al.*. Guest *et al.* instead report photodissociation of the μ-oxo dimer to form an ion pair, which then undergoes geminate recombination within 4 ns [33].

In this chapter, time resolved resonance Raman (TR^3) results are presented for the μ-oxo dimer, $[(TPP)Fe^{(III)}]_2O$, and the monomer, $(TPP)Fe^{(III)}Cl$, in an attempt to clarify the contradicting results of Peterson *et al.* and Guest *et al.*.

The RR study of porphyrin cation radicals has generated much interest, as these are models for a large range of heme enzymes. Porphyrin cation radicals are known to be able to exist in either an A_{1u} or A_{2u} ground state; this difference has a large effect on the RR spectra [34]. The character (A_{1u} or A_{2u}) of the cation radical is determined by the nature of the porphyrin, the central metal, and its axial ligands. Predictions of cation radical ground states have been made by M.O. calculations and from e.s.r and UV-vis. spectra [35]. Until very recently, there was confusion in the interpretation of the RR spectra of porphyrin cation radicals, which did not appear to follow the predictions from the expected ground state character (A_{1u} or A_{2u}) [36]. Some of the early confusion appears to have arisen from the presence of impurities in the sample [37]. Subsequently, Czernuszewicz *et al.* have made a careful study of the RR spectra of metallated octaethylporphine species, $MOEP^{+\cdot}$ and metallated TPP species, $MTPP^{+\cdot}$ and have found their results consistent with predictions of ground state character [34]. The

$MOEP^{+\cdot}$ species are found to have electronic ground states of predominantly A_{1u} character, whereas the $MTPP^{+\cdot}$ species have predominantly A_{2u} character. These results have already proved useful in interpreting the most recent RR data on HRP compound I [24].

6.2 EXPERIMENTAL

6.2.1 Materials and methods for catalase experiments

Materials

The chemicals and other items used for catalase experiments are listed below:

Catalase (Sigma C-100, suspension containing 0.1% thymol)

Catalase (Boehringer, crystalline high purity 'calibration standard')

Ce_2SO_4, cerium sulphate (BDH, AR grade)

Ferroin indicator (BDH)

KI, potassium iodide (Fisons, AR grade)

NaCl, sodium chloride (Fisons, SLR grade)

NaCN, sodium cyanide (BDH, SLR grade)

NaN_3, sodium azide (Fisons, SLR grade)

$Na_2HPO_4.12H_2O$, disodium hydrogen phosphate (Merck, AR grade)

$NaH_2PO_4.H_2O$, sodium dihydrogen phosphate (Merck, AR grade)

$Na_2S_2O_3.5H_2O$, sodium thiosulphate (BDH, AR grade)

Peroxyacetic (peracetic) acid, 32% $^{w}/_{v}$ in dilute acetic acid (Aldrich)

Starch indicator (BDH)

Tris(hydroxymethyl)aminomethane buffer, 'tris' (BDH, GPR)

Visking (dialysis) tubing, 8/32 (Medicell international)

Buffers

Phosphate and tris buffers were used for all experiments, at 0.01 M, between pH 6.0 and 7.8. Phosphate buffers of varying pH were made from different mixtures of solutions of disodium hydrogen phosphate and sodium dihydrogen phosphate, as described in ref.[38]. Tris buffers of pH 7.0 to 7.8 were made by adjusting tris solutions with dilute HCl.

Peroxyacetic acid (PAA) pretreatment and estimation

As noted by Middlemiss [10], commercial PAA preparations contain varying amounts of hydrogen peroxide, which will react rapidly with catalase to liberate oxygen. Relatively high proportions of H_2O_2 in PAA solutions are undesirable, as they will affect the kinetics of the reaction to form compounds I and II, and will cause bubbles to form in the Raman (or UV-vis.) cell.

PAA stock was diluted 400- to 800- fold (i.e. to concentrations in the range $5\text{-}10\times10^{-3}$ M), and the resulting solutions titrated with solutions of 0.01 M Ce_2SO_4 in 1 M H_2SO_4, using Ferroin indicator to detect the endpoint. Untreated solutions were found to contain as much H_2O_2 as PAA. To reduce the H_2O_2 content of PAA solutions, a pretreatment procedure was employed, as in ref. [10].

Dilute PAA solutions were pretreated by the addition of dilute catalase solutions. Typically, 50μl of stock (dialysed) catalase was added to 250 ml of 800x diluted PAA stock, i.e. to a catalase concentration of *ca.* 10^{-7} M. After 30 minutes at room temperature, nearly all the H_2O_2 was destroyed by such pretreatment. Pretreated PAA solutions could be kept at 0-4°C for up to 1 day before significant amounts of H_2O_2 were formed.

The concentrations of pretreated PAA solutions were determined iodometrically. A known volume (10 to 25 cm^3) of PAA was added to an excess of acidic KI (1% KI in 5 M H_2SO_4), then the liberated iodine was titrated with 0.01 M sodium thiosulphate, using starch indicator.

Catalase preparations

Several catalase sources were investigated, but most were too impure and too fluorescent to be suitable for spectroscopic studies. The Boehringer catalase (a generous gift from the company) was the most pure, but still produced significant fluorescence with excitation wavelengths longer than 413.1 nm. The Sigma catalase was suitable for use after dialysis to remove thymol (preservative) and other small impurities. To 1 cm^3 catalase suspension, 1-2 drops of 5% ammonia was added to dissolve the catalase. This solution was then dialysed overnight at 0-4°C against 0.01 M tris or phosphate buffer containing 0.1 M NaCl and a small amount of charcoal (added in an attempt to remove fluorescent impurities). The catalase solutions prepared by this method had purity values of *ca.* 0.9 or above, where purity is judged by the ratio A_{405}/A_{280} [10]. Fluorescence was prohibitive with excitation out of the Soret band. The concentration of the stock solution produced was calculated from the absorption at 405 nm, using $\epsilon_{405} = 3.4 \times 10^5\ M^{-1}cm^{-1}$ [10].

Attempts were made to purify dialysed catalase solutions further by column chromatography, using Sephadex G-25, G-50, G-100, G-150 and G-300 columns. None of the columns used were successful in either reducing fluorescence or increasing the purity value, so further purification was abandoned. Other workers have nevertheless reported success using Sephacryl S-200 [4] and Sephadex G-150

columns [10].

Preparation of catalase derivatives

The azide derivative of catalase was produced by the addition of small amounts of solid sodium azide to catalase solutions at pH 6.0. The formation of the catalase-azide complex was confirmed spectroscopically by observing the shift in the Soret band from 405 to 411 nm [39]. The cyanide derivative was similarly produced by the addition of small amounts of solid sodium cyanide (1 small crystal to 1 cm^3) to catalase in neutral or slightly alkaline solutions. The formation of the catalase-CN complex was confirmed by the shift in the Soret band from 405 to 424 nm [39].

Compound I of catalase was prepared by the addition of a *ca.* 10x excess of PAA to catalase. Typically, 30 μl of $1x10^{-3}$ M PAA was added to 1 cm^3 $3.5x10^{-5}$ M catalase. The reaction could be monitored either by Raman spectroscopy or by UV-vis. spectroscopy (using a 1 mm path length cell). The formation of compound I is immediate in the time resolution of these experiments. Middlemiss has shown that a 9:1 PAA to catalase ratio is necessary to maximise the formation of compound I, and that at this ratio, all catalase heme groups react [10]. At higher PAA to catalase ratios, it appears (from these experiments, and from those of Middlemiss [10]) that larger amounts of compound II are formed.

Raman spectroscopy

Raman spectra of the stable species, catalase-CN, catalase-azide and of native catalase were obtained using the Spex spectrometer system described in chapter 2, with 413.1 or 406.7 nm excitation. Typical laser powers were less than 40 mW at the sample.

A spinning cell was generally used for Raman experiments, although some spectra were recorded using thin (1 mm i.d.) capillaries, low (less than 10 mW) laser powers and a defocussed beam to avoid local heating.

Raman spectra of compound I (and II) were obtained using the multichannel CCD system described in chapter 2, with 413.1 or 406.7 excitation. Conventional right angle illumination and a spinning cell were used for all experiments. Calibration of spectra was performed using dioxan or dimethylformamide standards.

6.2.2 Materials and methods for porphyrin heme-model experiments.

$(TPP)Fe^{(III)}Cl$ and $[(TPP)Fe^{(III)}]_2O$

Iron(III)tetraphenylporphine chloride $(TPP)Fe^{(III)}Cl$ was a generous gift from Dr. J.R.Lindsay-Smith (York). The μ-oxo dimer, $[(TPP)Fe^{(III)}]_2O$, was prepared by shaking solutions of $(TPP)Fe^{(III)}Cl$ in dichloromethane (SLR grade) with 2 M NaOH (Fisons AR grade), followed by repetitive washing with distilled water. The formation of the dimer was not immediate. The UV-vis. (and Raman) spectra showed that $(TPP)Fe^{(III)}OH$ was first formed, which slowly (over one or more days) converted to $[(TPP)Fe^{(III)}]_2O$. The UV-vis. absorptions of these species in dichloromethane are given in Table 6.1.

Table 6.1 UV-vis. absorption maxima for FeTPP derivatives in dichloromethane.

Sample					
	λ max/nm				
$(TPP)Fe^{(III)}Cl$	378	412	506	569	608
$(TPP)Fe^{(III)}OH$	327	412	-	571	612
$[(TPP)Fe^{(III)}]_2O$	317	407	-	569	609

Raman spectroscopy

All time-resolved resonance Raman (TR^3) experiments were undertaken at the laser support facility, Rutherford Appleton Laboratory. The Triplemate spectrometer, OSMA detection system, and lasers used are described in chapter 2. The timing system necessary for one- and two- colour TR^3 experiments is also described in chapter 2.

Samples of $(TPP)Fe^{(III)}Cl$ and $[(TPP)Fe^{(III)}]_2O$ were made to appropriate concentrations (usually *ca.* A=10 per cm at the pump wavelength) in SLR dichloromethane. Further purification of dichloromethane did not affect the spectra or the amount of photodecomposition. In all experiments, samples were flowed through a quartz capillary tube (1 mm i.d.). Solutions were normally recycled, as the flow rate of the pump was fast - *ca.* 1 cm^3 per second. The capillary tube was translated slowly through the beam in pump-probe experiments to avoid excessive tube damage and build up of damaged porphyrin.

6.3 RESULTS

6.3.1 RR spectra of catalase and stable derivatives.

The RR spectra of native catalase (406.7 nm excitation), catalase-CN and of catalase-azide (413.1 nm excitation) are shown in Figs. 6.1 and 6.2. The spectra are typically accumulations of 4 or more scans, with a 1 second integration time. Fluorescence backgrounds have been subtracted where necessary. The wavenumber values and assignments are given in Table 6.2. The RR spectra of catalase from Boehringer and from Sigma were identical, and did not change markedly with pH in the range 6.0 to 7.8. There was a small change with pH in the 450-600 cm^{-1} region; in the high pH spectrum, a new band appeared at 502 cm^{-1}.

6.3.2 RR and UV-vis. spectra of catalase compounds I and II.

The UV-vis. spectrum of catalase in the Soret region is shown in Fig. 6.3, and shows a strong absorption maximum at 405 nm. Fig. 6.4 shows the visible absorption region with the weaker bands at *ca.* 500, 540 and 622 nm. Fig. 6.3 and 6.4 also show the spectrum of catalase immediately (i.e. < 15 s) after the addition of a 10x excess of PAA (---), i.e. the spectrum of compound I, and the spectra taken at intervals (-·-·, 2 minutes, — — —, 6 minutes) after the addition of PAA. Compound I absorbs comparatively weakly at 405 nm, and also at 540 and 660 nm (n.b. the 660 nm band is just offscale in Fig. 6.4). The original absorbance is never completely regained, there always appears to be an irreversible loss that is attributed to oxidation of ferrihaem to biliverdin [10], and, in the medium term, some loss is due to the formation of compound II. The presence of biliverdin does not affect the RR spectra; its

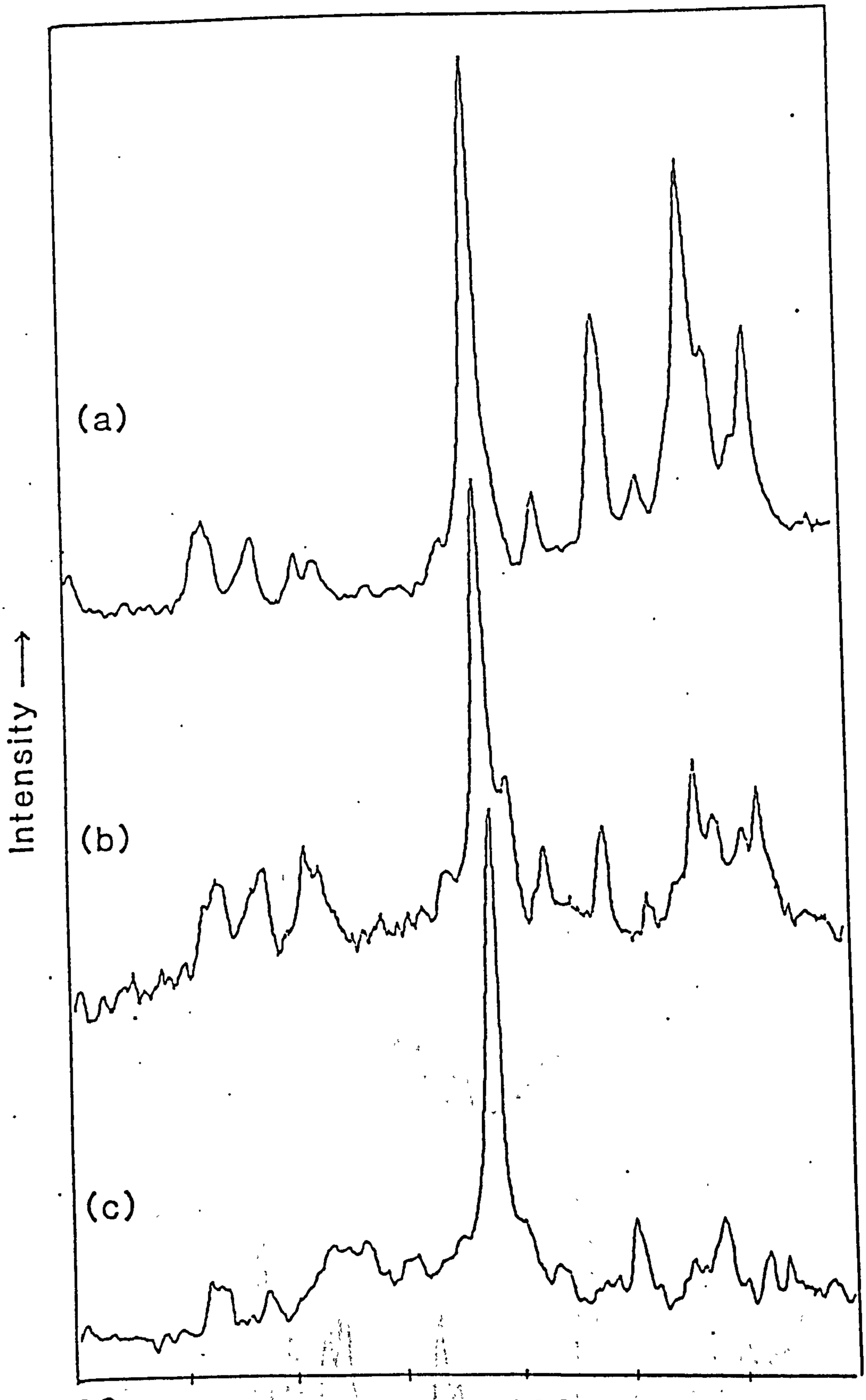

Figure 6.1 RR spectra of (a) native catalase, pH 7.8, 406.7 nm excitation, (b) catalase-azide, pH 6.0, 413.1 nm excitation, and (c) catalase-CN, pH 7.8, 413.1 nm excitation.

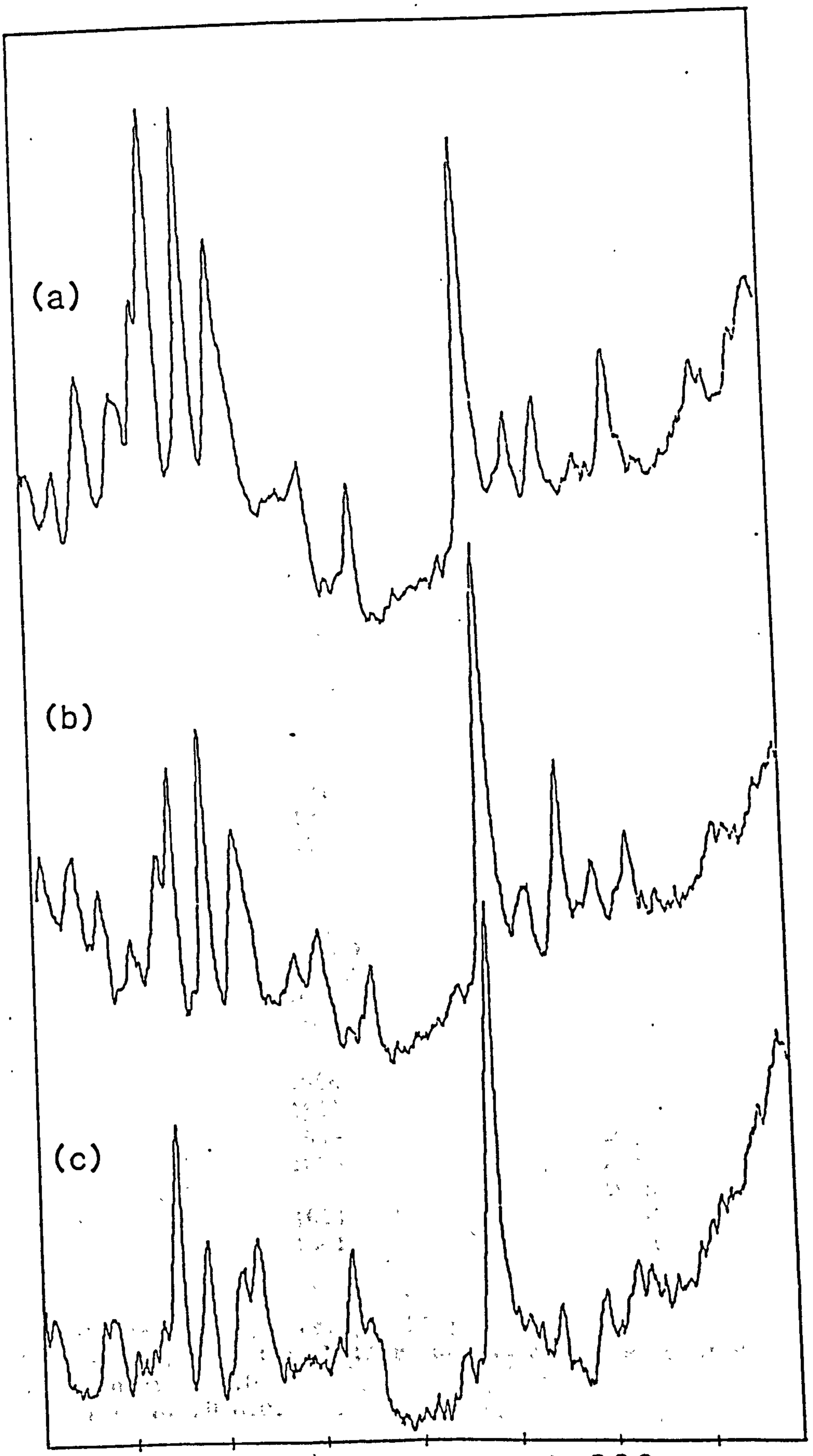

Figure 6.2 RR spectra. as Fig. 6.1. low wavenumber region.

Table 6.2: RR assignments for catalase and catalase derivatives

Wavenumber/cm^{-1}			Assignment[a]
Catalase[b]	Cat-N_3	Cat-CN	
	205	212	
237	239		
267	268	277	ν 9
307	301		γ (C_mC_a)
331	333	330	δ ($C_bC_\alpha C_\beta$)(2)
348	349	347	ν 8
384	385	380	γ (C_bS)
415	417	415	δ ($C_bC_\alpha C_\beta$)(1)
425sh	424sh	433	pyr fold
	476		
504[c]	506		ν(Fe-OH)
		530	
554	556		ν 49
		646	
677	680	679	ν 7
723	722		ν 16
756	759	751	ν 33 + ν 34
801[d]	797	799	
833	835	834w	γ (C_mH)
927	923		ν 46
992			ν 45
1006		1007w	γ (CH=)
1129	1120)	1121	)
	1132)	1130	) ν 6 + ν 8
1176	1177	1176	ν (C_bC_α)(1)
1215	1215		
1233	1229sh	1233	ν 13
1342	1340	1347	δ_s ($=CH_2$)(2)
1373	1371-2	1376-7	ν 4
	1394sh	1404sh	ν 29
1428	1426	1435	δ_s ($=CH_2$)(1)
1486	1480	1503	ν 3
1523	1520		ν 38, tyr
1549sh		1566	ν 11
		1555	ν 38
1569	1566	1584	ν 2, ν 19
1588	1584	1605	ν 37
1612sh	1610		ν 10 (or tyr)
1626	1624	1624	ν (C=C)
		1641	ν 10

[a] Assignments made using refs. [4, 13a]
[b] Catalase at pH 7.8 in tris buffer, unless otherwise stated.
[c] Not observed at pH 6.0.
[d] Only observed at pH 6.0.

absorption is weak compared with that of catalase.

Catalase compound I decays to form both native catalase and, depending on the precise conditions, compound II. The formation of small amounts of compound II was almost unavoidable. The spectra in Figs. 6.3 and 6.4 show very little compound II, which absorbs characteristically at *ca.* 425 and 567 nm. The formation of compound II from compound I is increased in the presence of phenols, alcohols, anions, or simply in a large excess of PAA. Fig. 6.5 shows the effects of adding an excess of PAA to the absorption spectrum of catalase. Clear bands appear at 425 and 567 nm.

The RR spectrum of catalase obtained with the CCD system and *ca.* 30 mW 406.7 nm excitation is shown in Fig. 6.6 (a). The spectrum of the same sample taken immediately after the addition of a 10x excess of PAA is shown in Fig. 6.6 (b). Spectra are shown to scale, and are the averaged result of two separate experiments. The spectra were accumulated for 40 seconds, under the same conditions of laser power, focus and spectral resolution. The spectrum of catalase immediately after the addition of PAA is about one-quarter of the intensity of the native catalase spectrum, but has a higher background. The positions of the main bands at 1374 (ν 4), 1487 (ν 3) and 1571 cm^{-1} (ν 2) remain unchanged, although the relative intensity of the 1571 cm^{-1} band drops markedly. The only new bands in the spectrum are those at 1645 and 1511 cm^{-1}. The latter changes are accompanied by the loss of the band at 1522 cm^{-1}. The RR spectrum gradually recovers to that of the original catalase, regaining most of the original intensity. The band at 1645 cm^{-1} disappears as the original spectrum recovers, although some intensity persists at 1511 cm^{-1} even after 10 minutes. Spectra of catalase before and after the addition of PAA were also recorded at

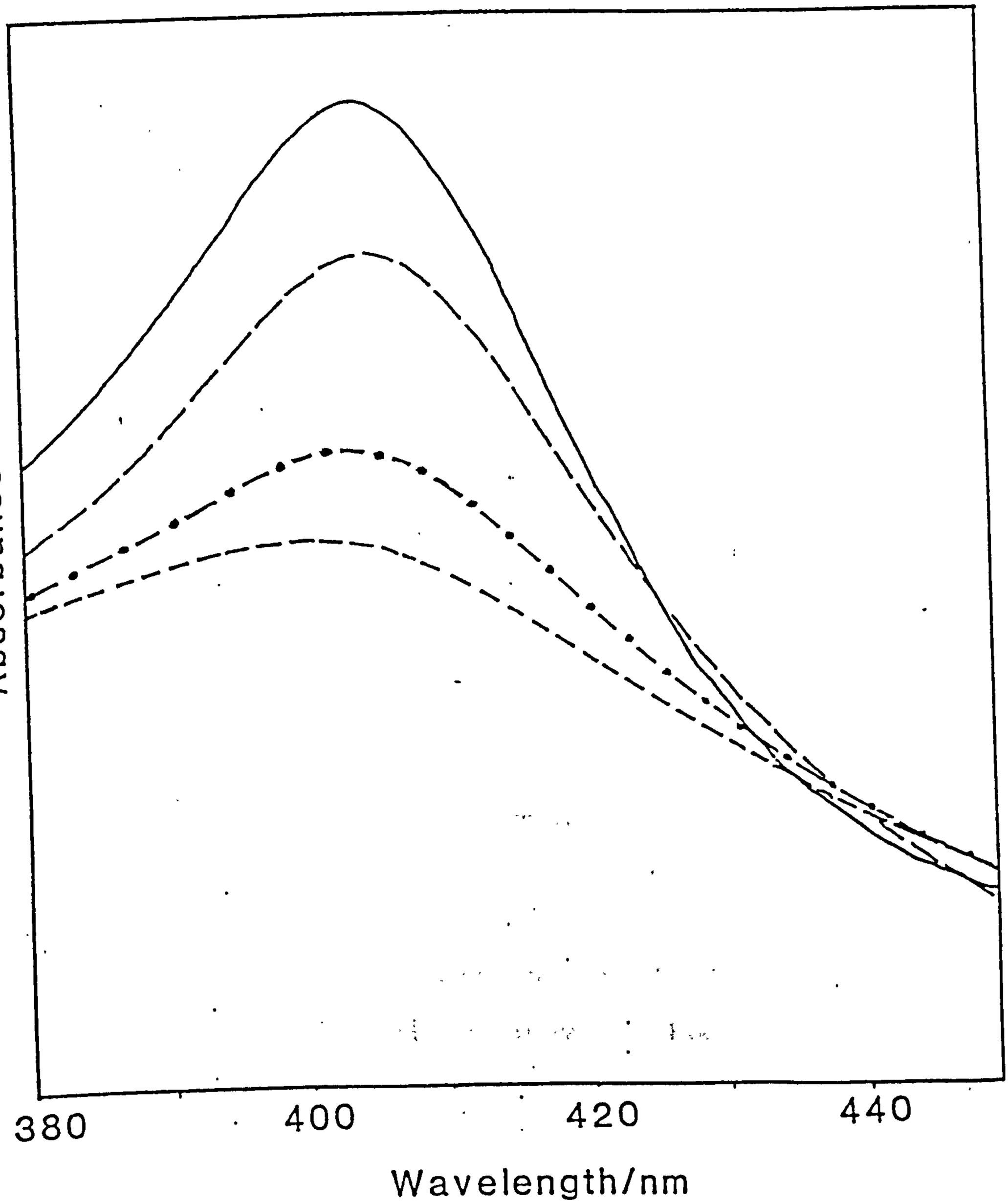

Figure 6.3 Soret region absorption spectrum of native catalase (———), and of catalase immediately (- - - - -), 2 minutes (-·-·-·), and 6 minutes (— — —) after the addition of a 10x excess of PAA. The dashed trace (------) shows the absorption spectrum of compound I.

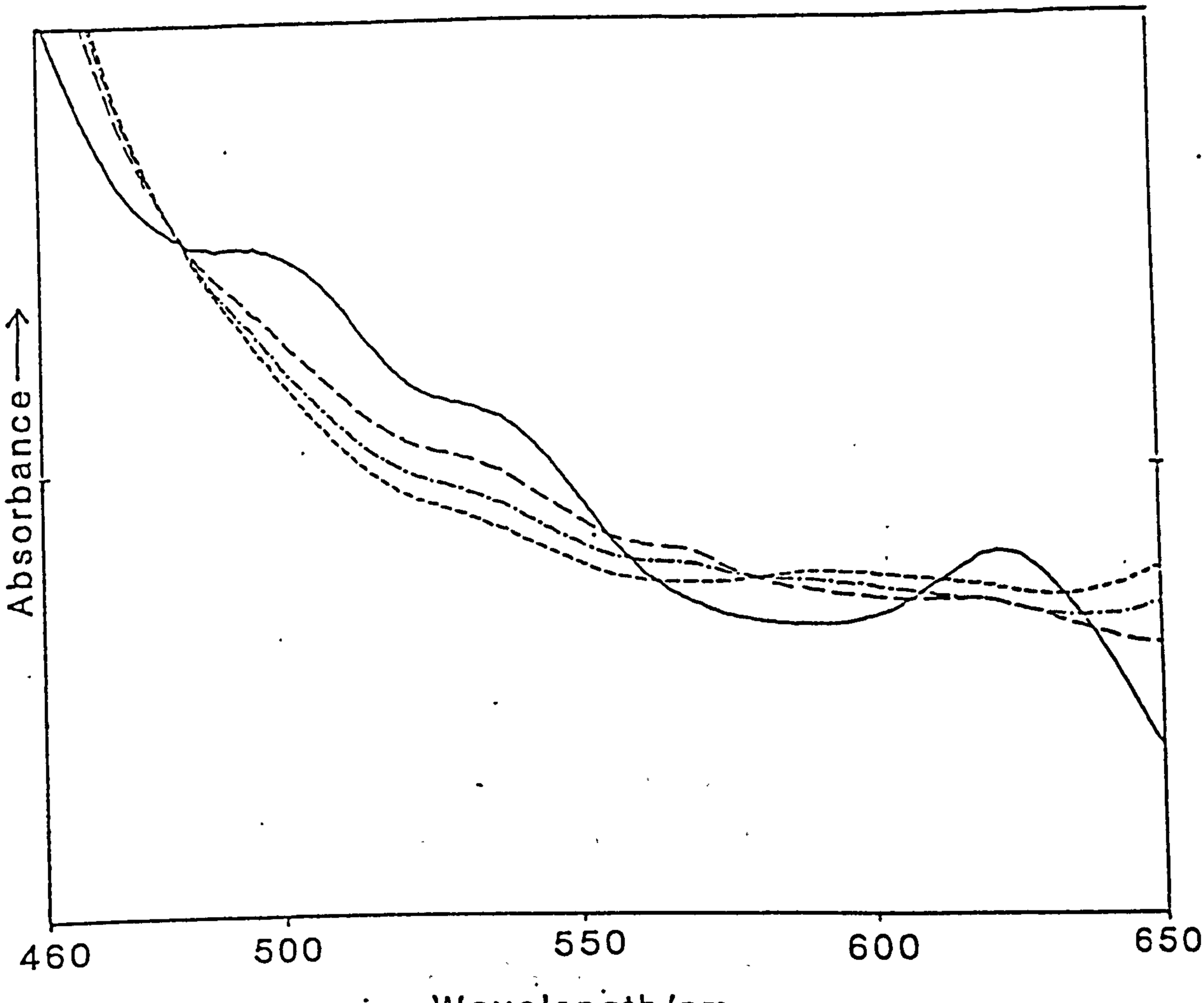

Figure 6.4 Visible absorption spectrum of catalase, and catalase after the addition of PAA, as Fig. 6.3.

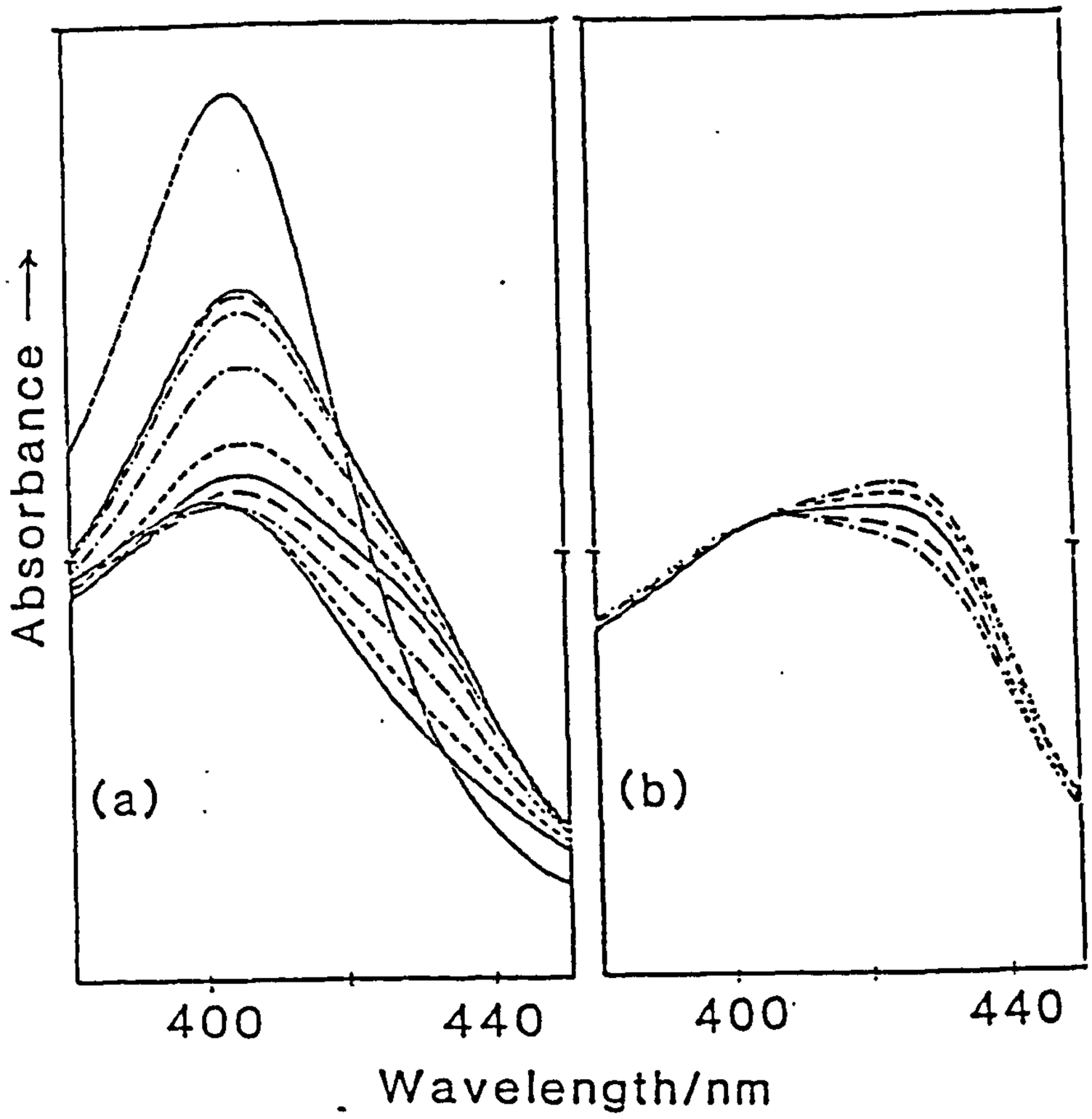

Figure 6.5 Soret region absorption spectra of catalase, and of catalase at varying time intervals after the addition of a 20x excess of PAA (a), and after the addition of a > 20x excess of PAA (b).

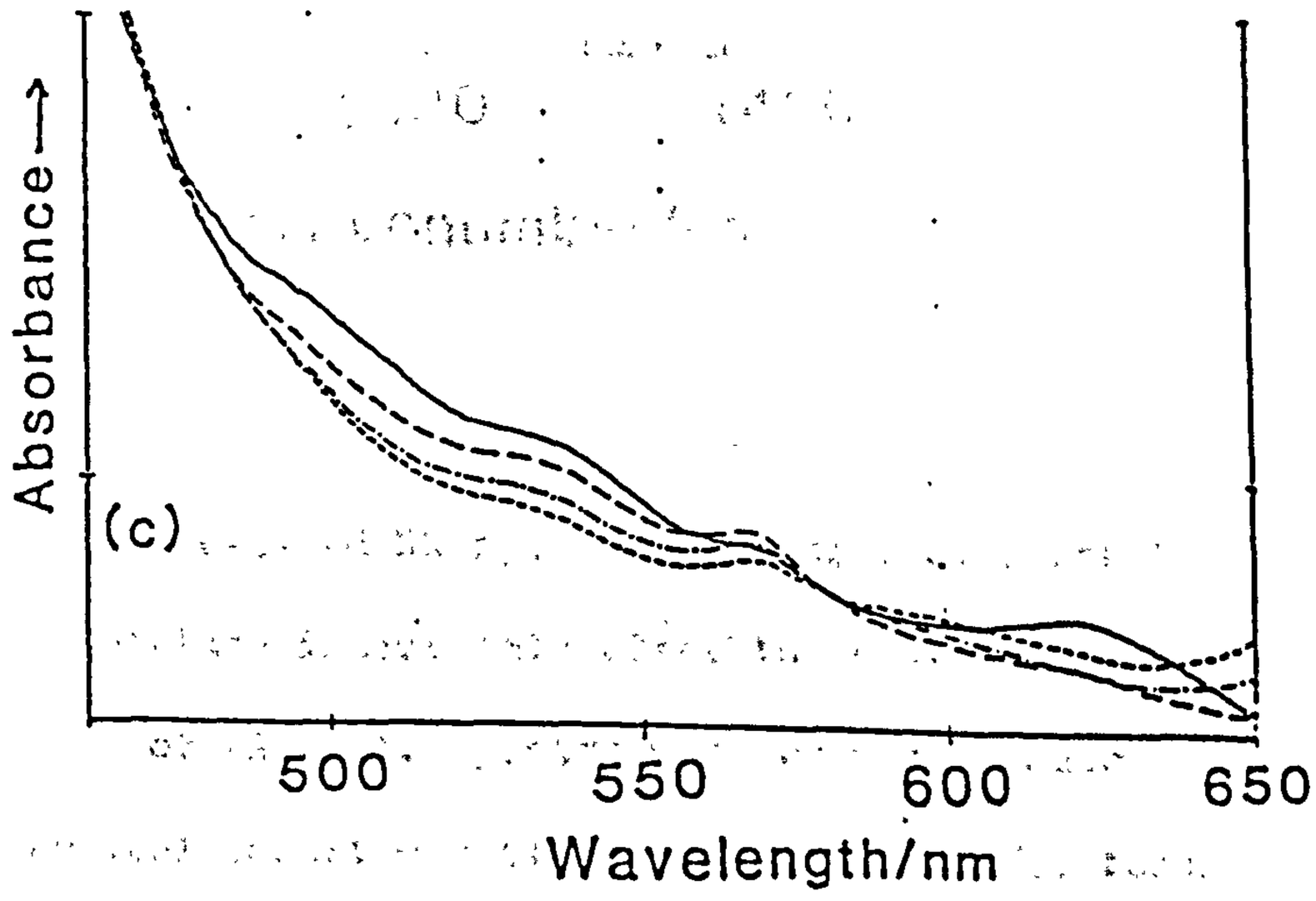

(c) Visible absorption region of catalase (——), and of catalase after the addition of a *ca.* 20x excess of PAA (------, 10 s, —·—·—·—, 2 minutes, — — — —, 6 minutes).

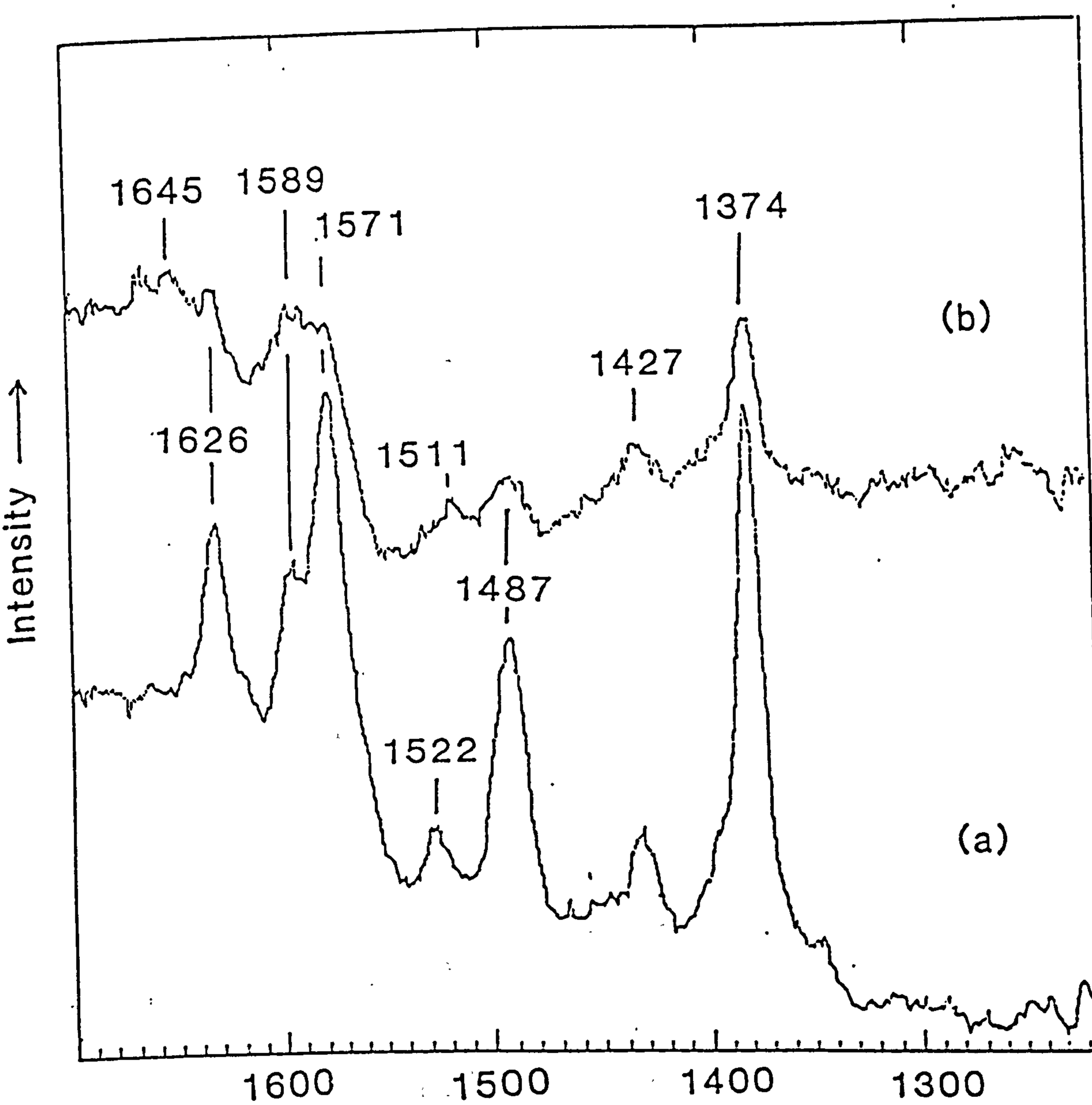

Figure 6.6 406.7 nm-excited RR spectra of native catalase (a), and catalase immediately after the addition of a 10x excess of PAA (b). Spectra were recorded under identical conditions of laser power (30 mW), focus, accumulation time, and are shown to scale.

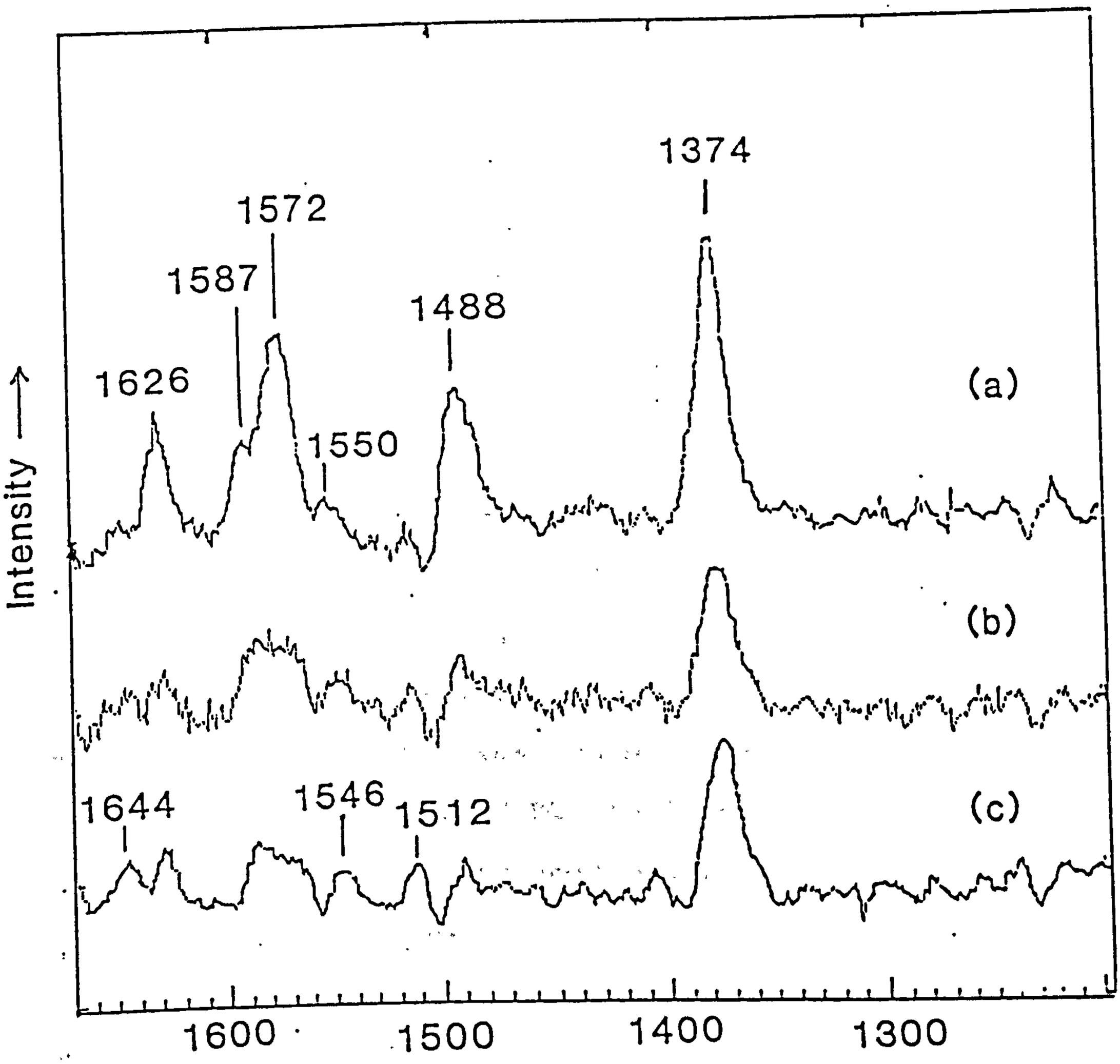

Figure 6.7 413.1 nm-excited RR spectra of (a) native catalase, (b) catalase immediately after the addition of a 10x excess of PAA, and (c), catalase after the addition of a > 30x excess of PAA. Fluorescence backgrounds have been subtracted.

much lower laser power (2 mW at sample), and appeared to be very similar to those obtained at high power.

On the addition of a second aliquot of PAA to the (mostly) regenerated catalase, the RR spectrum again dropped in intensity. In this spectrum, however, bands at 1645 and 1511 cm^{-1} were more prominent than in the spectrum in Fig. 6.6 (b).

The RR experiments were repeated using 413.1 nm excitation, closer to the absorption maximum of compound II (*ca.* 425 nm). Fig. 6.7 shows the RR spectra of (a) catalase, (b) catalase after the addition of PAA (10x excess), and (c) after the addition of a large excess of PAA. The UV-vis. spectrum taken after recording the spectrum shown in Fig. 6.7 (c) showed a large proportion of compound II in the sample. The results in Fig. 6.7 are essentially very similar to those in Fig. 6.6. However, a band at 1550 cm^{-1} in Fig. 6.7 (a) is distinct, and becomes relatively more intense, shifting to 1547 cm^{-1} on the addition of PAA. The bands at 1644 and 1512 cm^{-1} are surprisingly not vastly different in relative intensity in the spectra in Fig. 6.7 (b) and (c).

6.3.3 Model heme systems

The 406.7 nm (cw laser), 408 and 424 nm (pulsed laser) RR spectra of $(TPP)Fe^{(III)}Cl$ and $[(TPP)Fe^{(III)}]_2O$ in dichloromethane agree reasonably well with other reported spectra [40, 41], the dimer showing a characteristic Fe-O-Fe band at 363 cm^{-1}, see Fig. 6.8. This band was not observed immediately after shaking $(TPP)Fe^{(III)}Cl$ with NaOH; its absence was attributed to the slow formation of dimer from $(TPP)Fe^{(III)}OH$ (which has a similar UV-Vis. absorption, see Table 6.1). The 363 cm^{-1} band is not as resonantly enhanced at 406.7 nm as Burke *et al.* suggest [40], its Raman

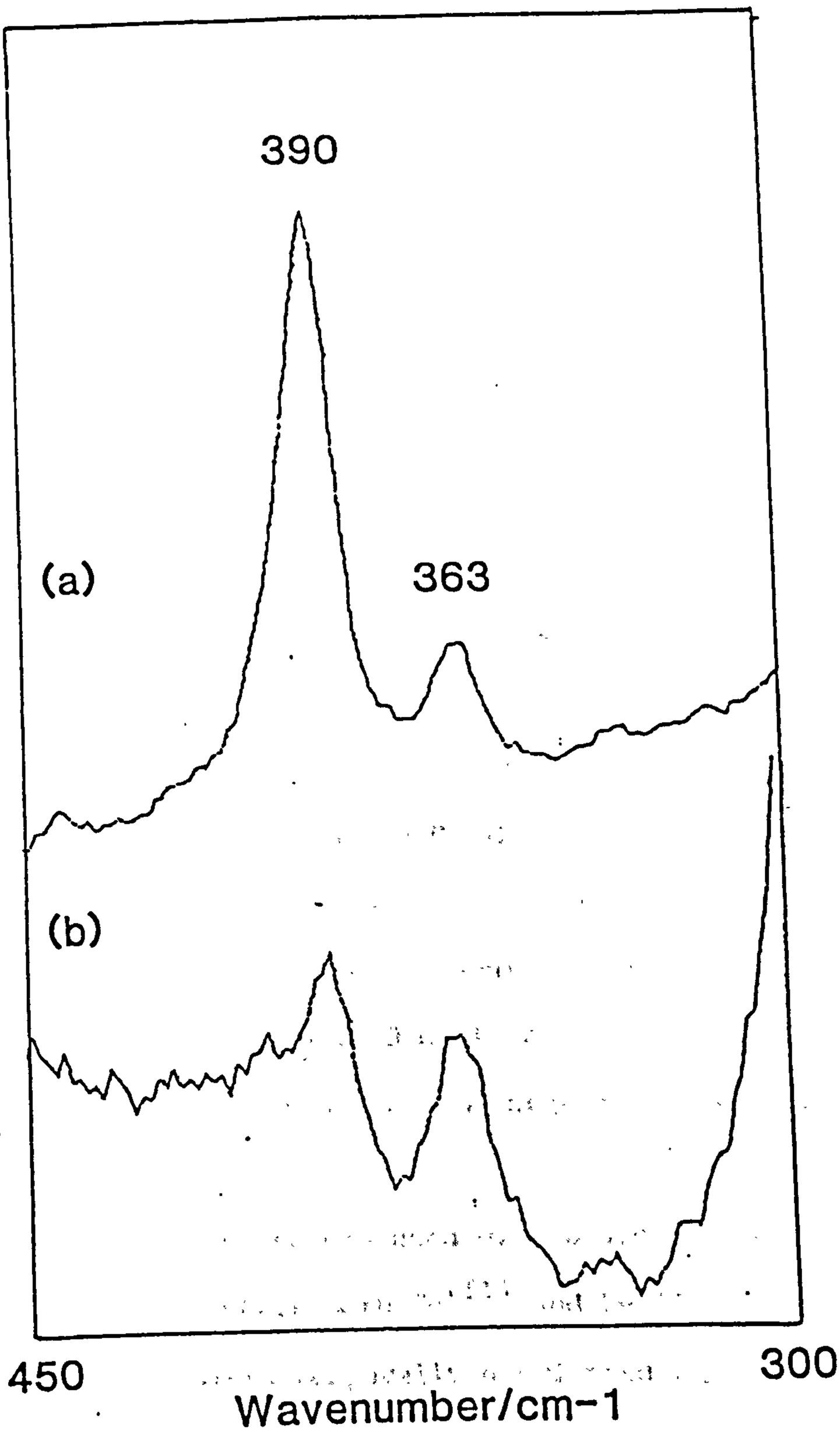

Figure 6.8 (a) 406.7 nm-excited RR spectrum of $[(TPP)Fe^{(III)}]_2O$ in dichloromethane. (b) 457.9 nm-excited RR spectrum of $[(TPP)Fe^{(III)}]_2O$ in dichloromethane.

excitation profile (REP) maximum appears to be to the red of the Soret absorption maximum (see Fig. 6.8). Fig. 6.9 shows the high wavenumber region of the 424 nm-excited RR spectra of $(TPP)Fe^{(III)}Cl$ (a), $(TPP)Fe^{(III)}OH$ (b), and $[(TPP)Fe^{(III)}]_2O$ (c). The wavenumber values of the bands are listed in Table 6.3.

Exciting into the Soret absorption maximum using 408 nm, 10 ns laser pulses, large differences in porphyrin band intensities with respect to the solvent band intensities were observed between spectra obtained using high (0.25-0.5 mJ/pulse) and low (3-10 μJ/pulse) laser power. Fig. 6.10 shows the 408 nm excited RR spectra of $[(TPP)Fe^{(III)}]_2O$ at high (a) and low (b) laser power, and of $(TPP)Fe^{(III)}Cl$ at high (c) and low (d) laser power. The solvent (dichloromethane) bands are marked **S**. The reduction in the intensity of the porpyrin RR bands with respect to the solvent bands at high laser powers represents a large 'bleaching', or loss of the ground state porphyrin. Using 424 nm, 10 ns laser pulses, a similar bleaching effect was observed, but no large new peaks appeared to grow in at high laser powers.

A 406 nm pump pulse was used with a 424 nm probe pulse to probe at a wavelength where both $Fe^{(II)}$ and $Fe^{(IV)}$=O species absorb strongly. With the pulses temporally overlapped (Δt = 0 ns), the bleaching effect was confirmed - loss in intensity of all the ground state porphyrin bands, and gain in intensity of solvent bands was observed. No new peaks were observed that could be attributed to $Fe^{(II)}$ or $Fe^{(IV)}$=O. Most of the bleaching appeared to be reversible; at Δt = 15 ns, the bleaching was much reduced. However, the residual bleaching observed at 15 ns was still present at 1 μs, and is probably due to some sort of permanent photodecomposition. Indeed, after exhaustively recycling the sample in the pump beam, shifts in

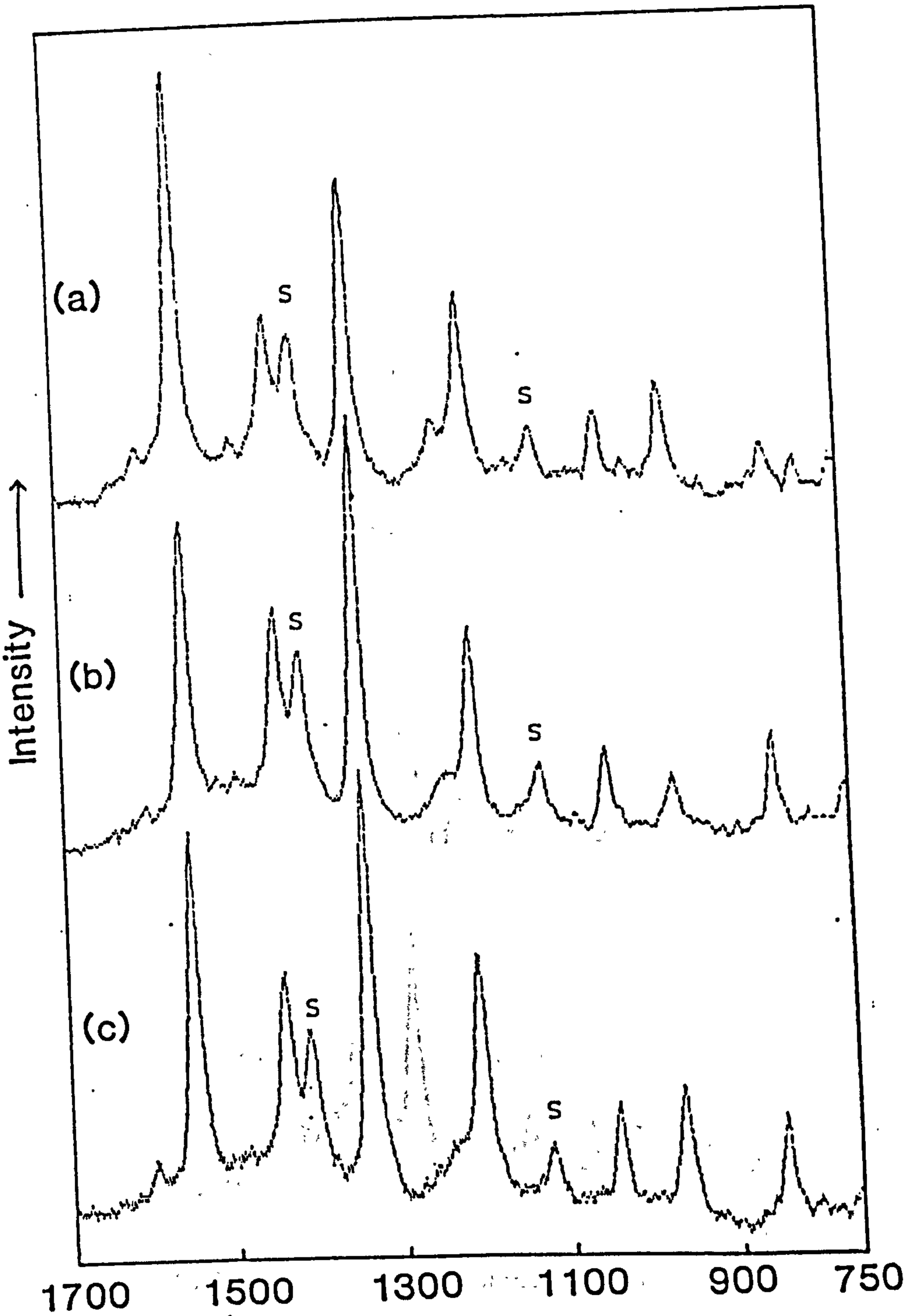

Figure 6.9 424 nm-excited RR spectrum of (a) $(TPP)Fe^{(III)}Cl$, (b) $(TPP)Fe^{(III)}OH$ and (c) $[(TPP)Fe^{(III)}]_2O$, in dichloromethane. Dichloromethane bands are marked S.

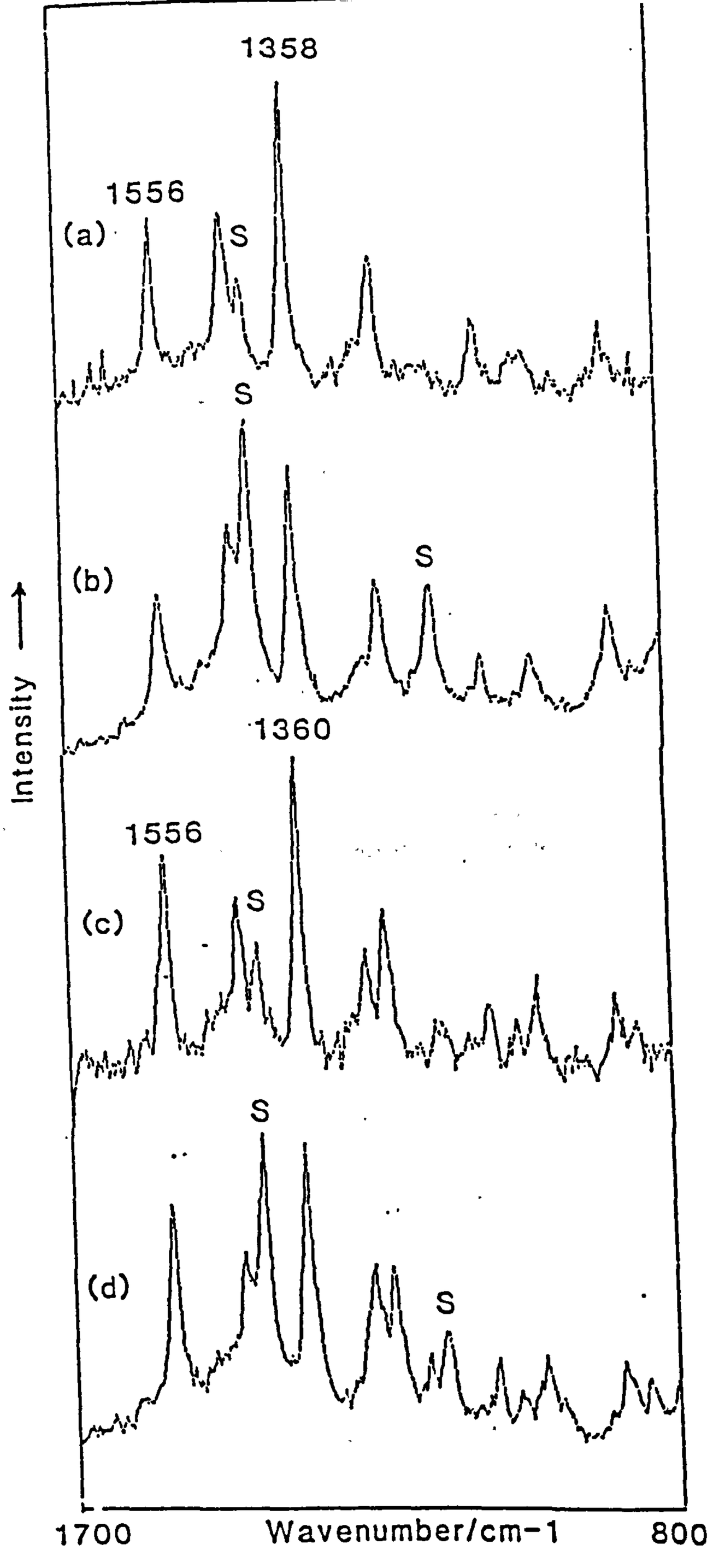

Figure 6.10 408 nm-excited RR spectra of

(a) $[(TPP)Fe^{(III)}]_2O$, high laser power,

(b) $[(TPP)Fe^{(III)}]_2O$, low laser power,

(c) $(TPP)Fe^{(III)}Cl$, high laser power,

(d) $(TPP)Fe^{(III)}Cl$, low laser power.

Dichloromethane (solvent) bands are marked S.

Table 6.3 Wavenumber values and assignments[a] of bands in the spectra of the $(TPP)Fe^{(III)}$ derivatives (Fig. 6.9).

Wavenumber/cm^{-1}			Assignment
$(TPP)Fe^{(III)}Cl$	$(TPP)Fe^{(III)}OH$	$[(TPP)Fe^{(III)}]_2O$	
1557	1556	1556	ν 2
1450	1450	1450	ν 3
1360	1360	1358	ν 4
1231	1231	1231	ν 1, ν (C_m-P)
1077	1077	1075	δ $(C_\beta H)_{sym}$
1001	1001	1001	ν 6, ν (pyr br)
886	884	883	ν 7, δ (pyr def)$_{sym}$

pyr=pyrrole, def=deformation, br=breathing, sym=symmetric,

P=phenyl.

[a] Assignments made using refs. [34] and [57], there is however, considerable conflict in some assignments between refs. [34] and [57].

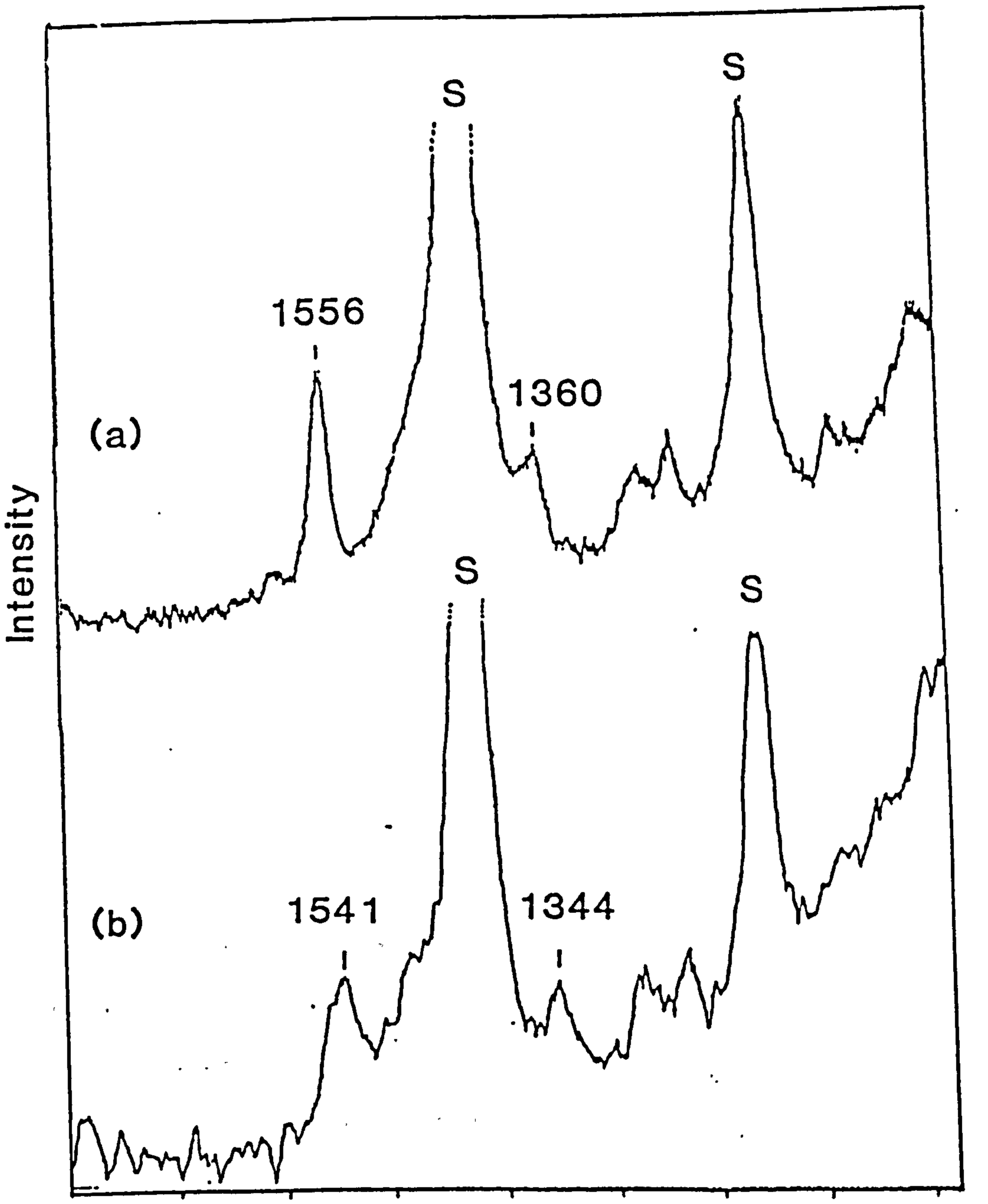

Figure 6.11 (a) 448 nm-excited (probe only) RR spectrum of $(TPP)Fe^{(III)}Cl$ in dichloromethane.

(b) 406 nm pump, 448 nm probe (Δt = 0 ns) TR^3 spectrum of $(TPP)Fe^{(III)}Cl$ in dichloromethane.

Dichloromethane bands are marked S.

UV-vis. absorption maxima could be observed for both monomer (Soret shift from 412 to 415 nm) and dimer (Soret shift from 407 to 415 nm). The change in the dimer absorption spectrum also indicated that photodissociation had taken place. Similar problems of photodecomposition of ZnTPP in dichloromethane have been reported [42].

A 408 nm pump pulse, to induce loss of ground state porphyrin was used with a 448 nm probe pulse, to probe at a wavelength where the porphyrin triplet state has been reported to absorb strongly [43]. At Δt = 0 ns, bleaching was accompanied by the growth of new bands. The probe only (i.e. ground state) spectrum, and the pump+probe spectrum (Δt = 0 ns) of (TPP)$Fe^{(III)}$Cl are shown in Fig. 6.11 (a) and (b). The band positions are given on the figure. Similar results were obtained with the dimer, although the new band at 1344 cm^{-1} shown in Fig. 6.11 (b) could not be observed in the corresponding dimer spectrum. In the pump+probe dimer spectrum, bands were observed at 1544 and 1229 cm^{-1}, with a very weak feature at *ca.* 1356 cm^{-1}. In the TR^3 spectra of both monomer and dimer, the new bands were not observed at Δt = 15 ns.

6.4 DISCUSSION

6.4.1 RR spectra of catalase and stable derivatives

The RR spectrum of catalase obtained at pH 7.8 (Fig. 6.1 (a) and 6.2 (a)) agrees well with the recently published RR spectrum of bovine liver catalase at pH 7.5 [4]. The positions of the oxidation, spin, and co-ordination state (or core size [13]) marker bands ν 4, ν 3, ν 2, and ν 37 confirm the identity of the heme iron in catalase as ferric high spin (see chapter 1, section 1.8).

The co-ordination of the iron, and the effects of co-ordination on the catalase RR spectrum are still debatable. On the proximal side, the heme iron is thought to be ligated to tyrosine [44]. Chuang *et al.* [4] have measured the Raman excitation profiles of catalase RR bands, and have tentatively assigned two bands, at 1612 and 1522 cm^{-1}, to tyrosine modes. The two bands are assigned to tyrosine modes on the basis of their positions and their excitation profile maxima at *ca.* 488 nm. Similar results have been observed for mutant Hb's with proximal tyrosines [45]. However, in the catalase spectrum, in contrast to the mutant Hb spectra, these two bands are weak and overlapped, and other tyrosine marker bands expected at *ca.* 600 and 1280-1310 cm^{-1} are not observed. It is possible that the intensity of the two bands arises almost entirely from ν 10 and ν 38, which are found in these positions for iron(III) high-spin, six-coordinate hemes such as aquomet Hb and Mb, and the model protoheme $(Me_2SO)_2Fe^{(III)}PP$ [46, 47]. These depolarised bands would be most enhanced with excitation in the visible region.

The sixth co-ordination position of catalase could be unoccupied in native catalase or occupied by a hydroxyl or aquo ligand. As pointed out above, the bands at 1612 and 1522 cm^{-1} can be assigned to ν 10 and ν 38 of a six-co-ordinate heme. The positions of the marker bands ν 3 (1486 cm^{-1}) and ν 2 (1569 cm^{-1}), in particular indicate a six- rather than a five- co-ordinate iron. Callaghan and Babcock, in their study of model hemes and hemeproteins (including aquomet Hb and Mb), assigned ν 3 and ν 2 bands occurring near 1482 and 1575 cm^{-1}, respectively, as indicating a six-coordinate iron [48]. The five-coordinate high spin species $Fe^{(III)}PPCl$ has ν 3 at 1495 cm^{-1} [46], much higher than ν 3 in catalase.

Recent X-ray studies resulted in the conclusion that native bovine liver catalase is five-coordinate [44]. Chuang *et al.* have also taken this view in their RR study [4]. It is also true that the six-co-ordinate catalase azide complex has $\nu 3$ and $\nu 2$ at significantly lower values than native catalase, at 1480 and 1566 cm^{-1}, respectively. The pH induced changes in the low wavenumber region of the catalase spectrum, and the lack of change in the high wavenumber region, are significant. The RR spectrum of HRP changes dramatically with pH as it changes from a five-coordinate high spin to a six-coordinate low spin [49] iron(III) heme. All the high wavenumber co-ordination and spin state marker bands shift to characteristic new positions and, significantly, a new band is observed at 503 cm^{-1}, which has been assigned to the $Fe^{(III)}$-OH stretching vibration [49].

The fact that the high wavenumber bands of catalase do not change with pH suggests that either (1) at all pH's catalase is five-coordinate, or (2) that catalase in solution is six-coordinate but the change between a hydroxyl and an aquo ligand (expected as pH is decreased) does not affect the core-size, and thus the marker bands of the heme. There is a band at 504 cm^{-1} in the RR spectrum of catalase at pH 7.8, which disappears in the spectrum obtained at pH 6.0. This could be indicative of a $Fe^{(III)}$-OH stretching band disappearing as the hydroxyl ligand is replaced by water. There is a band at 506 cm^{-1} in the catalase-azide RR spectrum, but this may be a coincidentally close porphyrin ring vibration.

In conclusion, although the core-size marker bands above 1400 cm^{-1} indicate a six-coordinate high-spin ferric iron, further work (e.g. isotope substitution) is needed to determine whether the band at 504 cm-1 in the spectrum of alkaline catalase is due to an

Fe-OH stretching vibration, or a co-ordination sensitive porphyrin vibration.

The RR spectrum of catalase-azide is firmly indicative of an $Fe^{(III)}$ six-coordinate high-spin heme. There is no evidence to suggest that the catalase-azide exists as a spin-state mixture, as suggested by Chuang *et al.* [3], and as exists for metMb-azide [50]. The very weak ν 3 and ν 10 bands at 1505 and 1638 cm^{-1} reported by Chuang *et al.* as indicators of some low spin catalase-azide are not observed in the spectrum shown in Fig. 6.1 (b). The low wavenumber region of the catalase-azide spectrum in Fig. 6.2 (b) does not show any bands that can be firmly assigned as Fe-N or internal azide modes. Asher and Schuster [51] have suggested that two bands at 413 and 570 cm^{-1} observed in the spectrum of metMb-azide are due to ν (Fe-N) of the low- and high- spin forms of the complex, respectively. Tsubaki *et al.* [52] have, on the other hand, assigned the bands to ν (Fe-N) and azide bending modes of the low spin complex. The spectrum in Fig. 6.2 (b) does not show a band at 573 cm^{-1}. A band at 417 cm^{-1} is strong, but also appears as a strong band in the native catalase and catalase-cyanide spectra. Thus, the lack of a band near 570 cm^{-1}, and the lack of a band that can be associated with azide at 413 cm^{-1}, supports the view of Tsubaki *et al.* that these bands in the catalase-azide apectrum are due to low spin forms of the azide complex. The catalase-azide complex appears to be totally high spin. Attempts were made to confirm this by recording the IR spectra of catalase-azide in the region 2000-2100 cm^{-1}, where azide stretching modes can be observed [53]. In metMb-azide, two bands have been observed at 2045 and 2023 cm^{-1}, and attributed to high- and low- spin complexes, respectively. In the catalase-azide IR spectrum, no band was observed at 2023 cm^{-1},

whilst a weak band was observed at *ca.* 2045 cm^{-1}. However, the spectra were troubled by the large absorption of water in this region, and also by the possibility of absorption of residual free azide at 2045 cm^{-1}.

The RR spectrum of catalase-cyanide shown in Figs. 6.1 (c) and 6.2 (c) is characteristic of a six-coordinate low spin ferric heme. The core size marker bands ν 3, ν 2, ν 37, and ν 10 are all upshifted from their positions in native catalase (see Table 6.2). Yu *et al.* [54] have recently assigned two bands in the spectrum of insect HbCN to δ ($Fe^{(III)}$-C-N) bending (at 410 cm^{-1}) and to ν ($Fe^{(III)}$-CN) stretching (at 453 cm^{-1}). The low wavenumber region of catalase-cyanide in Fig. 6.2 (c) shows marked differences from the spectra shown in Figs. 6.2 (a) and (b). However, there are no bands that can be unambiguously assigned as Fe-CN modes.

6.4.2 Spectra of catalase compounds I and II

The RR spectrum presented in Fig. 6.6 (b) was taken under conditions where the sample was almost entirely in the form of compound I, as can be seen from the corresponding UV-vis. spectra in Fig. 6.3 and 6.4. The RR spectrum in Fig. 6.6 (b) did show an overall loss of intensity, as expected from the corresponding loss of absorption. The spectrum does not show any large shift in ν 4 (1374 cm^{-1}), in contrast to the recently reported spectrum of HRP compound I [24], and the spectra of the MTPP cation radicals [34] (see section 6.1.2). The ν 4, ν 3 and ν 2 bands do change in relative intensity, the ν 3 and ν 2 bands dropping in intensity with respect to the ν 4 band. This could be due to the partial shift in ν 3 from 1487 cm^{-1} to 1511 cm^{-1}, and the partial shift in ν 2 from 1571 to *ca.* 1585 cm^{-1}, coincident with ν 37. These changes, and the

appearance of a band at *ca.* 1645 cm^{-1} are reasonably consistent with the formation of a compound II-type species. The RR spectrum of bovine liver catalase compound II has not been published, but the ν 4, ν 2 and ν 10 positions of horse blood catalase compound II have been reported to be at 1376, 1587 and 1641 cm^{-1}, respectively [4]. As discussed in section 6.1, studies of HRP compound I have been problematic, due to the apparent photolability of compound I [23b, 24]. The RR spectrum of compound I taken at relatively high irradiance bears a marked similarity to the spectrum of compound II (see section 6.1.1). In an attempt to avoid problems of compound I photodecomposition, spectra were obtained at 2 mW laser power; conditions which should have approached those of the 'successful' experiments of Paeng and Kincaid [24]. However, no differences could be observed between the results obtained at high and low power; thus, either the conditions were still inducing photodecomposition, or the spectrum in Fig. 6.6 (b) is that of compound I.

The spectra in Fig. 6.7, taken with 413.1 nm excitation, should show greater enhancement of any bands which might be due to the presence of compound II in the sample. But if compound I were to be immediately and entirely converted to compound II in the laser beam, then all that would be observed would be a greater overall enhancement of the spectrum after adding PAA (compared to the spectrum taken with 406.7 nm excitation). The latter change is difficult to measure, as the precise alignment of the sample and its concentration will affect the relative intensities of the catalase and compound I or II spectra, due to the differing absorption losses.

The spectra in Fig. 6.7, show catalase after the addition of a 10x excess (b), and a much larger excess (c) of PAA. These spectra

might be expected to show different, and generally greater intensities of the bands at 1642 and 1510 cm^{-1}, which increased in intensity under corresponding conditions with 406.7 nm excitation. Although there is some difference in the intensities of these bands between Figs. 6.7 (b) and (c), and between Figs. 6.7 (b) and 6.6 (b) the difference is not as large as the UV-vis. data (see Fig. 6.5) might lead us to expect. The main difference between the spectra taken with 413.1 nm and with 406.7 nm excitation is the appearance of a band of moderate intensity at 1547 cm^{-1} (see section 6.3). The band at 1550 cm^{-1} in the spectrum of native catalase can be assigned to ν 11 (see Table 6.2). In the case of HRP, ν 11 shifts up from 1550 cm^{-1} in native HRP to 1562 cm^{-1} in HRP compound II [11, 24]; a corresponding shift is not apparent in the catalase spectra in Fig. 6.7. In HRP compound I, however, a new band is observed at 1545 cm^{-1}, similar to the band at 1547 cm^{-1} in Fig. 6.7 (b). The 1545 cm^{-1} band in the HRP compound I spectrum has not been assigned, but is possibly ν 11. The model heme studies tentatively assign a 5 cm^{-1} downshift in ν 11 for the A_{2u} $CuTPP^{+\cdot}$ species, although there is a reported upshift in ν 11 for the A_{1u} $MOEP^{+\cdot}$ species [34].

In both spectra shown in Figs. 6.6 (b) and 6.7 (b), the ν 3 mode persists (with reduced intensity) at its original position of 1487 cm^{-1}, while a new band, previously assigned to ν 3 (of compound II), appears at 1511 cm^{-1}. The remaining intensity at 1487 cm^{-1} shows that either significant amounts of native catalase are regenerated in the laser beam, or that the ν 3 band in the spectrum of catalase compound I is not significantly shifted from 1487 cm^{-1}. The spectrum of HRP compound I shows ν 3 upshifted by only 3 cm^{-1} [24].

The lack of shift in the ν 4 band in the catalase spectra is

quite different from the observed shifts in the spectra of both compounds I and II of HRP [24]. As mentioned above, the only published data for catalase compound II also show $\nu 4$ to be relatively unshifted [3]. It appears that the $\nu 4$ band in catalase is unusually insensitive to the oxidation state changes accompanying the formation of compounds I and II, and thus comparisons with other compound I data may be misleading.

Summarising, there is strong evidence for some photodecomposition of catalase compound I to produce a compound II-type species, with associated RR bands at 1645 and 1511 cm^{-1}. However, there is still some evidence to suggest that there may be a significant spectral contribution from the compound I species. In particular the downshift of the band at 1550 cm^{-1} to 1547 cm^{-1} is similar to a shift observed on forming HRP compound I [24].

6.4.3 Spectra of model hemes

The observation of similar reversible loss (with 408 nm pump) of porphyrin ground state bands in **both** $[(TPP)Fe^{(III)}]_2O$ and $(TPP)Fe^{(III)}Cl$ shows that the largest changes that are occurring are not associated with fragmentation of the μ-oxo dimer. The lack of any new bands appearing in the dimer spectrum, or loss in solvent band intensity when a 424 nm probe is used (Δt = 0 ns) suggests that the process reported by Guest *et al.* [23] is not occurring in these experiments. Guest *et al.* observed an increase in absorption at 420 nm at 25 ps after a photolysis flash, the increase being of equal size to the loss in absorption at 408 nm. If this was occurring in the experiments presented here, then the 424 nm probe, 408 nm pump experiment would show loss of original porphyrin bands accompanied by a **loss** in the intensity of the solvent spectrum.

Growth of new bands due to the 'ion-pair' species would also be expected if the absorption at 424 nm was indeed of equal magnitude to the loss in 408 nm absorption. Using ns pulses, it is also true that the laser pulse energy and quantum yield for the photoprocess must be sufficiently high to observe a species with a 25-250 ps lifetime.

Cornelius *et al.* have observed reversible bleaching of the Soret absorption in $(TPP)Fe^{(III)}Cl$, with a concomitant new absorption appearing at 445 nm [43]. The absorption at 445 nm had a lifetime of $\tau \simeq 30$ ps, and was assigned to the first excited triplet state of $(TPP)Fe^{(III)}Cl$. By probing at 448 nm, at $\Delta t = 0$ ns after a 408 nm pump pulse, the spectrum of this triplet state might be expected to be observed. Fig. 6.11 indeed shows that new bands are observed for $(TPP)Fe^{(III)}Cl$ under these conditions. Thus, the bands at 1541 and 1344 cm^{-1} can probably be assigned to $\nu 2$ and $\nu 4$ of the triplet state of $(TPP)Fe^{(III)}Cl$. These values are considerably downshifted from the original positions at 1557 and 1360 cm^{-1}. This downshift reflects a large increase in the porphyrin core size (see chapter 1 and [13]).

The dimer also behaves in a similar manner, the ground state bands being replaced by new bands as the triplet state is formed. From the lack of ground state bands in the pump+probe spectrum it appears that both rings of the dimer molecule are excited to the triplet state. The changes in bands on forming the dimer triplet state are similar to those observed for the monomer, but the triplet state spectra are not identical. In the dimer triplet spectrum, $\nu 2$ shifts from 1556 to 1544 cm-1, but $\nu 4$ almost completely disappears. This is quite different from the case of the monomer, where $\nu 2$ and $\nu 4$ retain roughly the same relative intensities in the triplet

spectrum.

Both triplet state spectra are quite different from those reported recently for ZnTPP, which has a much longer triplet state lifetime [55, 56].

6.5 CONCLUSIONS

6.5.1 Catalase and stable derivatives

The balance of evidence from the RR spectra reported here indicates that the heme iron is 6-coordinate in native catalase. This contrasts with the conclusion from X-ray crystallography [44] and with the assumption of 5-coordination made by previous workers [4]. The spectra do however confirm that catalase contains iron in a ferric high-spin state at both alkaline and acidic pH. The spectra of catalase in alkaline (pH 7.8) and acidic (pH 6.0) solutions show differences that could be due to hydroxyl ligation at alkaline pH.

The RR spectrum of catalase-azide does not show any contribution from a low-spin ferric heme. This is in contrast to the conclusion of Chuang *et al.*, [4] who propose that catalase-azide exists as a spin state mixture, with the high spin form predominant.

6.5.2 Catalase and its reaction with PAA

There is strong evidence to suggest that catalase compound I is photolabile, and that the RR spectra of compound I contain a contribution from a species that is more like compound II. A similar photoprocess has been observed in HRP, and is thought to involve the transfer of the radical from the porphyrin to the protein, so as to leave the heme centre in a non-radical, 'compound II' ferryl form

[23b, 24]. There is some evidence for the contribution of a true compound I spectrum. However, if this contribution is significant, then it is surprising that $\nu 4$ is not apparently affected, as it is in both the model heme radical cation species, and in HRP compound I.

6.5.3 Heme models

With 408 nm excitation, the dominant process in both $(TPP)Fe^{(III)}Cl$ and $[(TPP)Fe^{(III)}]_2O$ appears to be formation of the short lived triplet state. There is no evidence to suggest that the photodissocation of the dimer to produce an ion-pair which absorbs at 420 nm, observed by Guest *et al.* [33], is occuring in these experiments. The photodissociation of the μ-oxo-dimer to produce long lived $Fe^{(IV)}=O$ and $Fe^{(II)}$ species, as observed by Peterson *et al.* [32], does not appear to be a major process. Photodissociation does take place, as evidenced by the gradual photodecomposition of the dimer to a monomer species. However, no Raman bands of the primary photoproduct species, $Fe^{(IV)}=O$ and $Fe^{(II)}$, could be observed.

6.6 FUTURE WORK

6.6.1 Catalase and stable derivatives

The coordination of hydroxide or water to the heme iron in native catalase could be confirmed by isotope substitution experiments using $H_2{}^{18}O$. The spin state equilibrium of the catalase-azide complex could be more unambiguously established by a number of experiments, including a careful measurement of the 2000-2100 cm^{-1} (azide stretching) region of both the IR and RR

spectra, and measurement of spectra at low temperature, where the low spin form may be favoured.

6.6.2 Catalase compounds I and II

The low wavenumber region of the spectrum of compound I should show the $Fe^{(IV)}$=O stretching band at *ca.* 737 cm^{-1} for a compound I species, but at 775-787 cm^{-1} for a compound II species. Unfortunately, attempts at obtaining low wavenumber region RR spectra of catalase with the CCD system have so far failed, due to problems with light scattering and other spectral artefacts. Using a low temperature Raman cell, the compound I species could probably be stabilised for long enough to record a spectrum on the Spex system, which gives better stray light rejection.

An experiment using a fast flow system, giving a μs residence time of the sample in the laser beam, might also show whether photodecomposition is taking place.

6.6.3 Heme models

It would be useful to confirm the identity of the species assigned to a triplet state with experiments using a picosecond laser. Power dependence studies on the dimer would be particularly useful in determining whether there really is a two photon process occurring that excites both rings of the dimer to separate triplet states. Polarisation measurements would also help in the assignment of the bands of the transient species.

6.7 REFERENCES

[1] T.Kitagawa in *"Advances in Spectroscopy, Vol. 13: Spectroscopy of Biological Systems"* Eds. R.J.H.Clark and R.E.Hester, p.443 (Wiley, Chichester, 1986).

[2] G.T.Babcock in *"Biological Applications of Raman Spectroscopy, Vol. 3: Resonance Raman Spectra of Heme and Metalloproteins"* Ed. T.G.Spiro, p.293 (Wiley, 1988).

[3] R.H.Felton, A.Y.Romans, N.-T.Yu, and G.R.Schonbaum, *Biochim. Biophys. Acta* **434**, 82 (1976).

[4] W.-J.Chuang, S.Johnson, and H.E.Van Wart, *Inorg.Chem* **34**, 201 (1988).

[5] (a) P.R.Ortiz de Montellano, *"Cytochrome P-450, Structure, Mechanism and Biochemistry"* (Plenum Press, New York, 1986).
(b) D.Dolphin, Ed. *"The Porphyrins, Physical Chemistry, Parts A-C"* (Academic Press, London, 1978).

[6] H.Theorell and A.Ehrenberg, *Arch.Biochem.Biophys.* **41**, 442 (1952).

[7] A.Brill, *Comp.Biochem.* **14**, 447 (1966).

[8] W.D.Hewson and L.P.Hager in *"The Porphyrins"* Ed. D.Dolphin, **7**, 295 (Academic Press, New York, 1979).

[9] J.E.Frew and P.Jones in *"Advances in Inorganic and Bioinorganic Mechanisms"* **3**, 175 (Academic Press, New York, 1984).

[10] D.N.Middlemiss, *Ph.D. Thesis, University of Newcastle-upon-Tyne* (1973).

[11] A.J.Sitter, C.M.Reczek and J.Terner, *J.Biol.Chem.* **261**, 8638 (1986).

[12] G.Rakshit, T.G.Spiro, and M.Uyeda, *Biochem.Biophys. Res.Commun.* **71**, 803 (1976).

[13] (a) T.G.Spiro, *Advances in Protein Chemistry* **37**, 111 (1985).
(b) N.Partasarathi, C.Hansen, S.Yamaguchi, and T.G.Spiro, *J.Am.Chem.Soc.* **109**, 3865 (1987).

[14] J.Terner, A.J.Sitter, and C.M.Reczek, *Biochim.Biophys. Acta* **828**, 73 (1985).

[15] S.Hashimoto, Y.Tatsuno, and T.Kitagawa, *Proc.Japan Acad.* **60 Ser.B**, 345 (1984).

[16] A.J.Sitter, C.M.Reczek, and J.Terner, *J.Biol.Chem.* **260**, 7515 (1985).

[17] S.Hashimoto, Y.Tatsuno, and T.Kitagawa, *Proc.Natl.Acad.Sci. USA* **83**, 2417 (1986).

[18] M.M.Palcic and H.B.Dunford, *J.Biol.Chem.* **255**, 6128 (1980)

[19] T.Araiso, R.Rutter, M.M.Palcic, L.P.Hager, and H.B.Dunford, *Can.J.Biochem.* **59**, 233 (1981).

[20] R.Rutter and L.P.Hager, *J.Biol.Chem.* **257**, 7958 (1982).

[21] C.E.Schulz, P.W.Devaney, H.Winkler, P.G.Debrunner, N.Doan, R.Chiang, R.Rutter, and L.P.Hager, *F.E.B.S. Lett.* **103**, 102 (1979).

[22] T.Ogura and T.Kitagawa, *J.Am.Chem.Soc.* **109**, 2177 (1987).

[23] (a) W.A.Oertling and G.T.Babcock, *J.Am.Chem.Soc.* **107**, 6406 (1985).
(b) W.A.Oertling and G.T.Babcock, *Biochemistry* in press (1989).

[24] K.-J.Paeng and J.R.Kincaid, *J.Am.Chem.Soc.* **110**, 7913 (1988).

[25] R.S.Czernuszewicz and K.A.Macor, *J.Raman Spectrosc.* **19**, 553 (1988).

[26] (a) K.Bajdor and K.Nakamoto, *J.Am.Chem.Soc.* **106**, 3045 (1984).
(b) L.M.Pronewicz, K.Bajdor, and K.Nakamoto, *J.Phys.Chem.* **90**, 1760 (1986).

[27] M.Schappacher, G.Chottard, and R.Weiss, *J.Chem.Soc.*

Chem.Commun. 93 (1986).

[28] R.T.Kean, W.A.Oertling, and G.T.Babcock, *J.Am.Chem.Soc.* **109**, 2185 (1987).

[29] A.Gold, K.Jayaraj, P.Doppelt, R.Weiss, G.Chottard, E.Bill, X.Ding, and A.X.Trautwein, *J.Am.Chem.Soc.* **110**, 5756 (1988).

[30] S.E.J.Bell, R.E.Hester, and J.R.Lindsay-Smith, *Proc. Int. Conf. on Time-Resolved Vibrational Spectroscopy*, Eds. T.G.Spiro and R.S.Czernuszewicz (1989).

[31] V.P.Shedbalkar, S.Modi, and S.Mitra, *J.Chem.Soc. Chem.Commun.* 1238 (1988).

[32] M.W.Peterson, D.S.Rivers, and M.Richman, *J.Am.Chem.Soc.* **107**, 2907 (1985).

[33] C.R.Guest, K.D.Straub, J.A.Hutchinson, and P.M.Rentzepis, *J.Am.Chem.Soc.* **110**, 5276 (1988).

[34] R.S.Czernuszewicz, K.A.Macor, X.-Y.Li, J.R.Kincaid, and T.G.Spiro, *J.Am.Chem.Soc.* **111**, 3860 (1989).

[35] L.K.Hanson, C.K.Chang, M.S.Davis, and J.Fajer, *J.Am.Chem.Soc.* **103**, 663 (1981).

[36] D.Kim, L.A.Miller, G.Rakshit, and T.G.Spiro, *J.Phys.Chem.* **90**, 3320 (1986).

[37] A.Salehi, W.A.Oertling, G.T.Babcock, and C.K.Chang, *J.Am.Chem.Soc.* **108**, 5630 (1986).

[38] R.M.C.Dawson, *"Data for Biochemical Research"* (Academic Press, 1969).

[39] P.Nicholls and G.R.Schonbaum, *"The Enzymes, 1st Edn."* **8**, 163 (1963).

[40] J.M.Burke, J.R.Kincaid, and T.G.Spiro, *J.Am.Chem.Soc.* **100**, 6077 (1978).

[41] G.Chottard, P.Battioni, J.-P.Battioni, M.Lange, and D.Mansuy,

Inorg.Chem. **20**, 1718 (1981).

[42] R.A.Reed, personal communication.

[43] P.A.Cornelius, A.W.Steele, D.A.Chernoff, and R.M.Hochstrasser, *Chem.Phys.Lett* **82**, 9 (1981).

[44] I.Fita and M.G.Rossmann, *J.Mol.Biol.* **185**, 21 (1985).

[45] K.Nagai, T.Kagimoto, A.Hayashi, F.Taketa, and T.Kitagawa, *Biochemistry* **22**, 1305 (1983).

[46] T.G.Spiro, J.D.Stong, and P.Stein, *J.Am.Chem.Soc.* **101**, 2648 (1979).

[47] S.Choi, T.G.Spiro, K.C.Langry, K.M.Smith, D.L.Budd, and G.N.LaMar, *J.Am.Chem.Soc.* **104**, 4345 (1982).

[48] P.M.Callaghan and G.T.Babcock, *Biochemistry* **20**, 952 (1981).

[49] A.J.Sitter, J.R.Shifflett, and J.Terner, *Proc.Int.Conf. on Raman Spectrosc. XI* Eds. R.J.H.Clark and D.A.Long, p.651 (Wiley, Chichester 1988).

[50] N.-T.Yu, *Meth.Enz.* **130**, 350 (1986).

[51] S.A.Asher and T.M.Schuster, *Biochemistry* **18**, 5377 (1979).

[52] M.Tsubaki, R.B.Srivastava, and N.-T.Yu, *Biochemistry* **20**, 946 (1981).

[53] S.McCoy and W.S.Caughey, *Biochemistry* **9**, 2387 (1970).

[54] N.-T.Yu, B.Benko, E.A.Kerr, and K.Gersonde, *Proc.Natl.Acad.Sci. USA* **81**, 5106 (1984).

[55] R.A.Reed, R.Purello, K.Kushmeider, and T.G.Spiro, *Proc.Int.Conf. on Time-Resolved Vibrational Spectroscopy* Eds. T.G.Spiro and R.S.Csernuszewicz (1989).

[56] V.A.Walters, J.C.de Paula, G.T.Babcock, and G.E.Leroi, *ibid.*

[57] T.G.Spiro and X.-Y.Li in "Biological Applications of Raman Spectroscopy, Vol. 3: Resonance Raman Spectra of Hemes and Hemeproteins", T.G.Spiro, Ed., p.1 (Wiley, New York, 1988).